JSCSEN 77(2)131–258(2012)

ISSN 1820-7421 (Online)

Journal of the Serbian Chemical Society

Electronic Version

Society 115th Anniversary 1897 - 2012

VOLUME 77

No 2

BELGRADE 2012

Available on line at

www.shd.org.rs/JSCS/

The full search of JSCS is available through

DOAJ DIRECTORY OF OPEN ACCESS JOURNALS

www.doaj.org

Штампање ове свеске је суфинансирао ЛУКОИЛ Србија АД

Publication of this issue is financially co-supported by LUKOIL Srbija AD

Journal of the Serbian Chemical Society
JSCS-info@shd.org.rs • www.shd.org.rs/JSCS

J. Serb. Chem. Soc. Vol. 77, No. 2 (2012)

CONTENTS

Published by the Serbian Chemical Society
Karnegijeva 4/III, 11000 Belgrade, Serbia
Printed by the Faculty of Technology and Metallurgy
Karnegijeva 4, P.O. Box 35-03, 11120 Belgrade, Serbia

Journal of the Serbian Chemical Society
JSCS-info@shd.org.rs • www.shd.org.rs/JSCS
J. Serb. Chem. Soc. *77* (2) 131–140 (2012)
JSCS–4255
UDC 547–304.2+542.913+66.095.83–916.2
Original scientific paper

Scalable methodologies for the synthesis of novel unsymmetrically substituted secondary amines

GHEORGHE ROMAN*

Department of Inorganic Polymers, Petru Poni Institute of Macromolecular Chemistry, 41A Aleea Gr. Ghica Vodă, Iaşi 700487, Romania

(Received 8 April, revised 2 July 2011)

Abstract: Fast, easy, and scalable methodologies for the synthesis of unsymmetrically substituted secondary amines containing naphthalene, indole, pyridine and imidazole moieties through reductive amination were explored. The investigated operating procedures were successful on a 50- to 30-mmol scale, and present a high potential for up-scaling.

Keywords: reductive amination; imine; secondary amine; scalability.

INTRODUCTION

Medicinal chemistry depends significantly on the generation of compound libraries for the discovery of leads, exploration of structure–activity relationship (SAR), and optimization of physical properties. However, the scope of a compound library can be limited by the commercial availability of the starting materials. Several chemical classes of starting materials, such as aldehydes and carboxylic acids, are well represented commercially. Amongst other important scaffolds in the preparation of numerous biologically active substances, a large number of structurally diverse amines are also available. Nonetheless, the significant use of amines as building blocks in drug-like molecules justifies the expansion of the available entities.

In connection with previous work concerning the synthesis,[1,2] reactivity,[3,4] and biological activity[5,6] of Mannich bases derived from *ortho*-hydroxyacetophenones, easy access to novel, biologically relevant secondary amines in 10-gram quantities was required. One-pot, solution-phase reductive alkylation of a primary amine with an aldehyde or a ketone is one of the most widely utilized methods for the synthesis of secondary amines. One of the drawbacks of this approach is the necessity for the removal (usually by column chromatography) of the unreacted primary amine along with other potential by-products, especially

* E-mail: gheorghe.roman@icmpp.ro
doi: 10.2298/JSC110408173R

the alcohol related to the initial carbonyl compound. Both solid-phase synthesis and solution-phase synthesis with resin-bound scavengers/reagents have been used to circumvent the shortcomings of the classical solution-phase synthesis.[7] Although these methodologies allow fast preparation of a virtually infinite number of pure secondary amines (either individually or in parallel synthesis) on a very small scale, the cost of the resins employed makes large- or even medium-scale synthesis prohibitive. Therefore, low-cost, classical, solution-phase synthetic strategies that are amenable to scaling up without the need for chromategraphic separation were considered for the achievement of this synthetic goal. In this paper, two of such strategies were employed for the multi-gram preparation of unsymmetrically substituted secondary amines having naphthalene, indole, pyridine and imidazole moieties in their structure; in addition, the potential for scale-up of these two strategies was explored.

EXPERIMENTAL

All chemical reagents were obtained from Sigma–Aldrich and were used without prior purification. Analytical thin-layer chromatography was performed on glass-backed SiliCycle precoated silica gel 60 F_{254} plates, and the compounds were visualized by UV illumination (254 nm). Melting points were taken on a Mel-Temp II apparatus and are uncorrected. Elemental analysis was conducted in-house, on a PerkinElmer 2400 Series II CHNS/O system. The ^{1}H- and ^{13}C-NMR spectra were recorded on a Bruker Avance 400-MHz spectrometer. The signals owing to residual protons in the deuterated solvents were used as internal standards for the ^{1}H-NMR spectra. The chemical shifts for the carbon atoms are given relative to $CDCl_3$ (δ = 77.16 ppm), CD_3OD (δ = 49.00 ppm), or DMSO-d_6 (δ = 39.52 ppm). The high-resolution mass spectra were obtained on an Applied Biosystems/MDS Sciex QSTAR XL spectrometer equipped with an Agilent HP1100 Cap-LC system in the electrospray ionization (ESI) mode.

General procedure for the synthesis of N-*(naphthalen-1-ylmethylene)benzylamines* ***1***

A mixture of the required amine (50 mmol) and 1-naphthaldehyde (7.81 g, 50 mmol) in ethanol (20 mL) was treated with 0.5 mL of ethereal HCl and stirred at room temperature for 1 h. The mixture was refrigerated overnight, and then the solid that separated was filtered and recrystallized.

General procedure for the synthesis of N-*(naphthalen-1-ylmethyl)benzylamines* ***2***

A solution of *N*-(naphthalen-1-ylmethylene)benzylamine **1** (20 mmol) in methanol (50 mL) was gradually treated with $NaBH_4$ (2.28 g, 60 mmol) at room temperature. The mixture was stirred at room temperature overnight, and then the solvent was removed under reduced pressure and the residue was partitioned between water (80 mL) and ethyl acetate (50 mL). The aqueous layer was further extracted with ethyl acetate (2× 20 mL) and the combined organic phase was washed with water and brine and dried over anhydrous Na_2SO_4. The solvent was removed under reduced pressure to give the pure secondary amine. The hydrochloride was prepared by treating a solution of the free base in diethyl ether with an excess of ethereal HCl. Filtration and recrystallization of the separated solid afforded the crystalline hydrochloride.

General procedure for the synthesis of N-*(arylidene)-2-(1*H-*indol-3-yl)ethanamines **3***

A mixture of tryptamine (4.81 g, 30 mmol) and aldehyde (30 mmol) in benzene (60 mL) was heated at reflux temperature for 4 h while the formed water was removed as an azeotrope. At the end of the reaction time, the solvent was removed under reduced pressure to give a residue that was recrystallized from the appropriate solvent.

*Reduction of imines **3** derived from tryptamine to amines **4***

Starting from imines **3** (20 mmol) and $NaBH_4$ (2.28 g, 60 mmol), the reduction was performed in a manner similar to the procedure reported previously for amines **2**. The hydrochlorides were prepared as described for the *N*-(naphthalen-1-ylmethyl)benzylamines **2**.

General procedure for the one-pot synthesis of N-*(pyridin-3-ylmethyl)benzylamines **5***

A mixture of 3-(aminomethyl)pyridine (3.24 g, 30.0 mmol) and aldehyde (36 mmol) in methanol (50 mL) was stirred at room temperature for 6 h, and then $NaBH_4$ (3.42 g, 90.0 mmol) was gradually added to the solution, and the mixture was further stirred at room temperature overnight. The solvent was removed under reduced pressure and the residue was partitioned between water (50 mL) and ethyl acetate (50 mL). The aqueous layer was further extracted with ethyl acetate (2×20 mL); the combined organic phase was washed with water (3×30 mL) and extracted with 1 M HCl (60 mL). The acid extract was washed with ethyl acetate (2×20 mL), and then the pH of the aqueous phase was rendered alkaline with 10 % aqueous K_2CO_3 solution. The separated oil was extracted in ethyl acetate (2×30 mL), washed with water and brine, and dried over anhydrous Na_2SO_4. The solvent was removed under reduced pressure to yield the pure amine. The dihydrochlorides were prepared as described for the *N*-(naphthalen-1-ylmethyl)benzylamines **2**.

General procedure for the synthesis of N-*(3-(1*H-*imidazol-1-yl)propyl)benzylamines **6***

A mixture of 1-(3-aminopropyl)-1*H*-imidazole (1.25 g, 10.0 mmol) and aldehyde (12 mmol) in methanol (20 mL) was stirred at room temperature for 24 h, and then $NaBH_4$ (1.14 g, 30.0 mmol) was gradually added. The mixture was further stirred at room temperature overnight, and then the solvent was removed under reduced pressure and the residue was partitioned between water (50 mL) and ethyl acetate (30 mL). The aqueous phase was further extracted with ethyl acetate (20 mL), and then the combined organic phase was washed with water (3×50 mL) and brine (20 mL) and dried over anhydrous Na_2SO_4. The solvent was removed under reduced pressure to give an oil that was purified by column chromatography. The dihydrochlorides were obtained by treating the solution of the free base in diethyl ether with excess of HCl in diethyl ether.

RESULTS AND DISCUSSION

The first methodology towards the large-scale synthesis of pure secondary amines investigated in this paper was based on the two-step reductive alkylation of a primary amine, an approach that entails the isolation of the intermediate imine. This methodology is less attractive for the preparation of secondary amines than the one-pot approach owing to the additional step. However, the two-step reductive alkylation becomes acceptable provided that the intermediate imine could be separated from the reaction mixture by filtration, and purified (preferably through recrystallization) prior to its reduction in the subsequent step; in this case, the reduction of the imine could yield the secondary amine in high pu-

rity even in bulk preparations. As a high molecular weight and the presence of fused carbocycles or heterocyles are usually grounds for an organic compound to be in the solid state at room temperature, it was hypothesized that imines having at least one naphthalene moiety could be good candidates for the exploration of this strategy. Furthermore, a naphthalene scaffold could be an interesting structural feature, as proved by its presence in the structure of the biologically active compounds that bind to a highly hydrophobic active site of an enzyme,[8] or by its effectiveness as a pharmacophore required for the binding to melanocortin receptors.[9] A brief search of the literature showed that the available information even on the common *N*-(naphthalen-1-ylmethylene)benzylamine or *N*-benzylidene-1-(naphthalen-1-yl)methylamine is scarce, and that the corresponding secondary amine is available from a limited number of commercial sources at considerable cost. Encouraged by these findings, the synthesis of a series of *N*-(naphthalen-1-ylmethyl)benzylamines **2** was undertaken starting from the commercially available naphthalene-1-carboxaldehyde and substituted benzylamines (Scheme 1). When an equimolar mixture of the starting materials in a small volume of ethanol and in the presence of catalytic amounts of ethereal HCl was stirred at room temperature for 1 hour and subsequently refrigerated overnight, the corresponding imines **1** separated as solids. However, 4-methylbenzylamine and 4-fluorobenzylamine did not lead to solid imines, but produced the Schiff bases as viscous oils that redissolved when the reaction mixture was allowed to warm to room temperature; the experiments with these two benzylamines were not pursued further. The solid imines **1** could be recrystallized from lower alcohols with only a moderate loss of material, except for the Schiff base derived from 4-methoxybenzylamine. Aside from 2-chloro-*N*-(naphthalen-1-ylmethylene)benzylamine **1b**, all other naphthalene-containing Schiff bases are novel, and were fully characterized (the analytic and spectral data are given as supplementary material). As a general feature, the ^{1}H-NMR spectra of imines **1** present one singlet integrating for one proton at approximately 9 ppm that can be associated with the

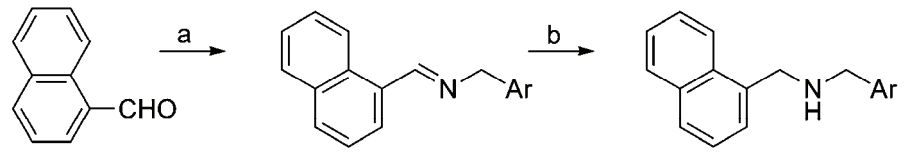

1 **2**

Ar = 4-$CH_3OC_6H_4$-; 2-ClC_6H_4-; 2-$CH_3C_6H_4$-; 2,4-$Cl_2C_6H_3$-; 3,4-$(OCH_2O)C_6H_3$-

Scheme 1. Synthesis of naphthalene-containing unsymmetrically substituted secondary amines. Conditions: a) substituted benzylamine, 36 % HCl, diethyl ether, rt for 1 h, then –10 °C overnight; b) $NaBH_4$, methanol, rt, overnight.

proton of the imine function, and one singlet integrating for two protons at around 5 ppm, corresponding to the methylene group. The signal of the carbon atom in the imine function just above 160 ppm and the peak of the carbon atom of the methylene group at about 60 ppm can also serve as markers for the validation of the structure of imines **1**.

As expected, the reduction of the pure imines with sodium borohydride in methanol[10] afforded the pure secondary amines **2** almost quantitatively. As the free amines are known to age badly or form carbamic acids in the presence of carbon dioxide from air, the novel compounds were also converted into their hydrochlorides by treating their solution in diethyl ether with ethereal HCl. A comparative inspection of the ^{1}H-NMR spectra of amines **2** as free bases revealed the presence of a new singlet integrating for two protons at around 4 ppm and the disappearance of the singlet that was noticeable downfield in the spectra of imines **1**. Moreover, an additional peak in the aliphatic region of the ^{13}C-NMR spectra can be attributed to the aliphatic carbon atom in the naphthalen-1-ylmethyl residue. The ^{1}H-NMR spectra of the hydrochlorides of amines **2** taken in deuterated DMSO feature a broad singlet at approximately 10 ppm that integrates for two protons. Since the addition of deuterated methanol to the NMR sample resulted in a decrease of the integration for this peak, the signal was attributed to the hydrogen atoms of the protonated secondary nitrogen atom.

The investigation was extended to a second series of secondary amines derived from tryptamine and aromatic aldehydes. A few *N*-benzyltryptamines with sedative, anticonvulsant, analgesic, and neuroleptic action,[11] or active as tuberculostatics[12] have been so far obtained through the condensation of tryptamine with aldehydes followed by the *in situ* reduction of the intermediate imine. On the other hand, imines derived from tryptamine have usually been reported in connection with the synthesis of tetrahydro-*β*-carbolines *via* the Pictet–Spengler reaction.[13] A brief examination of the methods described in the literature for the synthesis of imines **3** derived from tryptamine revealed that the most efficient method is based on the condensation of the reactants in benzene with the removal of the by-product water as an azeotrope (Scheme 2). For example, this method produced a 70 % yield of (2-(1*H*-indol-3-yl)-*N*-(2-thienylmethylene)ethanamine **3d** after recrystallization, whereas a low yield of only 24 % was reported when the same compound was prepared by heating the reactants in ethanol at reflux temperature for 30 min.[14] The analytic and spectral data for imines **3** are given in the Supplementary material to this paper. The ^{1}H-NMR spectra of the imines **3** showed two triplets around 3.1 and 3.9 ppm, attributable to the protons of the methylene groups originating from tryptamine, whereas the imine proton and the proton at the heterocyclic nitrogen atom were associated with a sharp singlet usually above 8 ppm and a broad singlet at approximately 8 ppm, respectively. In the ^{13}C-NMR spectra of imines **3**, the carbon atom of the imine function gave a

signal downfield at about 160 ppm. In the subsequent step, the reduction of the pure imines **3** with sodium borohydride in methanol at room temperature afforded, almost quantitatively, the pure secondary amines **4**. Amines **4a** and **4d** were crystalline compounds, whereas amines **4b** and **4c** were dense oils that were characterized both as free bases and as hydrochlorides.

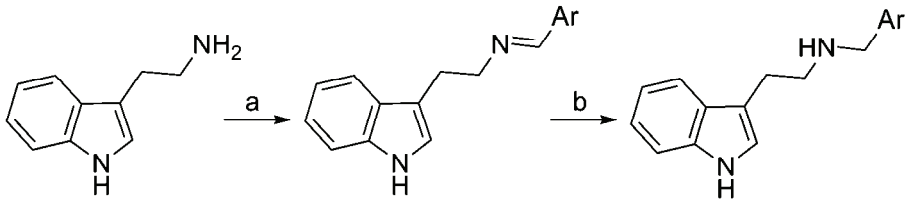

Ar = 4-BrC_6H_4-; 3,4-$(CH_3O)_2C_6H_3$-; naphthalen-1-yl; 2-thienyl

Scheme 2. Synthesis of tryptamine-derived unsymmetrically substituted secondary amines. Conditions: a) (hetero)aromatic aldehyde, benzene, reflux, 4 h; b) $NaBH_4$, methanol, rt, overnight.

A second hypothesized strategy that could provide uncomplicated access to multi-gram quantities of secondary amines was also explored in this study. This strategy relies on the association of the standard one-pot reductive alkylation with a procedure allowing the adequate separation of the desired product from the unreacted starting materials and any potential by-products. An inexpensive, fast separation procedure that is applicable for large-scale preparations could be based on the differential solubility of the components in the mixture. Thus, the simple partition of the crude reaction mixture between an organic solvent and an aqueous acid solution would result in the extraction in the latter phase of the basic components only (*i.e.*, the starting primary amine and the desired secondary amine), whereas the unreacted carbonyl compound and the alcohol by-product derived from it remain in the organic phase. Next, the mixture consisting of a hydrophilic primary amine and a more lipophilic secondary amine could be separated owing to their differential solubility in water. In order to test this hypothesis, the water-soluble 3-(aminomethyl)pyridine and 1-(3-aminopropyl)imidazole were selected as starting materials. These two primary amines are also good candidates for the generation of biologically active chemical entities. For example, the 3-pyridinyl moiety is important for the activity of several types of nicotinic acetylcholine receptor agonists,[15–17] or it is present as the pharmacophore in inhibitors of aldosterone synthase[18] or cytochromes P450,[19] whereas imidazole is ubiquitous in azole antifungal agents[20] and inhibitors of hemoenzymes, such as nitric oxide synthase[21] or heme oxygenase.[22]

Treatment of 3-(aminomethyl)pyridine with an excess of aromatic aldehydes in methanol for 6 hours led to the formation of the corresponding imines, which, in turn, were reduced *in situ* with sodium borohydride to the related secondary amines **5** (Scheme 3). Sequential removal of the solvent and partition between ethyl acetate and dilute hydrochloric acid allowed the separation of the basic components from the crude reaction mixture. Subsequent release of the amine (or amines, if unreacted 3-(aminomethyl)pyridine is still present) from their hydrochlorides, followed by extraction with ethyl acetate afforded the pure secondary amine in good yield, as shown by TLC; the unreacted 3-(aminomethyl)-pyridine, if present in the first ethyl acetate extract, appears to have remained in the aqueous phase after the second extraction. The analytic and spectral data for the secondary amines are given in the Supplementary material to this paper. The NMR characterization of the isolated amines **5** confirmed their purity and supported their structure through the two singlets integrating for two protons in the vicinity of 4 ppm in the ^{1}H-NMR spectra and the two signals around 50 ppm in the ^{13}C-NMR spectra, which are associated with the two methylene groups adjacent to the nitrogen atom. Inspection of the ^{1}H-NMR spectra of the salts prepared by treating the free bases of amines **5** with an excess of ethereal HCl revealed that the corresponding dihydrochlorides were obtained in all cases. The protonation of the heterocyclic nitrogen atom was supported by the displacement of the signals of the protons in the pyridine moiety to lower magnetic fields. The peak integrating for two protons noticeable above 10 ppm in ^{1}H-NMR spectra of the dihydrochlorides in deuterated DMSO confirmed the protonation of the nitrogen atom in the amine function; in contrast, the ^{1}H-NMR spectrum of dihydrochloride **5d** taken in deuterated methanol lacks this peak.

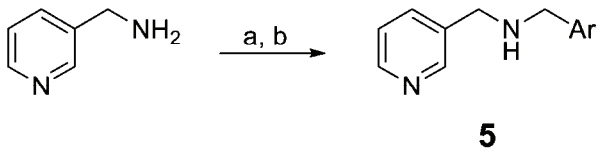

5

Ar = 4-BrC_6H_4-; 4-$CH_3O C_6H_4$-; 4-biphenylyl; naphthalen-1-yl; 2-thienyl

Scheme 3. Synthesis of pyridine-containing unsymmetrically substituted secondary amines. Conditions: a) (hetero)aromatic aldehyde, methanol, rt, 6 h; b) $NaBH_4$, methanol, rt, overnight.

Under similar reaction conditions, the condensation of 1-(3-aminopropyl)-imidazole with aromatic aldehydes to the corresponding imines (Scheme 4) was less straightforward. TLC analysis of the reaction mixture after 6 h revealed significant amounts of unreacted starting materials; extension of the reaction time to 24 h resulted in a slight improvement of the conversion. *In situ* reduction with sodium borohydride followed by the separation procedure detailed for amines **5**

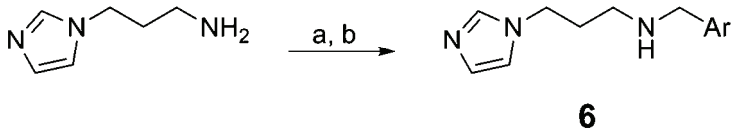

6

Ar = C_6H_5-; naphthalen-1-yl; 2-thienyl; 2,4-$(CH_3O)_2C_6H_3$-

Scheme 4. Synthesis of imidazole-containing unsymmetrically substituted secondary amines. Conditions: a) (hetero)aromatic aldehyde, methanol, rt, 24 h; b) $NaBH_4$, methanol, rt, overnight.

led to a mixture of 1-(3-aminopropyl)imidazole and secondary amines **6**, that required additional column chromatographic separation in order to afford modest yields of pure amines **6**. As a result, this strategy does not seem to be appropriate for a fast, medium-scale synthesis of amines derived from 1-(3-aminopropyl)imidazole. The analytic and spectral data of the synthesized amines **6** are given in the Supplementary material. The structure of the imidazole-containing secondary amines **6** was supported by NMR analysis. In the aliphatic region of the ^{1}H-NMR spectra, a multiplet at 2 ppm and two triplets at approximately 2.6 and 4 ppm are indicative for the propyl moiety, whereas the aromatic protons in the imidazole ring appear at 6.87, 7.03 and 7.43 ppm. The deliquescent dihydrochlorides of compounds **6a** and **6b** were also prepared and characterized by NMR. Again, the displacement of the protons in the heterocyclic ring towards higher chemical shifts confirmed the protonation of the imidazole, and the peak integrating for two protons at 10 ppm in the spectrum of compound **6b** taken in deuterated DMSO (which was absent in the spectrum of the compound **6a** taken in deuterated methanol) suggested the protonation of the nitrogen atom in the amine function.

CONCLUSIONS

Novel naphthalene- and indole-containing secondary amines were synthesized by a two-step reductive alkylation process, with the separation of the intermediate imine. The methodology was successfully applied to a 50-mmol scale synthesis of these novel amines, and the procedure could be scaled up for the production of even larger quantities. A second strategy, employing heterocyclic, water-soluble amines, and comprising the usual reductive alkylation process combined with an isolation procedure relying on the differential solubility of the initial primary amine and the resulting secondary amine, was successful only in the case of 3-(aminomethyl)pyridine; the methodology was valid on a 30-mmol scale, and its potential for scalability was high. On the other hand, the application of the same methodology with 1-(3-aminopropyl)imidazole as the starting material required chromatographic separation, making the procedure unsuitable for scaling up.

SUPPLEMENTARY MATERIAL

Analytical and spectral data of synthesized compounds are available electronically from http://www.shd.org.rs/JSCS/, or from the corresponding author on request.

ИЗВОД

МЕТОДОЛОГИЈА СИНТЕЗЕ НОВИХ АСИМЕТРИЧНО СУПСТИТУИСАНИХ СЕКУНДАРНИХ АМИНА

GHEORGHE ROMAN

Department of Inorganic Polymers, Petru Poni Institute for Macromolecular Chemistry, 41A Aleea Gr. Ghica Vodă, Iaşi 700487, Romania

Испитана је брза и једноставна синтеза асиметрично супституисаних секундарних амина који садрже нафталенски, индолски и имидазолски структурни фрагмент. Испитане процедуре успешно су примењене на скали 30 до 50 mmol и имају озбиљан потенцијал за примену на већим скалама.

(Примљено 8. априла, ревидирано 2. јула 2011)

REFERENCES

1. E. Comaniţă, I. Popovici, B. Comaniţă, G. Roman, *ACH – Models Chem.* **134** (1997) 3
2. E. Comaniţă, G. Roman, I. Popovici, B. Comaniţă, *J. Serb. Chem. Soc.* **66** (2001) 9
3. E. Comaniţă, I. Popovici, G. Roman, G. Robertson, B. Comaniţă, *Heterocycles* **51** (1999) 2139
4. G. Roman, E. Comaniţă, B. Comaniţă, *Tetrahedron* **58** (2002) 1617
5. I. Popovici, C. Lupuşoru, C. Ghiciuc, *Rev. Med. Chir. Soc. Med. Nat. Iasi* **101** (1997) 186
6. I. Popovici, I. Popovici, A. D. Mărculescu, *Farmacia (Bucharest)* **56** (2008) 221
7. R. N. Salvatore, C. H. Yoon, K. W. Jung, *Tetrahedron* **57** (2001) 7785
8. M. G. Götz, K. E. James, E. Hansell, J. Dvořák, A. Seshaadri, D. Sojka, P. Kopáček, J. H. McKerrow, C. R. Caffrey, J. C. Powers, *J. Med. Chem.* **51** (2008) 2816
9. F. Mutulis, I. Mutule, M. Lapins, J. E. S. Wikberg, *Bioorg. Med. Chem. Lett.* **12** (2002) 1035
10. J. H. Billman, A. C. Diesing, *J. Org. Chem.* **22** (1957) 1068
11. J. Boch, J. Molle (A.E.C. Société de Chimie Organique et Biologique), *Fr. Pat. 2,181,559* (1975)
12. S. Mahboobi, G. Grothus, W. Meindl, *Arch. Pharm.* **327** (1994) 105
13. S. W. Youn, *J. Org. Chem.* **71** (2006) 2521
14. Á. Szöllösy, T. Tischer, I. Kádas, L. Töke, G. Tóth, *Tetrahedron* **55** (1999) 7279
15. J. M. Frost, W. H. Bunnelle, K. R. Tietje, D. J. Anderson, L. E. Rueter, P. Curzon, C. S. Surowy, J. Ji, J. F. Daanen, K. L. Kohlhaas, M J. Buckley, R. F. Henry, T. Dyhring, P. K. Ahring, M. D. Meyer, *J. Med. Chem.* **49** (2006) 7843
16. W. H. Bunnelle, J. F. Daanen, K. B. Ryther, M. R. Schrimpf, M. J. Dart, A. Gelain, M. D. Meyer, J. M. Frost, D. J. Anderson, M. Buckley, P. Curzon, Y.-J. Cao, P. Puttfarcken, X. Searle, J. Ji, C. B. Putman, C. Surowy, L. Toma, D. Barlocco, *J. Med. Chem.* **50** (2007) 3627
17. W. H. Bunnelle, K. R. Tietje, J. M. Frost, D. Peters, J. Ji, T. Li, M. J. C. Scanio, L. Shi, D. J. Anderson, T. Dyhring, J. H. Grønlien, H. Ween, K. Thorin-Hagene, M. D. Meyer, *J. Med. Chem.* **52** (2009) 4126

18. S. Ulmschneider, U. Müller-Vieira, C. D. Klein, I. Antes, T. Lengauer, R. W. Hartmann, *J. Med. Chem.* **48** (2005) 1563
19. G. A. Wächter, R. W. Hartmann, T. Sergejew, G. L. Grün, D. Ledergerber, *J. Med. Chem.* **39** (1996) 834
20. L. Zirngibl, *Antifungal Azoles: A Comprehensive Survey of their Structures and Properties*, Wiley-VCH, Weinheim, Germany, 1998
21. L. Salerno, V. Sorrenti, C. Di Giacomo, G. Romeo, M. A. Siracusa, *Curr. Pharm. Des.* **8** (2002) 177
22. G. Roman, J. G. Riley, J. Z. Vlahakis, R T. Kinobe, J. F. Brien, K. Nakatsu, W. A. Szarek, *Bioorg. Med. Chem.* **15** (2007) 3225.

Journal of the Serbian Chemical Society
JSCS@tmf.bg.ac.rs • www.shd.org.rs/JSCS
J. Serb. Chem. Soc. 77 (2) S36–S44 (2012) *Supplementary material*

SUPPLEMENTARY MATERIAL TO

Scalable methodologies for the synthesis of novel unsymmetrically substituted secondary amines

GHEORGHE ROMAN*

Department of Inorganic Polymers, Petru Poni Institute of Macromolecular Chemistry, 41A Aleea Gr. Ghica Vodă, Iaşi 700487, Romania

J. Serb. Chem. Soc. 77 (2) (2012) 131–140

ANALYTICAL AND SPECTRAL DATA OF THE SYNTHESIZED COMPOUNDS

4-Methoxy-N-*(naphthalen-1-ylmethylene)benzylamine (**1a**)*. Yield: 6.48 g, 47 %; m.p. 44–45 °C (ethanol); Anal. Calcd. for $C_{19}H_{17}NO$: C, 82.88; H 6.22; N, 5.09 %. Found: C, 83.07, H, 6.11, N, 5.01 %; ^{1}H-NMR (400 MHz, $CDCl_3$, δ / ppm): 3.82 (3H, *s*), 4.91 (2H, *s*), 6.93 (2H, *d*, *J* = 8.4 Hz), 7.35 (2H, *d*, *J* = 8.4 Hz), 7.48–7.65 (3H, *m*), 7.85–8.02 (3H, *m*), 8.95 (1H, *d*, *J* = 8.4 Hz), 9.04 (1H, *s*); ^{13}C-NMR (100 MHz, $CDCl_3$, δ / ppm): 55.4, 65.6, 114.1, 124.5, 125.4, 126.1, 127.3, 128.7, 129.1, 129.3, 131.2, 131.5, 131.7, 134.0, 158.8, 161.4; HRMS (ESI) Calcd. for $C_{19}H_{18}NO$: 276.1388 $[M+H]^+$. Found: 276.1382.

2-Chloro-N-*(naphthalen-1-ylmethylene)benzylamine (**1b**)*.[1] Off-white solid. Yield: 9.65 g, 69 %; m.p. 60–61 °C (ethanol); Anal. Calcd. for $C_{18}H_{14}ClN$: C, 77.28; H 5.04; N, 5.01 %. Found: C, 77.20, H, 5.12, N, 4.94 %; ^{1}H-NMR (400 MHz, $CDCl_3$, δ / ppm): 5.05 (2H, *s*), 7.21–7.32 (2H, *m*), 7.43 (1H, *dd*, *J* = 0.8 and 8.0 Hz), 7.51–7.65 (4H, *m*), 7.88–8.00 (3H, *m*), 8.99 (1H, *d*, *J* = 8.4 Hz), 9.08 (1H, *s*); ^{13}C-NMR (100 MHz, $CDCl_3$, δ / ppm): 63.1, 124.5, 125.4, 126.2, 127.1, 127.4, 128.4, 128.8, 129.3, 129.4, 129.8, 131.4, 131.5, 131.6, 133.5, 134.0, 162.9; HRMS (ESI) Calcd. for $C_{18}H_{15}ClN$: 280.0893 $[M+H]^+$. Found: 280.0885.

2-Methyl-N-*(naphthalen-1-ylmethylene)benzylamine (**1c**)*. Off-white solid. Yield: 7.36 g, 57%; m.p. 52–53 °C (ethanol); Anal. Calcd. for $C_{19}H_{17}N$: C, 87.99; H 6.61; N, 5.40 %. Found: C, 87.88, H, 6.21, N, 5.31 %; ^{1}H-NMR (400 MHz, $CDCl_3$, δ / ppm): 2.47 (3H, *s*), 4.96 (2H, *s*), 7.20–7.26 (3H, *m*), 7.36–7.42 (1H, *m*), 7.50–7.63 (3H, *m*), 7.87–7.98 (3H, *m*), 8.98 (1H, *d*, *J* = 8.4 Hz), 9.03 (1H, *s*); ^{13}C-NMR (100 MHz, $CDCl_3$, δ / ppm): 19.5, 63.9, 124.5, 125.4, 126.2, 126.3, 127.2, 127.3, 128.6, 128.8, 129.2, 130.3, 131.2, 131.5, 131.8, 134.0,

* E-mail: gheorghe.roman@icmpp.ro

136.3, 137.8, 161.7; HRMS (ESI) Calcd. for $C_{19}H_{18}N$: 260.1439 $[M+H]^+$. Found: 260.1446.

2,4-Dichloro-N-*(naphthalen-1-ylmethylene)benzylamine* (***1d***). Yellowish solid. Yield: 12.21 g, 78 %; m.p. 97–98 °C (methanol); Anal. Calcd. for $C_{18}H_{13}Cl_2N$: C, 68.81; H 4.17; N, 4.46 %. Found: C, 68.68, H, 4.25, N, 4.37 %; ^{1}H-NMR (400 MHz, $CDCl_3$, δ / ppm): 4.98 (2H, *s*), 7.27 (1H, *dd*, *J* = 2.0 and 8.4 Hz), 7.44 (1H, *d*, *J* = 2.0 Hz), 7.47 (1H, *d*, *J* = 8.4 Hz), 7.51–7.65 (3H, *m*), 7.89––7.99 (3H, *m*), 8.98 (1H, *d*, *J* = 8.4 Hz), 9.07 (1H, *s*); ^{13}C-NMR (100 MHz, $CDCl_3$, δ / ppm): 62.6, 124.5, 125.4, 126.3, 127.4, 127.5, 128.8, 129.2, 129.5, 130.6, 131.4, 131.5, 131.6, 133.4, 134.0, 134.1, 136.1, 163.2; HRMS (ESI) Calcd. for $C_{18}H_{14}Cl_2N$: 314.0503 $[M+H]^+$. Found: 314.0498.

1-(1,3-Benzodioxol-5-yl)-N-*(naphthalen-1-ylmethylene)methylamine* (***1e***). Off-white solid. Yield: 10.29 g, 71 %; m.p. 63–64 °C (ethanol); Anal. Calcd. for $C_{19}H_{15}NO_2$: C, 78.87; H 5.23; N, 4.84 %. Found: C, 78.98, H, 5.31, N, 4.77 %; ^{1}H-NMR (400 MHz, $CDCl_3$, δ / ppm): 4.86 (2H, *s*), 5.96 (2H, *s*), 6.82 (1H, *d*, *J* = = 8.0 Hz), 6.88 (1H, *dd*, *J* = 0.8 and 8.0 Hz), 6.93 (1H, *d*, *J* = 0.8 Hz), 7.48–7.63 (3H, *m*), 7.86–7.98 (3H, *m*), 8.95 (1H, *d*, *J* = 8.4 Hz), 9.03 (1H, *s*); ^{13}C-NMR (100 MHz, $CDCl_3$, δ / ppm): 65.9, 101.1, 108.4, 108.8, 121.2, 124.4, 125.4, 126.2, 127.3, 128.8, 129.2, 131.3, 131.5, 131.6, 133.5, 134.0, 146.7, 147.9, 161.6; HRMS (ESI) Calcd. for $C_{19}H_{16}NO_2$: 290.1181 $[M+H]^+$. Found: 290.1183.

1-(4-Methoxybenzyl)-N-*(naphthalen-1-yl)methylamine* (***2a***). Yellowish oil. Yield: 5.31 g, 96 %; R_f 0.24 (hexane–ethyl acetate 3:1 v/v); Anal. Calcd. for $C_{19}H_{19}NO$: C, 82.28; H 6.90; N, 5.05 %. Found: C, 82.54, H, 6.71, N, 4.89 %; ^{1}H-NMR (400 MHz, $CDCl_3$, δ / ppm): 3.82 (3H, *s*), 3.87 (2H, *s*), 4.24 (2H, *s*), 6.90 (2H, *d*, *J* = 8.8 Hz), 7.32 (2H, *d*, *J* = 8.4 Hz), 7.40–7.57 (4H, *m*), 7.79 (1H, *d*, *J* = 8.0 Hz), 7.87 (1H, *dd*, *J* = 2.0 and 7.6 Hz), 8.09 (1H, *d*, *J* = 8.4 Hz); ^{13}C--NMR (100 MHz, $CDCl_3$, δ / ppm): 50.9, 53.3, 55.4, 113.9, 123.9, 125.5, 125.7, 126.1, 126.2, 127.9, 128.8, 129.5, 132.0, 132.6, 134.0, 136.1, 158.8; HRMS (ESI) Calcd. for $C_{19}H_{20}NO$: 278.1545 $[M+H]^+$. Found: 278.1553. *Hydrochloride*: colorless solid, m.p. 191–192 °C (ethanol); ^{1}H-NMR (400 MHz, DMSO-d_6, δ / ppm): 3.78 (3H, *s*), 4.24 (2H, *s*), 4.56 (2H, *s*), 7.00 (2H, *d*, *J* = 8.8 Hz), 7.51–7.65 (5H, *m*), 7.79 (1H, *d*, *J* = 7.2 Hz), 7.95–8.10 (3H, *m*), 9.89 (2H, *br s*); ^{13}C-NMR (100 MHz, DMSO-d_6, δ / ppm): 45.8, 49.7, 55.2, 113.9, 123.6, 123.7, 125.3, 126.2, 126.7, 128.1, 128.6, 129.1, 129.5, 131.1, 132.0, 133.2, 159.7.

1-(2-Chlorobenzyl)-N-*(naphthalen-1-yl)methylamine* (***2b***). Yellowish oil. Yield: 5.48 g, 97 %; R_f 0.24 (hexane–ethyl acetate 9:1 v/v); Anal. Calcd. for $C_{18}H_{16}ClN$: C, 76.72; H 5.72; N, 4.97 %. Found: C, 76.49, H, 5.53, N, 5.15 %; ^{1}H-NMR (400 MHz, $CDCl_3$, δ / ppm): 4.04 (2H, *s*), 4.27 (2H, *s*), 7.20–7.30 (2H, *m*), 7.37–7.56 (6H, *m*), 7.79 (1H, *d*, *J* = 8.0 Hz), 7.88 (1H, *dd*, *J* = 1.6 and 8.4

Hz), 8.12 (1H, *dd*, *J* = 1.2 and 8.0 Hz); ^{13}C-NMR (100 MHz, $CDCl_3$, δ / ppm): 51.0, 51.4, 123.9, 125.5, 125.7, 126.2, 126.3, 126.9, 128.0, 128.5, 128.8, 129.7, 130.5, 132.0, 134.0, 135.8, 137.7; HRMS (ESI) Calcd. for $C_{18}H_{17}ClN$: 282.1050 $[M+H]^+$. Found: 282.1055. *Hydrochloride*: colorless solid, m.p. 173–174 °C (ethanol); ^{1}H-NMR (400 MHz, DMSO-d_6, δ / ppm): 4.41 (2H, *s*), 4.74 (2H, *s*), 7.39–7.48 (2H, *m*), 7.49–7.67 (4H, *m*), 7.83–7.90 (2H, *m*), 8.02 (2H, *d*, *J* = 7.6 Hz), 8.19 (1H, *d*, *J* = 8.0 Hz), 10.02 (2H, *br s*); ^{13}C-NMR (100 MHz, DMSO-d_6, δ / ppm): 46.8, 47.0, 123.6, 125.3, 126.2, 126.8, 127.4, 127.7, 128.6, 129.4, 129.5, 129.6, 129.9, 130.7, 131.2, 132.0, 133.2, 133.6.

1-(2-Methylbenzyl)-N-*(naphthalen-1-yl)methylamine* (***2c***). Yellowish oil. Yield: 5.10 g, 97 %; R_f 0.29 (hexane–ethyl acetate 9:1 v/v); Anal. Calcd. for $C_{19}H_{19}N$: C, 87.31; H 7.33; N, 5.36 %. Found: C, 87.54, H, 7.14, N, 5.52 %; ^{1}H-NMR (400 MHz, $CDCl_3$, δ / ppm): 2.35 (3H, *s*), 3.92 (2H, *s*), 4.31 (2H, *s*), 7.17––7.23 (3H, *m*), 7.35–7.41 (1H, *m*), 7.42–7.56 (4H, *m*), 7.79 (1H, *d*, *J* = 8.0 Hz), 7.88 (1H, *dd*, *J* = 2.4 and 7.2 Hz), 8.13 (1H, *dd*, *J* = 2.4 and 7.2 Hz); ^{13}C-NMR (100 MHz, $CDCl_3$, δ / ppm): 19.1, 51.5, 51.7, 124.0, 125.5, 125.7, 126.0, 126.1, 126.2, 127.2, 127.9, 128.7, 128.8, 130.4, 132.1, 134.1, 136.1, 136.7, 138.4; HRMS (ESI) Calcd. for $C_{19}H_{20}N$: 262.1596 $[M+H]^+$. Found: 262.1590. *Hydrochloride*: colorless solid, m.p. 191–192 °C (ethanol); ^{1}H-NMR (400 MHz, DMSO-d_6, δ / ppm): 2.30 (3H, *s*), 4.26 (2H, *s*), 4.71 (2H, *s*), 7.21–7.33 (3H, *m*), 7.54–7.67 (4H, *m*), 7.88 (1H, *d*, *J* = 6.8 Hz), 7.99–8.05 (2H, *m*), 8.15–8.20 (1H, *m*), 9.90 (2H, *br s*); ^{13}C-NMR (100 MHz, DMSO-d_6, δ / ppm): 19.0, 46.5, 47.2, 123.6, 125.2, 125.9, 126.1, 126.7, 127.9, 128.6, 128.8, 129.3, 129.5, 130.4, 130.6, 131.2, 133.2, 137.5.

1-(2,4-Dichlorobenzyl)-N-*(naphthalen-1-yl)methylamine* (***2d***). Yellow solid. Yield: 5.98 g, 95 %; m.p. 69–70 °C; R_f 0.32 (hexane–ethyl acetate 9:1 v/v); Anal. Calcd. for $C_{18}H_{15}Cl_2N$: C, 68.37; H 4.78; N, 4.43 %. Found: C, 68.57, H, 4.61, N, 4.69 %; ^{1}H-NMR (400 MHz, $CDCl_3$, δ / ppm): 3.98 (2H, *s*), 4.25 (2H, *s*), 7.23 (1H, *dd*, *J* = 2.0 and 8.4 Hz), 7.38–7.55 (6H, *m*), 7.78 (1H, *d*, *J* = 8.0 Hz), 7.87 (1H, *dd*, *J* = 2.0 and 8.0 Hz), 8.10 (1H, *d*, *J* = 8.0 Hz); ^{13}C-NMR (100 MHz, $CDCl_3$, δ / ppm): 50.7, 51.1, 123.8, 125.5, 125.8, 126.2, 126.3, 127.2, 128.1, 128.9, 129.4, 131.1, 132.0, 133.4, 134.0, 134.6, 135.6, 136.5; HRMS (ESI) Calcd. for $C_{18}H_{16}Cl_2N$: 316.0660 $[M+H]^+$. Found: 316.0669. *Hydrochloride*: colorless solid, m.p. 224–225 °C (ethanol); ^{1}H-NMR (400 MHz, DMSO-d_6, δ / / ppm): 4.40 (2H, *s*), 4.74 (2H, *s*), 7.53 (1H, *dd*, *J* = 2.4 and 8.4 Hz), 7.55–7.67 (3H, *m*), 7.70 (1H, *d*, *J* = 2.4 Hz), 7.87 (1H, *d*, *J* = 7.2 Hz), 7.91 (1H, *d*, *J* = 8.4 Hz), 8.01 (2H, *d*, *J* = 8.0 Hz), 8.21 (1H, *d*, *J* = 8.4 Hz), 10.10 (2H, *br s*); ^{13}C--NMR (100 MHz, DMSO-d_6, δ / ppm): 46.5, 46.8, 123.6, 125.3, 126.2, 126.8, 127.5, 127.8, 128.6, 128.9, 129.1, 129.4, 129.6, 131.2, 133.2, 133.3, 134.4, 134.7.

1-(1,3-Benzodioxol-5-ylmethyl)-N-*(naphthalen-1-yl)methylamine (**2e**)*. Yellow oil. Yield: 5.52 g, 95 %; R_f 0.35 (hexane–ethyl acetate 3:1 v/v); Anal. Calcd. for $C_{19}H_{17}NO_2$: C, 78.33; H 5.88; N, 4.81 %. Found: C, 78.10, H, 6.06, N, 5.08 %; ^{1}H-NMR (400 MHz, $CDCl_3$, δ / ppm): 3.83 (2H, *s*), 4.23 (2H, *s*), 5.95 (2H, *s*), 6.76–6.86 (2H, *m*), 6.92 (1H, *s*), 7.39–7.56 (4H, *m*), 7.78 (1H, *d*, *J* = 8.0 Hz), 7.87 (1H, *dd*, *J* = 1.6 and 8.4 Hz), 8.11 (1H, *d*, *J* = 8.4 Hz); ^{13}C-NMR (100 MHz, $CDCl_3$, δ / ppm): 50.8, 53.6, 101.0, 108.2, 108.9, 121.4, 123.9, 125.5, 125.7, 126.2, 126.3, 127.9, 128.8, 132.0, 134.0, 134.5, 136.0, 146.7, 147.9; HRMS (ESI) Calcd. for $C_{19}H_{18}NO_2$: 292.1338 $[M+H]^+$. Found: 292.1331. *Hydrochloride*: colorless solid. m.p. 219–220 °C (ethanol); ^{1}H-NMR (400 MHz, DMSO-d_6, δ / ppm): 4.23 (2H, *s*), 4.55 (2H, *s*), 6.06 (2H, *s*), 6.98 (1H, *d*, *J* = 8.0 Hz), 7.12 (1H, *dd*, *J* = 1.6 and 8.0 Hz), 7.31 (1H, *d*, *J* = 1.6 Hz), 7.52–7.65 (3H, *m*), 7.79 (1H, *d*, *J* = 7.2 Hz), 7.96–8.03 (2H, *m*), 8.05–8.12 (1H, *m*), 9.87 (2H, *br s*); ^{13}C--NMR (100 MHz, DMSO-d_6, δ / ppm): 45.9, 50.1, 101.3, 108.3, 110.7, 123.6, 124.5, 125.3, 126.2, 126.7, 128.1, 128.7, 129.1, 129.5, 131.1, 133.2, 147.3, 147.7.

N-*(4-Bromobenzylidene)-2-(1*H-*indol-3-yl)ethanamine (**3a**)*. Colorless solid. Yield: 8.66 g, 88 %; m.p. 164–165 °C (ethyl acetate); Anal. Calcd. for $C_{17}H_{15}BrN_2$: C, 62.40; H 4.62; N, 8.56 %. Found: C, 62.30, H, 4.55, N, 8.64 %; ^{1}H-NMR (400 MHz, DMSO-d_6, δ / ppm): 3.03 (2H, *t*, *J* = 7.2 Hz), 3.86 (2H, *t*, *J* = 7.2 Hz), 6.96 (1H, *t*, *J* = 7.6 Hz), 7.06 (1H, *t*, *J* = 7.6 Hz), 7.14 (1H, *d*, *J* = 2.0 Hz), 7.33 (1H, *d*, *J* = 8.0 Hz), 7.56 (1H, *d*, *J* = 8.0 Hz), 7.63 (2H, *d*, *J* = 8.4 Hz), 7.67 (2H, *d*, *J* = 8.4 Hz), 8.26 (1H, *s*), 10.79 (1H, *s*); ^{13}C-NMR (100 MHz, DMSO-d_6, δ / ppm): 26.6, 61.4, 111.3, 112.2, 118.2, 118.5, 120.8, 122.8, 123.9, 127.3, 129.7, 131.7, 135.4, 136.2, 159.7; HRMS (ESI) Calcd. for $C_{17}H_{16}BrN_2$: 327.0497 $[M+H]^+$. Found: 327.0504.

N-*(3,4-Dimethoxybenzylidene)-2-(1*H-*indol-3-yl)ethanamine (**3b**)*. Cream--colored solid. Yield: 6.67 g, 72 %; m.p. 101–102 °C (ethyl acetate); Anal. Calcd. for $C_{19}H_{20}N_2O_2$: C, 74.00; H, 6.54; N, 9.08 %. Found: C, 73.88, H, 6.62, N, 9.01 %; ^{1}H-NMR (400 MHz, $CDCl_3$, δ / ppm): 3.17 (2H, *t*, *J* = 7.2 Hz), 3.91 (3H, *s*), 3.92 (3H, *s*), 3.93 (2H, *t*, *J* = 7.2 Hz), 6.86 (1H, *d*, *J* = 8.4 Hz), 7.00 (1H, *d*, *J* = = 2.4 Hz), 7.08–7.23 (3H, *m*), 7.35 (1H, *d*, *J* = 8.0 Hz), 7.44 (1H, *d*, *J* = 1.6 Hz), 7.68 (1H, *d*, *J* = 8.0 Hz), 8.10 (1H, *s*), 8.12 (1H, *br s*); ^{13}C-NMR (100 MHz, $CDCl_3$, δ / ppm): 27.2, 56.1, 62.1, 108.9, 110.6, 111.2, 114.3, 119.1, 119.3, 122.0, 122.2, 123.1, 127.7, 129.7, 136.4, 149.5, 151.4, 161.0; HRMS (ESI) Calcd. for $C_{19}H_{21}N_2O_2$: 309.1603 $[M+H]^+$. Found: 309.1595.

*2-(1*H-*Indol-3-yl)*-N-*(naphthalen-1-ylmethylene)ethanamine (**3c**)*. Cream-colored solid. Yield: 6.28 g, 70 %; m.p. 134–135 °C (lit.[2] m.p. 134–135 °C) (ethyl acetate); Anal. Calcd. for $C_{21}H_{18}N_2$: C, 84.53; H, 6.08; N, 9.39 %. Found: C, 84.41, H, 5.99, N, 9.47 %; ^{1}H-NMR (400 MHz, $CDCl_3$, δ / ppm): 3.28 (2H, *t*, *J* = = 7.0 Hz), 4.08 (2H, *t*, *J* = 7.0 Hz), 7.01 (1H, *d*, *J* = 2.0 Hz), 7.13–7.25 (2H, *m*),

7.36 (1H, *d*, *J* = 8.0 Hz), 7.48–7.58 (3H, *m*), 7.74 (1H, *d*, *J* = 8.0 Hz), 7.85–7.93 (3H, *m*), 7.99 (1H, *br s*), 8.59–8.65 (1H, *m*), 8.77 (1H, *s*); ^{13}C-NMR (100 MHz, $CDCl_3$, δ / ppm): 27.0, 62.8, 111.2, 114.0, 119.1, 119.4, 122.0, 122.5, 124.3, 125.4, 126.1, 127.0, 127.6, 128.2, 128.7, 130.9, 131.4, 132.0, 133.9, 136.4, 161.0; HRMS (ESI) Calcd. for $C_{21}H_{19}N_2$: 299.1548 $[M+H]^+$. Found: 299.1557.

*2-(1*H*-Indol-3-yl)*-N-*(2-thienylmethylene)ethanamine* ***(3d)***. Cream-colored solid. Yield: 5.20 g, 68 %; mp 127–128 °C (lit.[3] 133–134 °C) (ethyl acetate); Anal. Calcd. for $C_{15}H_{14}N_2S$: C, 70.83; H, 5.55; N, 11.01 %. Found: C, 70.98, H, 5.43, N, 10.93 %; ^{1}H-NMR (400 MHz, $CDCl_3$, δ / ppm): 3.16 (2H, *t*, *J* = 7.2 Hz), 3.90 (2H, *t*, *J* = 7.2 Hz), 7.00 (1H, *d*, *J* = 2.0 Hz), 7.05 (1H, *dd*, *J* = 3.6 and 5.2 Hz), 7.10–7.25 (3H, *m*), 7.35 (1H, *d*, *J* = 8.0 Hz), 7.39 (1H, *d*, *J* = 5.2 Hz), 7.67 (1H, *d*, *J* = 7.6 Hz), 8.03 (1H, *br s*), 8.22 (1H, *s*); ^{13}C-NMR (100 MHz, $CDCl_3$, δ / ppm): 26.9, 61.8, 111.2, 114.0, 119.1, 119.3, 122.0, 122.4, 127.4, 127.6, 128.8, 130.4, 136.3, 142.6, 154.8; HRMS (ESI) Calcd. for $C_{15}H_{15}N_2S$: 255.0956 $[M+H]^+$. Found: 255.0948.

N-*(4-Bromobenzyl)-2-(1*H*-indol-3-yl)ethanamine* ***(4a)***. Colorless solid. Yield: 6.33 g, 96%; m.p. 80–81 °C (lit.[4] 78–80 °C); Anal. Calcd. for $C_{17}H_{17}BrN_2$: C, 62.02; H, 5.20; N, 8.51 %. Found: C, 61.78, H, 5.38, N, 8.70 %; ^{1}H-NMR (400 MHz, $CDCl_3$, δ / ppm): 2.94–3.05 (4H, *m*), 3.76 (2H, *s*), 7.01 (1H, *d*, *J* = 2.4 Hz), 7.10–7.24 (4H, *m*), 7.33–7.37 (1H, *m*), 7.41 (2H, *d*, *J* = 8.4 Hz), 7.62 (1H, *d*, *J* = = 8.0 Hz), 8.09 (1H, *br s*); ^{13}C-NMR (100 MHz, $CDCl_3$, δ / ppm): 25.9, 49.5, 53.3, 111.3, 114.1, 119.0, 119.5, 120.7, 122.0, 122.2, 127.6, 129.9, 131.5, 136.6, 139.6; HRMS (ESI) Calcd. for $C_{17}H_{18}BrN_2$: 329.0653 $[M+H]^+$. Found: 329.0664.

N-*(3,4-Dimethoxybenzyl)-2-(1*H*-indol-3-yl)ethanamine* ***(4b)***. Light yellow oil. Yield: 5.88 g, 95 %; R_f 0.22 (ethyl acetate–methanol 4:1 v/v); Anal. Calcd. for $C_{19}H_{22}N_2O_2$: C, 73.52; H, 7.14; N, 9.03 %. Found: C, 73.32, H, 7.02, N, 8.86 %; ^{1}H-NMR (400 MHz, $CDCl_3$, δ / ppm): 2.95–3.04 (4H, *m*), 3.76 (2H, *s*), 3.82 (3H, *s*), 3.86 (3H, *s*), 6.77–6.84 (3H, *m*), 7.03 (1H, *d*, *J* = 2.0 Hz), 7.08–7.14 (1H, *m*), 7.16–7.22 (1H, *m*), 7.36 (1H, *d*, *J* = 8.0 Hz), 7.62 (1H, *d*, *J* = 8.0 Hz), 7.98 (1H, *br s*); ^{13}C-NMR (100 MHz, $CDCl_3$, δ / ppm): 25.9, 49.4, 53.8, 55.9, 56.0, 111.2, 111.3, 111.4, 114.0, 119.0, 119.3, 120.3, 122.1, 127.6, 133.2, 136.5, 148.1, 149.1; HRMS (ESI) Calcd. for $C_{19}H_{23}N_2O_2$: 311.1760 $[M+H]^+$. Found: 311.1766. *Hydrochloride*: colorless solid. m.p. 252–254 °C; ^{1}H-NMR (400 MHz, DMSO-d_6, δ / ppm): 3.04–3.19 (4H, *m*), 3.75 (3H, *s*), 3.78 (3H, *s*), 4.10 (2H, *s*), 6.93–7.02 (2H, *m*), 7.04–7.11 (2H, *m*), 7.21 (1H, *d*, *J* = 2.4 Hz), 7.34– –7.39 (2H, *m*), 7.57 (1H, *d*, *J* = 7.6 Hz), 9.56 (2H, *br s*); ^{13}C-NMR (100 MHz, DMSO-d_6, δ / ppm): 21.5, 46.4, 49.6, 55.5, 55.6, 109.4, 111.4, 111.6, 113.9, 118.1, 118.3, 121.1, 122.6, 123.1, 124.2, 126.7, 136.2, 148.6, 149.1.

*2-(1*H*-Indol-3-yl)*-N-*(naphthalen-1-ylmethyl)ethanamine* ***(4c)***. Light yellow oil. Yield: 5.75 g, 96 %; R_f 0.31 (ethyl acetate); Anal. Calcd. for $C_{21}H_{20}N_2$: C, 83.96; H, 6.71; N, 9.33 %. Found: C, 84.20, H, 6.87, N, 9.14 %; ^{1}H-NMR (400

MHz, $CDCl_3$, δ / ppm): 3.06 (2H, *t*, *J* = 6.8 Hz), 3.14 (2H, *t*, *J* = 6.8 Hz), 4.27 (2H, *s*), 6.96 (1H, *d*, *J* = 2.0 Hz), 7.11–7.25 (2H, *m*), 7.34 (1H, *d*, *J* = 8.0 Hz), 7.37–7.51 (4H, *m*), 7.66 (1H, *dd*, *J* = 0.8 and 8.0 Hz), 7.76 (1H, *d*, *J* = 8.0 Hz), 7.86 (1H, *dd*, *J* = 2.4 and 7.2 Hz), 8.02 (1H, *dd*, *J* = 1.6 and 8.0 Hz), 8.08 (1H, *br s*); ^{13}C-NMR (100 MHz, $CDCl_3$, δ / ppm): 25.9, 50.0, 51.6, 111.3, 114.1, 119.0, 119.4, 122.1 (2×), 123.7, 125.5, 125.7, 126.0, 126.1, 127.6, 127.8, 128.8, 131.9, 133.9, 136.1, 136.5; HRMS (ESI) Calcd. for $C_{21}H_{18}N_2$: 301.1705 $[M+H]^+$. Found: 301.1694. *Hydrochloride*: colorless solid. m.p. 234–235 °C (methanol); ^{1}H-NMR (400 MHz, DMSO-d_6, δ / ppm): 3.18–3.38 (4H, *m*), 4.70 (2H, *s*), 6.97––7.15 (2H, *m*), 7.23 (1H, *d*, *J* = 2.4 Hz), 7.38 (1H, *d*, *J* = 8.0 Hz), 7.53–7.70 (4H, *m*), 7.87 (1H, *d*, *J* = 6.8 Hz), 8.01 (2H, *d*, *J* = 7.6 Hz), 8.28 (1H, *d*, *J* = 8.4 Hz), 9.69 (2H, *br s*); ^{13}C-NMR (100 MHz, DMSO-d_6, δ / ppm): 21.6, 46.6, 47.6, 109.5, 111.5, 118.2, 118.3, 121.1, 123.1, 123.7, 125.2, 126.1, 126.7, 126.8, 128.2, 128.5, 128.9, 129.4, 131.0, 133.2, 136.2.

*2-(1*H*-Indol-3-yl)*-N-*(2-thienylmethyl)ethanamine (**4d**)*. Colorless solid. Yield: 4.99 g, 97 %; m.p. 63–64 °C; Anal. Calcd. for $C_{15}H_{16}N_2S$: C, 70.27; H, 6.29; N, 10.93 %. Found: C, 70.05, H, 6.48, N, 11.11 %; ^{1}H-NMR (400 MHz, $CDCl_3$, δ / / ppm): 2.98–3.08 (4H, *m*), 4.03 (2H, *s*), 6.88–6.93 (1H, *m*), 6.94 (1H, *dd*, *J* = 3.6 and 5.2 Hz), 7.02 (1H, *d*, *J* = 2.0 Hz), 7.10–7.25 (3H, *m*), 7.35 (1H, *d*, *J* = 8.4 Hz), 7.63 (1H, *d*, *J* = 8.0 Hz), 8.11 (1H, *br s*); ^{13}C-NMR (100 MHz, $CDCl_3$, δ / / ppm): 25.8, 48.5, 49.3, 111.3, 114.0, 119.0, 119.4, 122.1, 122.2, 124.4, 124.9, 126.7, 127.6, 136.5, 144.3; HRMS (ESI) Calcd. for $C_{15}H_{17}N_2S$: 257.1112 $[M+H]^+$. Found: 257.1120.

1-(4-Bromobenzyl)-N-*(pyridin-3-yl)methylamine (**5a**)*. Yellowish oil. Yield: 7.15 g, 86 %; R_f 0.39 (ethyl acetate–methanol 6:1 v/v); Anal. Calcd. for $C_{13}H_{13}BrN_2$: C, 56.34; H, 4.73; N, 10.11 %. Found: C, 56.56, H, 4.57, N, 9.92 %; ^{1}H-NMR (400 MHz, $CDCl_3$, δ / ppm): 3.76 (2H, *s*), 3.79 (2H, *s*), 7.18–7.29 (3H, *m*), 7.45 (2H, *d*, *J* = 8.0 Hz), 7.68 (1H, *d*, *J* = 7.6 Hz), 8.50 (1H, *dd*, *J* = 1.2 and 4.8 Hz), 8.56 (1H, *d*, *J* = 1.6 Hz); ^{13}C-NMR (100 MHz, $CDCl_3$, δ / ppm): 50.5, 52.6, 121.0, 123.6, 129.9, 131.7, 135.5, 135.9, 139.1, 148.735, 149.9; HRMS (ESI) Calcd. for $C_{13}H_{14}BrN_2$: 277.0340 $[M+H]^+$. Found: 277.0331. *Dihydrochloride*: colorless solid, m.p. 201–202 °C (ethanol); ^{1}H-NMR (400 MHz, CD_3OD, δ / ppm): 4.41 (2H, *s*), 4.63 (2H, *s*), 7.54–7.60 (2H, *m*), 7.61–7.67 (2H, *m*), 8.17–8.24 (1H, *m*), 8.88–8.94 (1H, *m*), 8.98 (1H, *d*, *J* = 5.6 Hz), 9.20 (1H, *d*, *J* = 2.0 Hz); ^{13}C-NMR (100 MHz, CD_3OD, δ / ppm): 48.3, 52.1, 125.1, 128.9, 131.3, 133.3, 133.4, 133.5, 143.7, 144.8, 149.9.

1-(4-Methoxybenzyl)-N-*(pyridin-3-yl)methylamine (**5b**)*. Yellow oil. Yield: 5.60 g, 82 %; R_f 0.33 (ethyl acetate–methanol 6:1 v/v); Anal. Calcd. for $C_{14}H_{16}N_2O$: C, 73.66; H, 7.06; N, 12.27 %. Found: C, 73.89, H, 6.88, N, 12.09 %; ^{1}H-NMR (400 MHz, $CDCl_3$, δ / ppm): 3.73 (2H, *s*), 3.79 (5H, *br s*), 6.86 (2H, *d*, *J* = 8.8 Hz), 7.21–7.28 (3H, *m*), 7.68 (1H, *d*, *J* = 7.6 Hz), 8.48 (1H, *dd*, *J* = 1.6

and 4.8 Hz), 8.55 (1H, *d*, *J* = 2.0 Hz); ^{13}C-NMR (100 MHz, $CDCl_3$, δ / ppm): 50.5, 52.7, 55.4, 114.0, 123.5, 129.4, 132.2, 135.8, 135.9, 148.5, 149.9, 158.9; HRMS (ESI) Calcd. for $C_{14}H_{17}N_2O$: 229.1341 $[M+H]^+$. Found: 229.1349. *Dihydrochloride*: colorless solid. m.p. 204–205 °C (ethanol); ^{1}H-NMR (400 MHz, DMSO-d_6, δ / ppm): 3.75 (3H, *s*), 4.14 (2H, *s*), 4.38 (2H, *s*), 6.95 (2H, *d*, *J* = 8.4 Hz), 7.54 (2H, *d*, *J* = 8.4 Hz), 8.06 (1H, *dd*, *J* = 5.6 and 8.0 Hz), 8.80 (1H, *d*, *J* = 8.0 Hz), 8.91 (1H, *dd*, *J* = 1.2 and 5.6 Hz), 9.13 (1H, *d*, *J* = 1.2 Hz), 10.32 (2H, *br s*); ^{13}C-NMR (100 MHz, DMSO-d_6, δ / ppm): 46.1, 49.6, 55.2, 113.9, 123.6, 126.4, 131.8, 131.9, 142.3, 144.1, 147.0, 159.7.

1-(4-Biphenylyl)-N-*(pyridin-3-yl)methylamine (**5c**)*. Yellow oil. Yield 7.51 g, 91 %; R_f 0.66 (ethyl acetate–methanol 6:1 v/v); Anal. Calcd. for $C_{19}H_{18}N_2$: C, 83.18; H, 6.61; N, 10.21 %. Found: C, 83.41, H, 6.42, N, 10.40 %; ^{1}H-NMR (400 MHz, $CDCl_3$, δ / ppm): 3.85 (2H, *s*), 3.86 (2H, *s*), 7.24–7.29 (1H, *m*), 7.31–7.37 (1H, *m*), 7.39–7.47 (4H, *m*), 7.55–7.63 (4H, *m*), 7.70–7.75 (1H, *m*), 8.52 (1H, *dd*, *J* = 1.6 and 4.8 Hz), 8.60 (1H, *d*, *J* = 2.0 Hz); ^{13}C-NMR (100 MHz, $CDCl_3$, δ / / ppm): 50.6, 53.0, 123.5, 127.2, 127.3, 128.7, 128.9, 135.8, 135.9, 139.2, 140.3, 141.1, 148.7, 149.9; HRMS (ESI) Calcd. for $C_{19}H_{19}N_2$: 275.1548 $[M+H]^+$. Found: 275.1554. *Dihydrochloride*: colorless solid, m.p. 258–260 °C (methanol); ^{1}H-NMR (400 MHz, DMSO-d_6, δ / ppm): 4.26 (2H, *s*), 4.43 (2H, *s*), 7.35–7.41 (1H, *m*), 7.43–7.51 (2H, *m*), 7.65–7.75 (6H, *m*), 8.03 (1H, *dd*, *J* = 6.4 and 8.0 Hz), 8.77 (1H, *d*, *J* = 8.0 Hz), 8.91 (1H, *dd*, *J* = 1.2 and 5.6 Hz), 9.14 (1H, *d*, *J* = = 1.2 Hz), 10.41 (2H, *s*); ^{13}C-NMR (100 MHz, DMSO-d_6, δ / ppm): 46.4, 49.7, 126.2, 126.7, 126.8, 127.8, 129.0, 130.9, 131.1, 131.4, 139.4, 140.6, 142.9, 144.7, 146.3.

1-(Naphthalen-1-ylmethyl)-N-*(pyridin-3-yl)methylamine (**5d**)*. Orange oil. Yield: 4.78 g, 64 %; R_f 0.37 (ethyl acetate–methanol 6:1 v/v); Anal. Calcd. for $C_{17}H_{16}N_2$: C, 82.22; H, 6.49; N, 11.28 %. Found: C, 82.00, H, 6.68, N, 11.07 %; ^{1}H-NMR (400 MHz, $CDCl_3$, δ / ppm): 3.91 (2H, *s*), 4.25 (2H, *s*), 7.23–7.29 (1H, *m*), 7.39–7.56 (4H, *m*), 7.73 (1H, *d*, *J* = 8.0 Hz), 7.78 (1H, *d*, *J* = 8.0 Hz), 7.86 (1H, *dd*, *J* = 1.6 and 7.6 Hz), 8.10 (1H, *d*, *J* = 8.0 Hz), 8.52 (1H, *dd*, *J* = 1.6 and 4.8 Hz), 8.62 (1H, *d*, *J* = 1.6 Hz); ^{13}C-NMR (100 MHz, $CDCl_3$, δ / ppm): 51.1, 51.2, 123.5, 123.8, 125.5, 125.8, 126.2, 126.3, 128.1, 128.8, 131.9, 134.0, 135.5, 135.8, 136.0, 148.7, 149.9; HRMS (ESI) Calcd. for $C_{17}H_{17}N_2$: 249.1392 $[M+H]^+$. Found: 249.1401. *Dihydrochloride*: Colorless solid. m.p. 236–237 °C (methanol); ^{1}H-NMR (400 MHz, DMSO-d_6, δ / ppm): 4.61 (2H, *s*), 4.74 (2H, *s*), 7.52–7.67 (3H, *m*), 7.85 (1H, *d*, *J* = 6.8 Hz), 7.96–8.07 (3H, *m*), 8.27 (1H, *d*, *J* = = 8.4 Hz), 8.80 (1H, *d*, *J* = 8.0 Hz), 8.90 (1H, *d*, *J* = 5.6 Hz), 9.16 (1H, *s*), 10.22 (2H, *br s*); ^{13}C-NMR (100 MHz, DMSO-d_6, δ / ppm): 47.0, 47.1, 123.9, 125.4, 126.4, 126.9, 128.0, 128.7, 129.3, 129.7, 131.1, 131.5, 133.3, 142.8, 144.7, 146.8.

1-(Pyridin-3-ylmethyl)-N-*(2-thienyl)methylamine* (***5e***). Orange oil. Yield: 3.85 g, 63 %; R_f 0.34 (ethyl acetate–methanol 6:1 v/v); Anal. Calcd. for $C_{11}H_{12}N_2S$: C, 64.67; H, 5.92; N, 13.71 %. Found: C, 64.90, H, 6.14, N, 13.48 %; ^{1}H-NMR (400 MHz, $CDCl_3$, δ / ppm): 3.84 (2H, *s*), 4.00 (2H, *s*), 6.90–6.98 (2H, m), 7.20–7.29 (2H, *m*), 7.70 (1H, *d*, *J* = 7.6 Hz), 8.50 (1H *dd*, *J* = 1.6 and 4.8 Hz), 8.56 (1H, *d*, *J* = 2.0 Hz); ^{13}C-NMR (100 MHz, $CDCl_3$, δ / ppm): 47.7, 50.1, 123.5, 124.7, 125.2, 126.8, 135.4, 136.0, 143.8, 148.7, 149.9; HRMS (ESI) Calcd. for $C_{11}H_{13}N_2S$: 205.0799 $[M+H]^+$. Found: 205.0807. *Dihydrochloride*: colorless solid. m.p. 228–230 °C (dec) (ethanol); ^{1}H-NMR (400 MHz, CD_3OD, δ / / ppm): 4.63 (2H, *s*), 4.67 (2H, *s*), 7.12 (1H, *dd*, *J* = 3.6 and 5.2 Hz), 7.45 (1H, *d*, *J* = 3.2 Hz), 7.59 (1H, *dd*, *J* = 0.8 and 5.2 Hz), 8.21 (1H, *dd*, *J* = 6.0 and 8.0 Hz), 8.89 (1H, *d*, *J* = 8.0 Hz), 8.98 (1H, *d*, *J* = 6.0 Hz), 9.18 (1H, *d*, *J* = 0.8 Hz); ^{13}C--NMR (100 MHz, CD_3OD, δ / ppm): 46.6, 47.8, 128.8, 128.9, 129.8, 132.6, 132.7, 133.3, 143.7, 144.7, 149.9.

N-*Benzyl-3-(1*H-*imidazol-1-yl)propylamine* (***6a***). Flash column chromategraphy (silica gel, ethyl acetate–methanol 1:1 v/v) afforded a colorless oil. Yield: 1.46 g, 68 %; R_f 0.25 (ethyl acetate–methanol 1:1 v/v); Anal. Calcd. for $C_{13}H_{17}N_3$: C, 72.52; H, 7.96; N, 19.52 %. Found: C, 72.81, H, 8.28, N, 19.85 %; ^{1}H-NMR (400 MHz, $CDCl_3$, δ / ppm): 1.87–1.97 (2H, *m*), 2.61 (2H, *t*, *J* = 6.8 Hz), 3.75 (2H, *s*), 4.04 (2H, *t*, *J* = 6.8 Hz), 6.87 (1H, *t*, *J* = 1.2 Hz), 7.03 (1H, *s*), 7.22–7.36 (5H, *m*), 7.43 (1H, *s*); ^{13}C-NMR (100 MHz, $CDCl_3$, δ / ppm): 31.5, 44.7, 45.8, 54.1, 119.0, 127.2, 128.2, 128.6, 129.5, 137.3, 140.3. *Dihydrochloride*: hygroscopic colorless crystals. Yield: 56 %; m.p. 144–145 °C (2-propanol); ^{1}H-NMR (400 MHz, CD_3OD, δ / ppm): 2.32–2.43 (2H, *m*), 3.16 (2H, *t*, *J* = 7.6 Hz), 4.25 (2H, *s*), 4.44 (2H, *t*, *J* = 7.2 Hz), 7.43–7.50 (3H, *m*), 7.53–7.59 (2H, *m*), 7.62 (1H, *t*, *J* = 1.6 Hz), 7.75 (1H, *t*, *J* = 1.6 Hz), 9.09 (1H, *s*); ^{13}C-NMR (100 MHz, CD_3OD, δ / ppm): 27.9, 45.3, 47.5, 52.5, 121.4, 123.3, 130.3, 130.7, 131.1, 132.4, 136.7; HRMS (ESI) Calcd. for $C_{13}H_{18}N_3$: 216.1501 $[M+H]^+$.

*3-(1*H-*Imidazol-1-yl)*-N-*(1-naphthalenylmethyl)propylamine* (***6b***). Flash column chromatography (silica gel, ethyl acetate–methanol 3:1 v/v) afforded a yellowish oil. Yield: 1.35 g, 51 %; R_f 0.18 (ethyl acetate–methanol 3:1 v/v); Anal. Calcd. for $C_{17}H_{19}N_3$: C, 76.95; H, 7.22; N, 15.84 %. Found: C, 77.29, H, 6.91, N, 16.15 %; ^{1}H-NMR (400 MHz, $CDCl_3$, δ / ppm): 1.89–2.00 (2H, *m*), 2.71 (2H, *t*, *J* = 6.8 Hz), 4.03 (2H, *t*, *J* = 6.8 Hz), 4.21 (2H, *s*), 6.84 (1H, *s*), 7.03 (1H, *s*), 7.38–7.45 (3H, *m*), 7.47–7.58 (2H, *m*), 7.75–7.83 (1H, *m*), 7.88 (1H, *dd*, *J* = 1.6 and 8.4 Hz), 8.13 (1H, *d*, *J* = 8.4 Hz); ^{13}C-NMR (100 MHz, $CDCl_3$, δ / ppm): 31.5, 44.7, 46.2, 51.9, 118.9, 123.8, 125.4, 125.8, 126.2, 126.3, 128.0, 128.9, 129.4, 131.8, 134.0, 135.8, 137.3; HRMS (ESI) Calcd. for $C_{17}H_{20}N_3$: 266.1657 $[M+H]^+$. Found: 266.1665. *Dihydrochloride*: hygroscopic colorless crystals. Yield: 61 %, m.p. 153–154 °C (ethanol); ^{1}H-NMR (400 MHz, DMSO-d_6, δ / / ppm): 2.29–2.43 (2H, *m*), 3.07 (2H, *t*, *J* = 6.8 Hz), 4.42 (2H, *t*, *J* = 6.8 Hz), 4.63

(2H, *s*), 7.52–7.66 (3H, *m*), 7.72 (1H, *t*, *J* = 1.6 Hz), 7.84–7.90 (2H, *m*), 7.96––8.03 (2H, *m*), 8.24 (1H, *d*, *J* = 8.0 Hz), 9.32 (1H, *s*), 9.83 (2H, *br s*); ^{13}C-NMR (100 MHz, DMSO-d_6, δ / ppm): 25.8, 43.9, 45.8, 46.7, 119.9, 122.0, 123.8, 125.3, 126.2, 126.8, 128.1, 128.6, 128.9, 129.4, 131.0, 133.2, 135.4.

*3-(1*H*-Imidazol-1-yl)*-N-*(2-thienylmethyl)propylamine* ***(6c)***. Flash column chromatography (silica gel, ethyl acetate–methanol 3:1 v/v) afforded a colorless oil. Yield: 1.15 g, 52 %; R_f 0.17 (ethyl acetate–methanol 3:1 v/v); Anal. Calcd. for $C_{11}H_{15}N_3S$: C, 59.69; H, 6.83; N, 18.99 %. Found: C, 60.02, H, 6.51, N, 19.29 %; ^{1}H-NMR (400 MHz, $CDCl_3$, δ / ppm): 1.86–1.95 (2H, *m*), 2.62 (2H, *t*, *J* = 6.8 Hz), 3.94 (2H, *s*), 4.04 (2H, *t*, *J* = 6.8 Hz), 6.86–6.91 (2H, *m*), 6.93 (1H, *dd*, *J* = 3.6 and 4.8 Hz), 7.02 (1H, *t*, *J* = 1.2 Hz), 7.20 (1H, *dd*, *J* = 1.2 and 4.8 Hz), 7.43 (1H, *br s*); ^{13}C-NMR (100 MHz, $CDCl_3$, δ / ppm): 31.4, 44.7, 45.4, 48.4, 118.9, 124.6, 125.0, 126.8, 129.4, 137.3, 144.0; HRMS (ESI) Calcd. for $C_{11}H_{16}N_3S$: 222.1065 $[M+H]^+$. Found: 222.1057.

N-*(2,4-Dimethoxybenzyl)-3-(1*H*-imidazol-1-yl)propylamine* ***(6d)***. Flash column chromatography (silica gel, ethyl acetate–methanol 1:1 v/v) afforded a colorless oil. Yield: 1.43 g, 52 %; R_f 0.18 (ethyl acetate–methanol 1:1 v/v); Anal. Calcd. for $C_{15}H_{21}N_3O_2$: C, 65.43; H, 7.69; N, 15.26 %. Found: C, 65.68, H, 8.03, N, 15.55 %; ^{1}H-NMR (400 MHz, $CDCl_3$, δ / ppm): 1.86–1.95 (2H, *m*), 2.53 (2H, *t*, *J* = 6.8 Hz), 3.66 (2H, *s*), 3.78 (3H, *s*), 3.80 (3H, *s*), 4.01 (2H, *t*, *J* = 6.8 Hz), 6.38–6.49 (2H, *m*), 6.88 (1H, *s*), 7.02 (1H, *s*), 7.07 (1H, *d*, *J* = 8.0 Hz), 7.44 (1H, *s*); ^{13}C-NMR (100 MHz, $CDCl_3$, δ / ppm): 31.4, 44.8, 45.4, 48.9, 55.4, 55.5, 98.7, 103.8, 119.0, 120.7, 129.4, 130.5, 137.3, 158.7, 160.3; HRMS (ESI) Calcd. for $C_{15}H_{22}N_3O_2$: 276.1712 $[M+H]^+$. Found: 276.1720.

REFERENCES

1. M. Crespo, M. Font-Bardia, S. Perez, X. Solans, *J. Organomet. Chem.* **642** (2002) 171
2. B.-T. Ho, W. M. McIsaac, L. W. Tansey, K. E. Walker, *Can. J. Chem.* **45** (1967) 2963
3. Á. Szöllösy, T. Tischer, I. Kádas, L. Töke, G. Tóth, *Tetrahedron* **55** (1999) 7279
4. Á. Patthy-Lukáts, Á. Kocsis, L. F. Szabo, B. Podányi, *J. Nat. Prod.* **62** (1999) 1492.

Journal of the Serbian Chemical Society
JSCS-info@shd.org.rs • www.shd.org.rs/JSCS
J. Serb. Chem. Soc. *77* (2) 141–146 (2012)
JSCS–4256
UDC 547–304.6+547.53+547.78+542.913
Original scientific paper

The synthesis of some new hydrazone derivatives containing the benzothiazole moiety

AHMET ÖZDEMİR[1]*, GÜLHAN TURAN-ZITOUNI[1], ZAFER ASIM KAPLANCIKLI[1] and MEHLİKA DİLEK ALTINTOP[1]

[1]*Anadolu University, Faculty of Pharmacy, Department of Pharmaceutical Chemistry, 26470, Eskişehir, Turkey*

(Received 21 March, revised 2 June 2011)

Abstract: Hydrazones are an important class of compounds found in many synthetic products. Due to their importance in synthetic chemistry, the present article reports the synthesis of a new series of ten compounds based on the coupling of 2-oxo-3(2*H*)-benzothiazoleacetic acid, hydrazide and 2-thioxo-3(2*H*)--benzothiazoleacetic acid, hydrazide with different aldehydes. The structures of the synthesized compounds were confirmed by elemental analyses, IR, ^{1}H--NMR, ^{13}C-NMR and FAB^{+}–MS spectral data.

Keywords: hydrazone; 2-benzothiazolinone; 2-mercaptobenzothiazole; aromatic aldehydes.

INTRODUCTION

Hydrazone derivatives have attracted a great deal of interest in synthetic chemistry and considerable research on them in relation to their synthetic utility has been accomplished. Hydrazones are extensively studied as reactants or reaction intermediates since they can readily undergo various ring closure reactions.[1]

Among the benzothiazole derivatives, benzothiazol-2-ones and 2-mercaptobenzothiazoles have received considerable attention in organic chemistry associated with their importance in nucleophilic substitution reactions.[2] The present study also confirmed that the ease of nucleophilic substitution depends on the nucleophilicity.

All these observations gave encouragement to commence a research program for the synthesis of new hydrazone derivatives containing a heterocyclic moiety. After careful screening of various heteronuclei, benzothiazole was chosen as the focus of attention. In this respect, it should be noted that this heterocyclic scaffold still attracts the attention of material chemists, because of its use as a chemically and thermally stable electron-withdrawing moiety in push-pull systems

* Corresponding author. E-mail: ahmeto@anadolu.edu.tr
doi: 10.2298/JSC110321171O

with potential application in nonlinear optics.[3–6] Furthermore, various derivatives bearing the benzothiazole moiety display antimicrobial and anticancer activities.[7–9] It was therefore expected that the newly synthesized hydrazone derivatives bearing a benzothiazole moiety might be of potential interest or could serve as potential intermediates in medicinal chemistry. Herein, the synthesis of new hydrazone derivatives bearing a benzothiazole moiety is described.

RESULTS AND DISCUSSION

Chemistry

Among several synthetic routes to derivatives **1a**–**j**, it was decided to investigate the synthesis of acylhydrazine derivatives as key intermediates. This compound could be transformed to **1a**–**j** using classical functional group interconversion, *i.e.* $CONHNH_2 \rightarrow CONHN{=}CH{-}CH_2{-}O{-}Ar$. Finally, the new target compounds **1a**–**j** were obtained, in good yields (70–88 %), by condensing hydrazides (**n**,**o**) with the corresponding appropriate aldehydes in absolute ethanol, as illustrated in Table I and Scheme 1.

TABLE I. Some characteristics of the synthesized compounds

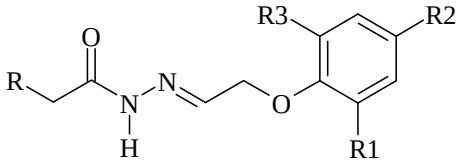

Compd.	Ar	R_1	R_2	R_3	Yield, %	Molecular formula	M.W., g mol^{-1}	M.p., °C
1a	**n**	H	CH_3	H	71	$C_{18}H_{17}N_3O_3S$	355.42	213–214
1b	**n**	H	$C(CH_3)_3$	H	88	$C_{21}H_{23}N_3O_3S$	397.50	209–211
1c	**n**	H	OCH_3	H	70	$C_{18}H_{17}N_3O_4S$	299.5	203–204
1d	**n**	CH_3	CH_3	H	77	$C_{19}H_{19}N_3O_3S$	369.45	218–220
1e	**n**	CH_3	H	CH_3	79	$C_{19}H_{19}N_3O_3S$	369.45	226–227
1f	**o**	H	CH_3	H	80	$C_{18}H_{17}N_3O_2S_2$	371.48	138–140
1g	**o**	H	$C(CH_3)_3$	H	78	$C_{21}H_{23}N_3O_2S_2$	413.56	142–144
1h	**o**	H	OCH_3	H	81	$C_{18}H_{17}N_3O_3S_2$	387.48	145–147
1i	**o**	CH_3	CH_3	H	79	$C_{19}H_{19}N_3O_2S_2$	385.51	136–137
1j	**o**	CH_3	H	CH_3	75	$C_{19}H_{19}N_3O_3S_2$	385.51	86–88

The nucleophilic substitution of 2(3*H*)-benzothiazolone shows an important difference when compared with that of 2-mercaptobenzothiazole. The enolizable character of the amide moiety allows several useful substitutions at the level of the *N* position of the 2(3*H*)-benzothiazolone under base-catalyzed conditions[10]. On the other hand, the nucleophilic reactivity of 2-mercaptobenzothiazole associated with the presence of nitrogen and sulfur atoms holding a pair of electrons on either side of the >C=S group increases the electron donating capacity of "S" to form a bond with a halogenated carbon atom.[11] The fact that the S-substituted

derivatives were the dominant species indicates that sulfur-containing anions are more stable and stronger nucleophiles due to d-orbital delocalization of sulfur compared to the nucleophilic properties of the nitrogen-containing anions.[2]

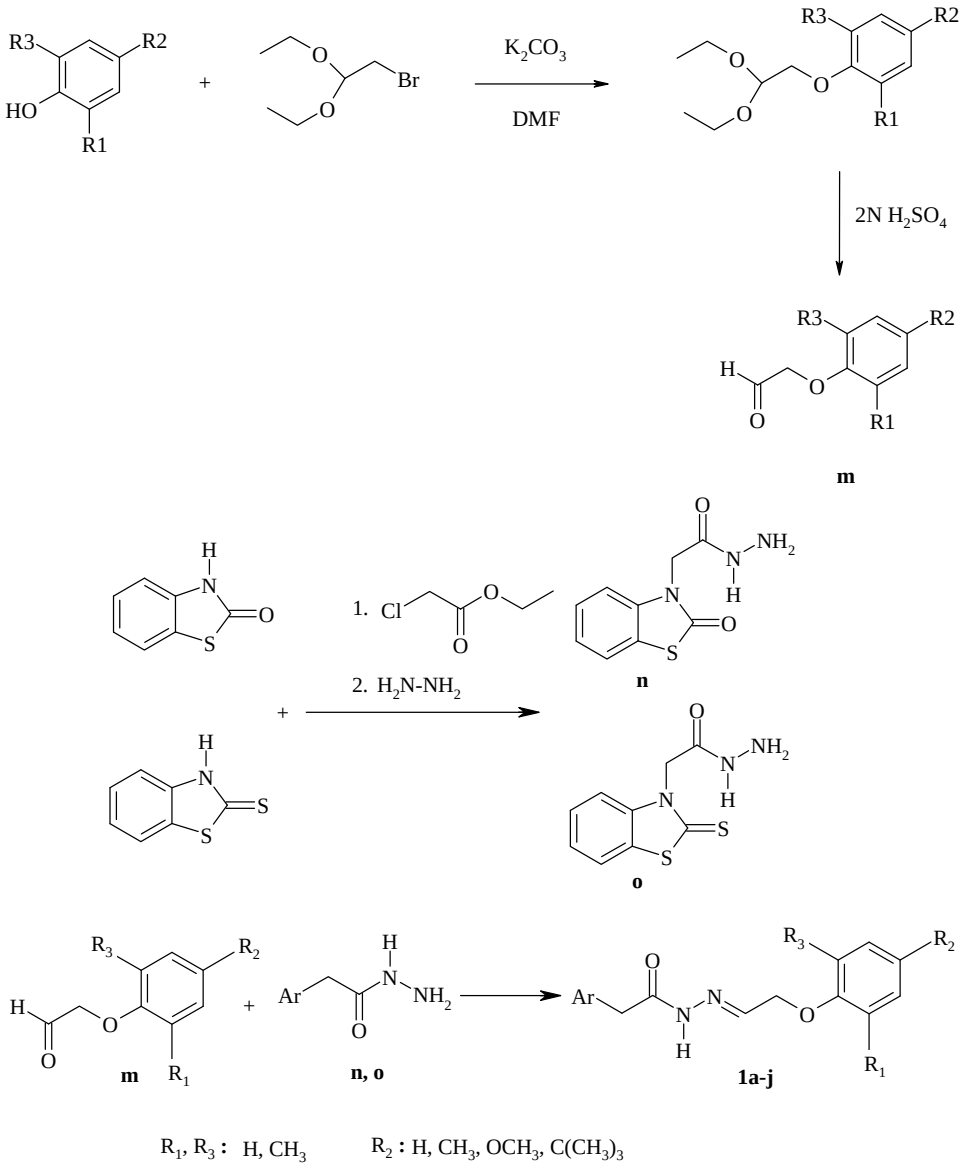

Scheme 1. The general synthetic reactions (see Table I for details of R, R_1 and R_2 of **1a**–**j**).

The purity of the synthesized compounds was checked by elemental analyses. The structures of the various synthesized compounds were determined based

on spectral data analysis, *i.e.*, IR, ^{1}H-NMR, ^{13}C-NMR and FAB^{+}-MS spectral data. These data are given in the Supplementary material to this paper.

The IR data provided functional group evidence for the formation of the expected structures. In the IR spectra, some significant stretching bands due to N–H, C=O, C=C and C=N were observed at 3339–3175 cm^{-1}, 1687–1680 cm^{-1} and 1610–1485 cm^{-1}, respectively. The IR spectra of the acid hydrazides **1a**–**e** showed a peak at 1680–1683 cm^{-1} due to the exocyclic carbonyl function derived from hydrazide structure, beside the endocyclic carbonyl peak (1770–1768 cm^{-1}) at position 2 of the 2(3*H*)-benzothiazolone ring.

According to the literature, hydrazones may exist as *E*/*Z* geometric isomers about the C=N double bonds and *cis*/*trans* amide conformers. In addition, hydrazones derived from aldehydes and substituted hydrazides are present in solution in the *E* form. It was reported that when hydrazones are dissolved in d_6-dimethyl sulfoxide solution, the *E* geometrical isomers of these compounds undergo a rapid *cis*/*trans* amide equilibrium, in which the *cis* conformer predominates.[12,13]

In the 400 MHz ^{1}H-NMR spectra of the compounds, the –O–CH_2–CO protons were observed as singlets at 4.55 and 4.87–4.90 ppm. The –O–C**H**$_2$–CH= protons appeared as multiplets at 4.63–4.72 ppm. The –N=CH– proton was observed as a triplet at 7.47–7.94 ppm. The –NH–N= proton was observed as two broad singlets at 11.41–11.47 ppm. All the other aliphatic and aromatic protons were observed within the expected regions.

The ^{1}H-NMR data were also consistent with the assigned structures. In the ^{1}H-NMR spectra of the compounds, paired peaks for each of the protons –O–C**H**$_2$–CH=, –N=CH– and –NH–N=, corresponding to the (*E*)- and (*Z*)-forms of the compounds, were observed. For each compound, the intensities of these paired peaks differed from others, due to the variable amounts of the (*E*)- and (*Z*)-isomers, which are usually unequal.

Additional support for the structures of the synthesized compounds was provided by their ^{13}C-NMR spectra, in which chemical shift values of the carbon atoms at around 164.56–164.64 ppm (hydrazide C=O), and 142.61–142.99 ppm (imine N=CH) corroborated the hydrazide character deduced from the ^{1}H-NMR data. The mass spectra of compounds showed [M+1] peaks in agreement with their molecular formula.

EXPERIMENTAL

All chemicals were obtained from Aldrich (Steinheim, Germany). All melting points (m.p.) were determined in open capillaries on a Gallenkamp apparatus (Weiss-Gallenkamp, Loughborough, UK) and are uncorrected. The purity of the compounds was routinely checked by thin layer chromatography (TLC) using silica gel 60G (Merck, Darmstadt, Germany). Elemental analyses were performed on a Perkin Elmer EAL 240 elemental analyzer. Spectroscopic data were recorded using the following instruments: ^{1}H-NMR, a Bruker 400 MHz spectrometer; ^{13}C-NMR, a Bruker 100 MHz spectrometer (Bruker, Billerica, Massachusetts,

USA) and MS-FAB, a VG Quattro Mass spectrometer (Agilent, Minnesota, USA). The NMR spectra were recorded in DMSO-d_6 using TMS as an internal standard.

General procedure for the synthesis of the compounds

*Synthesis of substituted phenoxyacetaldehyde (**m**).* These compounds used in the syntheses were prepared according to methods reported in the literature.[14,15]

*Synthesis of 2-oxo-3(2*H*)-benzothiazoleacetic acid, hydrazide (**n**).* This compound was prepared according to the literature, by reacting 2-oxo-3(2*H*)-benzothiazoleacetic acid, ethyl ester with hydrazine hydrate.[16,17]

*Synthesis of 2-thioxo-3(2*H*)-benzothiazoleacetic acid, hydrazide (**o**).* This compound was prepared in accordance with a previously described method, by reacting 2-thioxo-3(2H)-benzothiazoleacetic acid, ethyl ester with hydrazine hydrate.[16,17]

*Synthesis of the 2-phenoxyethylidene hydrazide derivatives (**1a–j**).* Equimolar quantities of acetylhydrazines (30 mmol) and an appropriate aldehyde in 25 ml of absolute ethanol were refluxed for 10–12 h. The reaction mixture was then cooled and the solid precipitated was recrystallized from an appropriate solvent. Some characteristics of the synthesized compounds are given in Table I.

CONCLUSIONS

In the present work, appropriate aldehyde derivatives were synthesized *via* the treatment of the compounds bearing an acetal group with sulfuric acid, which catalyzes the hydrolysis of acetals affording aldehydes proning to nucleophilic addition reactions. Hydrazone derivatives were obtained by reaction of the aldehyde derivatives with appropriate hydrazides.

SUPPLEMENTARY MATERIAL

Characteristics and spectral data of synthesized compounds are available electronically from http://www.shd.org.rs/JSCS/, or from the corresponding author on request.

ИЗВОД

СИНТЕЗА НОВИХ ХИДРАЗОНСКИХ ДЕРИВАТА КОЈИ САДРЖЕ БЕНЗОТИАЗОЛСКУ СТРУКТУРУ

AHMET ÖZDEMIR[1], GÜLHAN TURAN-ZITOUNI[1], ZAFER ASIM KAPLANCIKLI[1] и MEHLIKA DILEK ALTINTOP[1]

[1]*Anadolu University, Faculty of Pharmacy, Department of Pharmaceutical Chemistry, 26470, Eskişehir, Turkey*

Хидразони су важна класа једињења која се садржи у многим синтетичким производима. Због њихове важности у синтетској хемији, у овом раду је приказана синтеза нове серије од десет једињења. Синтеза се заснива на купловању хидразида 2-оксо-3(2*H*)-бензотиазолсирћетне киселине и хидразида 2-тиоксо-3(2*H*)-бензотиазолсирћетне киселине са различитим алдехидима. Структуре синтетисаних једињења одређене су на основу елементалне анализе, IC, ^{1}H-NMR, ^{13}C-NMR и FAB$^+$-MS спектроскопских података.

(Примљено 21. марта, ревидирано 2. јуна 2011)

REFERENCES

1. S. Rollas, Ş. G. Küçükgüzel, *Molecules* **12** (2007) 1910
2. J. H. Lee, S. H. Park, H. Lee, *Bull. Korean Chem. Soc.* **28** (2007) 1211

3. P. Hrobarik, I. Sigmundova, P. Zahradnik, P. Kasak, V. Arion, E. Franz, K. Clays, *J. Phys. Chem., C* **114** (2010) 22289
4. P. Hrobarik, P. Zahradnik, W. M. F. Fabian, *Phys. Chem. Chem. Phys.* **6** (2004) 495
5. V. Hrobarikova, P. Hrobarik, P. Gajdos, I. Fitilis, M. Fakis, P. Persephonis, P. Zahradnik, *J. Org. Chem.* **75** (2010) 3053
6. P. Hrobarik, I. Sigmundova, P. Zahradnik, *Synthesis* **4** (2005) 600
7. M. Zajac, P. Hrobarik, P. Magdolen, P. Foltinova, P. Zahradnik, *Tetrahedron* **64** (2008) 10605
8. L. Racane, V. Tralic-Kulenovic, S. K. Pavelic, I. Ratkaj, P. Peixoto, R. Nhili, S. Depauw, M. P. Hildebrand, M. H. David-Cordonnier, K. Pavelic, G. Karminski-Zamola, *J. Med. Chem.* **6** (2010) 2418
9. S. Saeed, N. Rashid, P. G. Jones, M. Ali, R. Hussain, *Eur. J. Med. Chem.* **45** (2010) 1323
10. J. Poupaert, P. Carato, E. Colacino, *Curr. Med. Chem.* **12** (2005) 877
11. S. R. Reddy, P. Kalyani, B. R. Rao, P. Manikyamba, *Indian J. Chem., A* **47** (2008) 236
12. G. Palla, G. Predieri, P. Domiano, *Tetrahedron* **42** (1986) 3649
13. E. Wyrzykiewicz, D. Prukała, *J. Heterocycl. Chem.* **35** (1998) 381
14. M. Ansar, S. Al Akoum Ebriki, R. Mouhoub, P. Berthelot, C. Vaccher, M. P. Vaccher, N. Flouquet, D. H. Caignard, P. Renard, B. Pirard, M. C. Rettori, G. Evrard, F. Durant, M. Debaert, *Eur. J. Med. Chem.* **31** (1996) 449
15. A. Alves, P. Fulcrand, G. Berge, A. M. Noelartis, J. Castel, H. Orzalesi, *Eur. J. Med. Chem.* **21** (1986) 297
16. H. L. Yale, K. Losee, J. Martins, M. Holsing, M. F. Perry, J. Bernstein, *J. Am. Chem. Soc.* **75** (1953) 1933
17. G. Turan-Zitouni, Z. A. Kaplancikli, K. Güven, *Farmaco* **52** (1997) 631.

Journal of the Serbian Chemical Society
JSCS@tmf.bg.ac.rs • www.shd.org.rs/JSCS
J. Serb. Chem. Soc. 77 (2) S45–S47 (2012) *Supplementary material*

SUPPLEMENTARY MATERIAL TO

The synthesis of some new hydrazone derivatives containing the benzothiazole moiety

AHMET ÖZDEMİR[1]*, GÜLHAN TURAN-ZITOUNI[1], ZAFER ASIM KAPLANCIKLI[1] and MEHLİKA DİLEK ALTINTOP[1]

[1]*Anadolu University, Faculty of Pharmacy, Department of Pharmaceutical Chemistry, 26470, Eskişehir, Turkey*

J. Serb. Chem. Soc. 77 (2) (2012) 141–146

CHARACTERISTICS AND SPECTRAL DATA OF THE SYNTHESIZED COMPOUNDS

*2-Oxo-3(2*H*)-benzothiazoleacetic acid, [2-(4-methylphenoxy)ethylidene]hydrazide (**1a**).* Yield 71 %; m.p. 213–214 °C; Anal. Calcd. for $C_{18}H_{17}N_3O_3S$: C, 60.83; H, 4.82; N, 11.82 %. Found: C, 60.70; H, 4.79; N, 11.74 %; IR (KBr, cm^{-1}): 3195, 1770, 1682, 1525, 1490; ^{1}H-NMR (400 MHz, DMSO-d_6, δ / ppm): 2.25 (3H, *s*), 4.63–4.70 (2H, *m*), 4.73 and 5.02 (2H, *s*), 6.86–6.95 (2H, *m*), 7.07–7.15 (2H, *m*), 7.17–7.27 (2H, *m*), 7.30–7.38 (1H, *m*), 7.55–7.61 (1H, *t*, J = 5.0 Hz), 7.64–7.68 (1H, *m*), 11.73 (1H, *m*); ^{13}C-NMR (100 MHz, DMSO-d_6 / δ ppm): 20.05 (CH_3), 43.23 (CH_2), 66.72 (CH_2), 111.40 (CH), 114.53 (2CH), 121.09, 122.73 (CH), 123.12 (CH), 126.51 (CH), 129.79, 129.89 (2CH), 137.22, 143.40 (CH), 155.75, 167.18, 162.66; MS-FAB$^+$ (*m*/*z*): 356 (M+1).

*2-Oxo-3(2*H*)-benzothiazoleacetic acid, [2-(4-*tert*-butylphenoxy)ethylidene]hydrazide (**1b**).* Yield 88 %; m.p. 209–211 °C; Anal. Calcd. for $C_{21}H_{23}N_3O_3S$: C, 63.46; H, 5.83; N, 10.57 %. Found: C, 63.79; H, 5.72; N, 10.64 %; IR (KBr, cm^{-1}): 3181, 1769, 1681, 1545, 1510; ^{1}H-NMR (400 MHz, DMSO-d_6, δ / ppm): 1.25 (9H, *s*), 4.70–4.74 (2H, *m*), 4.76 and 5.06 (2H, *s*), 6.90–6.97 (2H, *m*), 7.17––7.40 (5H, *m*), 7.56–7.63 (1H, *t*, J = 5.0 Hz), 7.64–7.68 (1H, *m*), 11.74–11.79 (1H, *m*); ^{13}C-NMR (100 MHz, DMSO-d_6, δ / ppm): 31.28 (3CH_3), 33.75, 43.25 (CH_2), 66.68 (CH_2), 111.40 (CH), 114.17 (2CH), 121.11, 122.72 (CH), 123.12 (CH), 126.15 (2CH), 126.50 (CH), 137.22, 143.26, 143.45 (CH), 155.60, 167.16, 162.65; MS-FAB$^+$ (*m*/*z*): 398 (M+1).

*2-Oxo-3(2*H*)-benzothiazoleacetic acid, [2-(4-methoxyphenoxy)ethylidene]hydrazide (**1c**).* Yield 70 %; m.p. 203-204 °C; Anal. Calcd. for $C_{18}H_{17}N_3O_4S$: C, 58.21; H, 4.61; N, 11.31 %. Found: C, 58.33; H, 4.70; N, 11.38 %; IR (KBr, cm^{-1}):

* Corresponding author. E-mail: ahmeto@anadolu.edu.tr

3175, 1770, 1683, 1602, 1500; ^{1}H-NMR (400 MHz, DMSO-d_6, δ / ppm): 3.70 (3H, *s*), 4.62–4.69 (2H, *m*), 4.73 and 5.02 (2H, *s*), 6.86–7.00 (4H, *m*), 7.17–7.27 (2H, *m*), 7.30–7.38 (1H, *m*), 7.54–7.72 (2H, *m*), 11.75–11.78 (1H, *bs*); ^{13}C-NMR (100 MHz, DMSO-d_6, δ / ppm): 43.24 (CH_2), 55.32 (CH_3), 67.25 (CH_2), 111.40 (CH), 114.63 (2CH), 115.70 (2CH), 121.08, 122.74 (CH), 123.13 (CH), 126.51 (CH), 137.22, 143.54 (CH), 151.83, 153.72, 167.18, 162.65; MS-FAB$^+$ (*m*/*z*): 372 (M+1).

*2-Oxo-3(2*H*)-benzothiazoleacetic acid, [2-(2,4-dimethylphenoxy)ethylidene]-hydrazide (**1d**)*. Yield 77 %; m.p. 218–220 °C; Anal. Calcd. for $C_{19}H_{19}N_3O_3S$: C, 61.77; H, 5.18; N, 11.37 %. Found: C, 61.79; H, 5.13; N, 11.34 %; IR (KBr, cm^{-1}): 3190, 1768, 1682, 1555, 1498; ^{1}H-NMR (400 MHz, DMSO-d_6, δ / ppm): 2.15 (3H, *s*), 2.21 (3H, *s*), 4.66–4.71 (2H, *m*), 4.75 and 5.02 (2H, *s*), 6.85–7.00 (3H, *m*), 7.17–7.39 (3H, *m*), 7.56–7.69 (1H, *t*, *J* = 5.0 Hz), 7.70 (1H, *d*, *J* = 7.7 Hz), 11.71–11.77 (1H, *bs*); ^{13}C-NMR (100 MHz, DMSO-d_6, δ / ppm): 15.93 (CH_3), 20.05 (CH_3), 43.22 (CH_2), 67.02 (CH_2), 111.41 (CH), 111.77 (CH), 121.07, 122.74 (CH), 123.13 (CH), 125.66, 126.51 (CH), 127.09 (CH), 129.42, 131.29 (CH), 137.23, 143.57 (CH), 153.87, 167.17, 162.65; MS-FAB$^+$ (m/z): 370 (M+1).

*2-Oxo-3(2*H*)-benzothiazoleacetic acid, [2-(2,6-dimethylphenoxy)ethylidene]-hydrazide (**1e**)*. Yield 79 %; m.p. 226–227 °C; Anal. Calcd. for $C_{19}H_{19}N_3O_3S$: C, 61.77; H, 5.18; N, 11.37 %. Found: C, 61.97; H, 5.11; N, 11.39 %; IR (KBr, cm^{-1}): 3339, 1770, 1680, 1595, 1486; ^{1}H-NMR (400 MHz, DMSO-d_6, δ / ppm): 2.26 (6H, *s*), 4.46–4.53 (2H, *m*), 4.73 and 5.01 (2H, *s*), 6.92–6.99 (1H, *m*), 7.02––7.08 (2H, *m*), 7.18–7.40 (3H, *m*), 7.63–7.70 (1H, *m*), 7.81–7.89 (1H, *t*, *J* = 5.2 Hz), 11.73 (1H, *m*); ^{13}C-NMR (100 MHz, DMSO-d_6, δ / ppm): 16.13 (2CH_3), 43.26 (CH_2), 71.08 (CH_2), 111.40 (CH), 121.07, 122.72 (CH), 123.11 (CH), 124.07 (CH), 126.50 (CH), 128.80 (2CH), 130.30 (2C), 137.23, 143.76 (CH), 155.23, 167.19, 162.71; MS-FAB$^+$ (*m*/*z*): 370 (M+1).

*2-Thioxo-3(2*H*)-benzothiazoleacetic acid, [2-(4-methylphenoxy)ethylidene]-hydrazide (**1f**)*. Yield 80 %; m.p. 138–140 °C; Anal. Calcd. for $C_{18}H_{17}N_3O_2S_2$: C, 58.20; H, 4.61; N, 11.31 %. Found: C, 58.42; H, 4.47; N, 11.18 %; IR (KBr, cm^{-1}): 3200, 1683, 1588, 1523, 1491; ^{1}H-NMR (400 MHz, DMSO-d_6, δ / ppm): 2.22 (3H, *s*), 4.27–4.58 (2H, *s*), 4.67–4.68 (2H, *d*, *J* = 5.0 Hz), 6.86–6.92 (2H, *m*), 7.09 (2H, *d*, *J* = 8.2 Hz), 7.33–7.40 (1H, *m*), 7.43–7.49 (1H, *m*), 7.56–7.75 (1H, *t*, *J* = 5.0 Hz), 7.84 (1H, *d*, *J* = 8.2 Hz), 8.01 (1H, *d*, *J* = 7.3 Hz), 11.70–11.94 (1H, 2*bs*); ^{13}C-NMR (100 MHz, DMSO-d_6, δ / ppm): 20.04 (CH_3), 35.21 (CH_2), 66.73 (CH_2), 114.52 (2CH), 121.09 (CH), 121.75 (CH), 124.43 (CH), 126.32 (CH), 129.73 (2CH), 134.69, 143.00 (CH), 152.47, 152.56, 155.74, 163.18, 165.83; MS-FAB$^+$ (*m*/*z*): 372 [M+1].

*2-Thioxo-3(2*H*)-benzothiazoleacetic acid, [2-(4-*tert*-butylphenoxy)ethylidene]-hydrazide (**1g**)*. Yield 78 %; m.p. 142–144 °C; Anal. Calcd. for $C_{21}H_{23}N_3O_2S_2$: C, 60.99; H, 5.61; N, 10.16 %. Found: C, 61.00; H, 5.64; N, 10.18 %; IR (KBr,

cm^{-1}): 3178, 1682, 1574, 1523, 1487; ^{1}H-NMR (400 MHz, DMSO-d_6, δ / ppm): 1.24 (9H, *s*), 4.27–4.58 (2H, *s*), 4.70 (2H, *d*, *J* = 5.0 Hz), 6.88–6.95 (2H, *m*), 7.27–7.32 (2H, *m*), 7.34–7.40 (1H, *m*), 7.43–7.50 (1H, *m*), 7.56–7.75 (1H, *t*, *J* = = 5.0 Hz), 7.84–7.85 (1H, 2*d*, *J* = 8.1 Hz), 8.02 (1H, *t*, *J* = 7.3 Hz), 11.70–11.97 (1H, 2*bs*); ^{13}C-NMR (100 MHz, DMSO-d_6, δ / ppm): 31.26 ($3CH_3$), 33.73, 35.18 (CH_2), 66.68 (CH_2), 114.16 (2CH), 121.08 (CH), 121.78 (CH), 124.44 (CH), 126.11 (2CH), 126.32 (CH), 134.67, 143.07 (CH), 143.19, 152.46, 155.60, 163.15, 165.85; MS-FAB$^+$ (*m*/*z*): 414 [M+1].

*2-Thioxo-3(2*H*)-benzothiazoleacetic acid, [2-(4-methoxyphenoxy)ethylidene]-hydrazide (**1h**)*. Yield 81 %; m.p. 145–147 °C; Anal. Calcd. for $C_{18}H_{17}N_3O_3S_2$: C, 55.80; H, 4.42; N, 10.84 %. Found: C, 55.97; H, 4.53; N, 10.92 %; IR (KBr, cm^{-1}): 3196, 1683, 1566, 1518, 1490; ^{1}H-NMR (400 MHz, DMSO-d_6, δ / ppm): 3.70 (3H, *s*), 4.26–4.58 (2H, *s*), 4.65 (2H, *d*, *J* = 5.0 Hz), 6.84–6.90 (2H, *m*), 6.95–6.98 (2H, *m*), 7.34–7.40 (1H, *m*), 7.43–7.49 (1H, *m*), 7.55–7.74 (1H, *t*, *J* = = 5.0 Hz), 7.84–7.85 (1H, *d*, *J* = 7.8 Hz), 8.02 (1H, *t*, *J* = 7.0 Hz), 11.69–11.96 (1H, 2*bs*); ^{13}C-NMR (100 MHz, DMSO-d_6, δ / ppm): 35.21 (CH_2), 55.29 (CH_3), 67.24 (CH_2), 114.59 (2CH), 115.67 (2CH), 121.08 (CH), 121.78 (CH), 124.44 (CH), 126.33 (CH), 134.67, 143.15 (CH), 151.81, 152.46, 153.70, 163.16, 165.85; MS-FAB$^+$ (*m*/*z*): 388 [M+1].

*2-Thioxo-3(2*H*)-benzothiazoleacetic acid, [2-(2,4-dimethylphenoxy)ethylide-ne]hydrazide (**1i**)*. Yield 79 %; m.p. 136–137 °C; Anal. Calcd. for $C_{19}H_{19}N_3O_2S_2$: C, 59.20; H, 4.97; N, 10.90 %. Found: C, 59.28; H, 4.93; N, 10.91 %; IR (KBr, cm^{-1}): 3195, 1682, 1562, 1528, 1494; ^{1}H-NMR (400 MHz, DMSO-d_6, δ / ppm): 2.14 (3H, *s*), 2.19 (3H, *s*), 4.26–4.58 (2H, *s*), 4.67–4.68 (2H, *d*, *J* = 5.0 Hz), 6.84––6.90 (1H, *m*), 6.91–6.98 (2H, *m*), 7.34–7.40 (1H, *m*), 7.44–7.50 (1H, *m*), 7.56––7.74 (1H, *t*, *J* = 5.0 Hz), 7.84 (1H, *d*, *J* = 7.8 Hz), 8.02 (1H, *t*, *J* = 7.4 Hz), 11.67–11.91 (1H, 2*bs*). ^{13}C-NMR (100 MHz, DMSO-d_6, δ / ppm): 15.91 (CH_3), 20.04 (CH_3), 35.20 (CH_2), 66.97 (CH_2), 111.75 (CH), 121.07 (CH), 121.77 (CH), 124.44 (CH), 125.63, 126.32 (CH), 127.05 (CH), 129.34, 131.26 (CH), 134.67, 143.17 (CH), 152.46, 153.85, 163.15, 165.83 (C); MS-FAB$^+$ (*m*/*z*): 386 [M+1].

*2-Thioxo-3(2*H*)-benzothiazoleacetic acid, [2-(2,6-dimethylphenoxy)ethylide-ne]hydrazide (**1j**)*. Yield 75 %; m.p. 86–88 °C; Anal. Calcd. for $C_{19}H_{19}N_3O_2S_2$: C, 59.20; H, 4.97; N, 10.90 %. Found: C, 59.08; H, 4.84; N, 10.98 %; IR (KBr, cm^{-1}): 3210, 1684, 1599, 1520, 1493; ^{1}H-NMR (400 MHz, DMSO-d_6, δ / ppm): 2.24 (6H, *s*), 4.27–4.56 (2H, *s*), 4.46 (2H, *d*, *J* = 5.3 Hz), 6.91–6.96 (1H, *m*), 7.01–7.05 (2H, *m*), 7.37 (1H, *m*), 7.47 (1H, *m*), 7.65–7.72 (1H, *t*, *J* = 5.3 Hz), 7.80–7.86 (1H, *m*), 8.01 (1H, *t*, *J* = 8.3 Hz), 11.69–11.87 (1H, 2*bs*); ^{13}C-NMR (100 MHz, DMSO-d_6, δ / ppm): 16.13 ($2CH_3$), 35.14 (CH_2), 71.11 (CH_2), 121.06 (CH), 121.75 (CH), 124.03 (CH), 124.42 (CH), 126.31 (CH), 128.77 (2CH), 130.30 (2C), 134.68, 143.33, 152.46, 155.20, 163.23, 165.81; MS–FAB$^+$ (*m*/*z*): 386 [M+1].

Journal of the Serbian Chemical Society
JSCS-info@shd.org.rs • www.shd.org.rs/JSCS
J. Serb. Chem. Soc. 77 (2) 147–157 (2012)
JSCS–4257
UDC 547.657.004.12:542.48:57–188
Original scientific paper

Fractionation of complex mixtures of naphthenic acids, their characterization and biological activity

LJUBICA GRBOVIĆ[1#], KSENIJA PAVLOVIĆ[1#], BOJANA PREKODRAVAC[1], KSENIJA KUHAJDA[1#], SLAVKO KEVREŠAN[2*#], MIRJANA POPSAVIN[1#], JELENA MILIĆ[1] and VERA ĆIRIN-NOVTA[1#]

[1]*Department of Chemistry, Biochemistry and Environmental Protection, Faculty of Sciences, University of Novi Sad, Trg Dositeja Obradovića 3, Novi Sad, Serbia and* [2]*Faculty of Agriculture, University of Novi Sad, Trg Dositeja Obradovića 8, Novi Sad, Serbia*

(Received 16 June, revised 22 September 2011)

Abstract: Naphthenic acids (NAs) are complex mixtures of cycloaliphatic and alkyl-substituted acyclic carboxylic acids, the overall characteristics of which are determined by the composition of the mixture. A complex mixture of NAs from a commercial fraction of atmospheric oil of the Vojvodina naphthenic crude oil "Velebit" (Serbia) was separated into narrower fractions based on their acidity. Electrospray ionization mass spectrometry analysis of the fractions showed the occurrence of structural differentiation of the acids. By extraction at pH 3–5, about 50 % of the total mass of acids, consisting predominantly of tricyclic and bicyclic structures, was separated. Acids of lower acidity, (about 22 %), separated at pH 9 and 10, and their dominant constituents were acids with three-, four- and five-membered rings. A correlation was found between the dominant structure and the biological activity of the NAs of the fractions. The fraction extracted at pH 8, also with dominant bicyclic and tricyclic structures, showed the highest auxin and gibberellin activities.

Keywords: naphthenic acids; fractionation; structural analysis; biological activity.

INTRODUCTION

Naphthenic acids (NAs) are carboxylic acids that are natural constituents of naphthenic oils.[1–3] In the process of commercial oil fractionation, the NAs are distributed into fractions and, in some commercial processes, they have to be extracted since they lower the quality of the crude oil product. The amount of NAs commercially extracted in the USA in 1992 was estimated to be 5500–6000 t.[4,5] About 80 % of the isolated NAs are transformed into their salts, primarily to cop-

* Corresponding author. E-mail: kevresan@polj.uns.ac.rs
# Serbian Chemical Society member.
doi: 10.2298/JSC110616195G

per naphthenates, which is used for wood protection. Besides this, naphthenates are used for the production of a variety of esters, amides, imidazolines and other derivatives that are widely used in the chemical industry. Due to this, but primarily because of the occurrence of NAs in oil sands process waters in Canada, there is a growing interest in the characterization, purification and application of NAs. This can be seen from the number of relevant papers with the key word "naphthenic acids", especially since the year 2000, when the annual number of papers increased by about eight fold compared to the annual number before 2000.[6]

At high concentrations (above 50 mg L^{-1}), NAs are corrosive and toxic substances,[4,7] and for these reasons they represent serious contaminants of refinery wastewaters, xenobiotics, and act as environmental pollutants.[8–10]. Low concentrations (up to 0.5 mg L^{-1}) of NAs and their salts have been studied for a long time as substances exhibiting biological activity, such as plant growth hormones,[11–13] rooting agents[14,15] or bactericides.[16]

Naphthenic acids represent complex mixtures of alkyl-substituted aliphatic and cyclic monocarboxylic acids of the general formula $C_nH_{2n-z}O_2$, where n is the number of carbon atoms and z the hydrogen deficiency due to ring formation. NAs may contain many individual structures. Despite of the advances in analytical techniques used to study NAs, a complete picture of the composition of these complex mixtures has yet to be obtained. In view of their complexity, it seems that this is an unattainable goal, although several recent advances have been made, including the identification of individual NA structures in both petroleum and oil sands by multidimensional comprehensive gas chromatography–mass spectrometry.[17–19] Literature data indicate that NAs from different sources have different structural compositions and ranges of molecular masses, as well as different mass ratios of the acids involved, which determine their chemical and biochemical properties, such as, for example, toxicity.[20] One of the approaches to dealing with this problem is to separate a complex NA mixture into narrower fractions according to their particular characteristics, determine the composition of these narrower fractions and their properties, and then correlate these properties to their chemical structures. Frank *et al.*[21] separated an NA into narrower fractions by fractional distillation of the methyl esters and showed that they differed slightly in respect to their toxicity. Based on these results, the authors established a quantitative structure–activity relationship that attempted to predict the toxicity of NAs.[22] Using five NA samples differing in total acid number, Ding-Rong *et al.*[23] attempted to establish a correlation between corrosivity and chemical structure and found that NAs with lower molecular weight and fewer ring structures usually were more corrosive. Apart from fractional distillation, NAs can be also separated in some other ways. Niemi *et al.*[24] developed a method of NAs fractionation by supercritical fluid extraction and tested the effects of different fractions on wood decay. Extraction and fractionation of petroleum NAs with solid media

was also performed on silica deposited with KOH, by which NA fractions of different acidity could be recovered from crude oils.[25] Separation of the acid components of crude oil on anionic ion-exchange resins resulted in carboxylic acids with a molecular mass distribution that differed from that of the normal alkanes in the crude oil.[26] Ashumov *et al*.[27] reported fractionation of NA mixtures by stepwise degradation of their soaps. The naphthenic acids were saponified with sodium hydroxide and then the soaps were decomposed gradually with HCl into different fractions.

Naphthenic acids are mainly weak acids with pK_a values in the range from 5 to 6.[28] They dissolve well in organic solvents, whereas their solubility in water depends on the pH. In a very acidic medium, when the NAs are present in the protonated form, they are practically insoluble, whereas in a very basic medium, they dissolve in the water as their salts. Headley *et al*.[28] showed that the mass profiles of water-soluble NAs differed significantly depending on the pH of the medium. This fact indicates that different classes of these acids are dissolved at different pH values. Based on this study,[28] and knowing the properties of NAs, such as their solubility in aqueous media and their pK_a values, it can be supposed that it is possible to fractionate a mixture of NAs by dissolving them as salts at a high pH and then, by addition of a strong mineral acid, achieve a successive and selective separation of the water-insoluble acids, which can then be readily extracted with an organic solvent.

The aim of the presented work was to investigate the possibility of fractionation of NAs based on their solubility in aqueous media of given pH values and then characterize the obtained fractions and study their biological activity of the type of the plant hormones auxin and gibberellin. These tests were realized in an attempt to explain the effect of these fractions on plant rooting, observed in a previous study.[28]

EXPERIMENTAL

General methods

All employed chemicals were purchased from Fluka.

Naphthenic acids were isolated from an atmospheric oil fraction (distillation interval 168–290 °C) of Vojvodina crude oil "Velebit" by the optimized procedure of alkaline extraction.[29] Further purification was performed by triple repeated alkaline extraction and drying with anhydrous Na_2SO_4. The average molecular mass of the naphthenic acids was determined[29] (ASTM D3238) to be 262, and this value was used in the further experiments.

Fractionation of NAs

The mixture of NAs (1.00 g, 3.82 mmol) was mixed with distilled water (300 mL) at room temperature and then 5 % NaOH solution (≈10 mL) was added under constant stirring until pH 11 was attained. After complete dissolution of the NAs, 5 % H_2SO_4 was added in small portions (1 mL) under cooling and constant stirring. When the pH had decreased by one unit, the insoluble NAs, separated on the top of the solution, were extracted three times with diethyl ether (30.0, 30.0 and 20.0 mL). Successive addition of acid and lowering of the pH by

one unit was continued until pH 2 was achieved. The extracts were dried over anhydrous Na_2SO_4 and the diethyl ether was removed by evaporation under reduced pressure.

Characterization of NAs

Group-structural analysis was performed by mass-spectrometric fragmentation to quasi-molecular ions by a soft ionization technique in either the positive or negative ion mode. Low-resolution high performance liquid chromatography coupled with electrospray ionization mass spectrometry (HPLC–ESI–MS) spectra were recorded on a Finningan LCQ advantage MAX spectrometer (Walthman, USA). The spectra encompassed a molecular series of protonated and sodiated molecular ions of the acids $[M+H]^+$ and $[M+2H]^+$ or $[M+23]^+$ recorded in the positive ion mode in 0.1 % trifluoroacetic acid in acetonitrile or acetonitrile–water mixture 1:1 and 0.1 % formic acid, as well as a series of $[M–H]^-$ recorded in the negative ion mode in a solution of 0.1 % triethylamine in acetonitrile–water (70:30) with the addition of 2 % NH_4OH. The injected sample volume was 50 μL, and the reference was the molecular ion of 5-cyclohexylpentanoic acid. The search range was 50–600 amu. Spectra were analyzed by the Xcalibur program (Thermo Fisher Scientific).

Determination of the auxin and gibberellin activities of the NA fractions

The auxin activity of the total NAs and its fractions was determined by the test of inhibition of germination of brown mustard (*Brassica juncea* L.), based on counting the germinated seeds after treatment with potassium naphthenates at a concentration of 1.0 mg dm^{-3} and the corresponding concentrations of 3-indoleacetic acid (IAA).[30] The gibberellin activity of the total NAs and its fractions (potassium salts, 1.0 mg dm^{-3}) was measured by the barley-endosperm test, using the corresponding concentrations of gibberellin GA_3 for comparison.[31] The experiments were repeated three times. Statistical significance was tested by one-way Anova followed by comparisons of means by the Duncan multiple range test ($p < 0.05$).

RESULTS AND DISCUSSION

Separation of NAs into narrower fractions

By the described fractionation of total NA preparation, the major part of the NAs was separated in the acidic range (pH 2–5, 62.5 %), then in the basic range (pH 9–10, 22.3 %), and the smallest in the neutral range (pH 6–8, 13.2 %) (Fig. 1). Bearing in mind that the procedure allows the gradual protonation of the acids and their separation into fractions, the obtained results suggest the existence of two groups of acids – weaker ones that were separated in the basic range and stronger ones that were separated in the acidic range.

Comparative structural analysis of the isolated NA fractions and the total NAs

Acids separated at pH 4. At pH 4, 23.9 % of the total NA mass was isolated, which means that the majority of acids had a higher relative acidity. The mass ratios of the NA classes as correlated with the homologous *z*-series in the mixture of acids extracted from the aqueous solution of the total NAs at pH 4 are presented in Table I. There were no pentacyclic structures among the isolated acids and the dominant acids being were structures having 18 to 21 carbon atoms in their molecule (36.5 %); additionally, the ratio of fatty acids was very small (9.7 %).

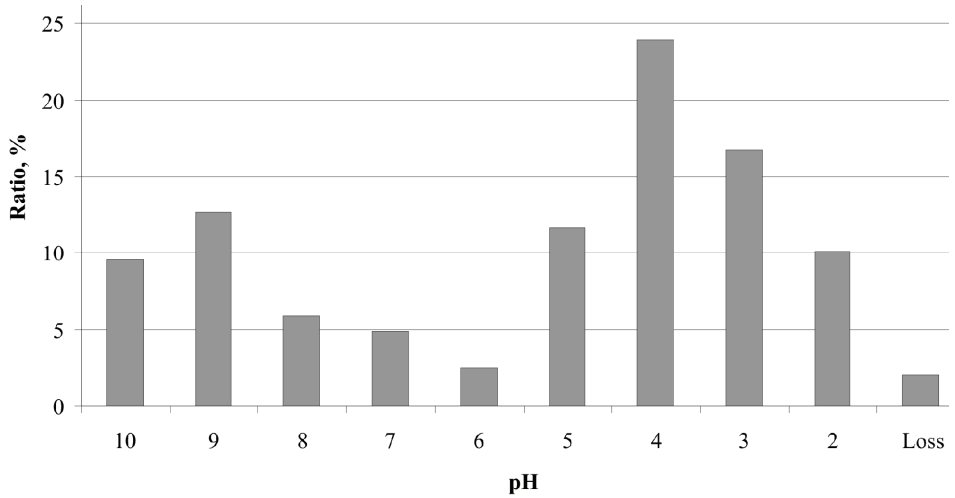

Fig. 1. Mass proportions (%) of particular NAs separated at different pH values.

TABLE I. Distribution of NA classes isolated at pH 4, based on the *m*/*z* values in the ESI-MS spectrum

Carbon number	Percentage of naphthenic acids by *z* number					Percentage by carbon number
	0	2	4	6	8	
14	0.00	0.00	0.56	0.00	0.00	0.56
15	0.00	0.87	0.44	0.00	0.00	1.31
16	0.00	1.06	1.37	1.06	0.00	3.49
17	0.62	0.00	2.62	3.56	0.00	6.80
18	0.94	1.87	3.37	5.05	0.00	11.23
19	1.12	1.81	3.43	5.18	1.18	12.72
20	1.18	1.87	1.68	6.24	4.43	15.40
21	1.25	2.31	3.24	6.11	4.56	17.47
22	1.25	1.87	2.06	3.56	3.56	12.30
23	1.44	1.12	1.50	2.06	2.00	8.12
24	1.18	0.00	1.25	1.56	0.75	4.74
25	0.75	0.00	1.12	1.06	0.62	3.55
26	0.00	0.00	0.75	0.62	0.00	1.37
27	0.00	0.00	0.00	0.00	0.00	0.00
28	0.00	0.00	0.50	0.44	0.00	0.94
Total	9.73	12.78	23.89	36.50	17.10	100.00

Acids separated at pH 8. Only 5.9 % of total acids were extracted at pH 8, and an analysis of the HPLC–ESI-MS spectra showed that dominant series of acids were bicyclic (z = 4, 32.5 %) and tricyclic (z = 6, 32.5 %) structures (Table II). The ratio of fatty acids was only 7.2 %; tricyclic acids were present at approximately the same level as at pH 4, but there are significantly more bicyclic structures with 20 to 25 C atoms in their molecule. No pentacyclic structures were found in this mixture.

TABLE II. Distribution of NA classes isolated at pH 8, based on the *m*/*z* values in the ESI-MS spectrum

Carbon number	Percentage of naphthenic acids by *z* number					Percentage by carbon number
	0	2	4	6	8	
15	0.00	0.00	0.78	0.00	0.00	0.78
16	0.00	0.00	0.00	0.00	0.00	0.00
17	0.00	0.00	0.88	0.00	0.00	0.88
18	0.00	0.00	0.78	0.97	0.00	1.75
19	0.97	0.00	1.07	1.07	0.00	3.11
20	0.97	1.07	2.72	2.92	1.85	9.53
21	0.88	0.78	3.41	3.99	0.00	9.06
22	0.97	2.24	5.26	3.02	0.00	11.49
23	1.70	1.75	4.87	5.26	0.00	13.58
24	0.78	1.07	3.31	7.01	4.77	16.94
25	0.00	2.82	3.60	2.72	0.00	9.14
26	0.00	5.26	2.72	2.34	2.14	12.46
27	0.88	0.00	1.65	2.14	1.75	6.42
28	0.00	1.17	1.46	1.07	1.17	4.87
Total	7.15	16.16	32.51	32.51	11.68	100.00

Acids separated at pH 10. Structures with the lowest acidity are the NAs that were insoluble in an aqueous medium of pH 10, and their ratio in the total mixture was 9.6 %. While the acid series with $z = 4$ and $z = 6$ were dominant in the fractions isolated at pH 4 and 8, this was not true for the fraction of weakest acids, isolated at pH 10 (Table III). In this fraction, the ratio of acyclic acids was 25.3 %, while pentacyclic acids ($z = 10$) appeared for the first time (12.0 %). Table III shows that structural differentiation occurred since the molecular ions of pentacyclic acids (12.0 %) of the series $[M+H]^+$ were evidenced. In the spectrum, acyclic *z*-class of acids were dominant (25.3 %), with the prevailing structures having 19, 20 and 21 C atoms (16.3 %). The ratio of tetracyclic acids was 17.7 %, with the dominant molecules having 22, 23 and 26 C atoms; the dominant tricyclic acids also had 22 to 26 C atoms in their molecules.

There was a sharp differentiation of acids not only into classes (*z*-series), but also within the same class with respect to the number of C atoms. Fatty acids, mono-, bi-, tri- and tetracyclic acids were differently distributed in all three fractions, as can be seen in Fig. 2. Pentacyclic acids, the content of which in the total mixture was the lowest, are the evidently weakest acids and hence the least soluble, so that they were concentrated in the fraction isolated at pH 10. At this pH, most of the fatty acids were isolated, whereas decreasing the pH resulted in less and less tricyclic structures in the mixture, which indicates their increasing average acidity. In this way, proof was obtained for the possible fractionation of NAs by their extraction with diethyl ether from aqueous media of different pH values. It is to be expected that naphthenic acids from different sources could be frac-

tionated in a similar way and the obtained results would depend on the composition of the mixture of naphthenic acids.

TABLE III. Distribution of NA classes isolated at pH 10, based on the *m*/*z* values in the ESI--MS spectrum

Carbon number	Percentage of naphthenic acids by *z* number						Percentage by carbon number
	0	2	4	6	8	10	
13	0.00	0.00	1.33	0.00	0.00	0.00	1.33
14	0.98	1.00	0.78	0.00	0.00	0.00	2.76
15	1.02	0.00	0.00	0.00	0.00	0.00	1.02
16	0.78	1.33	0.44	0.78	0.00	0.00	3.33
17	1.56	1.11	0.00	1.06	0.00	0.00	3.73
18	2.39	1.11	1.67	1.56	0.00	0.00	6.73
19	3.89	2.05	1.67	0.00	0.00	0.00	7.61
20	4.11	1.44	1.44	0.00	1.44	0.00	8.43
21	4.83	1.11	1.11	2.00	1.33	0.00	10.38
22	3.50	1.89	1.78	2.22	3.66	0.00	13.05
23	1.33	0.00	1.22	1.67	3.05	2.50	9.77
24	0.89	1.00	1.00	1.50	2.33	2.22	8.94
25	0.00	0.89	0.89	1.56	0.00	2.44	5.78
26	0.00	1.00	1.00	1.89	3.11	1.56	8.56
27	0.00	0.00	1.00	0.00	1.89	1.67	4.56
28	0.00	0.00	0.00	0.00	0.00	0.83	0.83
29	0.00	0.00	0.00	1.56	0.89	0.78	3.23
Total	25.28	13.93	15.33	15.80	17.70	12.00	100.00

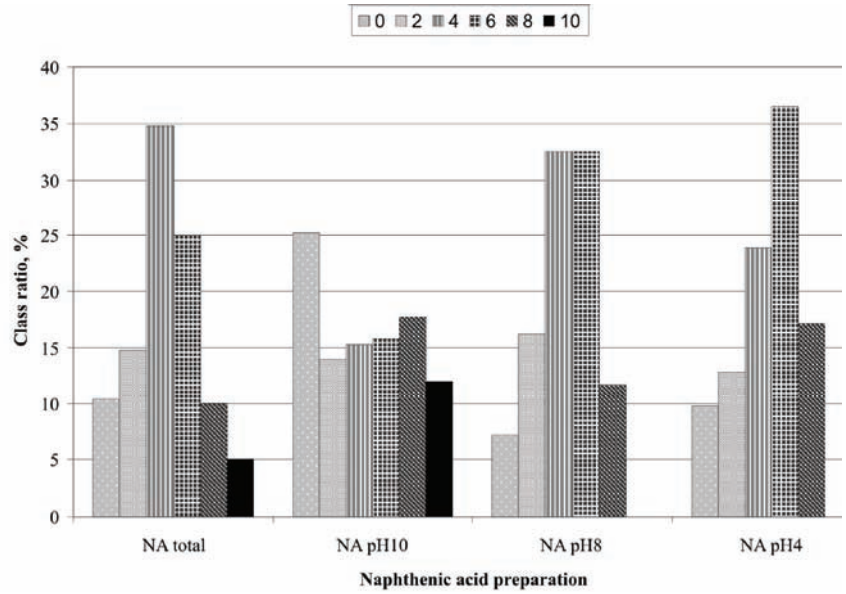

Fig. 2. Comparative distribution of the total NAs and NA classes isolated from aqueous solutions at pH 10, 8 and 4.

Auxin and gibberellin activities of the total NAs and its fractions

In respect of auxin activity, the total NA preparation and the fraction separated at pH 10 exhibit the same activity which corresponds to an IAA concentration of 0.05 mg L^{-1}, whereas the fraction separated at pH 4 showed a somewhat lower activity (16.4 % lower than that of the total preparation). The highest auxin activity (19.6 % higher than that of the total preparation) was exhibited by the fraction separated at pH 8, which corresponded to an IAA concentration of 0.5 mg L^{-1} (Fig. 3).

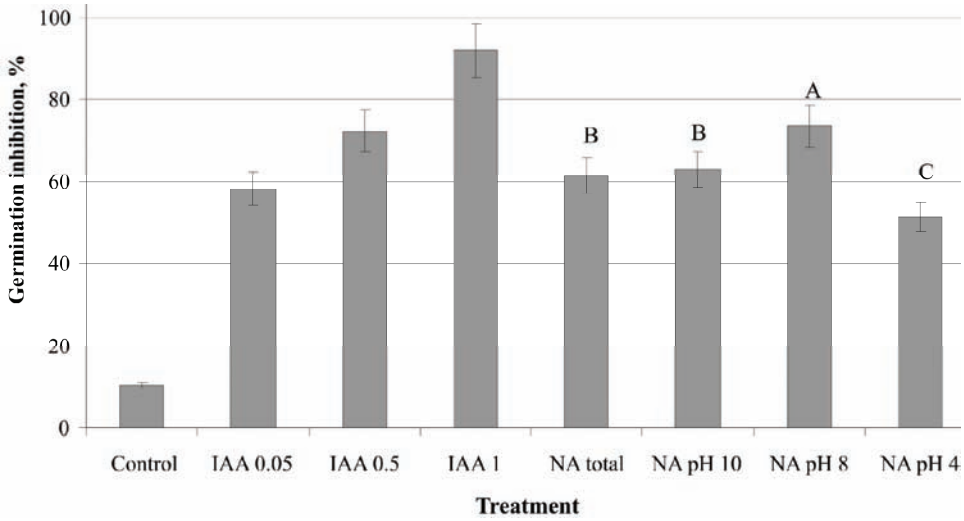

Fig. 3. Auxin activity of aqueous solutions of potassium naphthenates and the three NA fractions. Control (treatment with water, without IAA or K-naphthenates); IAA 0.05 – IAA 1 (treatments with IAA, concentrations: 0.05, 0.50 and 1.0 mg L^{-1}); NA total (treatment with total K-naphthenates, concentration: 1.0 mg L^{-1}); NA pH 10, NA pH 8, NA pH 4 (treatments with NA fractions obtained at the corresponding pH values, concentration: 1.0 mg L^{-1}). The bars represent the standard deviation. Columns labeled with different letters are significantly different (P<0.05, the Duncan multiple range test).

The separated NA fractions showed much greater mutual differences with respect to the gibberellin activity (Fig. 4). Again, the fraction separated at pH 8 showed the highest activity (92.3 % higher than that of the total preparation), which corresponds to a GA_3 concentration between 1×10^{-3} and 1×10^{-2} mg L^{-1}. The fraction separated at pH 4 showed an insignificantly higher activity compared to that of the total preparation, whereas the fraction separated at pH 10 exhibited a significantly lower activity (46.1 % lower than that of the total preparation). The NA fraction separated at pH 8 was characterized by the dominant presence of NAs with bicyclic and tricyclic structures, which were present in equal ratios.

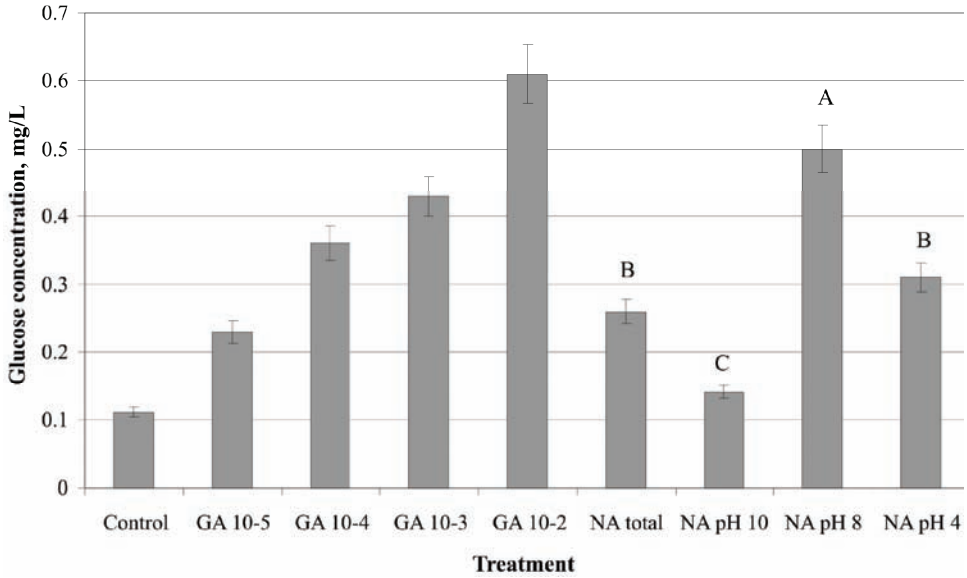

Fig. 4. Gibberellin activity of aqueous solutions of the NA fractions. Control (treatment with water, without GA or K-naphthenates); GA 10-5; GA 10-4; GA 10-3; GA 10-2 (treatments with GA_3, concentrations: 1×10^{-5}, 1×10^{-4}, 1×10^{-3} and 1×10^{-2} mg L^{-1}, respectively); NA total (treatment with total K-naphthenates, concentration 1.0 mg L^{-1}); NA pH 10, NA pH 8, NA pH 4 (treatment with NA fractions obtained at the corresponding pH values, concentration 1.0 mg L^{-1}). The bars represent the standard deviation. Columns labeled with different letters are significantly different (P<0.05, the Duncan multiple range test).

As is evident from Fig. 3, the treatment of brown mustard seeds with potassium naphthenate caused inhibition of their germination, which may be a result of an activity similar to that of plant hormones of the auxin-type, although phytotoxic activity cannot be excluded. Namely, it is known that naphthenic acids can exhibit phytotoxic effects which depend on the concentration and plant species.[32–34] That the activity of the total NAs and its fractions is similar to that of the plant hormones auxin is supported by the recently emerging hypothesis that the synthetic auxin 1-naphthaleneacetic acid (NAA) has a similar structure to those of the NAs in the z = 4 family. Although NAA has an aromatic ring structure whereas the NAs are aliphatic, there is a possibility that the NAs operate through the same receptors as the auxin NAA.[35] In addition, it was recently established that one or more of the compounds present in the naphthenic acid mixtures bind to the androgen receptor in a manner similar to that of flutamide, a powerful metabolite for binding to androgen receptors.[36]

CONCLUSIONS

Complex NA mixtures can be separated into narrower fractions based on the differences in their acidity. The obtained fractions differed in respect to their

group-structural composition. Pentacyclic acids, the content of which in the total NA mixture was otherwise the lowest, concentrate in the fraction isolated at pH 10. The differences in the compositions of the obtained fractions led to differences in their biological activity, and the fraction separated at pH 8 showed the highest auxin- and gibberellin-type activities. Based on the composition of this fraction, it can be concluded that such activities are due to the dominant presence of NAs with bicyclic and tricyclic structures in an equal ratio.

Acknowlegement. This study was supported by the Ministry of Education and Science of the Republic of Serbia, Project No. 172006.

И З В О Д

РАЗДВАЈАЊЕ КОМПЛЕКСНЕ СМЕШЕ НАФТЕНСКИХ КИСЕЛИНА, ЊИХОВА КАРАКТЕРИЗАЦИЈА И БИОЛОШКА АКТИВНОСТ

ЉУБИЦА ГРБОВИЋ[1], КСЕНИЈА ПАВЛОВИЋ[1], БОЈАНА ПРЕКОДРАВАЦ[1], КСЕНИЈА КУХАЈДА[1], СЛАВКО КЕВРЕШАН[2], МИРЈАНА ПОПСАВИН[1], ЈЕЛЕНА МИЛИЋ[1] и ВЕРА ЋИРИН-НОВТА[1]

[1]Департман за хемију, биохемију и заштиту животне средине, Природно–математички факултет, Универзитет у Новом Саду, Трг Доситеја Обрадовића 3,Ниви Сад и [2]Пољопривредни факултет, Универзитет у Новом Саду, Трг Доситеја Обрадовића 8, Нови Сад

Нафтенске киселине (НК) су комплексна смеша циклоалифатичних и алкил-супституисаних ацикличних карбоксилних киселина чије особине у многоме зависе од састава смеше. Комплексна смеша нафтенских киселина из комерцијалне фракције атмосферског уља војвођанске нафтенске нафте “Велебит” раздвојена је на уже фракције на основу различите киселости. Структурном ESI-MS анализом ужих фракција утврђено је да том приликом долази до структурне диференцијације киселина. Екстракцијом на pH 3–5 издвојено је око 50 % од масе укупних киселина са најдоминантнијим трицикличним и бицикличним структурама. Киселина мање киселости у смеши има око 22 %, издвојене су на pH 9 и pH 10, а доминантне структуре киселина су са три, четири и пет кондензованих прстенова у молекулу. Утврђено је да постоји корелација доминантних структура и биолошке активности нафтенских киселина ужих фракција. Фракција екстрахована на pH 8 има доминантне би- и три- цикличне структуре киселина и показује највећу ауксинску и гиберелинску активност.

(Примљено 16. јуна, ревидирано 22. септембра 2011)

REFERENCES

1. J. Cason, I. A. Khodair, *J. Org. Chem.* **32** (1967) 3430
2. J. R. Maxwell, C. T. Pillinger, G. Eglinton, *Q. Rev. Chem. Soc.* **25** (1971) 571
3. W. K. Seifert, R. M. Teeter, *Anal. Chem.* **41** (1969) 628
4. J. S. Clemente, P. M. Fedorak, *Chemosphere* **60** (2005) 585
5. J. A. Brient, P. J. Wessner, M. N. Doyle, *Kirk-Othmer Encyclopedia of Chemical Technology*, 4th ed., Wiley, New York, USA, 1995, p. 1017
6. D. M. Grewer, R. F. Young, R. M. Whittal, P. M. Fedorak, *Sci. Total Environ.* **408** (2010) 5997
7. E. Slavcheva, R. Shone, A. Turnbull, *Br. Corros. J.* **34** (1999) 125
8. D. C. L. Wong, R. van Compernolle, J. G. Nowlin, D. L. O’Neal, G. M. Johnson, *Chemosphere* **32** (1996) 1669

9. J. V. Headley, D. W. McMartin, *J. Environ. Sci. Health, Part A.* **39** (2004) 1989
10. S. S. Leung, M. D. MacKinnon, R. E. H. Smith, *Aquat. Toxicol.* **62** (2003) 11
11. R. Kastori, N. Petrović, T. Savkov, D. Miljković, *Acta Biol. Med. Exp.* **13** (1988) 83
12. V. Ćirin-Novta, K. Kuhajda, S. Kevrešan, J. Kandrač, Lj. Grbović, P. Rodić, *Acta Period. Technol.* **35** (2004) 87
13. V. Ćirin-Novta, K. Kuhajda, S. Kevrešan, J. Kandrač, Lj. Radić, *Acta Period. Technol.* **33** (2002) 135
14. S. Kevrešan, B. Kovačević, V. Ćirin-Novta, K. Kuhajda, J. Kandrač, K. Pavlović, Lj. Grbović, *J. Serb. Chem. Soc.* **72** (2007) 953
15. A. Halmagyi, S. Kevrešan, B. Kovačević, V. Ćirin-Novta, K. Pavlović, Lj. Grbović, K. Kuhajda, *Propag. Ornam. Plants* **8** (2008) 148
16. M. A. Samedov, L. I. Alieva, V. M. Abbasov, *Prot. Met.* **44** (2008) 397
17. S. J. Rowland, A. G. Scarlett, D. Jones, C. E. West, R. A. Frank, *Environ. Sci. Technol.* **45** (2011) 3154
18. S. J. Rowland, C. E. West, A. G. Scarlett, D. Jones, *Rapid Commun. Mass Spectrom.* **25** (2011) 1741
19. S. J. Rowland, C. E. West, A. G. Scarlett, D. Jones, R. A. Frank, *Rapid Commun. Mass Spectrom.* **25** (2011) 1198
20. C. C. Lo, B. G. Brownlee, N. J. Bunce, *Water Res.* **40** (2006) 655
21. R. A. Frank, R. Kavanagh, B. K. Burnison, G. Arsenault, J. V. Headley, K. M. Peru, G. Van der Kraak, R. Kavanagh, B. K. Burnison, G. Arsenault, J. V. Headley, *Chemosphere*, **72** (2008) 1309
22. R. A. Frank, R. Kavanagh, B. K. Burnison, G. Arsenault, J. V. Headley, K. M. Peru, G. Van Der Kraak, K. R. Solomon, *J. Environ. Sci. Health, Part A.* **73** (2010) 319
23. Q. Ding-Rong, Y. Zheng, X. Jiang, K. Wei, *Anti-Corros. Methods Mater.* **54** (2007) 211
24. B. Niemi, W. St. John, B. Woodward, R. De Groot, G. McGinnis, *Proc.-Annu. Meet. Am. Wood-Preserv. Assoc.* **94** (1998) 168
25. A. M. R. Teixeira, K. C. Dutra, C. H. Muniz, M. A. G. Teixeira, *Prepr. – Am. Chem. Soc., Div. Pet. Chem.* **47** (2002) 1
26. Yu. V. Savinykh, E. E. Sirotkina, *Soversh. Metodov Anal. Neftei*, Akad. Nauk SSSR, Sib. Otd., Tomsk, USSR, 1983, p. 104 (in Russian)
27. G. G. Ashumov, L. M. Kosheleva, B. A. Gadzhieva, *Sbornik Trudov - Akademiya Nauk Azerbaidzhanskoi SSR, Institut Neftekhimicheskikh Protsessov im. Yu. G. Mamedalieva* **8** (1977) 77 (in Russian)
28. J. V. Headley, K. M. Peru, D. W. McMartin, M. Winkler, *J. AOAC Int.* **85** (2002) 182
29. V. S. Ćirin-Novta, S. E. Kevrešan, K. N. Kuhajda, J. E. Kandrač, Lj. M. Grbović, P. Rodić, *Acta Period. Technol.* **34** (2003) 49
30. E. N. Polyakova, *Metody opredeleniya fitogormonov i fenolov v semenah*, Nauka, Leningrad, USSR, 1979, p. 12 (in Russian)
31. B. G. Coombe, D. Cohen, L. G. Paleg, *Plant Physiol.* **42** (1967) 113
32. M. Kamaluddin, J. Zwiazek, *Tree Physiol.* **22** (2002) 1265
33. K. G. Apostol, J. J. Zwiazek, M. D. MacKinnon, *Plant Soil* **263** (2004) 183
34. S. A. Armstrong, J. V. Headley, K. M. Peru, J. J. Germida, *J. Environ. Sci. Health, Part A.* **43** (2008) 26
35. S. A. Armstrong, Ph. D. Thesis, University of Saskatchewan, Saskatoon, Canada, 2008
36. K. V. Thomas, K. Langford, K. Petersen, A. J. Smith, K. E. Tollefsen, *Environ. Sci. Technol.* **43** (2009) 8066.

Journal of the Serbian Chemical Society
JSCS-info@shd.org.rs • www.shd.org.rs/JSCS
J. Serb. Chem. Soc. *77* (2) 159–176 (2012)
JSCS–4258
UDC 547.262+546.48:549.323.4–099
Original scientific paper

Oxidative stress in rat liver during acute cadmium and ethanol intoxication

TATJANA RADOSAVLJEVIĆ[1]*, DUŠAN MLADENOVIĆ[1], MILICA NINKOVIĆ[2], DANIJELA VUČEVIĆ[1], IVAN BORIČIĆ[3], RADA JEŠIĆ-VUKIĆEVIĆ[4], TAMARA ŠLJIVANČANIN[1], SRDJAN LOPIČIĆ[1] and VERA TODOROVIĆ[5]

[1]Department of Pathophysiology, School of Medicine, University of Belgrade, Serbia, [2]Institute for Medical Research, Military Medical Academy, Belgrade, Serbia, [3]Department of Pathology, School of Medicine, University of Belgrade, Serbia, [4]Institute for Digestive Diseases, Clinical Centre of Serbia, Belgrade, Serbia and [5]Faculty of Stomatology Pančevo, University Business Academy, Novi Sad, Serbia

(Received 30 March, revised 8 July 2011)

Abstract: The aim of this study was to investigate the effects of binge drinking on the prooxidant/antioxidant system in rat liver in acute cadmium (Cd) intoxication. Male Wistar rats were used in the experiments. They were divided into the following groups: 1. control, 2. ethanol-treated group, in five subsequent doses of 2 g kg^{-1}, administered by an orogastric tube, 3. Cd-treated group in a single dose of 2.5 mg kg^{-1}, administered intraperitoneally, 4. group that received Cd 12 h after the last dose of ethanol. Blood and liver samples for determination of oxidative stress parameters, were collected 24 h after treatment. When administered in combination, ethanol and Cd induced a more pronounced increase in the serum and liver malondialdehyde levels than either of the substances alone (p<0.01). Liver manganese superoxide dismutase (MnSOD) activity was increased in both the ethanol- and Cd-treated groups (p<0.01), while liver copper/zinc superoxide dismutase (Cu/ZnSOD) activity was elevated in the Cd group only. However, when administered in combination, ethanol and Cd induced a more pronounced decrease in liver MnSOD and Cu/ /ZnSOD activity 24 h after treatment (p<0.01). Based on our study, it can be concluded that ethanol may act synergistically with Cd in inducing lipid peroxidation and reduction in liver SOD activity.

Keywords: ethanol; reactive oxygen species; cadmium; liver injury; rat.

INTRODUCTION

Cadmium is one of the most toxic substances in the environment due to its toxic effects on multiple organ systems and long elimination half-time.[1] The initial site of its accumulation is liver; hence, acute exposure to large Cd doses re-

* Corresponding author. E-mail: tatjana.radosavljevic@mfub.bg.ac.rs; tanjamm@med.bg.ac.rs
doi: 10.2298/JSC110330174R

sults in liver injury. Morphologic changes in the liver that follow acute Cd exposition depend on the administered dose and on time when these changes are observed and may vary from dilation of the rough endoplasmic reticulum with loss of ribosomes to hepatocellular necrosis, becoming evident 10–12 h after exposure.[2] The mechanisms of acute Cd hepatotoxicity are not completely understood. Cd ions have a high affinity for thiol groups and form cadmium–thiol complexes. Interaction of Cd ions with thiol-containing molecules (glutathione, GSH, and metallothionein, MT) could protect cells and body from the toxicity of Cd. MT I and II are small proteins rich in cysteine thiols. Since thiol groups are involved in the function of many enzymes, structure proteins and receptors, the cadmium-thiol complexes possibly disturb many functions of cells. It is strongly believed that the toxic effects develop in two phases. Primary injury to hepatocytes is induced by Cd binding to sulfhydryl groups and their inactivation leads to mitochondrial dysfunction, mitochondrial permeability transition and oxidative stress.[2] Oxidative stress, at least partly, may develop as a result of GSH depletion.[3] An additional direct mechanism of acute Cd hepatotoxicity includes ischemia of hepatocytes due to Cd-induced direct injury of sinusoidal endothelial cells.[4–6] Secondary injury to the liver appears as a result of inflammation initiated by the activation of Kupffer cells. Infiltrating neutrophiles, macrophages, as well as resident cells (hepatocytes, endothelial cells, and stellate cells) synthesize and release various cytokines, chemokines and other proinflammatory mediators, thus aggravating initial injury caused directly by Cd.[2]

Ethanol, an active compound of alcoholic beverages, is a well-known hepatotoxin, when administered either acutely or chronically. Various mechanisms are involved in its hepatotoxicity, including direct damage by ethanol or its metabolite acetaldehyde, oxidative stress, release of endotoxin from gut lumen, induction of immune response and release of various cytokines and proinflammatory mediators from infiltrating leukocytes.[7–12] In addition, ethanol may induce hypoxia of hepatocytes, due to increased consumption of oxygen in ethanol metabolism.[13]

Interactions between ethanol and Cd are of great medical importance, since many people exposed to Cd are also prone to excessive alcohol consumption. Possible interactions between these hepatotoxins have been studied in various investigations, usually in models of chronic Cd intoxication.[14–17] It has been suggested that ethanol modifies Cd metabolism and its effect on the metabolism of other bioelements, including iron, zinc and copper.[14,18] On the other hand, precise data related to interactions between ethanol and Cd during acute intoxication are still lacking from the currently available literature. Since oxidative stress was suggested to be a possible mechanism of both Cd- and ethanol-induced liver injury, the aim of the present study was to investigate the effects of binge

drinking on the prooxidant/antioxidant system in rat liver in acute cadmium intoxication.

EXPERIMENTAL

Animals

The experiment was performed on adult male Wistar rats weighting 220–250 g, raised at the Military Medical Academy, Belgrade. The animals were kept under standard laboratory conditions (temperature 22±2 °C, relative humidity 50±10 %, 12/12 light–dark cycle with lights turned on at 9 am) and had free access to tap water and standard pelleted LM2 food (Veterinary Institute "Subotica", Subotica, Serbia). The diet, which had metabolizable energy of the least 11.5 MJ kg^{-1}, was composed of a maximum of 7 % cellulose, and a minimum of 19 % protein. On the day prior to the sacrifice, the rats were fasted overnight. The study was performed according to the Guidelines for Animal Study No. 282-12/2002 and was approved by the Ethic Committee of the Military Medical Academy for animal experiments.

All animals (n = 32) were randomly divided into the following groups: 1. control, saline--treated group (0.9 % NaCl) (n = 8); 2. ethanol-treated group (E; n = 8) in five subsequent doses of 2 g kg^{-1}, administered at 12 h intervals by the oral route (orogastric tube); 3. cadmium-treated group (Cd; n = 8) in a dose of 2.5 mg kg^{-1} intraperitonally (i.p.); 4. cadmium- and ethanol-treated group (CdE; n = 8). Ethanol was administered to the CdE group in five subsequent doses in the same manner as was employed for the E group. 12 h after the last dose of ethanol, the animals were treated with cadmium in a dose of 2.5 mg kg^{-1} i.p. The animals in the Cd and E group received saline instead of Cd and ethanol, respectively. For oral administration, ethanol was dissolved in distilled water in a 30 % v/v concentration. Cadmium was dissolved in saline (0.9 % NaCl) before intraperitonal administration.

Rats were sacrificed by cervical dislocation 24 h after cadmium administration (or saline for E and control group). Blood samples for determination of oxidative stress parameters were collected from the right side of the heart. For the same purpose, livers were excised and stored as described below.

Analysis

Liver samples for biochemical analysis were homogenized on ice (Ultrasonic homogenizer Sonopul), in cold buffered 0.25 M sucrose medium (Serva, Heidelberg, New York), 10 mM phosphate buffer (pH 7.0) and 1.0 mM ethylenediaminetetraacetic acid (EDTA) (Sigma, USA). The homogenates were centrifuged at 2000×g for 15 min at 4 °C (Eppendorf centrifuge 5804 R). The crude sediments were dissolved in the sucrose medium and centrifuged in the same manner. The supernatants were transferred into tubes and centrifuged at 3200×g for 30 min at 4 °C. The obtained sediments were dissolved in deionized water. After one hour of incubation, the samples were centrifuged at 3000×g for 15 min at 4 °C, and supernatants were stored at –70 °C. Proteins were determined by the Lowry method using bovine serum albumin as the standard.[19]

Lipid peroxidation analysis in the plasma and liver homogenates was measured as malondialdehyde (MDA) production, assayed in the thiobarbituric acid reaction as described by Girotti *et al*.[20] The results are expressed as μmol L^{-1} in the plasma or nmol mg^{-1} proteins in the liver homogenates.

The serum concentration of nitrates and nitrites (NO_x) as a measure of nitric oxide (NO) production was determined using Griess reagent. The nitrates were reduced to nitrites by incubating the serum sample with a nitrate reductase and the total amount of nitrite was then

determined by the Griess method. With nitrites, the Griess reagent forms a purple azo dye, which can be measured spectrophotometrically at 492 nm (Ultrospec 2000 spectrophotometer, Pharmacia Biotech).[21]

The thiol group of GSH reacts with DTNB (5,5'- dithiobis[2-nitrobenzoic acid], Ellman reagent) and produces yellow colored 5-mercapto-2-nitrobenzoic acid (TNB). The mixed disulfide, GSTNB that is concomitantly produced, is reduced by glutathione reductase to recycle the GSH and produce more TNB. The rate of TNB production is directly proportional to the concentration of GSH in the deproteinized sample. Measurement of the absorbance of TNB at 414 nm provides an accurate estimation of GSH in the sample and a GSH standard curve.[22]

Total content of sulfhydryl groups (–SH) in the plasma was measured spectrophotometrically at 412 nm in phosphate buffer (0.20 M + 2.0 mM EDTA, pH 9) using 5,5'--dithiobis[2-nitrobenzoic acid] (DTNB, 0.01 M, Sigma).[23]

Total superoxide dismutase (EC1.15.1.1.;SOD) activity in the liver was measured spectrophotometrically, as the inhibition of epinephrine auto-oxidation at 480 nm. After addition of 10 mM epinephrine (Sigma, USA), the analysis was performed in sodium carbonate buffer (50 mM, pH 10.2; Serva, Heidelberg, New York) containing 0.1 mM EDTA (Sigma, St. Louis, CA, USA). Samples for MnSOD were previously treated with 8 mM potassium cyanide (KCN) (Sigma, USA) and then analyzed as described.[24]

For all analyses, three probes were used.

Histological examination

For light microscopic evaluation, the liver tissues were fixed in 10 % neutral buffered formaldehyde and embedded in paraffin wax. Sections from paraffin blocks were cut at 5 mm, mounted on slides, stained with Masson Trichrome and examined by a Leica DFC280 light microscope.

Chemicals

All reagents and chemicals were of analytical grade or higher purity. Ethanol was purchased from Merck (Germany). Cadmium was obtained from Sigma (USA).

Statistical analysis

The results are expressed as means±*SD*. For testing the difference among groups, one--way analysis of variance with Fisher's post hoc test was used. The difference was considered statistically significant for $p<0.05$. Statistica 7.0 was used for the statistical analysis.

RESULTS

The obtained results showed that the liver MDA level was significantly higher in the groups that received ethanol (27.82±4.42 nmol mg^{-1} prot.) or cadmium (73.54±11.62 nmol mg^{-1} prot.) in comparison with the control group (14.19±3.23 nmol mg^{-1} prot.) 24 h after treatment ($p<0.05$ and $p<0.01$, respectively). Previous binge drinking was found to induce a more pronounced increase in the liver MDA level (86.62±22.09 nmol mg^{-1} prot.) than cadmium alone ($p<0.01$). The serum MDA concentration was significantly higher in all the treated animals. The highest MDA concentration (about 120 % higher than in control group) was measured in the serum of animals that were co-exposed to ethanol and cadmium (266.59±23.62 μmol L^{-1}).

The serum nitrates and nitrites (NO_x) concentration was significantly higher in the ethanol and in the cadmium-treated group (7.618±0.907 and 16.374±1.821 μmol L^{-1}, respectively) in comparison with the control group (121.65±6.82 μmol L^{-1}), as well as in the Cd-treated group compared to the ethanol group, 24 h after treatment (p<0.01). Moreover, administration of cadmium 12 h after the last dose of ethanol caused a significant rise in the serum NO_x concentration (16.079± ±2.546 μmol L^{-1}) in comparison with group that received ethanol alone (p<0.01) (Fig. 1). No significant difference in the NO_x concentration was detected between the Cd and CdE group (p>0.05).

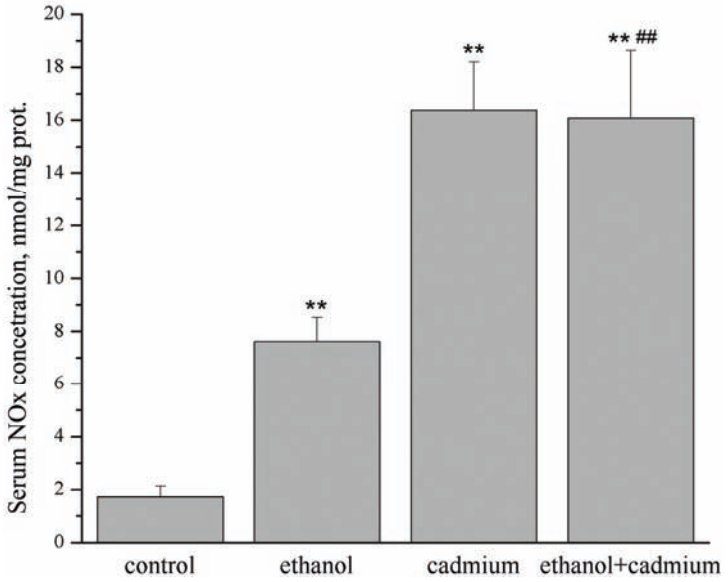

Fig. 1. Serum concentration of nitrites and nitrates (NO_x) in animals 24 h after treatment. For statistical evaluation, the one-way Anova with the Fisher *post hoc* test were used; **p<0.01 *vs.* the control group, $^{\#\#}p$<0.01 in comparison with the ethanol-group.

The liver GSH content was found to be significantly decreased in the ethanol-treated group (20.26±2.57 nmol mg^{-1} prot.) in comparison with the control group (29.41±4.21 nmol mg^{-1} prot.) (p<0.01). In contrast, a single dose of cadmium did not induce significant changes in the GSH level 24 h after administration (p>0.05). However, prior ethanol treatment induced a significant decrease in the liver GSH content (20.42±3.08 nmol mg^{-1} prot.) (p<0.01), but the extent of this decrease was not different from the decrease induced by ethanol alone (Fig. 2).

The plasma concentration of total sulfhydryl groups was significantly lower in ethanol-treated group (0.239±0.031 μmol L^{-1}) in comparison with the control animals (0.372±0.047 μmol L^{-1}) 24 h after ethanol administration (p<0.01). In

contrast, cadmium induced a significant increase in plasma concentration of total sulfhydryl groups (0.461±0.078 μmol L^{-1}) in the same time interval (p<0.05). When animals were exposed to ethanol prior to cadmium, a significant decrease in total sulfhydryl group concentration (0.225±0.020 μmol L^{-1}) was detected in comparison with animals that received cadmium alone (0.461±0.078 μmol L^{-1}) (p<0.01) (Fig. 3). However, no significant change was observed between E and CdE groups (p>0.05).

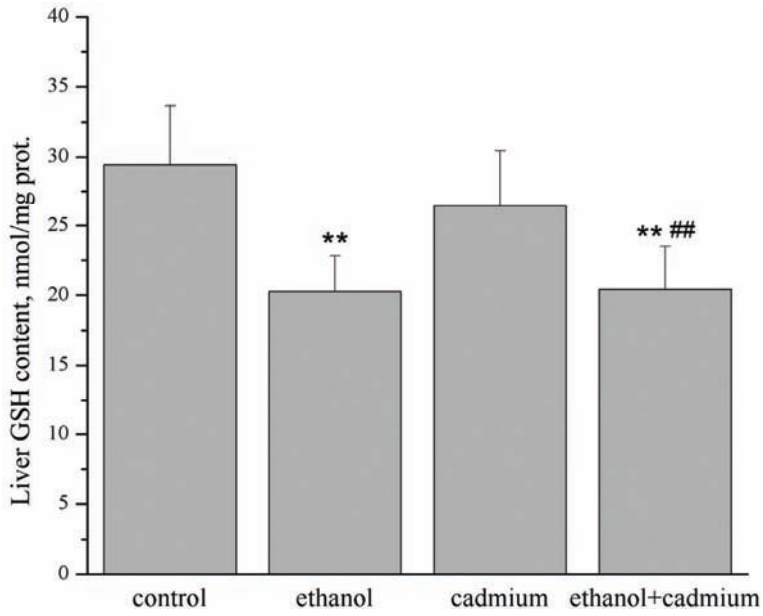

Fig. 2. The liver glutathione (GSH) level in the experimental animals. For statistical evaluation, the one-way Anova with the Fisher *post hoc* test were used. **p<0.01 *vs.* the control group, $^{\#\#}p$<0.01 in comparison with the Cd-group.

Total liver SOD activity was significantly higher 24 h after cadmium administration (2204.7±111.8 U mg^{-1} prot.) in comparison with the control group (570.5±27.3 U mg^{-1} prot.) (p<0.01). However, the total liver SOD activity was significantly lower in the CdE group (346.7±67.7 U mg^{-1} prot.) in comparison with Cd and E group (2204.7±111.8 and 563.2±29.6 U mg^{-1} prot., respectively) (p<0.01) (Fig. 4). No significant change was found in the total liver SOD activity in animals that received ethanol in comparison with control animals (p>0.05).

In addition to the total SOD activities, the activities of the hepatic isoforms of this enzyme were altered in a different manner in the various experimental groups. Cadmium was found to induce a significant increase of the activities of both SOD isoforms, but to a different extent. The Cu/Zn SOD activity was approximately fivefold higher in comparison with the control group (1931.9±111.2 and

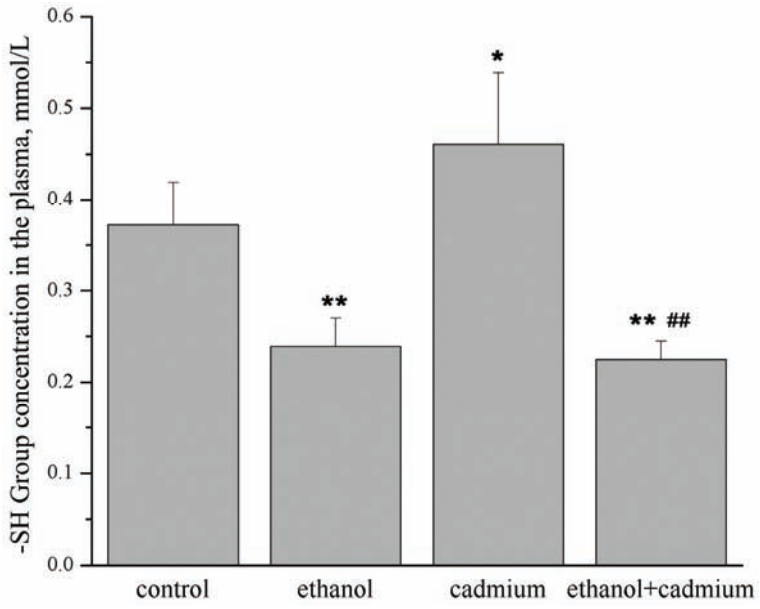

Fig. 3. Plasma sulfhydryl group (–SH) concentration in the experimental animals. For statistical evaluation, the one-way Anova with the Fisher *post hoc* test were used. *p<0.05, **p<0.01 *vs*. the control group, $^{\#\#}p$<0.01 in comparison with the Cd-group.

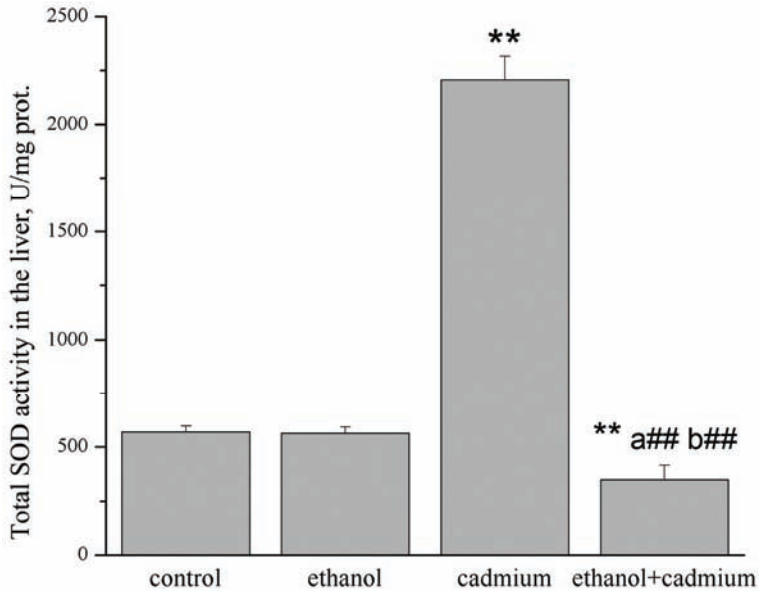

Fig. 4. Total liver superoxide dismutase activity (SOD) in the experimental animals. For statistical evaluation, the one-way Anova with the Fisher *post hoc* test were used. **p<0.01 *vs*. the control group, $^{\#\#}p$<0.01 in comparison with the ethanol- (a) or cadmium-treated group (b).

402.7±6.7 U mg^{-1} prot. in the Cd and control group, respectively) (p<0.01), while the rise in the MnSOD activity was only, approximately, 60 % in the Cd group (272.8±19.8 U mg^{-1} prot.) compared to the control group (167.8±30.9 U mg^{-1} prot.) (p<0.01). A similar rise in the MnSOD activity was measured in ethanol-treated animals (292.4±22.9 U mg^{-1} prot.). In contrast to cadmium, ethanol administration was followed by a significant decrease in the Cu/ZnSOD activity (270.8±40.8 U mg^{-1} prot.) (p<0.01) (Fig. 5). While the administration of either cadmium or ethanol caused a significant increase in the liver MnSOD activity; co-exposure of rats to these hepatotoxins induced a significant fall in its activity (86.2±19.3 U mg^{-1} prot.) in comparison with the control group (167.8± ±30.9 U mg^{-1} prot.) (p<0.01) (Fig. 6). In addition, the lowest Cu/ZnSOD activity was detected in the CdE group (260.5±73.6 U mg^{-1} protein), but its activity was not significantly different in comparison with the E group (p>0.05).

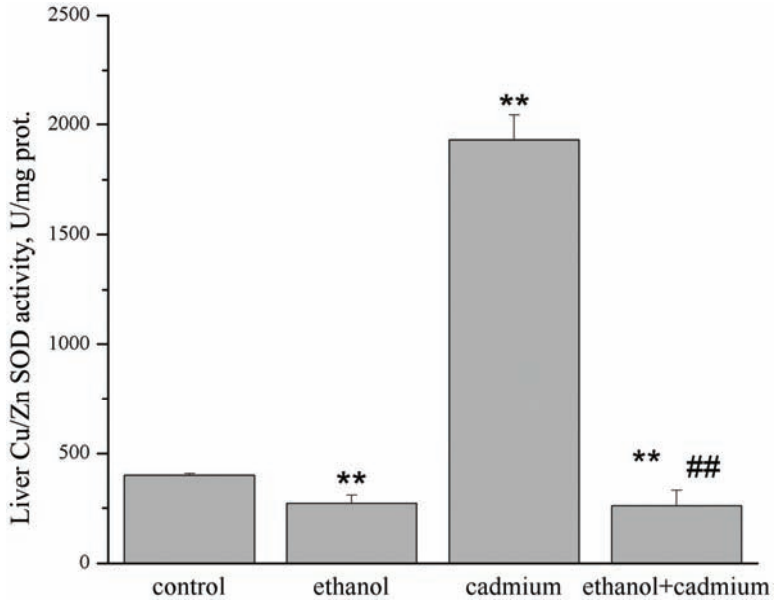

Fig. 5. Copper/zinc superoxide dismutase (Cu/ZnSOD) activity in the hepatocytes of treated animals. For statistical evaluation, the one-way Anova with the Fisher *post hoc* test were used. **p<0.01 *vs.* control group, $^{\#\#}p$<0.01 in comparison with the animals treated with cadmium alone.

Histological analysis

Histological examination confirmed liver damage in all groups that received cadmium or ethanol. Cadmium in a dose of 2.5 mg kg^{-1} caused vacuolar degeneration of hepatocytes with focal necrosis 24 h after administration. Ethanol was found to cause mild congestion with focal necrosis. Additionally, an apoptotic

body may be observed in the pericentral area. Kupffer cells were more numerous than in the control liver. In rats co-exposed to cadmium and ethanol, more extensive liver damage was observed in comparison with the ethanol- or cadmium-treated groups. A severe congestion with a prominent mononuclear infiltrate may be detected in the pericentral area. Vacuolar degeneration and necrosis were more pronounced in this group in comparison with the animals treated with cadmium (Fig. 7).

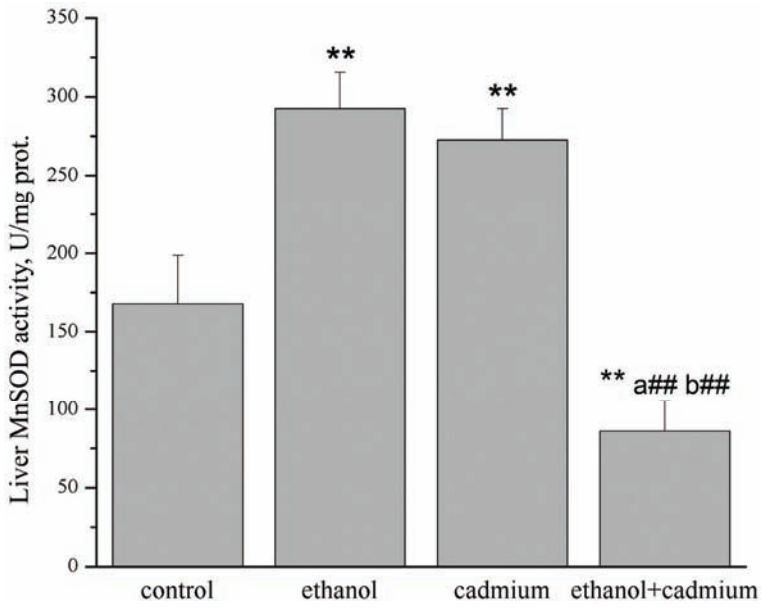

Fig. 6. Manganese superoxide dismutase (MnSOD) activity in the hepatocytes of treated animals. For statistical evaluation, the one-way Anova with the Fisher *post hoc* test were used. $^{**}p<0.01$ *vs*. control group, $^{\#\#}p<0.01$ in comparison with the animals treated with ethanol (a) or cadmium (b) alone.

DISCUSSION

Cd is a very toxic environmental pollutant that causes the production of reactive oxygen species (ROS), such as superoxide anions, hydrogen peroxide, hydroxyl radicals and NO,[1,25,26] thus impairing the balance between prooxidant and antioxidant systems.[27–29] In the present study, oxidative stress was found to be induced in the liver during acute co-exposure to ethanol and Cd. The results showed that ethanol and Cd increased the serum and liver MDA concentrations 24 h after administration. This indicates that lipid peroxidation is an important mechanism of acute Cd- and ethanol-induced hepatotoxicity. The role of lipid peroxidation in acute Cd intoxication was demonstrated in numerous studies using various doses and routes of its administration.[30–32] Cd in a dose of 2.5 mg

kg^{-1} body weight increased the MDA levels in the liver, kidney, and blood of rats 24 h after administration.[33,34] It was also observed that prior administration of antioxidants prevented Cd toxicity.[29,32,35–38] In accordance with the significant role of lipid peroxidation in the pathogenesis of acute Cd intoxication is also the fact that a rise in the concentrations of substances that react with thiobarbituric acid (TBARS) is less pronounced after previous α-tocopherol administration.[35] However, antioxidant substances may prevent Cd hepatotoxicity by various additional mechanisms, such as increasing metallothioneine (MT) and endothelial nitric oxide (eNOS) expression,[37] increasing the activities of antioxidant enzymes and improvement of the GSH level.[29,35,36]

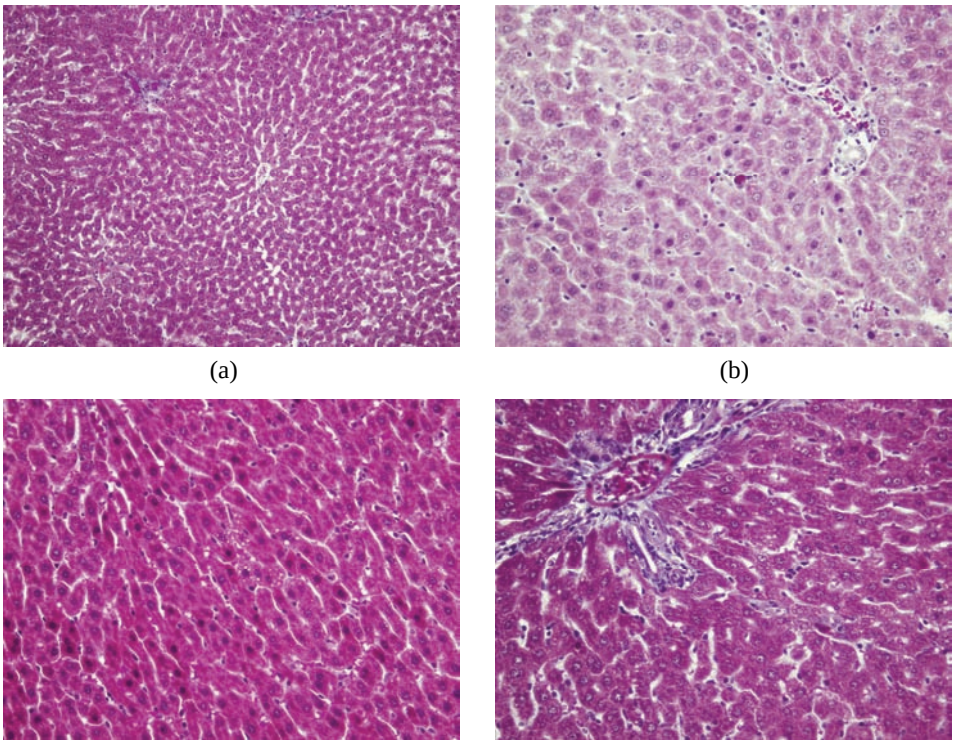

Fig. 7. a) Normal liver histology in the control group (Masson Trichrome X200); b) focal necrosis, increased number of Kupffer cells and an apoptotic body in the ethanol-treated group (Masson Trichrome X400); c) vacuolar degeneration in the pericentral area, necrosis and mild congestion in the cadmium-treated group (Masson Trichrome X400); d) severe vacuolar degeneration, necrosis and a mononuclear infiltrate with congestion in animals treated with cadmium and ethanol (Masson Trichrome X400).

In the present study, prior binge drinking was found to potentiate Cd-induced lipid peroxidation in the liver. This potentiation may lead to more exten-

sive vacuolar degeneration, inflammatory infiltration and necrosis of hepatocytes, observed after ethanol and Cd administration than after either of these hepatotoxins alone. Possible synergistic effects of ethanol and Cd are not surprising, since previous studies indicated that even acute ethanol intoxication causes lipid peroxidation in the liver, thus contributing to acute ethanol-induced liver injury.[39–41]

Serum NO_x, indicators of NO production, were increased in all groups treated with either ethanol or Cd, 24 h after administration. These findings suggest that reactive nitrogen species (RNS) are involved in acute ethanol- and Cd-induced liver injury. The role of NO in acute Cd liver damage is still not completely understood. In some studies, it was found that Cd administration at a dose of 30 μmol kg^{-1} in rats caused a twofold increase in the serum nitrate concentration 48 h after treatment.[42] However, administration of inducible nitric synthase (iNOS) inhibitors did not prevent Cd-induced liver injury; thus indicating that other sources, independent of iNOS, are responsible for the increased NO production.[43] A possible mechanism of NO-induced liver injury may be an increase in free cellular Cd level, due to the release of Cd from its association with MT. The mechanism by which NO mediates the release of Cd from MT appears to involve NO_x in liver injury. Nitrosation of intracellular GSH by NO_x is thought to play a key role in detoxication of this reactive intermediate. NO_x could nitrosate cysteine residues coordinated to Cd, resulting in the formation of *S*-nitrosothiol adducts and the release of Cd from MT. While such an occurrence would indeed result in the detoxification of NO_x, it would simultaneously "activate" Cd, posing a new toxicological threat to cells.[44]

Cd bound to MT was found to exert no hepatotoxic effects.[45,46] In contrast, Qu *et al.*[47] suggested that a liver-selective NO donor, which is metabolized by cytochrome P450 enzymes, protects against Cd hepatotoxicity. It was suggested that the protective effect of NO is mediated by potentiation of the Cd-induced increase in MT synthesis.[47] These discrepancies may be related to the dual effects of NO, depending on its amount. In low concentrations, NO exerts hepatoprotective effects, while in high concentrations, it reacts with superoxide radicals to form peroxynitrite as a potent oxidant.[48–50] Since the importance of NO as a mediator of liver injury depends on its amount and source,[49] its precise role in acute Cd-induced liver injury should be further investigated.

It has been reported that ethanol causes an increase in NO synthesis.[51] Alcohol administration increases inducible iNOS expression,[52] which, together with the alcohol-mediated increase in superoxide anion formation, could increase hepatic peroxynitrite formation. Peroxynitrite and/or peroxynitrite-generated reactive intermediates can nitrate proteins and can damage lipids and DNA.[53] The present results, in accordance with other studies,[54,55] show that ethanol induced a significant increase in the serum NO_x concentration, although its level was significantly lower than after Cd administration. This significant increase of NO_x in

the Cd-treated group could be explained by the more pronounced toxic effects of Cd compared to ethanol (Cd is a pollutant ranked eighth in the top 20 hazardous substances).[33] When administered prior to Cd, ethanol had no influence on the Cd-induced rise in NO_x generation. This indicates that binge drinking does not aggravate nitrosative stress induced by acute Cd exposition.

The obtained results showed that the liver GSH content was decreased in the ethanol-treated animals 24 h after its administration. Other studies indicated that GSH depletion plays an important role in ethanol-induced liver injury.[40,41,56,57] Among others, GSH depletion in the liver is recognized as a mechanism that may contribute to acute ethanol-induced oxidative injury within a few hours after intoxication. It was shown that silymarin and betaine exerted protective effects on binge-drinking mice by reducing GSH depletion.[41,57]

In the present study, Cd did not induce any change in the reduced GSH level in the liver 24 h after its administration. GSH is an intracellular non-enzymatic antioxidant that provides the first line of defense against oxidative injury. Similar to the present study, Siegers *et al.*[58] showed no change in the liver GSH level in acute Cd-hepatotoxicity. This indicates that GSH depletion is not a major mechanism of oxidative stress in acute Cd-induced liver injury. These results may be surprising, since the major direct Cd effect refers to its binding to sulfhydryl groups. However, Cd-induced inflammation in the liver is another important mechanism for Cd-induced oxidative stress. The activation of Kupffer cells is an important source for Cd-induced inflammatory mediators such as IL-1β, TNFα, IL-6, and IL-8, which in turn contribute to Cd-generated free radicals in the liver. Moreover, mitochondrion is an important target of Cd toxicity. It has been proposed that Cd initially binds to protein thiols in the mitochondrial membrane, affects mitochondrial permeability transition, inhibits the respiratory chain reaction and then generates ROS.[59] In addition, the lack of change in the liver GSH content could be explained by the simultaneous activation of adaptive mechanisms in hepatocytes. This adaptive response was also suggested by other studies that found an increase in GSH content within 24 h after acute Cd exposition.[60] However, this effect is dependent on the administered dose, and time and route of application.[35,60] Inside the cell, Cd elicits a number of reactions that may lead to stress adaptation and survival. These processes are mediated by signaling pathways that induce up-regulation of various protective molecules.[61] It was found that MT is relevant in Cd toxicity and survival.[62] Namely, the different localization and physiological functions of MTs, including the metal-free (apo-MT) and metal-bound (holo-MT) forms, in various organs and intracellular organelles affect the redox and energy status of cells. The double-edged role of MT in organ toxicity is emphasized by its involvement as a protein preventing (antioxidant, chelator) and mediating (carrier) of Cd toxicity.[62]

Kitamura and Hiramatsu[63] reviewed recent evidence for the involvement of ER stress signaling and the unfolded protein response (UPR) in Cd apoptosis *in vivo* and *in vitro*. Cd-induced cellular stress disturbs the proper folding of membranes and secreted proteins in the ER and triggers UPR, which determines whether damage control or death by apoptosis occurs. ROS may operate up- or downstream of the ER stress. The superoxide radical anion, but not H_2O_2, appears to trigger selectively activation of the pro-apoptotic branches of the UPR induced by Cd. In addition to the ER stress-UPR signaling, other pathways with broad anti-apoptotic potential are also activated by Cd and ROS, namely calcium and NF-κB signaling[63].

Additionally, Cuypers *et al*.[64] described the mechanisms and sources of ROS formation in the presence of Cd, which involved enhancement of ROS formation by the mitochondrial respiratory chain and induction of NADPH oxidases (NOX) enzymes. Induction of these enzymes play the key role of ROS in cellular adaptation to Cd. NADPH oxidases function as multi-component enzymes, and use electrons derived from intracellular NADPH to generate O_2^- from O_2. The NOX family of ROS-generating NADPH oxidases consists of seven members that participate in important cellular processes, related to signaling, cell proliferation and apoptosis. Thus, increased NOX4 gene expression probably may have led to increased NOX activity in mice kidneys following Cd exposure in this tissue. The exact role of NOX4 in Cd toxicity has not been described, but it may be linked to the production of free radicals for signal transduction to activate the antioxidative defense system or adaptive mechanisms.[64] NADPH-dependent oxidase could trigger signaling leading to protective measures in HepG2 cells.[65]

Generally, potentially all NOX expressing cells can be targeted by Cd and the influence of Cd on NADPH oxidase activity could result in signaling leading to the onset of cellular protection mechanisms or, alternatively, of cell death. Controlled levels of ROS production (*via* NADPH oxidase or other sources) are therefore necessary to ensure correct ROS levels for signaling or defense. Persistent NOX expression results from an amplification loop triggered by ROS and ROS-sensitive transcription factors, whereas a defense loop is mediated by ROS, which also trigger up-regulation of protective antioxidative mechanisms.[64]

The role of oxidative stress in chronic cadmium intoxication is well known. Chronic cadmium exposition inhibits the activity of antioxidant enzymes, including catalase, MnSOD, and Cu/ZnSOD.[28] Moreover, it is reported that chronic exposition to cadmium decreases the antioxidant capacity of hepatocytes, due to glutathione depletion and sulfhydryl groups inactivation in the liver.[35] It was shown that prior α-tocopherol administration reduced cadmium-induced GSH depletion in the liver.[35] On the other hand, adaptive mechanisms after chronic, low-dose exposure, including induction of MT, GSH, and cellular antioxidants, could diminish Cd-induced oxidative stress.[59] The increase in GSH content in

hepatocytes is probably due to the expression of gamma-glutamylcysteine synthetase, which catalyzes the key reaction of GSH biosynthesis.[66]

In the present study, co-exposure to ethanol and Cd was found to induce GSH depletion to the same extent as exposure to ethanol alone. This indicates that ethanol does not interact with Cd in inducing GSH depletion. Changes in liver GSH levels in these groups were accompanied by similar changes in the plasma –SH group concentration. Plasma proteins, as sources of –SH groups, reflect systemic toxic damages, which are caused by protein oxidation upon the action of Cd.

The results obtained in the present study showed that the total liver SOD activity was not altered in ethanol-treated animals 24 h after binge drinking, while Cd was found to increase its activity at the same time-point. However, the activities of its isoenzymes were significantly different in both groups. Ethanol was found to induce a significant increase in MnSOD with a simultaneous decrease in the Cu/ZnSOD activity. The increase in the MnSOD activity may be a result of an adaptive response of the hepatocytes to an increased production of ROS. Since mitochondria are the major source of ROS,[11] it is not surprising that activity of mitochondrial isoenzyme was increased after binge drinking. Similar results were obtained within 6 h after administration of a single dose of ethanol.[67] In contrast, Cd induced a significant increase in the activities of both SOD isoenzymes, with a more pronounced rise in the Cu/ZnSOD activity. The results of other studies related to the influence of Cd on SOD activity are contradictory. In accordance with the present study, Cd in a dose of 0.4 mg kg^{-1} was found to induce an adaptive increase in SOD activity.[34] In contrast, high doses of Cd (5 mg kg^{-1}) caused a decrease in both mitochondrial and cytosolic SOD activity,[68] probably because the antioxidative capacity of the hepatocytes was surmounted. *In vitro* investigations showed that MnSOD is more vulnerable to inhibitory effect of Cd than Cu/ZnSOD.[33] Possible mechanisms of greater sensitivity of MnSOD to Cd may be a substitution of Cd for manganese at active site of this enzyme or binding of Cd to another site at the active centre of the enzyme.[33]

When animals were co-exposed to ethanol and Cd, the activities of both SOD isoenzymes were decreased in comparison with the control group. Additionally, no adaptive response was observed 24 h after treatment. This finding, together with increased lipid peroxidation, indicates that prior binge drinking potentiates Cd-induced ROS production, thus causing decreased activities of these enzymes. This increased ROS generation could be responsible for suppression of the adaptive increase in MnSOD and Cu/ZnSOD activity.

CONCLUSIONS

According to this study, it can be concluded that oxidative stress plays an important role in liver injury caused by acute Cd intoxication and binge ethanol

drinking. However, its role in the interactions between these hepatotoxins remains incompletely understood. This study suggests that previous binge drinking may act synergistically with cadmium in inducing lipid peroxidation and consumption of SOD, especially its mitochondrial isoenzyme. Ethanol and cadmium, in contrast, were found to induce no synergistic effect on RNS production and glutathione depletion. Although the type of interactions between these agents are still unclear, increased lipid peroxidation and decreased SOD activity after co-exposure to ethanol and cadmium indicate that application of antioxidant therapy may be reasonable in the early phase of acute ethanol and cadmium intoxication.

Acknowledgements. This work was supported by the Ministry of Education and Science of Republic of Serbia, Grant No. 175015. The authors are also thankful to colleagues from Institute for Medical Research of the Military Medical Academy in Belgrade for providing useful assistance for the experimental procedures, as well as Vladimir Miljković for his technical assistance during experimental procedures.

И З В О Д

ОКСИДАТИВНИ СТРЕС У ЈЕТРИ ПАЦОВА У ТОКУ АКУТНЕ ИНТОКСИКАЦИЈЕ КАДМИЈУМОМ И ЕТАНОЛОМ

ТАТЈАНА РАДОСАВЉЕВИЋ[1], ДУШАН МЛАДЕНОВИЋ[1], МИЛИЦА НИНКОВИЋ[2], ДАНИЈЕЛА ВУЧЕВИЋ[1], ИВАН БОРИЧИЋ[3], РАДА ЈЕШИЋ-ВУКИЋЕВИЋ[4], ТАМАРА ШЉИВАНЧАНИН[1], СРЂАН ЛОПИЧИЋ[1] и ВЕРА ТОДОРОВИЋ[5]

[1]Институт за патофизиологију, Медицински факултет, Универзитет у Београду, Др Суботића 9, [2]Институт за медицинска истраживања, Војномедицинска академија, Црнотравска 17, Београд, [3]Институт за патологију, Медицински факултет, Универзитет у Београду, Др Суботића 1, [4]Институт за болести дигестивног система, Клинички центар Србије, Београд и [5]Стоматолошки факултет Панчево, Универзитет Привредна Академија у Новом Саду

Циљ студије је био да се испита ефекат викенд пијанства на прооксидантни/антиоксидантни систем у јетри пацова у акутној интоксикацији кадмијумом (Cd). У експерименту су коришћени пацови, мужјаци Wistar соја подељени у следеће групе: 1. контрола, 2. животиње третиране етанолом (5 појединачних доза од по 2 g kg^{-1} путем орогастричне сонде), 3. животиње третиране Cd (појединачна доза од 2.5 mg kg^{-1} интраперитонеално), 4. животиње које су примиле Cd 12 сати после последње дозе етанола. За одређивање параметара оксидативног стреса узимани су узорци крви и јетре, 24 сата након третмана. Када су администрирани у комбинацији, етанол и кадмијум изазивају значајно повећање нивоа малондиалдехида (MDA) у серуму и јетри, него када су ове супстанце даване појединачно (p<0.01). Активност манган-супероксид-дисмутазе (MnSOD) је повећана у групама третираним етанолом и Cd (p<0.01), док је активност бакар/цинк-супероксид-дисмутазе (Cu/ /ZnSOD) повећана само у групи третираној Cd. Међутим, када је етанол администриран заједно са Cd дошло је до значајног смањења активности MnSOD и Cu/ZnSOD у јетри 24 сата после третмана (p<0.01). На основу нашег истраживања може се закључити да етанол може деловати синергистички са кадмијумом у настанку липидне пероксидације и смањењу активности SOD у јетри.

(Примљено 30. марта, ревидирано 8. јула 2011)

REFERENCES

1. P. Andujar, L. Bensefa-Colas, A. Descatha, *Rev. Med. Interne* **31** (2010) 107
2. L. E. Rikans, T. Yamano, *Biochem. Toxicol*. **14** (2000) 110
3. D. Bagchi, M. Bagchi, E. A. Hassoun, S. J. Stohs, *Biol. Trace Elem. Res.* **52** (1996) 143
4. C. V. Nolan, Z. A. Shaikh, *Life Sci*. **39 (**1986) 1403
5. W. C. Prozialeck, J. R. Edwards, J. M. Woods, *Life Sci.* **79** (2006) 1493
6. W. C. Prozialeck, J. R. Edwards, D. W. Nebert, J. M. Woods, A. Barchowsky, W. D. Atchison, *Toxicol. Sci*. **102** (2008) 207
7. P. Dandona, A. Aljada, A. Bandyopadhyay, *Trends Immunol*. **27** (2004) 4
8. G. M. Thiele, T. K. Freeman, L. W. Klassen, *Semin. Liver Dis.* **24** (2004) 273
9. E. Albano, *Proc. Nutr. Soc.* **65** (2006) 278
10. A. Dey, A. I. Cederbaum, *Hepatology* **43** (2006) S63
11. S. K. Das, D. M. Vasudevan, *Life Sci.* **81** (2007) 177
12. Y. Tang, A. Banan, C. B. Forsyth, J. Z. Fields, C. K. Lau, L. J. Zhang, A. Keshavarzian, *Alcohol. Clin. Exp. Res.* **32** (2008) 355
13. L. Li, S. H. Chen, Y. Zhang, C. H. Yu, S. D. Li, Y. M. Li, *Hepatobiliary Pancreat. Dis. Int.* **5** (2006) 560
14. M. M. Brzóska, J. Moniuszko-Jakoniuk, M. Jurczuk, M. Gałazyn-Sidorczuk, J. Rogalska, *Alcohol Alcohol.* **35** (2000) 439
15. M. M. Brzóska, J. Moniuszko-Jakoniuk, B. Pilat-Marcinkiewicz, B. Sawicki, *Alcohol Alcohol*. **38** (2003) 2
16. M. Jurczuk, M. M. Brzóska, J. Rogalska, J. Moniuszko-Jakoniuk, *Alcohol Alcohol.* **38 (**2003) 202
17. M. Jurczuk, M. M. Brzoska, J. Moniuszko-Jakoniuk, M. E. Gałazyn-Sidorczuk, E. Kulikowska-Karpinska, *Food Chem. Toxicol.* **42** (2004) 429
18. J. Moniuszko-Jakoniuk, M. Gałazyn-Sidorczuk, M. M. Brzóska, M. Jurczuk, M. Kowalczyk, *Bull. Environ. Contam. Toxicol*. **66** (2001) 25
19. O. H. Lowry, N. J. Rosenbrough, A. L. Farr, R. J. Randall, *J. Biol. Chem.* **193** (1951) 265
20. M. Girotti, N. Khan, B. McLellan, *J. Trauma* **31** (1991) 32
21. J. B. Hibbs, R. Taintor, Z. Vavrin, E. Rachlin, *Biochem. Biophys. Res. Commun.* **157** (1989) 87
22. M. E. Anderson, in *The DTNB-GSSG reductase recycling assay for total glutathione (GSH + 1/2GSSG)*, R. A. Greenwald, Ed., CRC Press, Boca Raton, 1986, p 317
23. G. L. Elman, *Arch. Biochem. Biophys*. **82** (1959) 70
24. M. Sun, S. Zigman, *Anal. Biochem.* **90** (1978) 81
25. S. J. Stohs, D. Bagchi, E. Hassoun, M. Bagchi, *J. Environ. Pathol. Toxicol. Oncol.* **20** (2001) 77
26. J. Liu, S. Y. Qian, Q. Guo, J. Jiang, M. P. Waalkes, R. P. Mason, M. B. Kadiiska, *Free Radical Biol. Med.* **45** (2008) 475
27. S. Sarkar, P. Yadav, R. Trivedi, A. K. Bansal, D. Bhatnagar, *J. Trace Elem. Med. Biol*. **9** (1995) 44
28. A. Koyu, A. Gokcimen, F. Ozguner, D. S. Bayram, A. Kocak, *Mol. Cell. Biochem*. **284** (2006) 81
29. A. A. Newairy, A. S. El-Sharaky, M. M. Badreldeen, S. M. Ewedaa, S. A. Sheweita, *Toxicology* **242** (2007) 23

30. S. A. El-Maraghy, M. Z. Gad, A. T. Fahim, M. A. Hamdy, *J. Biochem. Mol. Toxicol.* **15** (2001) 207
31. V. Eybl, D. Kotyzová, M. Bludovská, *Toxicol. Lett.* **151** (2004) 79
32. V. Eybl, D. Kotyzova, J. Koutensky, *Toxicology* **225** (2006) 150
33. E. Casalino, G. Calzaretti, C. Sblano, C. Landriscina, *Toxicology* **179** (2002) 37
34. B. I. Ognjanović, S. D. Marković, S. Z. Pavlović, R. V. Žikić, A. S. Stajn, Z. S. Saičić, *Physiol. Res.* **57** (2008) 403
35. S. Nemmiche, D. Chabane-Sari, P. Guiraud, *Chem.-Biol. Interact.* **170** (2007) 221
36. A. Karadeniz, M. Cemek, N. Simsek, *Ecotoxicol. Environ. Saf.* **72** (2009) 231
37. C. Vicente-Sánchez, J. Egido, P. D. Sánchez-González, F. Pérez-Barriocanal, J. M. López-Novoa, A. I. Morales, *Food Chem. Toxicol.* **46** (2008) 2279
38. L. P. Borges, R. Brandao, B. Godoi, C. W. Nogueira, G. Zeni, *Chem.-Biol. Interact.* **171** (2008) 15
39. K. Nagata, H. Suzuki, S. Sakaguchi. *J. Toxicol. Sci.* **32**(2007) 453
40. E. Albano, *Mol. Aspects Med.* **29** (2008) 9
41. S. J. Kim, Y. S. Jung, Y. do Kwon, Y. C. Kim, *Biochem. Biophys. Res. Commun.* **368** (2008) 893
42. S. Satarug, J. R. Baker, P. E. Reilly, H. Esumi, M. R. Moore. *Nitric Oxide* **4** (2000) 431
43. E. B. Harstad, C. D. Klaassen, *Toxicology* **175** (2002) 83
44. R. R. Misra, J. F. Hochadel, G. T. Smith, J. C. Cook, M. P. Waalkes, D. A. Wink, *Chem. Res. Toxicol.* **9** (1996) 326
45. C. D. Klaassen, J. Liu, *Drug Metab. Rev.* **29** (1997) 79
46. C. D. Klaassen, J. Liu, *Environ. Health Perspect.* **1** (1998) 297
47. W. Qu, J. Liu, R. Fuquay, R. Shimoda, T. Sakurai, J. E. Saavedra, L. K. Keefer, M. P. Waalkes, *Nitric Oxide* **12** (2005) 114
48. J. A. Hinson, S. L. Pike, N. R. Pumford, P. R. Mayeux, *Chem. Res. Toxicol.* **11** (1998) 604
49. M. G. Clemens, *Hepatology* **30** (1999) 1
50. R. Radi, A. Cassina, R. Hodara, C. Quijano, L. Castro, *Free Radical Biol. Med.* **33** (2002) 1451
51. T. Zima, L. Fialova, O. Mestek, M. Janebova, J. Crkovska, I. Malbohan, S. Stipek, *J. Biomed. Sci.* **8** (2001) 59
52. G. J. Yuan , X. R. Zhou, Z. J. Gong , P. Zhang , X. M. Sun, S. H. Zheng, *World J. Gastroenterol.* **12** (2006) 2375
53. A. Venkatraman, S. Shiva, A. Wigley, E. Ulasova, D. Chhieng, S. M. Bailey, V. M. Darley-Usmar, *Hepatology* **40** (2004) 565
54. X. S. Deng, P. Bludeau, R. A. Deitrich, *Alcohol* **34** (2004) 217
55. E. Oekonomaki, G. Notas, I. A. Mouzas, V. Valatas, P. Skordilis, C. Xidakis, E. A. Kouroumalis, *Alcohol Alcohol.* **39** (2004) 106
56. J. C. Fernandez-Checa, N. Kaplowitz, *Toxicol. Appl. Pharmacol.* **204** (2005) 263
57. Z. Song, I. Deaciuc, M. Song, D. Y. Lee, Y. Liu, X. Ji, C. McClain, *Alcohol. Clin. Exp. Res.* **30** (2006) 407
58. C. P. Siegers, M. Schenke, M. Younes, *J. Toxicol. Environ. Health* **22** (1987) 141
59. J. Liu, W. Qu, M. B. Kadiiska, *Toxicol. Appl. Pharmacol.* **238** (2009) 209
60. T. Yamano, M. Shimizu, T. Noda, *Toxicol. Appl. Pharmacol.* **51** (1998) 9
61. J. M. Moulis, F. Thévenod, *Biometals* **23** (2010) 763

62. I. Sabolic, D. Breljak, M. Skarica, C. M. Herak-Kramberger. *Biometals* **23** (2010) 897
63. M. Kitamura, N. Hiramatsu. *Biometals* **23** (2010) 941
64. A. Cuypers, M. Plusquin, T. Remans, M. Jozefczak, E. Keunen, H. Gielen, K. Opdenakker, A. R. Nair, E. Munters, T. J. Artois, T. Nawrot, J. Vangronsveld, K. Smeets, *Biometals* **23** (2010) 927
65. V. Souza, M. Escobar, L. Bucio, E. Hernández , L. E. Gómez-Quiroz, M. C. Gutiérrez Ruiz, *Toxicol. Lett.* **187** (2009) 180
66. A. C. Wild, R. T. Mulcahy, *Free Radical Res.* **32** (2000) 281
67. O. R. Koch, M. E. De Leo, S. Borrello, G. Palombini, T. Galeotti, *Biochem. Biophys. Res. Commun.* **201 (**1994) 1356
68. S. Yalin, U. Comelekoglu, S. Bagis, N. O. Sahin, O. Ogenler, R. Hatungil, *Ecotoxicol. Environ. Saf.* **65** (2006) 140.

Journal of the Serbian Chemical Society
JSCS-info@shd.org.rs • www.shd.org.rs/JSCS
J. Serb. Chem. Soc. *77* (2) 177–185 (2011) UDC 547.584+546.472+542.913:548.7:544.18
JSCS–4259 *Original scientific paper*

Synthesis, crystal structure and computational chemistry research of the zinc(II) complex: [Zn(pt)(Biim)$_2$]

FEI TENG[1], NAN JIANG[2], ZHONGHUI WANG[3], YUNCHENG CUI[2] and JIAJUN WANG[2,4]*

[1]*Mathematics College of Jilin Normal University, Siping 136000, China,* [2]*Key Laboratory of Preparation and Application of Environmental Friendly Materials (Jilin Normal University), Ministry of Education, Chemistry Department of Jilin Normal University, Siping 136000, China,* [3]*Acrylonitrile Plant of PetroChina Jilin Petrochemical Company, Jilin 132021, China and* [4]*State Key Laboratory of Theoretical and Computational Chemistry, Institute of Theoretical Chemistry Jilin University, Changchun 130023, China*

(Received 9 December 2010, revised 7 September 2011)

Abstract: The title metal–organic coordination complex **1**, [Zn(pt)(Biim)$_2$] (pt = = phthalate, benzene-1,2-dicarboxylate, Biim = 2,2'-biimidazole), was obtained by hydrothermal synthesis and characterized by single crystal X-ray diffraction. The complex crystallized as monoclinic, space group $P2_1/n$ with a = 8.5466(15) Å, b = 11.760(2) Å, c = 20.829(4) Å, β = 95.56(2)°, V = 2083.5(6) Å^3, Mr = = 497.78, Dc = 1.587 g cm^{-3}, μ(MoK$_\alpha$) = 1.226 mm^{-1}, F(000) = 1016, Z = 4, the final R = 0.0564 and wR = 0.1851 for 3656 observed reflections ($I > 2\sigma(I)$). The complex was also investigated by elemental analysis, IR spectroscopy, themogravimetry and theoretical calculations.

Keywords: 2,2'-biimidazole; phthalic acid; zinc(II) complex; crystal structure; quantum chemistry.

INTRODUCTION

The design and synthesis of metal–organic framework structures have been studied widely during the past decade not only because of their intriguing architectures but also because of their unexpected properties for potential practical applications in a wide number of fields, such as asymmetric catalysis, magnetism, photoluminescence, *etc.*[1–3] These novel structures can be rapidly and efficiently synthesized from some subunits, whereby the metal ion, bi- or multidentate organic ligand and coordinate bonding are the important factors for the self-assembly processes. Consequently, investigations in this field have led to many materials with interesting structures.[4]

* Corresponding author. E-mail: yccuisp@yahoo.cn
doi: 10.2298/JSC101209184T

The structural characteristics of and characterization of some metal complexes, such as $[Cd(C_8H_4O_4)(C_7H_6N_2)_3]_n$, has been reported[5] and some metal complexes containing the pt ligand (pt = phthalate, benzene-1,2-dicarboxylate) were synthesized and characterized. 2,2'-Biimidazole (Biim), a good nitrogen and hydrogen donor, can regard as a robust heteromeric hydrogen-bonded synthon. As the five-membered rings also contain π electrons, π–π interactions may be formed when the distance between the two rings is befitting.[6,7] In this article, a new Zn(II) complex with pt as the first ligand is reported.

EXPERIMENTAL

2,2'-Biimidazole was prepared according to a reported method.[8] Other chemicals from commercial sources were of reagent grade and used without further purification. Infrared spectra (KBr pellets) were taken on a Perkin–Elmer 240C spectrometer. The thermal analysis was performed on a Diamond DSC type thermal analyzer.

*Synthesis of bis(2,2'-biimidazole)phthalato zinc(II) [Zn(pt)(Biim)$_2$] (**1**)*

Complex **1** was prepared from a mixture of $Zn(OAc)_2 \cdot 2H_2O$ (0.109 g), phthalic acid (0.166 g), biimidazole (0.268 g) and H_2O (18 mL) in a 30 mL Teflon-lined autoclave under an autogenous pressure at 160 °C for six days. After cooling to room temperature, white block crystals of **1** were collected by filtration and washed with distilled water. Yield 73 % (based on Zn). Anal. Calcd. for $C_{20}H_{16}N_8O_4Zn$: C, 48.2; H, 3.2; N, 22.5 %. Found: C, 48.1; H, 3.2; N, 22.3 %.

Crystal structure determination and physical measurements

A single crystal with dimensions of 0.360 mm×0.316 mm×0.218 mm was mounted at 293(2) K. All measurements were performed on a Bruker CCD diffractometer using graphite-monochromated MoK_α (λ = 0.71073 Å) radiation in the ω scan mode ($5.00 < 2\theta < 52.14°$). A total of 17514 reflections were collected and 4134 were independent with R_{int} = 0.0252, of which 3656 were observed with $I > 2\sigma(I)$. A correction for *Lp* factors was applied. The structure was solved by direct methods using the SHELX-97 program and refined with SHELXL-97[9] by full-matrix least-squares techniques on F^2. All H atoms were positioned geometrically and refined as riding atoms, with C–H = 0.93 Å and N–H = 0.86 Å, and with *U*iso(H) = 1.2 *U*eq(C,N). All non-hydrogen atoms were refined anisotropically and hydrogen atoms isotropically. The final $R = 0.0564$ and $wR = 0.1851$, $w = 1/(\sigma 2(Fo^2) + (0.1466P)^2 + 1.1882P)$ where $P = (Fo^2 + 2Fc^2)/3$. $S = 1.057$, $(\Delta\rho)_{max} = 0.70$, $(\Delta\rho)_{min} = -0.71$ e/Å^3 and $(\Delta/\sigma)_{max} = 0.002$. The selected important bond parameters are given in Table I.

*Crystal structure deposition for complex **1***. Supplementary crystallographic data for complex **1** is deposited at the Cambridge Crystallographic Data Centre under CCDC 739928. Further details of the crystal structure investigation may be obtained *via* http://www.ccdc.cam.ac.uk/data_request/cif.

RESULTS AND DISCUSSION

*Crystal structure of [Zn(pt)(Biim)$_2$] **1***

The single crystal X-ray diffraction analysis revealed that complex **1** crystallizes in the $P2_1/n$ space group. There are one Zn(II) ion, one pt ligand and two Biim ligands in the asymmetric unit (Fig. 1).

TABLE I. Selected bond lengths (Å) and bond angles (°) of the title complex obtained from X-ray analysis and theoretical calculations at the B1B95/(6-311+G(2df,2p) (for C, H, N and O) and the Lanl2dz (for Zn) level of theory, as well as the relative errors (%)

Bond	Experimental	Calculated	Error, %
	Bond length, Å		
Zn–O(2)	2.265(4)	2.2653	0.004
Zn–N(1)	2.342(5)	2.3425	0.000
Zn–N(5)	2.333(4)	2.3327	0.029
Zn–O(3)	2.321(3)	2.3219	0.026
Zn–N(4)	2.266(4)	2.2658	0.026
Zn–N(8)	2.265(5)	2.2647	0.035
	Bond angle, °		
N(4)–Zn–O(2)	86.31(15)	86.2986	0.015
O(2)–Zn–N(8)	165.09(17)	165.0567	0.021
O(2)–Zn–O(3)	78.26(15)	78.2608	0.001
N(4)–Zn–N(5)	92.29(16)	92.3217	0.033
N(8)–Zn–N(5)	74.76(15)	74.7555	0.008
N(4)–Zn–N(1)	74.69(14)	74.6713	0.027
N(8)–Zn–N(1)	89.54(14)	89.5631	0.024
N(5)–Zn–N(1)	155.52(14)	155.5279	0.004
N(4)–Zn–N(8)	108.41(16)	108.4539	0.039
N(4)–Zn–O(3)	163.03(15)	163.0163	0.009
N(8)–Zn–O(3)	87.40(16)	87.3638	0.043
O(2)–Zn–N(5)	103.00(14)	102.9839	0.017
O(3)–Zn–N(5)	97.97(14)	97.9603	0.011
O(2)–Zn–N(1)	96.86(14)	96.8661	0.005

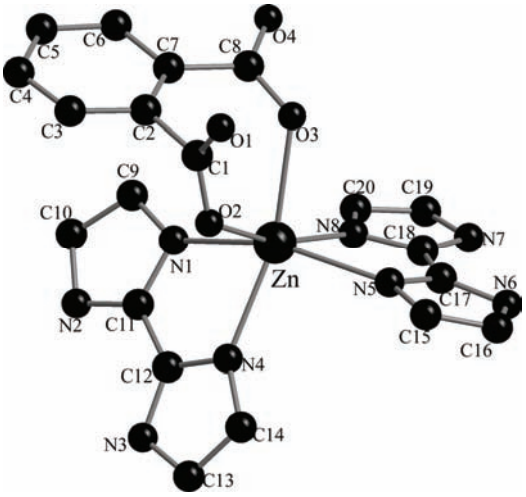

Fig. 1. The coordination geometry of complex **1**.

The coordination number of each zinc(II) atom is six. The Zn is coordinated by two carboxylate oxygen atoms from the two carboxyls of one pt (Zn–O(2),

2.266(5) Å and Zn–O(3), 2.317(5) Å), the other two oxygen atoms were deprotonated, and four nitrogen atoms from two different Biim ligands, giving a distorted octahedron geometry. The Zn–N bond distances range from 2.259(5) to 2.331(6) Å, the O(N)–Zn–O(N) angles range from 74.89(18) to 165.1(2)° (Table I).

Each carboxyl group of pt is in a single-dentate coordination mode, *i.e.*, the two carboxyl groups are both deprotonated; this was proved by the absence of the characteristic double peak at around 1600 cm^{-1} in the IR spectrum. In this coordination mode, the title complex formed a monomeric structure.

In the crystal lattice of the title complex, strong N–H···O hydrogen bonds exist (Table II). The nitrogen atoms N(2), N(3), N(6) and N(7) of the biimidazole ligands act as donors, while the acceptor O atoms come from the carboxyl oxygen of the pt ligands. The individual structures linked by strong hydrogen bonds form a two dimensional planar grid structure (Fig. 2).

TABLE II. The hydrogen bonds of the title complex (symmetry transformations used to generate the equivalent atoms: #1: $-x+3/2$, $y+1/2$, $-z+1/2$; #2: $-x+1$, $-y$, $-z$; #3: $x-1/2$, $-y+1/2$, $z+1/2$)

D–H···A	*d*(D–H) / Å	*d*(H···A) / Å	*d*(D···A) / Å	∠(DHA) / °
N(3)–H(3B)···O(1)#1	0.86	1.91	2.736(6)	161.2
N(7)–H(7A)···O(3)#2	0.86	1.91	2.722(6)	155.8
N(2)–H(2A)···O(2)#1	0.86	1.86	2.702(6)	165.1
N(6)–H(6B)···O(4)#2	0.86	1.88	2.736(6)	173.3
C(13)–H(13A)···O(4)#3	0.93	2.38	3.273(7)	160.4

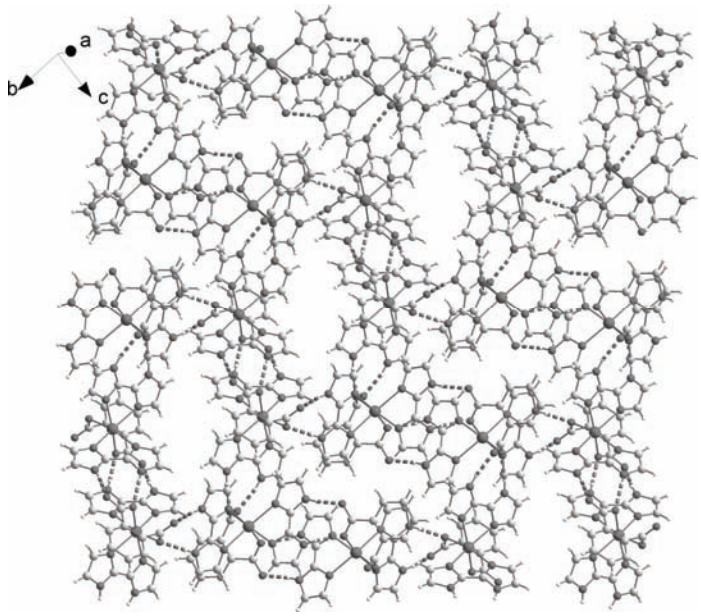

Fig. 2. The two-dimensional planar grid structure extended parallel to the plane (the dotted single lines indicate hydrogen bonds).

In addition, C(13)–H···O(4)# (#: –1/2+*x*, 1/2–*y*, 1/2+*z*) hydrogen bond interactions exist.[10] These inter-molecular contacts link neighboring two-dimensional planar structures to a three dimensional supramolecular structure. Complex **1** also contains π–π interactions and C–H···π interactions (Table III). These intermolecular interactions stabilize the crystal structure.

TABLE III. Intermolecular π–π interactions (dist. centroids < 4.0 Å) and C–H···π interactions (H···Cg < 3.0 Å, γ < 30.0°) parameters of complex **1** (Cg(1): N(5)→C(15)→C(16)→N(6)→→C(17)→5, Cg(2): N(7)→C(18)→N(8)→C(20)→C(19)→6, Cg(3): C(2)→C(3)→C(4)→→C(5)→C(6)→C(7)→7, Cg(4): N(3)→C(12)→N(4)→C(14)→C(13)→4; Cg(I) = plane number I (= ring number in () above), dihedral angle = dihedral angle between planes I and J (°), dist. centroids = distance between ring centroids (Å), CgI_Perp = perpendicular distance of Cg(I) on ring J (Å), CgJ_Perp = perpendicular distance of Cg(J) on ring I (Å), γ = angle Cg(I)→Cg(J) vector and normal to plane J (°), symmetry codes: a = 1–*x*, –*y*, –*z*; b = –1+*x*, *y*, *z*; c = 1+*x*, *y*, *z*)

Cg(I)→Cg(J)	Dist. centroids, Å	Dihedral angle, °	CgI_Perp, Å	CgJ_Perp, Å
Cg(1)→Cg(2)	3.677(4)	6.04	3.327	3.344
Cg(2)→Cg(1)	3.677(4)	6.04	3.345	3.327
Cg(2)→Cg(3)	3.916(4)	18.72	3.670	3.612
Cg(3)→Cg(2)	3.916(4)	18.72	3.611	3.670
	C–H(I)→Cg(J)			
C(3)–H(3A)→Cg(4)	Distance H···Cg, Å	H-Perp γ / °	C–H···Cg angle, °	
	2.90	8.68	131	

*IR Spectrum of complex **1***

The IR spectrum of complex **1** contained a weak band at 3144 cm^{-1} of $\nu_{N–H}$ and $\nu_{C–H}$, which is a characteristic absorption of Biim. The medium bands at 1608 and 1397 cm^{-1} are, respectively, the asymmetric and symmetric stretch vibration of the carboxylate groups; Δ > 200 cm^{-1} shows the presence of monodentate linkages of the carboxylates in the dianions, which is consistent with the X--ray diffraction results. The bands at 1559*w*, 1483*w*, 1424*w* and 1257*s* cm^{-1} can be attributed to C=C and C=N[11–13] stretch vibrations of the imidazole ring. The band at 827*s* cm^{-1} arises from N–H bend vibrations, and those at 771*w*, 758*w*, 745*w* cm^{-1} can be attributed to C=C and C=N bend vibrations of imidazole. The band at 445*w* cm^{-1} is in the low frequency region and can be regarded as arising from the metal coordinated to the Biim ligand (Zn–N stretching vibration).[13]

Thermal analysis

The TG measurement was performed under a N_2 atmosphere at a heating rate of 10 °C min^{-1}. The TG curve of complex **1** is shown in Fig. 3. TG curve of complex **1** shows a first weight loss of 31.4 % from 190 to 310 °C, corresponding to the removal of the pt ligand molecules (calcd. 32.9 %). Upon further heating, a weight loss (54.6 %) occurred in the temperature range of 510–595 °C, corres-

ponding to the release of the organic ligand Biim (calcd. 53.9 %). After 600 °C, no weight loss was observed, which indicates the complete decomposition of complex **1**. The residual weight of 16.8 % (calcd. 16.4 %) corresponds to ZnO.

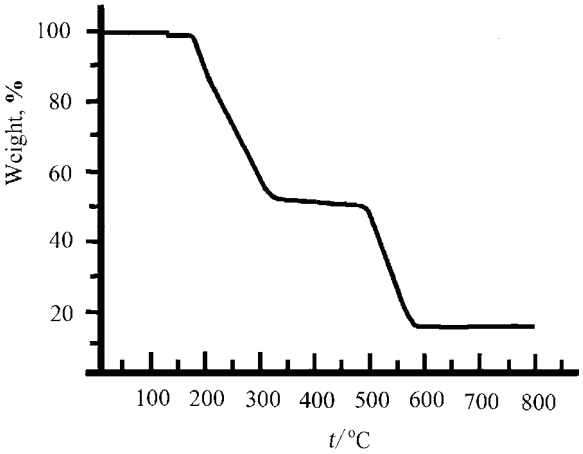

Fig. 3. The TG curve for the title complex **1**.

Computational chemistry research

The geometric structure with real frequence was optimized by the density functional theory (DFT)[14] method with a Becke one parameter hybrid functional (B1B95).[15] There were no symmetry constraints on the complex. In the calculation, the effective core potentials of Zn atoms proposed by Hay and Wadt[16] were employed, and a "double-ζ" quality basis set LANL2DZ was adopted for the Zn metal. There are lone-pair electrons and a conjugated system in the complex, the 6-311++G(2df, 2p) basis set was employed for C, H, O, N optimization, which involved 49 atoms, 1266 basis functions, 1895 primitive Gaussians, 118 alpha electrons and 118 beta electrons. All calculations were performed with the Gaussian 09 software package[17] and Natural Bond Orbital (NBO)[18] analyses were obtained based on the optimized geometries.

From Table I, it can be seen that the relative errors of the bond lengths and bond angles were all in the range of 0.00–0.04 %. This led to the belief that the employed theoretical method was suitable for complex **1**.

The atomic net charges for complex **1** calculated in the NBO analysis are listed in Table IV. The results of calculation show that electronic arrangement of the central zinc atom is $4s^{0.273}d^{9.984}p^{0.42}$. The covalent valence of zinc is +2, but the zinc partially obtains electrons from the pt and Biim ligands, illustrating that the charge of the central Zn metal for complex **1** is 1.31799. The net charges of the other coordinated N and O atoms (N1, N4, N5, N8, O2 and O3) are –0.53277, –0.51940, –0.53279, –0.51939, –0.86153 and –0.86151, respectively. Thus, the net charges of the coordinated O atoms are more negative than those of the coor-

dinated N atoms. The calculated Weiberg bond orders (Zn–O (0.2220), Zn–N4, Zn–N8 (0.1707) and Zn–N1, Zn–N5 (0.1579)) indicate that the bonds around the metal are covalent in nature.

TABLE IV. Selected atom net charges and electronic configuration of the title complex at the B1B95/(6-31+G(2df) (for C, H, N and O) and the Lanl2dz (for Zn) level

Atom	Charge	Electronic c
Zn	1.31799	[core] 4s(0.27) 3d(9.98) 4p(0.42)
N1	–0.53277	[core] 2s(1.35) 2p(4.14) 3d(0.02) 4p(0.01)
N2	–0.55498	[core] 2s(1.23) 2p(4.30) 3d(0.01) 4p(0.01)
N3	–0.55533	[core] 2s(1.23) 2p(4.30) 3d(0.01)
N4	–0.51940	[core] 2s(1.35) 2p(4.13) 3d(0.02) 4p(0.01)
N5	–0.53279	[core] 2s(1.35) 2p(4.14) 3d(0.02) 4p(0.01)
N6	–0.55498	[core] 2s(1.23) 2p(4.30) 3d(0.01) 4p(0.01)
N7	–0.55532	[core] 2s(1.23) 2p(4.30) 3d(0.01)
N8	–0.51939	[core] 2s(1.35) 2p(4.13) 3d(0.02) 4p(0.01)
O1	–0.71567	[core] 2s(1.70) 2p(4.98) 3p(0.01) 3d(0.02)
O2	–0.86153	[core] 2s(1.68) 2p(5.15) 3p(0.01) 3d(0.02)
O3	–0.86151	[core] 2s(1.68) 2p(5.15) 3p(0.01) 3d(0.02)
O4	–0.71569	[core] 2s(1.70) 2p(4.98) 3p(0.01) 3d(0.02)

It can be seen from Fig. 4 that in the highest molecular occupied orbital (HOMO, Orbital No. 118, Fig. 4a), the electron is mainly located at the pt ligand,

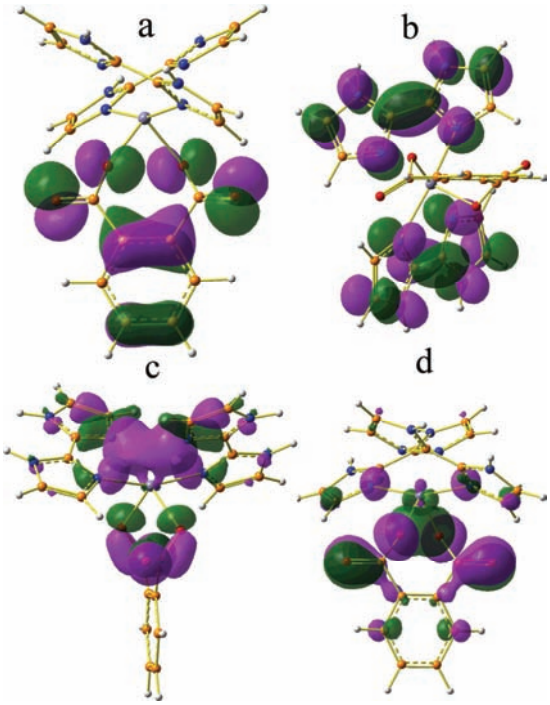

Fig. 4. The LUMO No. 94 0.036 (a) and No. 109 0.029 isosurface (b), HOMO 0.034 (c) and LUMO 0.030 isosurface (d) orbitals of the title complex **1**.

while in the lowest unoccupied molecular orbital (LUMO, Orbital No. 119, Fig. 4b), the electron is mainly situated on the two Biim ligands. There are four Zn–N coordinate bonds and two Zn–O coordinate bond around the central Zn. After examination of both molecular orbital graphs, it is known that the Zn–N bonds are related to the orbital No. 94 (Fig. 4c), correspondingly, the Zn–O bonds are related to the orbital No. 109 (Fig. 4d). These two orbitals reveal that the Zn center uses its d orbitals to interact with N or O p orbital to form the coordinate bonds of the title complex.

CONCLUSION

In this article, the metal–organic coordination complex **1**, $[Zn(pt)(Biim)_2]$, which exhibits a three-dimensional network structure, is reported. The complex was investigated by IR spectroscopy, elemental analysis and TG analysis. The density functional theory (DFT) calculation was performed at the B1B95 level. Analysis of the orbitals revealed that the Zn center mainly uses its d orbitals to coordinate to the ligands. The net charges and the bond orders were also investigated. The obtained results are consistent with the X-ray diffraction results.

ИЗВОД

СИНТЕЗА, КРИСТАЛНА СТРУКТУРА И ТЕОРИЈСКА ИСПИТИВАЊА ЦИНК(II) КОМПЛЕКСА $[Zn(pt)(Biim)_2]$

FEI TENG[1], NAN JIANG[2], ZHONGHUI WANG[3], YUNCHENG CUI[2] и JIAJUN WANG[2,4]

[1]Mathematics College of Jilin Normal University, Siping 136000, China, [2]Key Laboratory of Preparation and Application of Environmental Friendly Materials (Jilin Normal University), Ministry of Education, Chemistry Department of Jilin Normal University, Siping 136000, China, [3]Acrylonitrile Plant of PetroChina Jilin Petrochemical Company, Jilin 132021, China и [4]State Key Laboratory of Theoretical and Computational Chemistry, Institute of Theoretical Chemistry Jilin University, Changchun 130023, China

Хидртермалном синтезом изолован је цинк(II) комплекс **1**, $[Zn(pt)(Biim)_2]$ (pt = фталат, бензен-1,2-дикарбоксилат, Biim = 2,2'-биимидазол). Карактеризација комплекса је извршена на основу дифракције X-зрака са монокристала. Моноклинични кристали комплекса имају просторну групу $P2_1/n$ са вредностима: a = 8,5466(15) Å, b = 11,760(2) Å, c = = 20,829(4) Å, β = 95,56(2)°, V = 2083,5(6) Å^3, Mr =497,78, Dc = 1,587 g/cm^3, $\mu(MoK_\alpha)$ = 1,226 mm^{-1}, $F(000)$ = 1016, Z = 4, коначни фактор поузданости R = 0,0564 и wR = 0,1851 за 3656 употребљених рефлексија ($I > 2\sigma(I)$). Поред тога, за карактеризацију комплекса употребљени су елементална анализа, IR, TG и теоријска израчунавања.

(Примљено 9. децембра 2010, ревидирано 7. септембра 2011)

REFERENCES

1. P. A. Schofield, H. Adams, N. A. Bailey, E. Cesarotti, C. White, *J. Organomet. Chem.* **16** (1991) 273
2. S. A. Komaei, G. A. van Albada, I. Mutikainen, U. Turpeinen, J. Reedijk, *Eur. J. Inorg. Chem.* **11** (1998) 1577
3. W. B. Lin, L. Ma, O. R. Evans, *Chem. Commun.* (2000) 2263

4. K. D. Subrata, M. Nijhuma, M. Mondal, E. F. Salah, V. Ramon, E. Albert, S. Xavier, M. B. Font, M. Matsushita, V. Gramlich, M. Samiran, *Inorg. Chem.* **43** (2004) 2427
5. Y. C. Cui, J. J. Wang, G. B. Che, C. B. Li , *Acta Crystallogr*., *E* **62** (2006) m2761
6. B. H. Ye, B. B. Ding, Y. Q. Weng, X. M. Chen, *Cryst. Growth Des*. **5** (2005) 801
7. B. B. Ding, Y. Q. Weng, Z. W. Mao, C. K. Lam, X. M. Chen, B. H. Ye, *Inorg. Chem.* **44** (2005) 8336
8. B. F. Fieselmann, D. N. Hendrickson, G. D. Stucky, *Inorg. Chem.* **17** (1978) 2078
9. G. M. Sheldrick, *Acta Crystallogr., A* **64** (2008) 112
10. Th. Steiner. *Crystallogr. Rev. **6*** (1996) 1
11. D. Boinnard, P. Cassoux, V. Petrouleas, J. M. Savariault, J. P. Tuchagues *Inorg. Chem.* **29** (1990) 4114
12. K. Ramirez, J. A. Reyes, A. Brieeno, R. Atencio, *CrystEngComm* **4** (2002) 208
13. K. Golcuk, A. Altun, M. Kumru. *Spectrochim. Acta, A* **59** (2003) 1841
14. R. G. Parr, W. Yang, *Density-functional theory of atoms and molecules*, Oxford University Press, Oxford, UK, 1989
15. A. D. Becke, *J. Chem. Phys.* **104** (1996) 1040
16. a). P. J. Hay, W. R. Wadt, *J. Chem. Phys.* **82** (1985) 270; b). P. J. Hay, W. R. Wadt, *J. Chem. Phys.* **82** (1985) 299
17. *Gaussian 09, Revision A.1, Gaussian, Inc*, Wallingford CT, USA, 2009
18. A. E. Reed, L. A. Curtiss, F. Weinhold, *Chem. Rev.* **88** (1988) 899.

Journal of the Serbian Chemical Society
JSCS-info@shd.org.rs • www.shd.org.rs/JSCS
J. Serb. Chem. Soc. 77 (2) 187–199 (2012)
JSCS–4260
UDC 546.472'562+547.979.733+
544.032.6:66.022.362
Original scientific paper

Zinc(II) and copper(II) complexes with pheophytin and mesoporphyrin and their stability to UV-B irradiation: Vis spectroscopy studies

JELENA B. ZVEZDANOVIĆ*, DEJAN Z. MARKOVIĆ and SANJA M. MILENKOVIĆ

University of Niš, Faculty of Technology, Bulevar oslobodjenja 124, 16000 Leskovac, Serbia

(Received 10 March, revised 20 July 2011)

Abstract: The stability of Zn(II) and Cu(II) complexes of porphyrin derivatives (pheophytin and mesoporphyrin) to UV-B irradiation was studied by absorbance spectroscopy in 95 % ethanol. The chosen porphyrins and their heavy metal complexes underwent first-order photochemical decomposition. In general, pheophytin was more stable than mesoporphyrin to UV-B irradiation. Moreover, the stabilities of the Zn(II) complexes were lower than those of the Cu(II)-complexes for both pheophytin and mesoporphyrin. However, while the Cu(II)-complex with pheophytin was more stable than the one with mesoporphyrin, the situation was *vice versa* for the Zn(II)-complexes.

Keywords: pheophytin; mesoporphyrin; heavy metal; complexes; UV-B kinetics.

INTRODUCTION

Pheophytin and mesoporphyrin belong to the family of porphyrin compounds. The structure of mesoporphyrin IX (MP), 7,12-diethyl-3,8,13,17-tetramethyl-porphyrin-2,18-dipropionic acid, is shown in Fig. 1A.[1,2] Insertion of heavy metals (HM) such as zinc or copper (in the form of ions) into the center of the porphyrin structure leads to the formation of a heavy metal–mesoporphyrin (HM–MP) complexes, in which the new metal coordinates the four symmetric pyrrole rings.[3] On the other hand, pheophytin (Pheo – shown in Fig. 1B) is a derivative of the major photosynthesis pigment, chlorophyll (Chl), with an isocyclic cyclopentanone ring fused to a C-pyrrole ring of the porphyrin core between the C-13 and C-15 positions. In chlorophyll, the central magnesium (Mg) atom is bonded with the N-atoms from the four symmetric pyrrole rings by two covalent and two coordination bonds.[3] Pheophytin is formed when chlorophyll is depleted of magnesium (Fig. 1B). It is known that heavy metals can replace the labile bonded central Mg-atom

* Corresponding author. E-mail: jelite74@yahoo.com
doi: 10.2298/JSC110310175Z

of chlorophyll to form substitutional or "central" complex of chlorophyll, *i.e.* heavy metal complex of pheophytin, HM–Pheo.[4,5]

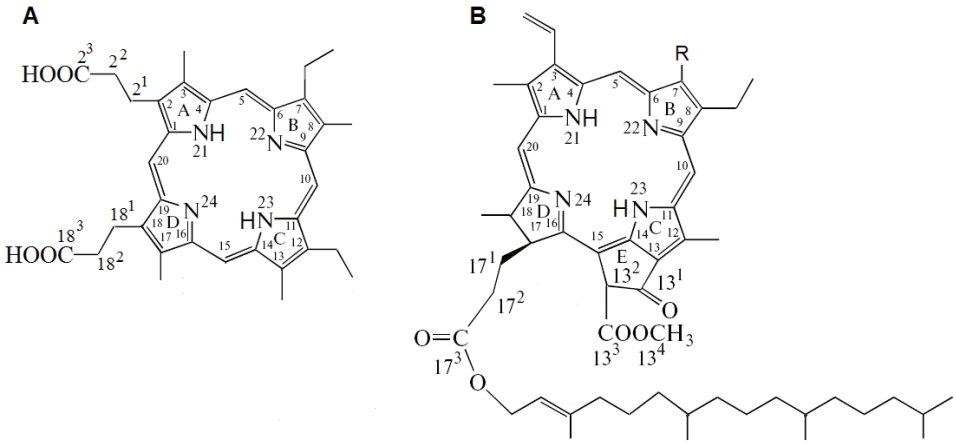

Fig. 1. Structure of mesoporphyrin (A), and pheophytin (B) with numerated C-positions; R = CH_3 in pheophytin *a*; R = CHO in pheophytin *b*.

It is well known that porphyrins and their metal derivatives have attracted significant attention in many areas because of their spectral properties; their characteristic absorption spectrum consists of an intense (Soret or *B*) band close to 400 nm and a less intense (Q) band in the region 500–700 nm.[6,7] They make a core in many other types of molecules, such are chlorophyll and hemoglobin, as well as in many enzymes where they play a heme role.[8] In numerous biological and solar energy applications,[3,9] it is often important to examine the basic properties of porphyrins and their metal-complexes when they are irradiated by UV light (*e.g.*, UV-B). Treatment of chlorophyll with strong UV and visible light in solutions and in isolated photosynthetic organelles results in irreversible breakdown of chlorophyll, *i.e.*, bleaching.[10–12]

This work deals with the stability of two porphyrin derivatives, *i.e.*, pheophytin and mesoporphyrin, and their heavy metal complexes to continuous UV-B irradiation. The irradiation was performed in 95 % ethanol for different irradiation periods, providing possibilities for kinetic analysis.

EXPERIMENTAL

All experiments, beginning with the extraction, were performed under dim light as far as possible, and inside vessels and equipment covered with aluminum foil or black cloth, thus preventing exposure of the pigments to light.[13]

Mesoporphyrin IX (Sigma Aldrich) was a gift from the Hugo Scheer Laboratory, Botanisches Institute, LMU University, Munich, Germany.

Chlorophyll isolation and preparation of pheophytin

The chlorophylls were isolated from plant pigments (extracted from spinach leaves, *Spinacia oleracea*) using an already published method.[4,14] Chlorophyll fraction (containing Chl*a* and Chl*b* in molar ratio ≈ 6:1, respectively) was isolated by column chromatography with silica gel as the adsorbent (silica gel 60, Merck, 0.063–0.200 mm) and an *n*-hexane/acetone mixture as the eluent.[15] The *n*-hexane/acetone ratio was changed from initial 1:0 to final 1:1, to permit easier elution of the polar fractions. Chlorophyll was eluted at an eluent composition 1:0.1 (*n*-hexane/acetone, respectively). To prove the purity of the Chl-fraction, high pressure liquid chromatography (HPLC) was employed using a Chla-standard (Sigma–Aldrich) in acetone; the chlorophyll fractions were then run through HPLC as reported, proving large content of Chl*a* in each of them and a minor contribution of Chl*b* (the peaks ratio 8.5:1).[15] The total Chl content (Chl*a* + Chl*b*) in the isolated Chl-fraction has been calculated as reported.[16]

Pheophytins (*a* and *b*) were made from the collected chlorophyll in 95% ethanol by the dropwise addition of 1.0 M HCl.[17] Conversion was completed in approximately 2 h in the dark as observed by the color change from green to olive brown. The freshly made Pheo matter was then extracted by *n*-hexane and then dissolved in 95 % ethanol. The Pheo*a* and Pheo*b* content in the pheophytin fraction in 95% ethanol was calculated as reported previously.[16]

Preparation of pheophytin and mesoporphyrin heavy metal complexes

Zinc(II) and copper(II) complexes of pheophytin – denoted as Cu–Pheo and Zn–Pheo*, were prepared from Chl using a modified method proposed by Kupper.[18] Chlorophyll, dried at room temperature, was dissolved in 95 % ethanol and a solution of $CuSO_4$, or $ZnSO_4$, was then added. The substitution reaction of the central Mg in the Chl molecule by Zn, or Cu, (formation of the central Zn– or Cu–Pheo complexes) was performed by heating the reaction mixture in a reflux apparatus for 1 h at 40 °C, followed by 24 h at room temperature.

The copper and zinc complexes of mesoporphyrin (Cu–MP and Zn–MP) were prepared using the patent method of Inoue.[19] Mesoporphyrin was placed in 95 % ethanol and a 50 % ethanolic solution of $CuSO_4$, or $ZnSO_4$, was then added. Formation of the Cu–, or Zn–MP, complex was performed by heating the reaction mixture in a reflux apparatus for 1 h at 40 °C, followed by 24 h at room temperature.

Before metal ions addition to the pigment solutions, control experiments were performed in order to check the stability of the pigment solutions, and to assign all potential absorption changes to other factors other than metal–porphyrin interactions. The controls were realized in a period of 3 days (with porphyrin solutions only) by controlling their absorption spectra over the indicated period.

* Strictly speaking, those complexes should be denoted as Cu(II)–Pheo and Zn(II)–Pheo. However, essentially the pheophytin complex with Cu(II) or Zn(II) and chlorophyll (Chl) complex with Cu(II) or Zn(II) are basically the same, and the manner of their formation is practically the same: with chlorophyll, the formation these complexes is preceded by the removal of the central Mg atom (*i.e.*, pheophytin formation); then Cu(II) or Zn(II) ions (from surrounding solution) fill “the hole” and the complexes are formed. Therefore in most citations, Cu(II)–Pheo and Zn(II)–Pheo are denoted like Chl-complexes with these metals, *i.e.*, Cu(II)–Chl and Zn(II)–Chl, or just Cu–Chl and Zn–Chl.

UV-B Treatment

In all the experiments, the final concentration of pheophytin and mesoporphyrin was adjusted to 2.4 μM. Continuous irradiation of Pheo and MP solutions, as well as their Zn(II)- and Cu(II)-complexes in 95 % ethanol was performed in a cylindrical photochemical reactor "Rayonnet" with 8 symmetrically placed UV-B lamps having an emission maximum at 300 nm. The samples were irradiated in quartz cells (1 cm×1 cm×4.5 cm) placed on a circular rotating holder. The total measured energy flux (hitting the samples) was about 12.0 W m^{-2} at a distance of 10 cm from the lamps.

Vis spectroscopy

The spectrophotometric measurements were made on a Varian Cary-100 spectrophotometer equipped with 1.0 cm quartz cells. All spectra before and after irradiation were recorded from 300 to 750 nm with a 1.0 nm bandwidth.

HPLC Analysis

HPLC analysis of the isolated chlorophyll was performed under isocratic conditions; apparatus: Agilent 1100 series, Waldborn, Germany; column: Zorbax Eclipse XDB-C18; mobile phase: acetonitrile/methanol/ethyl acetate, 60:20:20; flow rate: 0.5 cm^3 min^{-1}; temperature: 25 °C. The monitoring wavelengths were 430 and 660 nm.

RESULTS AND DISCUSSION

Vis (absorption) spectra of UV-B-irradiated porphyrin derivatives

Absorption spectra of pheophytin (A), Zn–Pheo complex (B) and Cu–Pheo complex (C) following increasing periods of continuous UV-B irradiation in 95 % ethanol are shown in Fig. 2. Similarly, absorption spectra of mesoporphyrin (A), Zn–MP complex (B) and Cu–MP complex (C) following increasing periods of UV-B irradiation in 95 % ethanol are shown in Fig. 3*.

It is well known that porphyrins have two major absorption bands in the visible range, due to extended π-delocalization at the edge of the cyclic tetrapyrrole (porphyrin) skeleton: a ''red'' (Q) band and a ''blue'' (Soret or B) band.[6,7,20] HM–Pheo complexes showed spectroscopic behavior different from those of Chl and Pheo themselves, both qualitatively (shifts of the characteristic bands maximums, A_{Qmax}), as well as quantitatively (different intensities of the corresponding bands).[6,7,18,21] For example, the formation of the Cu–Pheo complex was followed by a characteristic hypsochromic ("blue") shift of the Q absorption band, compared to Chl itself;[4,21] this effect was not clearly seen with the Zn–Pheo complex.[4,21] The absorption maximum of the Q-band (A_{Qmax}) for Pheo a in 95 % ethanol was located at 665.0 nm, while same absorption maximum for Zn–Pheo and Cu–Pheo in 95 % ethanol were located at 664.0 and 654.0 nm, respectively (Fig. 1S of the Supplementary material and Fig. 2).[16] On the other hand, the Cu–MP and Zn–MP complexes expressed very different spectral behavior in comparison to

* The absorption spectra of: pheophytin (a), Zn–Pheo (b), Cu–Pheo (c) and mesoporphyrin (d), Zn–MP (e), Cu–MP (f) in 95 % ethanol are shown in Fig. 1S of the Supplementary material to this paper.

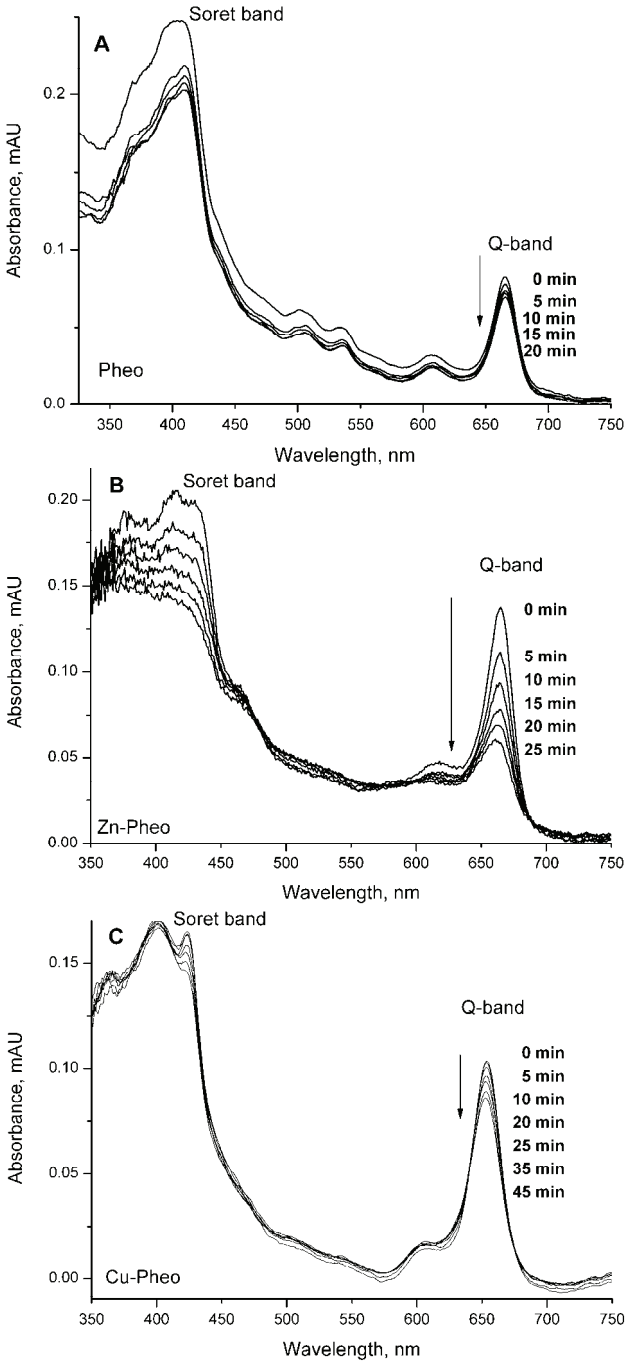

Fig. 2. UV-B-induced decomposition of Pheo (A), Zn––Pheo (B) and Cu–Pheo (C) in 95 % ethanol – changes in the absorption spectra followed their exposure to UV-B radiation. The exposure times are displayed for all three irradiated samples. The initial samples concentration was 2.4 μM.

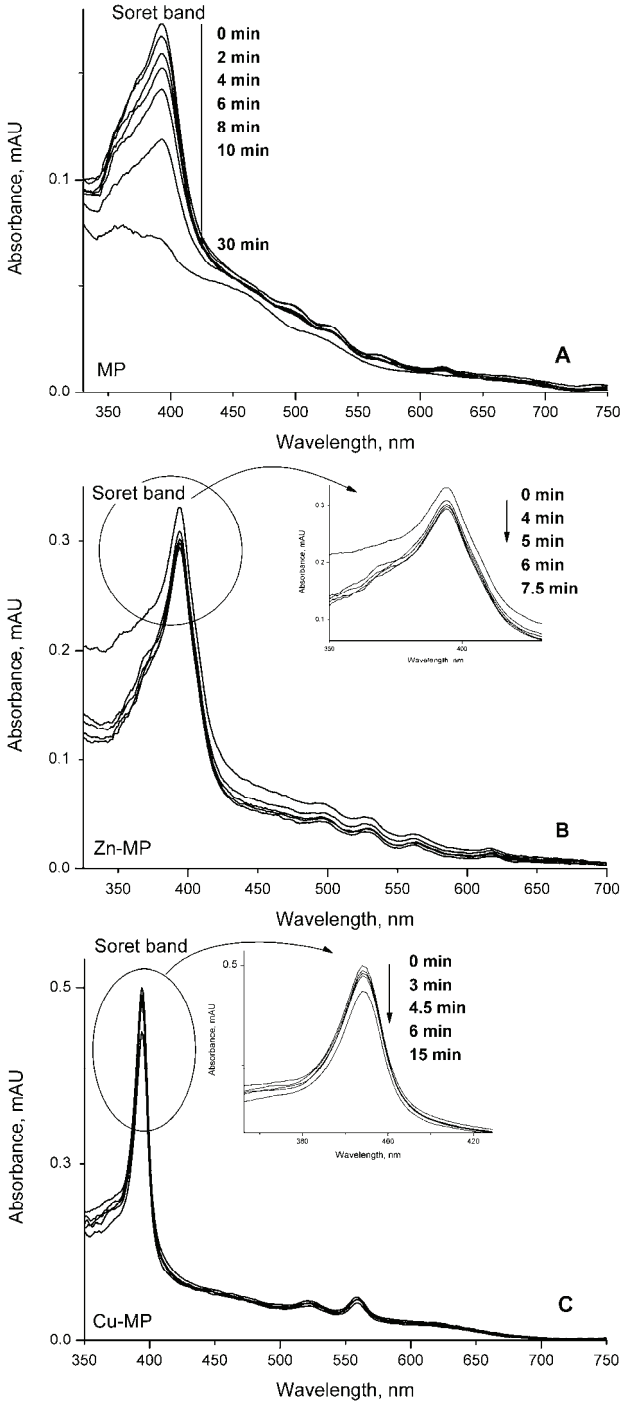

Fig. 3. UV-B-induced decomposition of MP (A), Zn–MP (B) and Cu–MP (C) in 95 % ethanol – changes in the absorption spectra followed their exposure to UV-B radiation. The exposure times are displayed for all three irradiated samples. The initial samples concentration was 2.4 μM.

MP itself; seen through the higher absorption in "blue" region, *i.e.*, the Soret (B) band (Fig. 1S of the Supplementary material and Fig. 3).[3,22,23] The absorption maximum of the Soret band, ($A_{\text{Soret-max}}$) of MP and the Zn– and Cu–MP complexes in 95 % ethanol were found at ≈ 394 nm and the maxima were, respectively, ≈ 2 and ≈ 3 times higher for Zn– and Cu–MP, compared to MP. The metal coordination of the four N-atoms leads to an increase of the porphyrin symmetry (in comparison to the free base porphyrin) and consequently to a rise in the intensity of the Soret band.[24,25]

The UV-induced changes of chlorophylls were already detected in various solvents, such as acetone and *n*-hexane, using the Q-band as a sensitive indicator.[10] Similar to this, in the present study, it was found that UV-B irradiation induced a gradual decrease of the absorption over the whole measured spectral range (300–750 nm), *e.g.*, a hypochromic effect was clearly observed for irradiated pheophytin, and the Zn– and Cu–Pheo complexes in 95 % ethanol, as shown in Figs. 2A–2C. In addition, it was also found that UV-B irradiation of mesoporphyrin and its Zn– or Cu–MP complexes induced a clear decrease of the Soret band intensity ($A_{\text{Soret-max}}$), as shown in Fig. 3. Clearly, UV-B irradiation of pheophytin and its Zn(II)- and Cu(II)-complexes, as well as of MP and its Zn(II)- and Cu(II)-complexes in 95 % ethanol results in their irreversible photochemical decomposition – bleaching.

Kinetics of the UV-B-induced photochemical decomposition the porphyrin derivatives

Photochemical decomposition kinetics of pheophytin and HM–Pheo complexes (Cu–Pheo and Zn–Pheo), as well as of MP and the HM–MP complexes (Cu–MP and Zn–MP), *i.e.*, logarithmic (ln) plots of the absorption *vs*. time of irradiation with UV-B light, are shown in Figs. 4 and 5, respectively. The decomposition (bleaching) rate constants, *k*, for Pheo and the HM–Pheo complexes, and for MP and the HM–MP complexes were calculated from the slopes given in Figs. 4 and 5:

$$y = n - kx$$

where *y* is the ln of the absorbance maximum, ln A_{Qmax} and ln $A_{\text{Soret-max}}$, respectively, and *x* is the UV-B irradiation time (in min). The decomposition kinetics of Pheo and the Zn– and Cu–Pheo complexes were followed by recording the value of the absorption maximum of the Q band, A_{Qmax} (665 nm for Pheo, 664 nm for Zn–Pheo and 654 nm for Cu–Pheo, Fig. 2). On the other hand, the decomposition kinetics of MP, and the Zn– and Cu–MP complexes were followed by recording absorption the maximum of the Soret band, $A_{\text{Soret-max}}$ at ≈ 394 nm (Fig. 3). The UV-B-induced decomposition (bleaching) of the porphyrin derivatives fits the first order kinetic model, as shown in Figs. 4 and 5. The calculated rate constants,

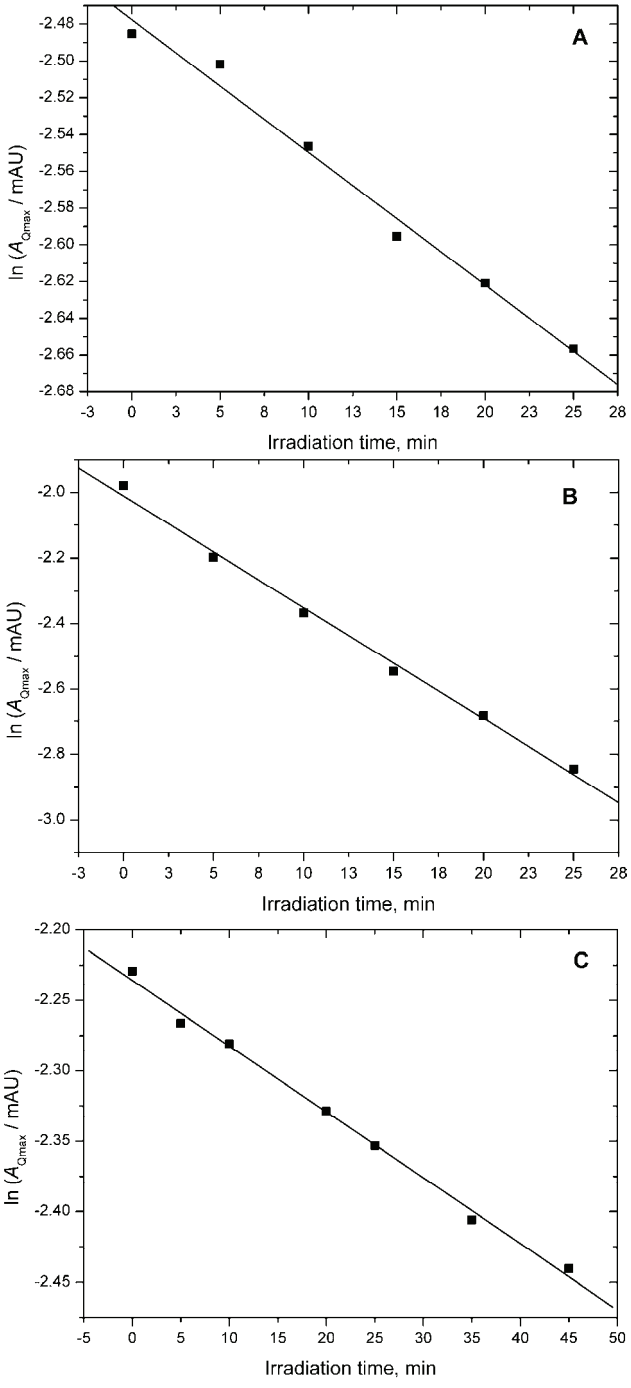

Fig. 4. First order kinetic plots for the photochemical decomposition of pheophytin (A), Zn–Pheo (B) and Cu––Pheo (C) in 95 % ethanol under UV-B irradiation. The absorbances were taken from the Q-band maximum.

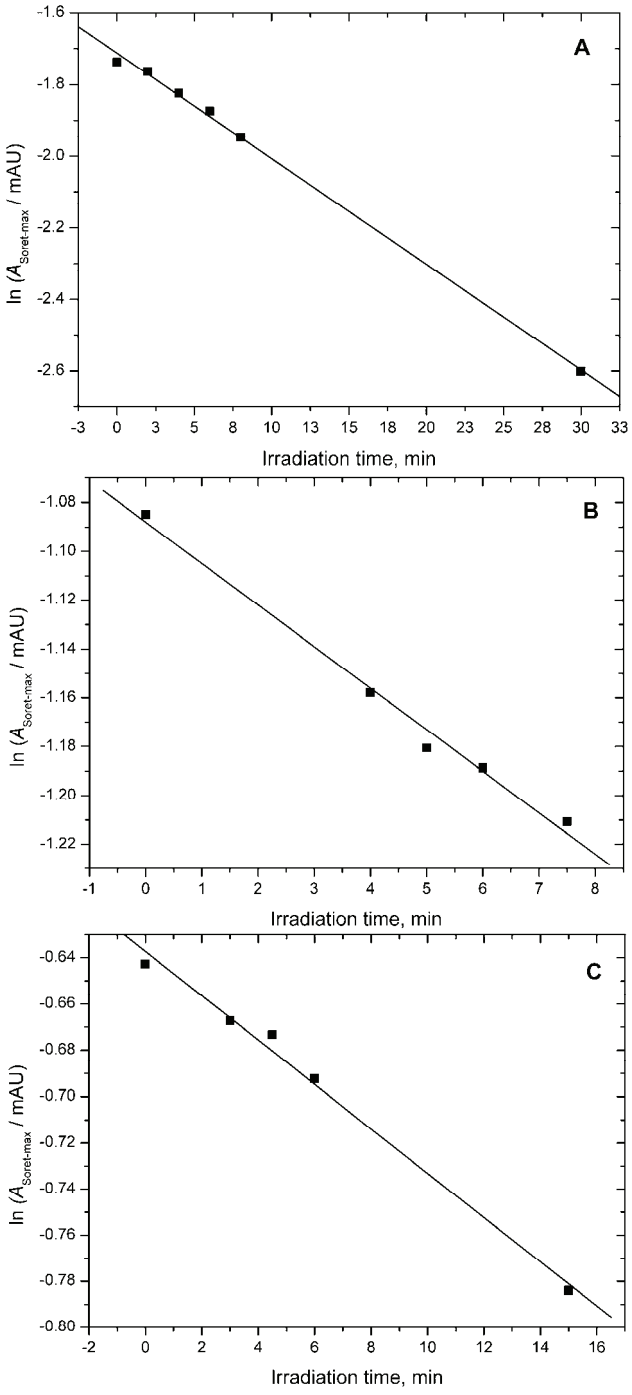

Fig. 5. First order kinetic plots for photochemical decomposition of mesoporphyrin (A), Zn–MP (B) and Cu––MP (C) in 95 % ethanol under UV-B irradiation. The absorbances were taken from the Soret-band maximum.

k (in min^{-1}), for Pheo and MP as well as for their Zn- and Cu-complexes in 95 % ethanol are given in Table I (correlation coefficient $r^2 \approx 0.99$).

TABLE I. First order rate constants (k / 10^{-3} min^{-1}) for photochemical decomposition of pheophytin, mesoporphyrin and their Zn(II)- and Cu(II)-complexes in 95 % ethanol under UV-B irradiation

Compound	Derivatives of pheophytin	Derivatives of mesoporphyrin
No metal	7.2	30
Zn(II)-complex	34	17
Cu(II)-complex	4.7	9.6

The bleaching rate constants of the Zn–Pheo and Zn–MP complexes generally exhibited higher values than those for the Cu(II)-complexes (Table I). The ratios of the UV-B induced decomposition rate constants of the Zn(II)- and Cu(II)--complexes of Pheo and MP, taken separately (*i.e.*, $k_{Zn–Pheo}/k_{Cu–Pheo}$ and $k_{Zn–MP}/k_{Cu–MP}$) were 7.3 and 1.8, respectively (Table I). In porphyrins, the energy levels of the corresponding electronic transitions are determined by the electrostatic interactions between the N (nitrogen)-tetrapyrolles-mediated π-electron densities and the metal center, and hence the effect of the central metal is related to its electronegativity.[26] In general, the stability of the metal complexes of pheophytin and mesoporphyrin in solution can be explained by theoretical analysis of the Falk "stability factor" (including charge number of the metal ion, effective radius of the metal ion in Å and the Pauling electronegativity).[13] According to the Falk equation, the stability of the complexes is ordered as: Mg(II)-complex ≈ ≈ Zn(II)-complex << Cu(II)-complex.[13] In addition, a similar order for the tendency of metal ions to fill "the hole" in the center of the chlorophyll molecule was already found in the cited reports.[18,21] On the other hand, metal complexes of porphyrins can be divided into two groups based on the properties of their electronic structure.[2] Complexes which contain closed-shell metal ions (d^0 or d^{10}), such as Zn(II), have relatively low energy in d–π metal-based orbitals. These interactions have very little effect on the porphyrin π–π* energy gap in electronic spectra. On the other hand, metal complexes of porphyrins which contain metals such as Cu(II) with a d^m configuration of the corresponding energy levels (m = 6–9, number of electrons) have significant metal to porphyrin orbital interaction (*i.e.*, metal to ligand d–π-backbonding), resulting in an increased π–π* energy separation, which is seen as a blue-shift in the appropriate spectra.[2–4] A heavy metal in the central position of the porphyrin structure (Fig. 1) seems to play a significant role in the stability of HM–Pheo and HM–MP complexes to UV-B irradiation; the affinity of heavy metals to the four nitrogen atoms (N-(21--24)) in the center of the porphyrin molecule could play the role of stability factor for HM-complexes against UV-B irradiation.

The photochemical decomposition rate constants for Pheo and its Cu-complexes (Cu–Pheo) generally showed smaller values than the same rate constants for MP and its Cu-complexes (Cu–MP), as given in Table I. The ratios of UV-B induced decomposition constants for MP and Pheo (k_{MP}/k_{Pheo}) and their Cu–MP and Cu–Pheo complexes ($k_{Cu–MP}/k_{Cu–Pheo}$) are 4.1 and 2.1, respectively. Mesoporphyrin differs from pheophytin by an additional double bond in the D pyrrole ring (Fig. 1A). In the mesoporphyrin structure, the extended delocalization at the edge of the cyclic tetrapyrrole (porphyrin) skeleton contains 11 π–bonds (Fig. 1A). In the pheophytin structure, the extended delocalization contains 10 π-bonds and two more π-bonds belonging to: 1) the C=O carbonyl group in position C--13[1] and 2) the C=C bond in position C-3[1]; the phytil chain is bonded to the propionic acid residue in position C-17[3] and isocyclic cyclopentanone ring fused to a C-pyrrole ring between the C-13 and C-15 positions (Fig. 1B) makes substantial differences between the Pheo and MP molecules. These differences between the two chosen porphyrin molecules and the related energy distributions seems to be related to the stability of the Pheo molecule against UV-B irradiation, compared to MP.

Pheophytin is more stable compared to its Zn(II) complex, but, on the other hand, the Zn–MP complex is more stable than MP itself to UV-B irradiation, as shown in Table I. The ratios of UV-B induced decomposition constants for Zn––Pheo and Pheo ($k_{Zn–Pheo}/k_{Pheo}$), as well as of MP and the Zn–MP complex ($k_{MP}/k_{Zn–MP}$) are 4.7 and 1.7, respectively (Table 1). It is known that the Zn––Pheo complex is more labile than Chl itself in solution: Zn(II) was shown to be involved in the formation of a peripheral complex at the right edge of the Chl molecule that includes at least two C=O groups in different positions.[4,21]

CONCLUSIONS

The chosen porphyrins, pheophytin and mesoporphyrin, and their heavy metal complexes undergo UV-induced photochemical decomposition obeying first--order kinetics. Pheophytin and its Cu(II)-complex are more stable to UV-B irradiation than mesoporphyrin and its Cu(II)-complex; contrarily, the Zn(II)-complex of mesoporphyrin is more stable than the same complex of pheophytin.

SUPPLEMENTARY MATERIAL

Absorbance spectra of porphyrin derivatives are available electronically from http:////www.shd.org.rs/JSCS/, or from the corresponding author on request.

Acknowledgements. This work was supported by the Ministry of Education and Science of the Republic of Serbia under project number TR 34012. We thank Dr Hugo Scheer who donated the mesoporphyrin standard.

И З В О Д

КОМПЛЕКСИ ФЕОФИТИНА И МЕЗОПОРФИРИНА СА ЦИНКОМ(II) И БАКРОМ(II) И ЊИХОВА СТАБИЛНОСТ ПРЕМА ДЕЈСТВУ UV-B ЗРАЧЕЊА: VIS СПЕКТРОСКОПСКА АНАЛИЗА

ЈЕЛЕНА Б. ЗВЕЗДАНОВИЋ, ДЕЈАН З. МАРКОВИЋ и САЊА М. МИЛЕНКОВИЋ

Универзитет у Нишу, Технолошки факултет, Булевар ослобођења 124, 16000 Лесковац

Стабилност Zn(II) и Cu(II) комплекса са дериватима порфирина (феофитином и мезопорфирином) према дејству UV-B зрачења у 95 % етанолу, анализирана је апсорпционом спектроскопијом. Изабрани порфирини као и њихови комплекси са тешким металима подлежу деструкцији (деградацији), пратећи кинетику првог реда. Генерално посматрајући, у односу на мезопорфирин, феофитин је стабилнији према дејству UV-B зрачења. Са друге стране, Zn(II) комплекси су мање стабилни од Cu(II) комплекса са оба испитивана порфирина – феофитином и мезопорфирином; ипак, док је Cu(II) комплекс феофитина стабилнији од оног са мезопорфирином, у случају комплекса са Zn(II) ситуација је обрнута.

(Примљено 10. марта, ревидирано 20. јула 2011)

REFERENCES

1. H. Fisher, *On haemin and the relationships between haemin and chlorophyll*, Nobel Lecture, 1930, p. 165
2. L. R. Milgrom, *The Colours of Life: An Introduction to the Chemistry of Porphyrins and Related Compounds*, OUP, Oxford, UK, 1997
3. A. Kay, M. Grätzel, *J. Phys. Chem.* **97** (1993) 6272
4. J. Petrović, G. Nikolić, D. Marković, *J. Serb. Chem. Soc*. **71**, 501 (2006)
5. L. J. Boucher, J. J. Katz, *J. Am. Chem. Soc*. **89** (1967) 4703
6. M. Gouterman, in *The Porphyrins*, D. Dolphyn, Ed., Academic Press, New York, 1978, p. 3
7. L. K. Hanson, in *Chlorophylls*, H. Scheer, Ed., CRC Press, Boca Raton, 1991, p. 994
8. M. R. Pereira, A. J. Ferreira, G. Hungerford, *J. Photochem. Photobiol., A* **172** (2005) 7
9. A. Kay, R. Humphry-Baker, M. Graetzel, *J. Phys. Chem*. **98** (1994) 952
10. J. Zvezdanović, D. Marković, *J. Serb. Chem. Soc.* **73** (2008) 271
11. M. N. Merzlyak, S. I. Pogosyan, L. Lekhimena, T. V. Zhigalova, I. F. Khozina, Z. Cohen, S. S. Khrushchev, *Russ. J. Plant Physiol*. **43** (1996) 160
12. S. Santabarbara, *Arch. Biochem. Biophys.* **455** (2006) 77
13. P. H. Hynninen, in *Chlorophylls*, H. Scheer, Ed., CRC Press, Boca Raton, 1991, p. 145
14. W. A. Svec, in *The Porphyrins*, D. Dolphyn, Ed., Academic Press, New York, 1978, p. 341
15. J. Zvezdanović, T. Cvetić, S. Veljović-Jovanović, D. Marković, *Radiat. Phys. Chem.* **78** (2009) 25
16. H. K. Lichtenthaler, *Meth. Enzymol*. **148** (1987) 350
17. H. Küpper, F. Küpper, M. Spiller, *J. Exp. Bot.* **47** (1996) 259
18. H. Küpper, M. Spiller, F. Küpper, *Anal. Biochem*. **286** (2000) 247
19. Y. Inoue, V. Borovkov, J. Lintuluoto, US patent, US 6,420,553 B1 (2002)
20. A. J. Hoff, J. Amesz, in *Chlorophylls*, H. Scheer, Ed., CRC Press, Boca Raton, 1991, p. 723
21. J. Zvezdanović, D. Marković, Russ. *J. Phys. Chem., A* **83** (2009) 1542
22. F. C. Belanger, A. R. Constantin, *J. Biol. Chem*. **257** (1982) 1360

23. R. Franco, J.-G. Ma, Y. Lu, G. C. Ferreira, J. A. Shelnutt, *Biochemistry* **39** (2000) 2517
24. M. Gouterman, *J. Chem. Phys*. **30** (1959) 1139
25. W. Zheng, N. Shan, L. Yu, X. Wang, *Dyes Pigm*. **77** (2008) 153
26. A. Drzewiecka-Matuszek, A. Skalna, A. Karocki, G. Stochel, L. Fiedor, *J. Biol. Inorg. Chem*. **10** (2005) 453.

Journal of the Serbian Chemical Society
JSCS@tmf.bg.ac.rs • www.shd.org.rs/JSCS
J. Serb. Chem. Soc. 77 (0) S48–S49 (2012) *Supplementary material*

SUPPLEMENTARY MATERIAL TO

Zinc(II) and copper(II) complexes with pheophytin and mesoporphyrin and their stability to UV-B irradiation: Vis spectroscopy studies

JELENA B. ZVEZDANOVIĆ*, DEJAN Z. MARKOVIĆ and SANJA M. MILENKOVIĆ

University of Niš, Faculty of Technology, Bulevar oslobodjenja 124, 16000 Leskovac, Serbia

J. Serb. Chem. Soc. 77 (2) (2012) 187–199

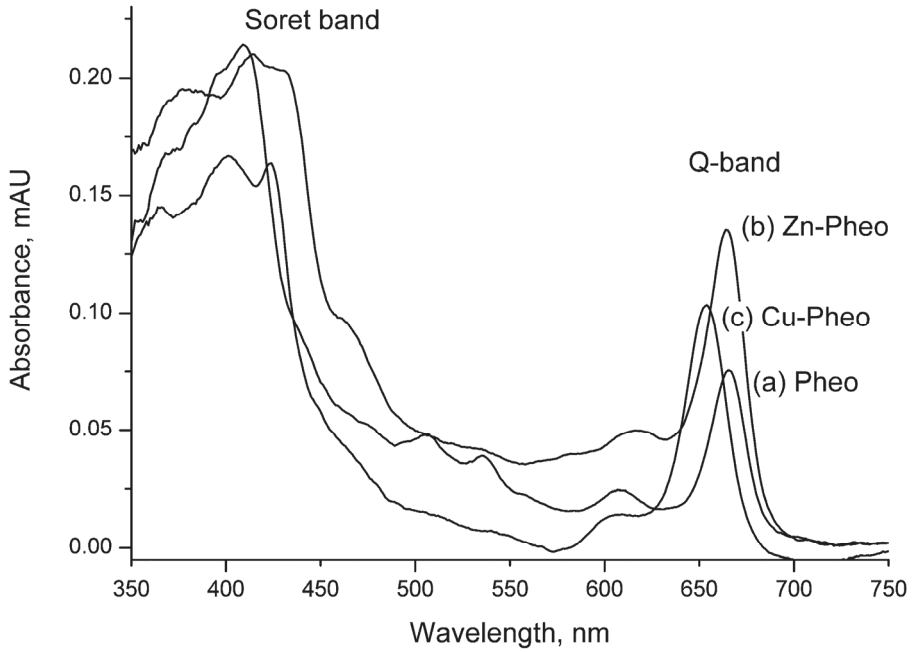

Fig. 1S. Absorbance spectra of porphyrin derivatives: a) pheophytin, b) Zn(II)-complex and c) Cu(II)-complex of pheophytin.

* Corresponding author. E-mail: jelite74@yahoo.com

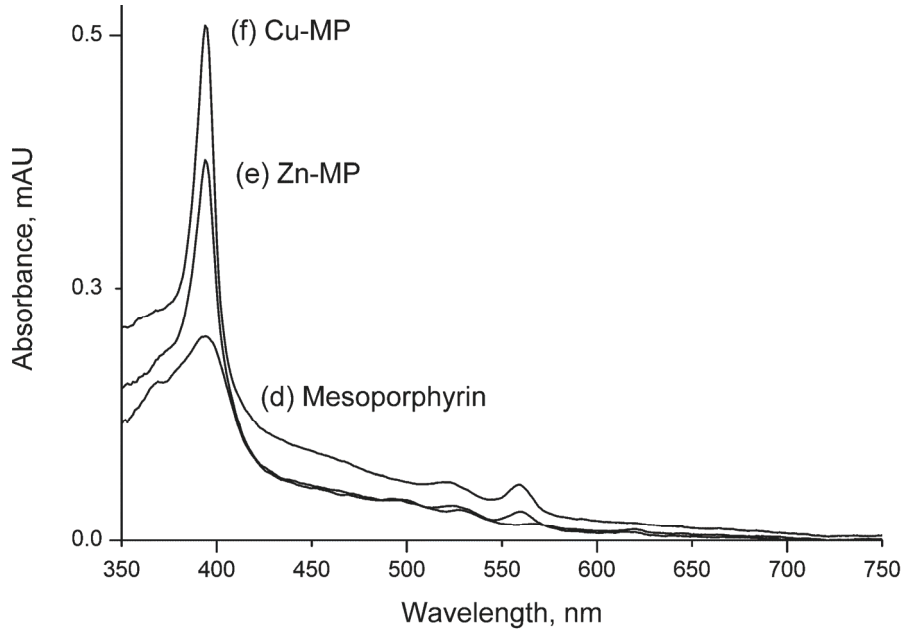

Fig. 1S. (Continued) Absorbance spectra of porphyrin derivatives: d) mesoporphyrin, e) Zn(II)-complex and f) Cu(II)-complex of mesoporphyrin.

Journal of the Serbian Chemical Society
JSCS-info@shd.org.rs • www.shd.org.rs/JSCS
J. Serb. Chem. Soc. 77 (2) 201–210 (2012)
JSCS–4261
UDC 547.586.1/.7+544.351+543.42+544.77.022.532
Original scientific paper

Interactions of short chain phenylalkanoic acids within ionic surfactant micelles in aqueous media

KASHIF NAEEM[1]*, SYED W. H. SHAH[2], BUSHRA NASEEM[3] and SYED S. SHAH[2]

[1]*Central Analytical Facility Division, PINSTECH, PO Nilore, Islamabad 45650, Pakistan,* [2]*Department of Chemistry, Hazara University, Mansehra, Pakistan and* [3]*Department of Chemistry, Lahore College for Women University, Lahore, Pakistan*

(Received 21 January, revised 10 August 2011)

Abstract: The solubilization and interactions of phenylalkanoic acids induced by the cationic surfactant, cetyltrimethylammonium bromide (CTAB) and the anionic surfactant sodium dodecyl sulfate (SDS) was investigated spectrophotometrically at 25.0 °C. The UV spectra of the additives (acids) were measured with and without surfactant above and below the critical micelle concentration (*cmc*) of the surfactant. The presence of an alkyl chain in phenylalkanoic acids was responsible for hydrophobic interactions resulting in a shift of the spectra towards longer wavelengths (red shift). The value of partition coefficient (K_x) between the bulk water and surfactant micelles and, in turn, the standard free energy change of solubilization ($\Delta G_p^{\ominus}$) were also estimated by measuring the differential absorbance (ΔA) of the additives in micellar solutions.

Keywords: alkanoic acids; solubilization; *cmc*; CTAB; SDS.

INTRODUCTION

The augmented solubility of sparingly soluble solutes in water brought about by a surfactant micellar solution is well known as solubilization, a phenomenon that plays an important role in industrial and biological processes.[1,2] The process of solute (additive) transfer from one medium to another is of widespread importance and characterized by a free energy change of transfer in relation to the partition coefficient. The solute transfer from one medium to another can be used to predict the solubilization of small molecules and anesthetic drugs in biological membranes.[3]

Amphiphilic additives containing a benzene ring are convenient to investigate spectrophotometrically.[4] The physical behavior of the surfactant micelles can be envisaged as the construction of a model membrane to mimic a biological system. This experimental model is useful for studying the interaction of biolo-

* Corresponding author. E-mail: naeemkashif@yahoo.com
doi: 10.2298/JSC110121182N

gical surfaces with the additive molecule.[5] Phenylalkanoic acids and their derivatives are being used in pharmaceutical research. These compounds act as agonists for hPPARs (human peroxisome proliferator activated receptors), in particular the human PPARα isoform, and are effective in the treatment of abnormal lipid metabolism, diabetes and other disorders.[6,7]

In the past, the solubilization of various hydrophobic additives in aqueous micellized ionic surfactant systems were investigated.[8–12] Recently, spectroscopic studies of diverse organic additives in different ionic surfactant systems were reported.[13–15] In the current study, short chain phenylalkanoic acids in aqueous solution of anionic sodium dodecyl sulfate (SDS) and cationic cetyltrimethylammonium bromide (CTAB) surfactants were investigated. The additives studied were phenylmethanoic acid (PhMA), phenylethanoic acid (PhEA), 3-phenylpropionic acid (3-PhPA) and 3-phenylpropeonic acid or cinnamic acid (CA). The general structures of the additives are given below:

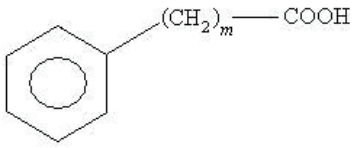

m = 0–2
Phenylalkanoic acids

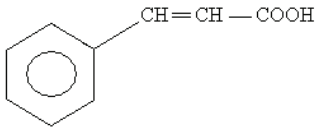

Cinnamic acid

In this current study, the effect of increasing the alkyl chain length in acid molecules on their solubilization in cationic and anionic surfactant solutions was studied using UV spectroscopy. The incremental free energy change of transfer per methylene group, $\Delta G^{\ominus}(CH_2)$, and site of solubilization were evaluated and are discussed.

EXPERIMENTAL

Reagents

The CTAB and SDS were obtained from Sigma and Fluka, respectively. Phenylalkanoic acids ($C_6H_5(CH_2)_mCOOH$, *m* = 0–2) and cinnamic acid were obtained from Merck. All chemicals were used without further purification. The water used throughout was distilled twice over alkaline permanganate in a Pyrex all-glass set-up.

Simple absorbance measurements

The UV absorption spectra of phenylalkanoic acids, each of concentration 1×10^{-6} mol dm^{-3} in aqueous solution, were measured at 25.0±0.1 °C on a Hitachi double beam UV-220 type spectrophotometer equipped with 10 mm matched quartz cells. Then the absorption spectra of 1×10^{-6} mol dm^{-3} phenylalkanoic acid solution containing CTAB and SDS were taken at 25.0 °C using water as the blank.

Differential absorbance measurements

An additive solution (phenylalkanoic acid) of a particular concentration (1×10^{-6} mol dm^{-3}) was prepared. One portion of this solution was used as a solvent for SDS micellar solutions. Measurements were made at 25.0±0.1 °C in such a way that a cuvette filled with an additive solution was set on the reference side and cuvette filled with SDS micellar solutions at the same additive concentration on the sample side of the instrument.

Conductance measurements

The specific conductance of twenty CTAB (1.29×10^{-4} to 13.5×10^{-4}) and SDS (1.14×10^{-3} to 12.0×10^{-3}) aqueous solutions were measured on a microprocessor conductivity meter (WTW), LF 2000/C at 25.0 °C. A water thermostat was used to control the temperature within ±0.1 °C. The critical micelle concentration (*cmc*) was determined from plots of the specific conductance *versus* the concentration of the surfactant solution. The *cmc* values for SDS and CTAB in water were determined to be 8.0×10^{-3} and 9.0×10^{-4} mol dm^{-3}, respectively.

RESULTS AND DISCUSSION

The absorption spectra of a representative acid (PhMA) in water and at certain concentrations of SDS and CTAB are shown in Fig. 1. Surfactant solutions are known to cause a red shift in the spectra of organic additives. The effect of various concentrations (c_s) of CTAB and SDS on the maximum absorption wavelength (λ_{max}) of the phenylalkanoic acids are shown in Figs. 2 and 3. In addition, the absorbance (A) for two representative acids, PhMA and 3-PhPA, are given in Tables I and II. It can be inferred from Figs. 2 and 3 that the UV spectra shift continuously to higher wavelengths. The increase in absorbance with increasing c_s is due to the increased number of additive molecules in the micellar phase.[16] At surfactant concentrations above the *cmc*, the spectra no longer change with increasing c_s assuming all the additive molecules are taken into the micelles.

The value of red shift was greater for the more hydrophobic acid (3-PhPA) than the less hydrophobic acid (PhMA) in presence of both the surfactants. The more hydrophobic acid exhibited a larger red shift even at surfactant concentra-

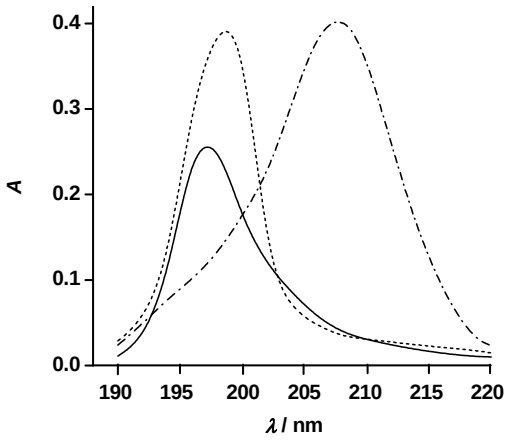

Fig. 1. Absorption spectra of PhMA in water (–), in 6.0 mmol dm^{-3} SDS (···) and in 0.6 mmol dm^{-3} CTAB (–··–).

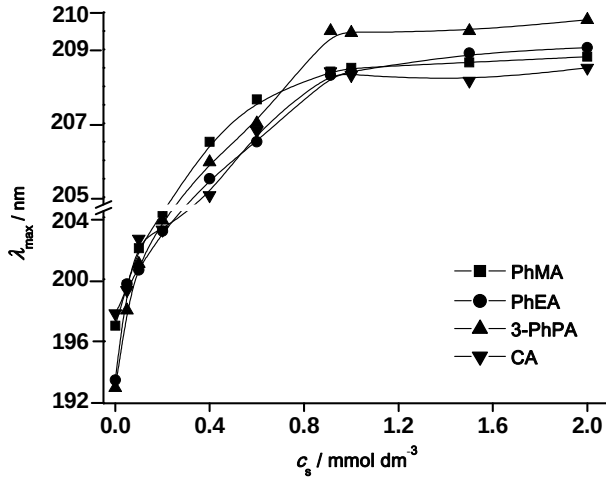

Fig. 2. Effect of increasing concentration of CTAB on the λ_{max} of phenylalkanoic acids.

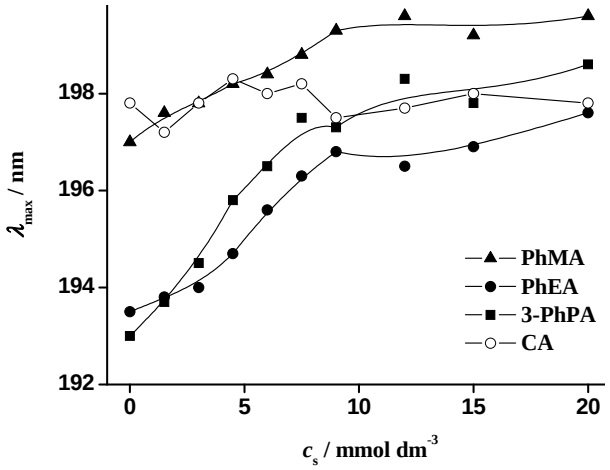

Fig. 3. Effect of increasing concentration of SDS on the λ_{max} of phenylalkanoic acids.

tions below their observed *cmc*. The shift also depends on the nature of charge (positive or negative) present on the surfactant head group. In the case of 3-PhPA, the value of red shift in the cationic surfactant (CTAB) was $\Delta\lambda_{max}$ = 16.9 nm as compared to the anionic surfactant (SDS), where $\Delta\lambda_{max}$ = 5.6 nm. Hence, the red shift for each acid in the anionic surfactant solutions was smaller. The red shifts in the spectra are generally representative of the interaction between surfactant and additive acid. The initial shifts represent the association between additive and monomeric surfactant, while the λ_{max} value becomes more uniform in the micellar region. The red shift also represents changes in the micropolarity around the orientated chromophore, due to which the energy of transition is reduced. The red shift in the case of acids could also be due to their conversion to anions, the bands of which are likely to appear at higher wavelength values compared to the un-

dissociated acids. The anions are attached significantly to cationic CTAB and the binding phenomenon could involve the parallel stacking of acid molecules with surfactant monomer, and later reorientation to incorporate them into the micelles as the *cmc* is reached. On the other hand, owing to the repulsive interaction between the acid anion and SDS head, the only possibility of interaction is through water bridging, hence the wavelength was not altered much with the anionic surfactant. As c_S is increased, there is a continuous change in the wavelength, initially due to complex formation or binding with monomeric surfactant and later due to appearance of premicellar aggregates and ultimately due to presence of polarity gradient offered by the organized solutions of the two surfactants.

TABLE I. Absorbance (A) of phenylalkanoic acids at various concentrations (c_s) of CTAB

c_s / mmol dm^{-3}	PhMA	3-PhPA
0.0	0.256	0.291
0.050	0.305	0.304
0.10	0.339	0.327
0.20	0.351	0.349
0.40	0.389	0.403
0.60	0.402	0.435
0.91	0.409	0.539
1.0	0.539	0.552
1.5	0.618	0.591
2.0	0.620	0.588

TABLE II. Absorbance (A) of phenylalkanoic acids at various concentrations (c_s) of SDS

c_s / mmol dm^{-3}	PhMA	3-PhPA
0	0.256	0.291
1.5	0.248	0.282
3.0	0.273	0.221
4.5	0.283	0.248
6.0	0.389	0.248
7.5	0.406	0.272
9.0	0.420	0.304
12	0.411	0.326
15	0.429	0.335
20	0.435	0.344

However, the λ_{max} values of the CA obtained in pure water are comparable to those obtained in the surfactant solutions of SDS. This means “no change in polarity” around the oriented chromophore of the CA or, in other words, the incapability of the CA molecules to penetrate into the SDS micelles. It was suggested that the anions of CA are incapable of penetrating into the SDS micelles owing to repulsive interactions between the negatively charged oxygen of the CA anion and the anionic head of SDS.[17] Similar behavior was observed for cationic hemi-

cyanine dyes into CTAB micellar solutions.[8] The CTAB, which contains positive head group, interacts with the negative charge present on the phenylalkanoic acid molecules. In turn, the acid molecules penetrate easily into the CTAB micelles.

The differential absorbances (ΔA) spectra of PhMA solutions in the presence of SDS at different concentrations are shown in Fig. 4. The ΔA values were obtained at the wavelength λ_{max}, where the highest peak appears in the spectra. The shift of each peak with increasing c_s can be ignored within experimental error (±0.5 nm). The λ_{max} wavelengths for the respective acids are given in Table III. The increase in ΔA with increasing surfactant concentration is attributed to the increase in the number of solubilized additive molecules in the micellar phase, as observed for other additives.[8–14,18]

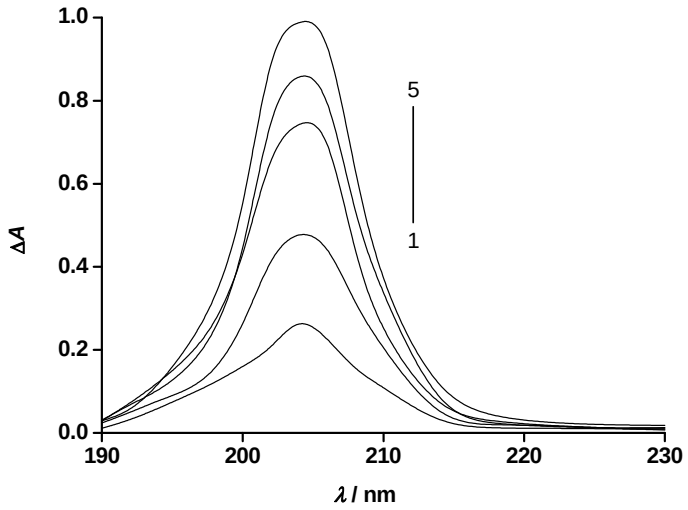

Fig. 4. Differential absorption spectra of PhMA in: 1) 18.0, 2) 36.0, 3) 54.0, 4) 72.0 and 5) 90.0 mmol dm^{-3} solutions of SDS.

The ΔA values of solutions of phenylalkanoic acids in the presence of various concentrations of SDS at 25.0 °C are shown in Fig. 5. In the pre-micellar region, ΔA is practically zero and increases for each acid with increasing concentration of SDS. ΔA was recorded at the respective maximum wavelength (λ_{max}). Kawamura *et al.*,[18] developed a relationship for the determination of the water–micelle partition coefficient, K_c.

$$\frac{1}{\Delta A} = \frac{1}{K_c \Delta A_\infty (c_a + c_s^{mo})} + \frac{1}{\Delta A_\infty} \quad (1)$$

where ΔA_∞ represents the ΔA value at infinitive c_s, c_a is the concentration of additive and c_s^{mo} is the micellized concentration of the surfactant and is given by c_s–cmc_0 (cmc_0 is the *cmc* of the surfactant in water). The dimension of K_c in Eq.

(1) is $dm^3\ mol^{-1}$, which is related to K_x as $K_c = K_x/n_w$, where n_w is the number of moles of water per dm^3, *i.e.*, 55.5 mol dm^{-3}.

TABLE III. Values of λ_{max} and K_x for the added phenylalkanoic acids in SDS and CTAB solutions

Additive	SDS			CTAB[10]		
	λ_{max}	K_x	$\Delta G_p^{\ominus}$ / kJ mol^{-1}	λ_{max}	K_x	$\Delta G_p^{\ominus}$ / kJ mol^{-1}
PhMA	204.3	1358	17.87	208.7	13123	23.49
PhEA	203.4	2204	19.07	211.6	34776	25.91
3-PhPA	203.8	3105	19.92	210.7	54851	27.04
CA	–	–	–	207.0	41658	26.35

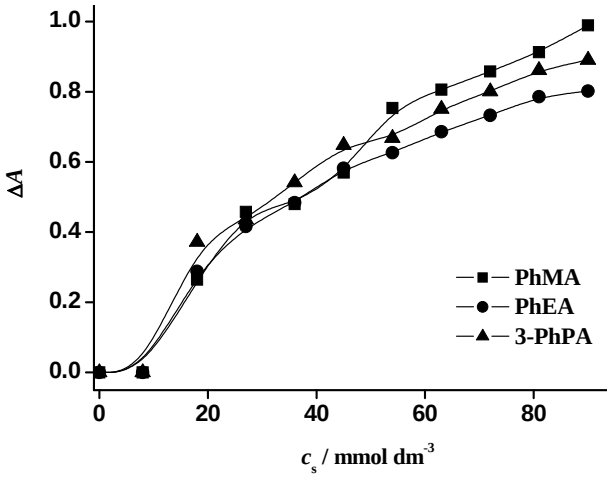

Fig. 5. Effect of the SDS concentration on the differential absorbance of phenylalkanoic acids.

The plots of $1/\Delta A$ against $1/(c_a + c_s^{mo})$ for phenylalkanoic acids at a certain concentration of additive ($c_a = 1.0\times10^{-6}$ mol dm^{-3}) are presented in Fig. 6. The intercept and slope of the linear relationship in Eq. (1) give the values of ΔA_∞ and K_c. The values of K_x calculated from K_c are given in Table III.

The standard free energy change, $\Delta G_p^{\ominus}$, of the transfer of the additives from bulk water to micelles is given by the relationship:

$$\Delta G_p^{\ominus} = -RT \ln K_x \tag{2}$$

where R is the general gas constant and T is the absolute temperature. The $\Delta G_p^{\ominus}$ values are summarized in Table III.

Free energy change per methylene group, $\Delta G^{\ominus}(CH_2)$, from water to micelles is obtained from straight-line plots using the following equation:

$$-\Delta G^{\ominus}(CH_2) = RT \frac{d \ln K_x}{dm} \tag{3}$$

where R and T are defined parameters and m refers to the number of methylene groups in alkyl chain of the acid molecules. The plots of ln K_x *vs.* m for both systems are shown in Fig. 7. The values of $\Delta G^{\ominus}(CH_2)$ evaluated from the plots are –1.03 and –1.77 kJ mol^{-1} for the SDS and CTAB system, respectively.

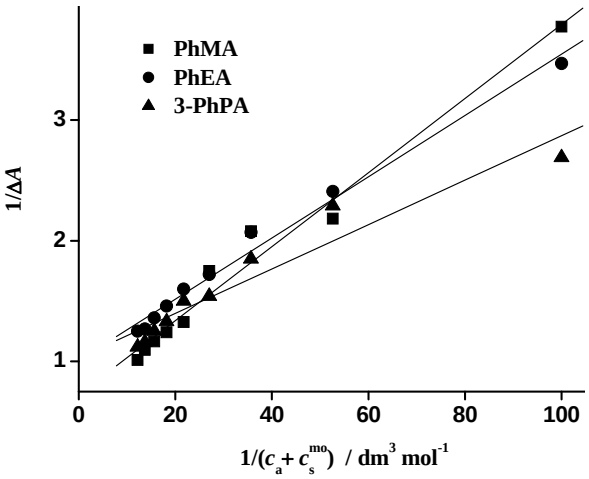

Fig. 6. Relationship between $1/\Delta A$ and $1/(c_a + c_s^{mo})$ for phenylalkanoic acids.

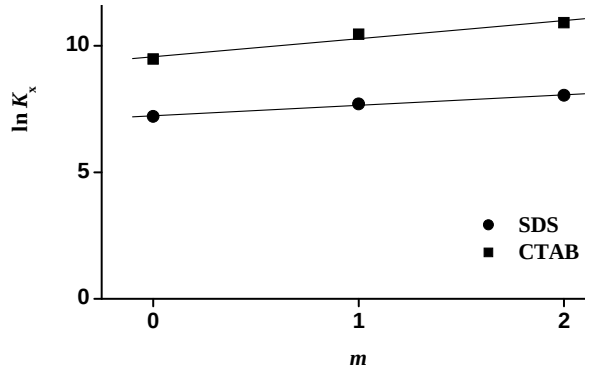

Fig. 7. ln K_x *vs.* the number of carbon atoms in hydrocarbon chain of phenylalkanoic acids.

The values of the free energy change per methylene group of transfer from water to ionic micelles were reported to be –1.3 kJ mol^{-1} for alkyl phenoxide ions and alkyl phenols, and –1.25 kJ mol^{-1} for benzoic acid and aniline.[19] The free energy of transfer per CH_2 group of the same compounds from water to *n*--heptane was close to –3.76 kJ mol^{-1}. These results were taken to imply that the compounds were solubilized within an aqueous environment, such as near the micellar interface region.[20] It may be concluded from the above results that the solubilization site of phenylalkanoic acids in the ionic micelles was the water––micelle interface. The lower value of $\Delta G^{\ominus}(CH_2)$ in the CTAB system suggests that this system was more favorable for solubilization than the SDS system. The

negative value of $\Delta G^{\ominus}(CH_2)$ indicates that the solubilization of phenylalkanoic acids into micelles was a spontaneous phenomenon.

In view of the fact that the phenyl ring was common in the phenylalkanoic acids, the alkyl chain appears to be an important factor for the solubilization. The insignificant shifts in the λ_{max} of phenylalkanoic acids in SDS solutions show the presence of electrostatic repulsion between the anions of the acids and SDS. However, phenylalkanoic acids were expected to interact favorably with CTAB. The partition coefficients, K_x, obtained in CTAB micellar solutions were higher than those found for the SDS micellar solutions. The higher K_x values indicate stronger interaction and hence enhanced solubility of the acids in the CTAB micelles. It is recognized that aromatic acids counter ions are more efficient with cationic micelles.[21] Furthermore, it was reported that CTAB micelles cause more ionization of aromatic acids, which leads to increase in the van der Waals association between the surfactant molecules and the additive molecules.[22] It is suggested that additive molecule forms an ion pair with the surfactant monomer. The adhesion of this ion pair to the micellar surface enhances the incorporation of additive molecule at a later stage. Where hydrophobic interactions allow for parallel stacking of additive acids with monomeric surfactants[13] and incorporation of acids into the micelles is in such a way that their hydrophobic part is directed inwards towards micellar core, both these factors change the polarity of microenvironment around the oriented chromophore and hence cause a red shift by lowering the energy of transition.

CONCLUSIONS

The differential absorbance of the phenylalkanoic acids increased with increasing surfactant concentration, indicating that the acid molecules absorbed light more favorably in the micellar phase than in the aqueous phase. However, cinnamic acid is incapable of penetrating into SDS micelles due to analogous charge. An increase in the hydrophobicity of the acid molecules affects an increase in the K_x values. Moreover, the solubilization site of phenylalkanoic acids in ionic micelles is the water–micelle interface.

Acknowledgements. The authors gratefully acknowledge the donation of the microprocessor conductivity meter by the German Academic Exchange Program (DAAD). The authors are grateful to an anonymous referee for fruitful comments and suggestions.

ИЗВОД

INTERAKCIJA KRATKOLANČANIH FENILALKANSKIH KISELINA SA MICELAMA POVRŠINSKI AKTIVNIH SUPSTANCI U VODENOJ SREDINI

KASHIF NAEEM[1], SYED W. H. SHAH[2], BUSHRA NASEEM[3] и SYED S. SHAH[2]

[1]Central Analytical Facility Division, PINSTECH, PO Nilore, Islamabad 45650, [2]Department of Chemistry, Hazara University, Mansehra, Pakistan и [3]Department of Chemistry, Lahore College for Women University, Lahore, Pakistan

Растворљивост и интеракција фенилалканских киселина у присуству катјонске, цетилтриметиламонијум-бромида (CTAB), и анјонске површински активне супстанце натријум-додецилсулфата (SDS) испитивана је спектрофотометријски на 25,0 °C. UV спектри адитива (киселина) су мерени без присуства и у присуству површински активних супстанци, испод и изнад критичне мицеларне концентрације (*cmc*). Присуство алкилног ланца у фенилалканским киселинама је одговорно за хидрофобну интеракцију и померај у спектру према већим таласним дужинама. Вредност партиционог коефицијента (K_x) између воде и мицеле површински активне супстанце и стандардна слободна енергија растварања ($\Delta G_p^{\ominus}$) су такође одређени мерењем диференцијалне абсорбанције (ΔA) адитива у мицеларном раствору.

(Примљено 21. јануара, ревидирано 10. августа 2011)

REFERENCES

1. P. H. Elworthy, A. T. Florence, C. B. Macfarlane, *Solubilization by Surface-Active Agents.*, Chapman & Hall, London, 1968
2. M. J. Rosen, *Surfactant and Interfacial Phenomena.*, Wiley, New York, 1978
3. J. A. Marqusee, K. A. Dill, *J. Chem. Phys.* **85** (1986) 434
4. L. Sepulveda, *J. Colloids Interface Sci*. **46** (1974) 372
5. H. Sato, Y. Kusumoto, N. Nakashima, K. Yoshihara, *Chem. Phys. Lett*. **71** (1980) 326
6. J. Kasuga, M. Makishima, Y. Hashimoto, H. Miyachi, *Bioorg. Med. Chem. Lett*. **16** (2006) 554
7. M. Pal, *Tetrahedron* **65** (2009) 433
8. S. S. Shah, R. Ahmad, S. W. H. Shah, K. M. Asif, K. Naeem, *Colloids Surf., A* **137** (1998) 301
9. S. S. Shah, G. M. Laghari, K. Naeem, S. W. H. Shah, *Colloids Surf., A* **143** (1998) 115
10. S. S. Shah, K. Naeem, S. W. H. Shah, H. Hussain, *Colloids Surf., A* **148** (1999) 299
11. S. S. Shah, K. Naeem, S. W. H. Shah, G. M. Laghari, *Colloids Surf., A* **168** (2000) 77
12. K. Naeem, S. S. Shah, S. W. H. Shah, G. M. Laghari, *Monatsh. Chem.* **131** (2000) 767
13. S. W. H. Shah, K. Naeem, B. Naseem, S. S. Shah, *Colloids Surf., A* **331** (2008) 227
14. B. Naseem, S. W. H. Shah, A. Hasan, S. S. Shah, *Spectrochim. Acta A* **75** (2010) 1341
15. S. W. H. Shah, K. Naeem, B. Naseem, M. Hasan, S. S. Shah, *Phys. Chem. Liq.* **48** (2010) 316
16. Y. Miyashita, S. Hayano, *Bull. Chem. Soc. Jpn*. **54** (1981) 3249
17. M. Foti, M. Piatteli, M. T. Baratta, G. J. Ruberto, *J. Agric. Food Chem*. **44** (1996) 497
18. H. Kawamura, M. Manabe, Y. Miyamoto, Y. Fujita, S. Tokunaga, *J. Phys. Chem.* **93** (1989) 5536
19. C. A. Bunton, L. Sepulveda, *J. Phys. Chem*. **83** (1979) 680
20. C. Hirose, L. Sepulveda, *J. Phys. Chem.* **85** (1981) 3689
21. S. Kumar, Z. A. Khan, Kabir-ud-Din, *J. Surfact. Deterg.* **5** (2002) 55
22. C. A. Bunton, M. J. Minch, *J. Phys. Chem.* **78** (1974) 1490.

Journal of the Serbian Chemical Society
JSCS-info@shd.org.rs • www.shd.org.rs/JSCS
J. Serb. Chem. Soc. 77 (2) 211–224 (2012)
JSCS–4262
UDC 547.478+546.11+544.35:542.8
Original scientific paper

On the kinetics of the hydrogen evolution reaction on Ni–MoO_x composite catalysts in alkaline solutions

BORKA M. JOVIĆ[1], UROŠ Č. LAČNJEVAC[1#], VLADIMIR D. JOVIĆ[1], LJILJANA M. GAJIĆ-KRSTAJIĆ[2#] and NEDELJKO V. KRSTAJIĆ[3]

[1]Institute for Multidisciplinary Research, University of Belgrade, P. O. Box 33, 11030 Belgrade, Serbia, [2]Institute of Technical Sciences SASA, Knez Mihajlova 35, 11000 Belgrade, Serbia and [3]Faculty of Technology and Metallurgy, University of Belgrade, Karnegijeva 4, 11000 Belgrade, Serbia

(Received 21 June, revised 19 September 2011)

Abstract: MoO_3 particles were co-deposited with Ni onto smooth or rough Ni supports from modified Watt baths of different compositions. Morphology and composition of the electrodeposits were characterized by means of cyclic voltammetry, X-ray diffraction analysis, scanning electron microscopy, transmission electron microscopy and energy dispersive X-ray spectroscopy. The electrocatalytic activity of the composite catalysts for H_2 evolution in alkaline solutions was determined by quasi-stationary polarization curves. Activity increases with MoO_x content in the Ni deposit up to a limiting value. The composite Ni–MoO_x catalysts exhibited high catalytic activity, similar to that of a commercial Ni–RuO_2 catalyst. Stability tests showed that the Ni–MoO_x co-deposits were stable under constant current conditions and exhibited excellent tolerance to repeated short-circuiting.

Keywords: hydrogen evolution; nickel; molybdenum trioxide; composite catalyst; co-deposition.

INTRODUCTION

The hydrogen evolution reaction (HER) is one of the most studied electrochemical reactions because it occurs through a limited number of reaction steps with only one reaction intermediate involved. It is a unique electrochemical reaction for which the complete theory of electrocatalysis was developed.[1,2]

Hydrogen evolution is the most frequent cathodic reaction in industrial electrolytic processes and has been recognized as a valuable fuel that may well replace oil as an energy source. It also plays a major role in synthetic organic chemistry in the well-known catalytic hydrogenation process.[3] One major aspect of

* Corresponding author. E-mail: nedeljko@tmf.bg.ac.rs
# Serbian Chemical Society member.
doi: 10.2298/JSC112106185J

the research undertaken is to improve catalytic electrode materials in terms of their activity, efficiency and mechanical and corrosion stability. Nickel-based materials were shown to exhibit these characteristics and are widely used in industrial processes.

Alloying two metals has long appeared to be the most straightforward way of achieving electrocatalytic activation. In the case of the hydrogen evolution reaction, it seems that Ni–Mo catalysts, either electrodeposited,[4] or thermally prepared,[5] or added *in situ*,[6] have constituted the main objective of research during the past twenty years.

Synergetic effects were explicitly ruled out in the case of *in situ* activation with molybdate.[7,8] As molybdate was deposited from technical solutions, a co-deposit of Mo and Ni (Fe, Co) was in fact formed, but the Tafel slope remained the same as that for pure Ni. The same was the case of Ni–Mo bulk alloys.[9] In the case of Ni–Mo catalysts prepared by thermal decomposition of suitable precursors, synergetic effects were observed, with a maximum at around 30 at. % Ni.[10] The Tafel slope decreased to 40 mV and extended to very high current densities, while the exchange current density close to 10 mA cm^{-2} was by three orders of magnitude higher than that for bulk Ni. However, these electrodes did not possess the expected stability during prolonged electrolysis, mainly due to the drastic irreversible reduction of the corresponding metal oxides during cathodic polarization, which caused the collapse of the oxide lattice.[11]

Ni–Mo coatings obtained by electroplating exhibited so-called "synergetic effects" in contrast to Ni–Mo bulk alloys.[12,13] The specific role of Mo in Ni–Mo electroplated coatings could be explained by the fact that the molybdenum was present more likely as an amorphous oxides phase than as a pure metallic phase. However, the morphology of Ni (Fe,Co)–Mo electroplated coatings were characterized by the presence of numerous micro-cracks down to the support.[14–18] Accumulation of molecular hydrogen in localized areas, such as micro-cracks, in the coating may result in the formation of internal bursts or blisters and the coating becomes mechanically fragile. In addition, it was found that Mo is not at all stable in alkaline solution when a cell is shut down, as it tends to be leached out, which could be the origin of deactivation on cathodic load.[19]

Improved performances are to be expected if a composite compact layer of Ni and some Mo oxides could be prepared by the simultaneous electrodeposition of Ni and MoO_3 from an electrolyte solution in which MoO_3 particles are suspended. It seems a unique way for solving the problem of porosity of electroplated Ni–Mo coatings and low mechanical stability of thermally prepared Ni–Mo catalysts. Therefore, the aim of this study was to determine the conditions for the preparation of compact Ni–MoO_x composite coatings possessing high catalytic activity towards the HER.

EXPERIMENTAL

Electrode preparation

The Ni/(Ni–MoO_x) active cathodes were prepared by the simultaneous electrodeposition of Ni and suspended MoO_3 particles onto a Ni substrate from a Watt bath of the following composition: $NiSO_4 \cdot 6H_2O$ – 330 g dm^{-3}; $NiCl_2 \cdot 6H_2O$ – 45 g dm^{-3}; H_3BO_3 – 38 g dm^{-3}; pH: 3.2–4.0. The deposition was performed at 40 °C. Nickel platelets (10 mm×10 mm×0.2 mm) with a very thin stem were used as substrates.

The MoO_3 powder was prepared by thermal decomposition of $(NH_4)_6Mo_7O_{24} \cdot 4H_2O$ at 500 °C for 2 h under an air atmosphere[20] and was dispersed by means of a magnetic stirrer. The amount of MoO_3 particles in the bath was varied between 0 and 20 g dm^{-3}.

The pre-treatment of the Ni support consisted of either etching (HCl) or mechanical polishing (emery paper). Electrodeposition was performed galvanostatically in a stirred solution (magnetic stirrer at 400 rpm) at 40 °C by varying the current density, typically from 5 to 50 mA cm^{-2}, for a constant electricity (72 C cm^{-2}). All deposition experiments were performed using a self-made rectifier.

Electrode characterization

Scanning electron microscopy (SEM, on JOEL 840) was used to characterize the morphology of the as-deposited surface. Transmission electron microscopy (TEM) measurements were performed using the FEI (Fillips Electronic Instruments) – CM200 super-twin and CM300 ultra-twin microscopes operating at 200 and 300 kV, equipped with Gatan 1k×1k and 2k×2k CCD cameras, respectively. Specimens for TEM analysis were prepared by making a suspension of the catalyst powder in ethanol, using an ultrasonic bath. The catalyst powder was prepared by grounding the Ni–MoO_x coating electrodeposited onto a glassy carbon support. XRD Analysis of Ni–MoO_3 composite coatings was carried out by Siemens D-500 diffractometer. CuK radiation was used in conjunction with a CuK (nickel filter). Obtained X-ray diffraction pattern was used to evaluate the phase structure and crystallite size of the coatings.

Cell and chemicals

A conventional three-compartment cell was used. The working electrode (WE) compartment was separated by fritted glass discs from the other two compartments. The WE compartment was jacketed and thermostated during measurements at 25.0 °C or at 85 °C, using a thermostat. All measurements were performed in 1.0 mol dm^{-3} or 33 wt. % NaOH solution (Spectrograde, Merck), prepared in deionized water. The WE compartment was saturated with purified hydrogen at standard pressure during measurements. A saturated calomel electrode (SCE) or a reversible hydrogen electrode (RHE) in the same solution were used as the reference electrodes while a flat Pt sheet served as the counter electrode.

Electrochemical measurements

Tafel lines were recorded using potentiostatic steady-state voltammetry, point by point at 60 s intervals, using a PAR 273 potentiostat, with good reproducibility of measurement. Whenever the potential of the WE approached approximately –1.3 V (SCE) (or when current densities were close to, above approximately 0.1 A cm^{-2}) it was found that the uncompensated solution resistance (IR drop) was significant. Therefore, the IR drop was systematically determined in all measurements, using ac impedance methods. All data presented in this report are corrected for the IR drop.

RESULTS AND DISCUSSION

Efficiency of electrodeposition

The variation of the current efficiency for Ni electrodeposition as a function of the concentration of MoO_3 particles in the solution at a constant current density of 10 mA cm^{-2} is shown in Fig. 1. The current efficiency was estimated from deposition charge and weight increase measurements, assuming that the latter was due to Ni only, without correction for the contribution to the overall weight increase of the dispersed phase. As can be seen from Fig. 1, the current efficiency did not depend significantly on the concentration of suspended MoO_3 particles in the range from 1 to 20 g dm^{-3}. The current efficiency for Ni electrodeposition was generally very low, indicating a high catalytic activity of the Ni–MoO_x co-deposits for the HER, which occurred as a parallel reaction during electrodeposition. However, it is important to emphasize that partial reduction of MoO_3 can also takes place during electrodeposition, according to the following overall reactions:

$$MO_3 + xH^+ + xe \rightleftarrows H_xMoO_3 \quad (1)$$

or

$$MO_3 + 2yH^+ + 2ye \rightleftarrows MoO_{3-y} + yH_2O \quad (0<y<1) \quad (2)$$

Reaction (1) or (2) could additionally reduce the current efficiency for Ni electrodeposition.

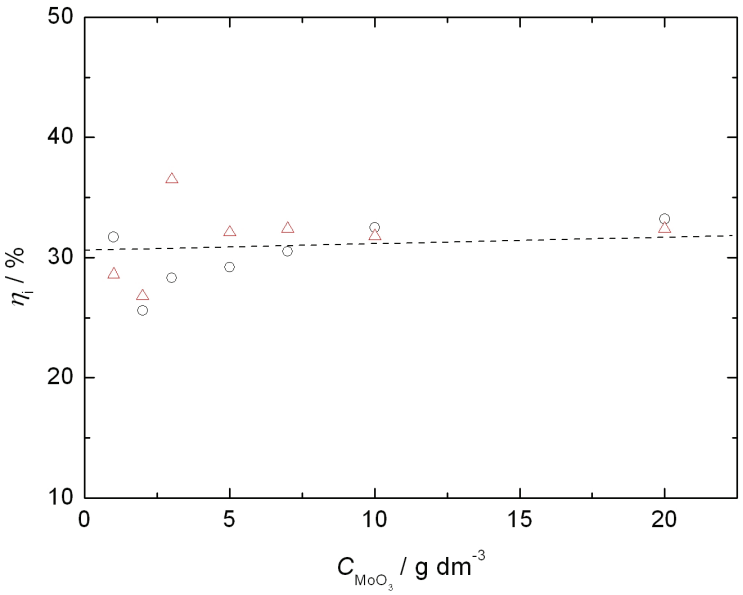

Fig. 1. Effect of the MoO_3 content in the Watt bath on the current efficiency of Ni+MoO_3 co-deposition at j_{Ni} = 10 mA cm^{-2} (circles and triangles present two different measurements).

This speculation is based on previous experiments that showed the reduction of MoO_3 powder in a hydrogen atmosphere at temperature of 623 K proceeded *via* the formation of hydrogen molybdenum bronze, H_xMoO_3. Therefore, during Ni+MoO_3 co-deposition, the formation of similar reduced phases of MoO_3 could occur in which hydrogen species adsorbed onto the Ni surface participate in this reaction.

The dependence of the current efficiency on the applied current density of deposition at a constant concentration of suspended MoO_3 particles in the bath (1 g dm^{-3}) is shown in Fig. 2. The current efficiency decreases with increasing applied current density, probably due to the increase in the relative deposition rate of Ni to MoO_3 particles, which leads to an increase of the catalytic activity of composite (Ni–MoO_x) coatings for the HER.

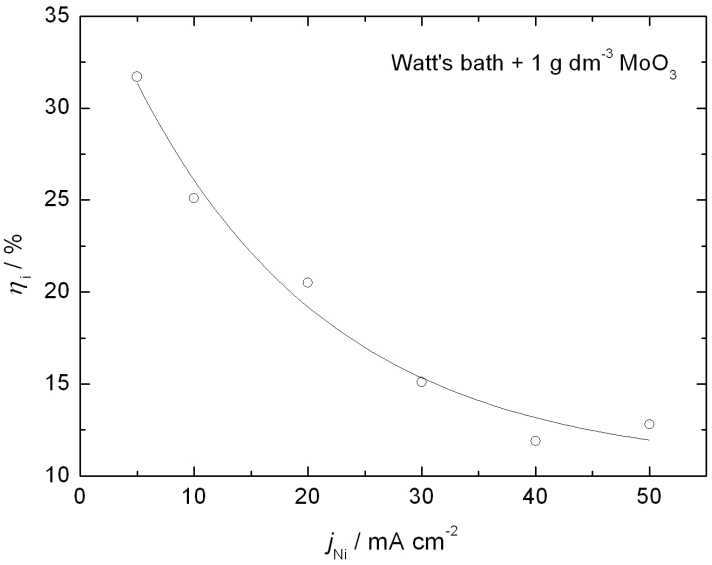

Fig. 2. Current efficiency for Ni+MoO_3 co-deposition as a function of the applied current, determined in a Watt bath containing 1 g dm^{-3} of MoO_3 particles.

Morphology and chemical composition of composite the Ni–MoO_x electrodeposits

Typical top views of the Ni–MoO_x composites electrodeposited at different current densities from a Watt bath containing 1 g dm^{-3} of suspended particles MoO_3. As can be seen, the morphology of the Ni–MoO_x coating deposited at a lower current density is characterized by the presence of micro-cracks, with some 2 μm in width (Fig. 3a), and a high concentration of MoO_3 particles. However, the electrodeposit formed at a higher current density is microcrystalline and compact (Fig. 3c).

The X-ray diffraction (XRD) pattern for a Ni–MoO_x electrodeposit is shown in Fig. 4. It was found that the XRD peaks of MoO_3 had disappeared after co-deposition with Ni and that the Ni–MoO_x composite coating was completely amorphous in nature. The reason for the disappearance of the corresponding XRD peaks is not clear at this stage; the change to an amorphous MoO_x phase during the co-deposition is probably the result of a reduction process in which H_{ads} species participate. Thus, due to amorphous nature of the coating, it was necessary to characterize the composite coating by energy dispersive X-ray spectroscopy (EDS) to determine the chemical composition of the Ni–MoO_x coatings.

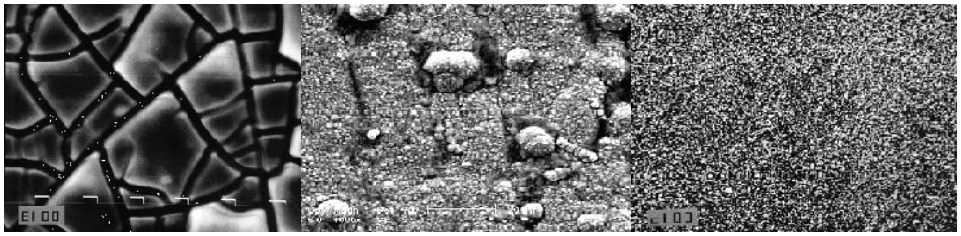

(a) (b) (c)

Fig. 3. Scanning electron micrographs of the Ni–MoO_x electrode surfaces electrodeposited at: a) j_{Ni} = 10 mA cm^{-2}; b) j_{Ni} = 20 mA cm^{-2}; c) j_{Ni} = 50 mA cm^{-2}. The concentration of MoO_3 particles in the Watt bath was 1 g dm^{-3}. Magnification 1000×.

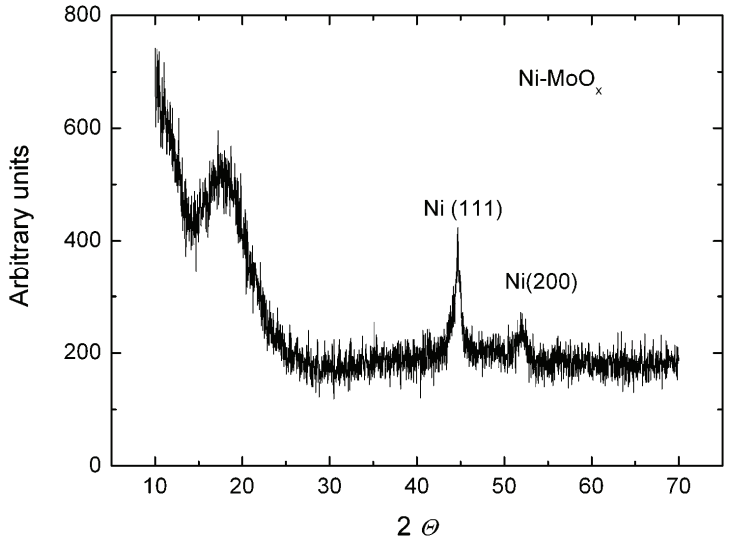

Fig. 4. XRD Pattern (2Θ in degrees) of the composite (Ni–MoO_x) coating prepared by electrodeposition from a Watt bath containing 1 g dm^{-3} of MoO_3 particles at j_{Ni} = 10 mA cm^{-2}.

The amount of MoO_x could hardly be determined by surface spectroscopies, because of the localization of the MoO_x particles, but TEM analysis showed that

MoO_x particles (white spots) were relatively uniformly distributed in Ni matrices (Fig. 5). The chemical composition of the coating (sample obtained by electrodeposition at 30 mA cm^{-2}) at different positions (EDS spectra) is presented in Fig. 5.

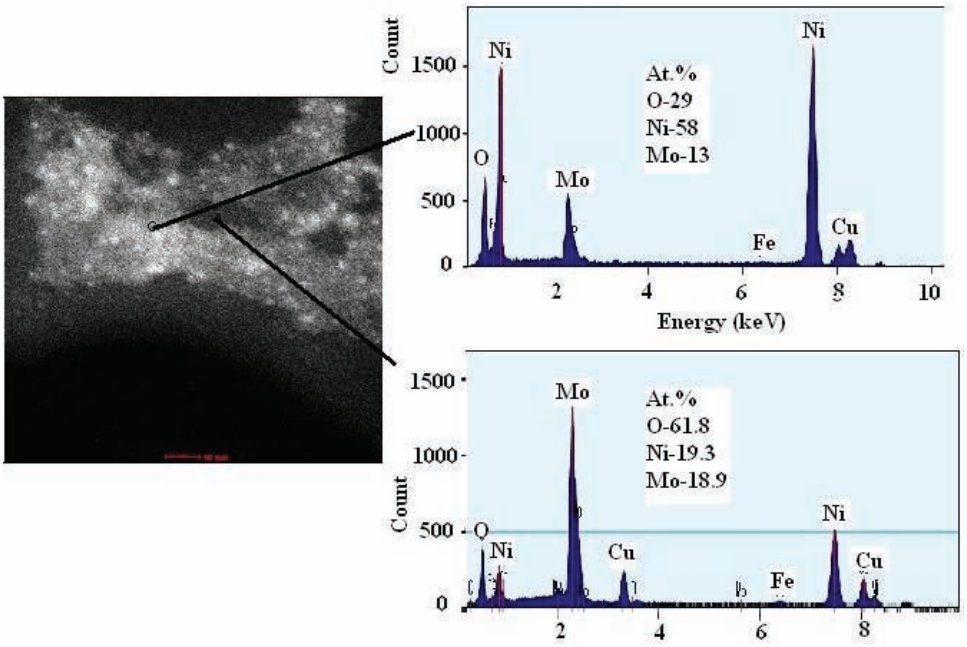

Fig. 5. TEM dark field image and EDS spectra of an electrodeposited Ni–MoO_x layer (j_{Ni} = 50 mA cm^{-2}; 1 g dm^{-3} MoO_3) on a smooth Ni support from a Watt bath. The MoO_x particles are presented by white spots and the corresponding EDS spectra of the region with a low and a high content of Mo oxides.

The average content of Mo oxides in the composite coating generally decreased with increasing deposition current density.

Cyclic voltammetry in 1.0 mol dm^{-3} NaOH

The electrode surfaces of the Ni–MoO_x catalysts were characterized by means of their voltammetric curves (VC). A series of VCs recorded at different scan rates is shown in Fig. 6. The corresponding curves of Ni in the same solution are shown in Fig. 7, for comparison. Reproducible and characteristic voltammograms were obtained. Both electrodes are characterized by a highly reversible peak prior to the oxygen evolution reaction. The reactions occurring at potentials in the range of both the anodic current and the cathodic current peaks are apparently complementary processes, which are represented by the overall reaction:

$$\mathrm{NiO(hydrated)} + \mathrm{OH^-} \rightleftarrows \mathrm{NiOOH} + e^- \quad (3)$$

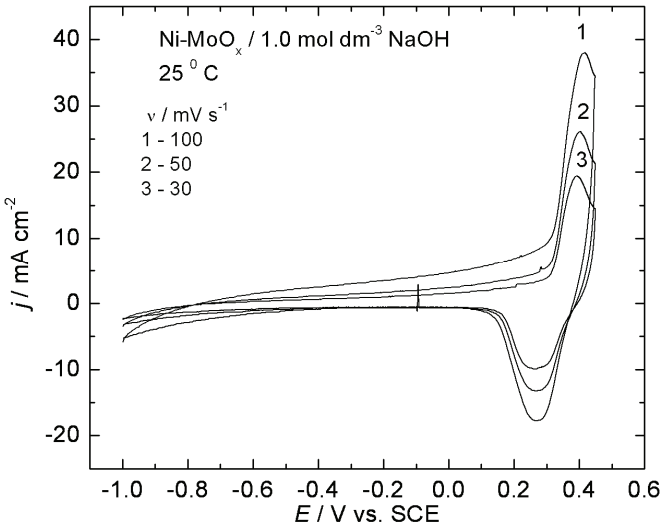

Fig. 6. Cyclic voltammetric curves over the potential range of –1.0 to 0.45 V (SCE) of a Ni/(Ni–MoO_) composite electrode (prepared by electroplating at 50 mA cm^{-2} in a Watt bath containing 1 g dm^{-3} of MoO_3 particles) in 1.0 mol dm^{-3} NaOH solution at 25 °C.

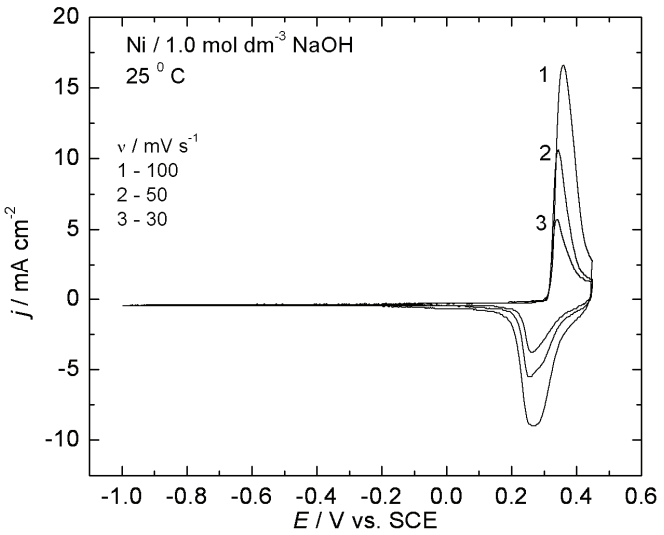

Fig. 7. Cyclic voltammetric curves over the potential range –1.0 to 0.45 V (SCE) of a Ni electrode in 1.0 mol dm^{-3} NaOH solution.

The anodic and cathodic processes referred to in Eq. (3) are highly reversible, in which the solid-state diffusion of hydroxide ions is the rate determining step. It is interesting to emphasize that the introduction of MoO_3 particles into the Ni deposit increased the peak of NiO oxidation and shifted it towards a more

positive value (≈ 50 mV). Consistently, O_2 evolution commenced at a *ca.* 50 mV more negative potential on the Ni electrode than on the composite. The increase of both the anodic and cathodic peaks could be explained by the surface of Ni–MoO_x being rougher than that of the etched Ni surface, because the participation of Mo oxides redox reactions could not be expected, according to the thermodynamic data. Anodic peak current density of the Ni–MoO_x composite catalyst was around two times higher, which means that the real surface area of this electrode is approximately two times higher than the real surface area of the etched Ni electrode.

Polarization measurements in 1.0 mol dm^{-3} NaOH

The polarization curves for the HER obtained on different Ni/(Ni–MoO_x) electrodes prepared by co-deposition onto a mechanically polished Ni substrate, from 1.0 mol dm^{-3} NaOH solution are shown in Fig. 8. The polarization curves were recorded after holding the electrodes at a constant cathodic current density of 100 mA cm^{-2} for about 1 h. The polarization curves are characterized by two Tafel slopes at all electrodes, $b_1 \approx -40$ mV in the lower overpotential region and $b_2 \approx -120$ mV in the high overpotential region. The composite Ni–MoO_x coating obtained by electroplating at j_{Ni} = 50 mA cm^{-2} was found to have the lowest hydrogen overpotential (Fig. 9) and the highest exchange current density, $j_0 \approx$ ≈ 7.9×10^{-4} A cm^{-2} (Fig. 8). The corresponding kinetic parameters for the HER for these electrodes are presented in Table I.

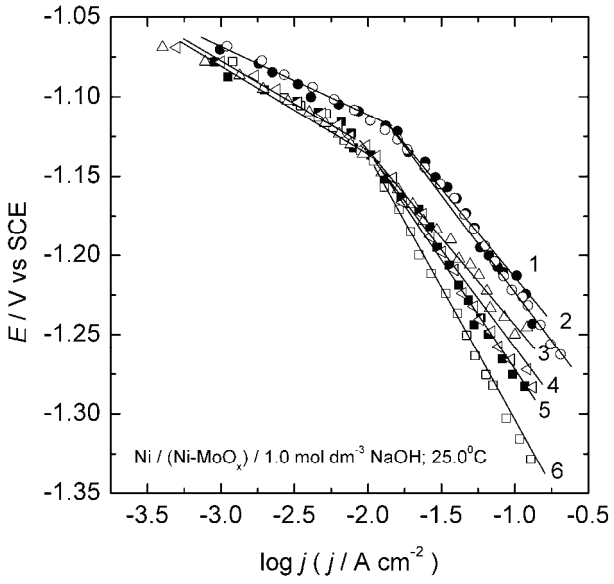

Fig. 8. Tafel polarization curves for the HER on Ni/(Ni–MoO_x) electrodes in 1.0 mol dm^{-3} NaOH solution at 25 °C. The electrodes were prepared by electrodeposition from a Watt bath containing 1.0 g dm^{-3} of MoO_3 particles at different current densities (mA cm^{-2}): 1) 50; 2) 40; 3) 30; 4) 20; 5) 10; 6) 5.

Typical polarization curves for the HER on polished Ni and the most active Ni/(Ni–MoO_x) electrode are shown in Fig. 10, for comparison. In contrast to Ni/

/(Ni–MoO_x), only one Tafel slope of about –120 mV dec^{-1} is present over the complete potential range for the HER on Ni. At the same potential, the activity of Ni/(Ni–MoO_x) was about four orders of magnitude higher than that of the Ni electrode. It is clear from the morphological investigations that the incorporation of MoO_3 particles into a Ni deposit produces roughness, but undoubtedly, syner-

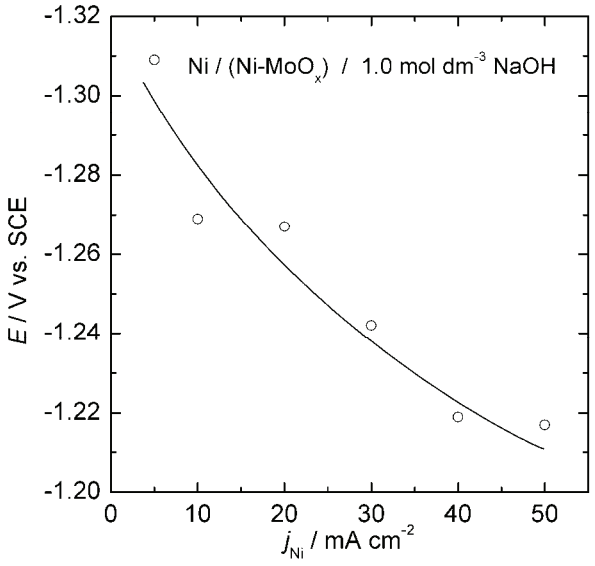

Fig. 9. Potential for the HER at j_{H_2} = 100 mA cm^{-2} on Ni/(Ni–MoO_x) composite electrodes in 1.0 mol dm^{-3} NaOH, prepared by electroplating at different current densities.

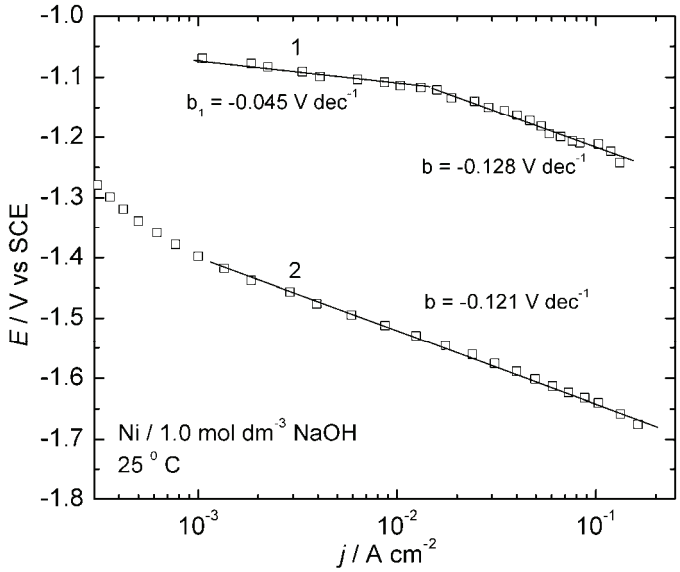

Fig. 10. Tafel polarization curves for the HER on the most active Ni/(Ni–MoO_x) electrode (electrode 1 from Fig. 8) and on an etched Ni electrode in 1.0 mol dm^{-3} NaOH solution at 25 °C.

getic effects are achieved, because the Tafel slope decreases to –40 mV in the lower overpotential region and extends to relatively high current densities. It was shown[21] that the reaction mechanism of the HER on Ni is a consecutive combination of a Volmer and a Heyrovsky step, and that the Heyrovsky step prevails over the Tafel step in the low overpotential region and that the reaction rate is controlled by the Heyrovsky reaction with an almost full coverage by $H_{ads.}$ However, the presence of Tafel slope of –40 mV for the HER on the Ni/(Ni–MoO_x) electrode indicates that the Heyrovsky step controls the rate of the overall reaction in the lower potential range, but with a low coverage by H_{ads} intermediates. In accordance with the mechanism of the HER, both the Volmer and the Heyrovsky steps occurred at a single adsorption site and the reaction occurred at the Ni electrode with an almost full coverage by H_{ads}, but with a low coverage by H_{ads} in the case of the Ni/(Ni–MoO_x) electrode. The fact that the reaction rate was almost four orders of magnitude higher on the latter electrode, indicates an increased catalytic activity of the adsorption sites for the HER on the Ni/(Ni––MoO_x) electrode.

Electrochemical characteristics of the composite Ni–MoOx catalyst in 33 wt.% NaOH solution

The polarization characteristics of the most active Ni/(Ni–MoO_x) cathode were tested in a 33 wt. % NaOH solution at 85 °C, which are typical conditions for industrial chlor–alkali electrolysis.

The polarization curve for the HER at the Ni/(Ni–MoO_x) electrode is shown in Fig. 11. The polarization curve for the HER at a commercial DN3 electrode (Ni–RuO_2, DeNora cathode) is also presented in the same figure, for comparison. It is interesting to note that both electrodes possessed practically the same activity for HER at j = –0.3 A cm^{-2}.

In industrial chlor–alkali electrolysis, one of the technical methods for replacing some the electrodes by new ones is the short-circuiting of a cathode and an anode in the electrolysis bath. Then a reverse current flows through a bypass circuit and the cathode is oxidized, resulting in the loss of electrocatalytic activity for the HER. In the case of the Raney-Ni active cathode, the potential was sharply shifted in the positive potential direction immediately after the short-circuiting and reached 0.30 V *vs.* SCE within about 3 min. It was reported by Yoshida and Morimoto[22] that the reverse current on short-circuiting caused a shift of the potential toward oxidation of the Raney-Ni electrode to lower its electrocatalytic activity, due to formation of NiOOH surface oxide. In order to simulate short-circuiting condition, Ni/Ni–MoO_x cathode was repeatedly polarized at 0.30 V (SCE) for 1000 s, and polarization curves for the HER were recorded after short-circuiting (Fig. 12). At an applied current density of 300 mA cm^{-2}, a decrease of the overvoltage by about 20 mV was observed after the short-circuiting, suggesting

that the Ni/(Ni–MoO_x) active cathode kept an excellent activity irrespective of the presence and the absence of a reverse current due to short-circuiting.

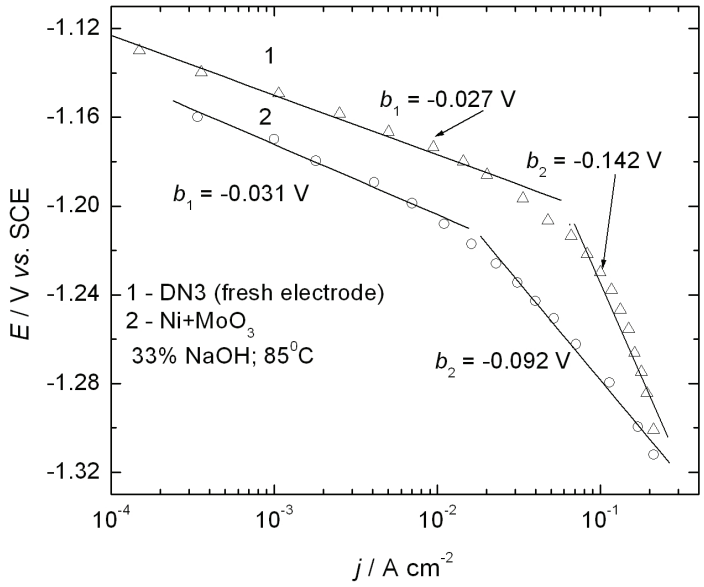

Fig. 11. Tafel polarization curves for the HER on a commercial DN3 electrode (1) and Ni/(Ni–MoO_x) electrode (2) in 33 wt. % NaOH solution at 85 °C. The composite electrode was prepared by electrodeposition from a Watt bath containing 1 g dm^{-3} of MoO_3 particles at j_{Ni} = 50 mA cm^{-2}.

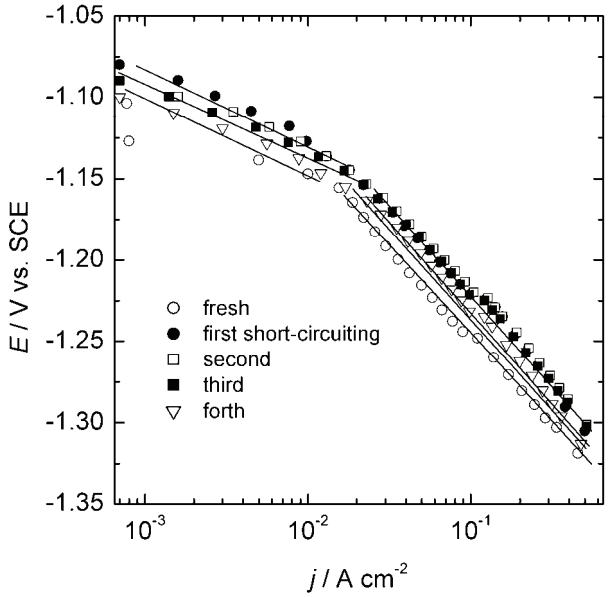

Fig. 12. Tafel polarization curves for the HER on a Ni/(Ni–MoO_x) electrode in 33 wt. % NaOH solution at 85 °C, recorded after short-circuiting. The composite electrode was prepared by electrodeposition from a Watt bath containing 1.0 g dm^{-3} of MoO_3 particles at j_{Ni} = 50 mA cm^{-2}.

CONCLUSIONS

Co-deposition of Ni and MoO_3 particles from a Watt bath produced composite catalysts that possessed high activity for the HER in strong alkaline solutions.

During co-deposition, partial reduction of the MoO_3 particles occurred and the Ni–MoO_x composite coatings prepared by deposition at lower current densities were completely amorphous in nature.

The maximum activity was obtained already at 1 g dm^{-3} MoO_3 in solution (suspension).

Co-deposition resulted in increased surface roughness. The roughness factor for the Ni–MoO_x composite electrode was two orders of magnitude higher than that of a polished Ni electrode.

The true catalytic activities of the composite Ni–NiO_x catalysts for the HER were about two orders of magnitude higher than that of an etched Ni electrode.

The Ni–MoO_x composite catalyst possessed the same activity at high current density for the HER as a commercial DeNora (DN3) electrode in 33 wt. % NaOH solution at 85 °C.

Preliminary stability tests showed that anodic pretreatment of the composite catalyst that simulated short-circuiting conditions did not deactivate the electrode for the HER.

Acknowledgment. This work is financially supported by the Ministry of Education and Science of the Republic of Serbia, under contract No. 172054.

И З В О Д

КИНЕТИКА ЕЛЕКТРОХЕМИЈСКЕ РЕАКЦИЈЕ ИЗДВАЈАЊА ВОДОНИКА НА КОМПОЗИТНИМ NI–MoO_x КАТАЛИЗАТОРИМА У АЛКАЛНИМ РАСТВОРИМА

БОРКА М. ЈОВИЋ[1], УРОШ Ч. ЛАЧЊЕВАЦ[1], ВЛАДИМИР Д. ЈОВИЋ[1], ЉИЉАНА М. ГАЈИЋ-КРСТАЈИЋ[2] и НЕДЕЉКО В. КРСТАЈИЋ[3]

[1]Институт за мултидисциплинарна истраживања, Универзитет у Београду, 11030 Београд, [2]Институт техничких наука САНУ, Кнез Михајлова 35, 11000 Београд и [3]Технолошко–металуршки факултет, Универзитет у Београду, Карнегијева 4, 11000 Београд

Композитне Ni–MoO_x превлаке су формиране истовременим таложењем никла и MoO_3 честица које су суспендоване у Watt-овом купатилу различитог састава. Морфологија и састав композитних превлака испитивани су применом цикличне волтаметрије, трансмисионе и скенирајуће електронске микроскопије и дифракцијом X-зрака. Електрокаталитичка активност композитних превлака за реакцију издвајања водоника у алкалним растворима је одређена стационарним поларизационим мерењима. Показано је да активност катализатора расте са садржајем MoO_3 у Ni превлакама до одређене граничне вредности. Композитне Ni–MoO_x превлаке испољавају високу каталитичку активност, која је слична активности комерцијалног Ni–RuO_2 (De Nora) катализатора. Тестови стабилности су показали да Ni–MoO_x катализатор задржава високу каталитичку активност при константној густини струје издвајања водоника као и одличну толеранцију према реверсној поларизацији.

(Примљено 21. јуна, ревидирано 19. септембра 2011)

REFERENCES

1. R. Parsons, *Trans. Faraday Soc*. **54** (1958) 1053
2. S. Trasatti, *J. Electroanal. Chem*. **39** (1972) 163
3. R. L. Augustine, in *Catalytic Hydrogenation*, Marcel Dekker, New York, 1985, p. 26
4. N. Elezović V. D. Jović, N. V. Krstajić, *Electrochim. Acta* **50** (2008) 5594
5. D. E. Brown, M. N. Mahmood, A. K. Turner, S. M. Hall, P. O. Fogarty, *Int. J. Hydrogen Energy* **7** (1982) 405
6. J. Y. Huot, L. Brossard, *J. Appl. Electrochem.* **18** (1988) 815
7. J. Y. Huot, L. Brossard, *J. Appl. Electrochem*. **20** (1990) 281
8. J. Y. Huot, L. Brossard, *Surf. Coat. Technol*. 34 (1998) 373
9. B. E. Conway, L. Bai, *J. Chem. Soc., Faraday Trans. 1* **81** (1985) 1841
10. M. M. Jakšić, *Mat. Chem. Phys*. **1** (1989) 22
11. M. Yoshida, Y. Noaki, in *Performance of Electrodes for Industrial Electrochemical Processes*, F. Hine, B. V. Tilak, J. M. Fenton, J. D. Lisius, Eds., The Electrochemical Society, Penington, NJ, USA, 1989, p. 15
12. L. S. Sanches, S. H. Domingues, A. Carubelli, L. H. Mascaro, *J. Braz. Chem. Soc*. **14** (2003) 556
13. L. S. Sanches, S. H. Domingues, C. B. Marino, L. H. Mascaro, *Electrochem. Commun*. **6** (2004) 543.
14. E. J. Podlaha, D. Landolt, *J. Electrochem. Soc*. **143** (1996) 893
15. E. Chassaing, N. Portail, A. F. Levy, G. Wang, *J. Appl. Electrochem*., **34** (2004)1085.
16. M. Donten, H. Cesiulis, Z. Stojek, *Electrochim. Acta* **50** (2005) 1405
17. M. Donten, H. Cesiulis, Z. Stojek, *Electrochim. Acta* **45** (2000) 3389
18. H. Cesiulis, A. Baltutiene, M. Donten, M. L. Donten, Z. Stojek, *J. Solid State Electrochem.* **6** (2002) 237
19. J. Divisek, H. Schmitz, J. Balej, *J. Appl. Electrochem*. **19** (1989) 519
20. Z. M. Hanafa, M. A. Khilla, M. H. Askae, *Thermochim. Acta* **45** (1981) 221
21. N. Krstajić, M. Popović, B. Grgur, M. Vojnović, D. Šepa, *J. Electroanal. Chem*. **512** (2001) 16
22. N. Yoshida, T. Morimoto, *Electrochim. Acta* **39** (1994) 1733.

Journal of the Serbian Chemical Society
JSCS-info@shd.org.rs • www.shd.org.rs/JSCS
J. Serb. Chem. Soc. 77 (2) 225–234 (2012)
JSCS–4263
UDC 677.21+539.24+546.57:
615.281–188+66.022.362
Original scientific paper

A study of the antibacterial activity and stability of dyed cotton fabrics modified with different forms of silver

VESNA LAZIĆ[1], ZORAN ŠAPONJIĆ[2], VESNA VODNIK[2], SUZANA DIMITRIJEVIĆ[3], PETAR JOVANČIĆ[1], JOVAN NEDELJKOVIĆ[2] and MAJA RADETIĆ[1*#]

[1]*Textile Engineering Department, Faculty of Technology and Metallurgy, Karnegijeva 4, 11000 Belgrade, Serbia,* [2]*Vinča Institute of Nuclear Sciences, P. O. Box 522, 11001 Belgrade, Serbia and* [3]*Department of Bioengineering and Biotechnology, Faculty of Technology and Metallurgy, Karnegijeva 4, 11000 Belgrade, Serbia*

(Received 5 May, revised 31 May 2011)

Abstract: This study compares the effect of colloidal silver nanoparticles and the commercial RUCO-BAC AGP agent with silver chloride as the active component on the antibacterial activity of dyed cotton fabrics. Cotton fabrics were dyed with vat dyes Bezanthren Olive T and Bezanthren Grey FFB. The antibacterial activities of the silver-loaded dyed cotton fabrics were tested against the Gram-positive bacterium *Staphylococcus aureus* and the Gram-negative bacterium *Escherichia coli*. Unlike RUCO-BAC AGP, the synthesized silver nanoparticles deposited onto the dyed cotton fabrics provided maximum bacteria reduction, independent of the applied dye. The stability of the modified cotton fabrics was analyzed in artificial sweat at pH 5.5 and 8.0. Approximately the same amount of silver was released from the differently modified cotton fabrics in artificial sweat. Larger amounts of silver were released in the sweat at pH 8.0.

Keywords: cotton; silver nanoparticles; RUCO-BAC AGP; antibacterial efficiency; artificial sweat.

INTRODUCTION

Approximately 50 % of textiles today are made of cotton (Co) since these fibers are particularly suitable for the manufacture of sport and leisure textiles, medical non-implantables (different bandages, plasters, gauze dressings, lint, wadding, adsorbent pads) and healthcare/hygiene products (surgical gowns and hosiers, sheets, pillowcases, uniforms, blankets).[1] However, Co fibers may act as a nutrient, becoming a suitable medium for microorganism growth and thus frequently antimicrobial properties have to be imparted to cotton products.[2]

* Corresponding author. E-mail: maja@tmf.bg.ac.rs
# Serbian Chemical Society member.
doi: 10.2298/JSC110505167L

Various agents have been used for supplying textile materials with antimicrobial properties, but poor efficiency or high toxicity made them unsuitable for long-term use.[3] Silver nanoparticles (Ag NPs) are potent and broad-spectrum antibacterial agents.[4] Ag NPs can be found in room sprays, detergents and wall paints, as well as in washing machines, refrigerators, vacuum cleaners and air conditioners. The concept of Ag NPs application to textile materials relies on the fact that a small amount of deposited nanoparticles can provide the desired antimicrobial activity with long-term durability and stability without the use of highly toxic organic compounds. The antibacterial effect of Ag NPs on Co fabrics has already been studied by several research groups.[5–12] However, less attention has been paid to the synergism between antibacterial finishing with Ag NPs and dyeing, which is a very important issue from the technological point of view. Hitherto, the influence of reactive dyes and direct dyes on the antibacterial efficiency of Co fabrics treated with Ag NPs was investigated.[6,10]

In this study, the effect of silver in different forms on the antibacterial properties and color change of Co fabrics dyed with vat dyes were investigated. Comparative examination of colloidal Ag NPs that were synthesized without the employment of any stabilizer and the commercial RUCO-BAC AGP (RB) agent with silver chloride as the active component was performed. Namely, RB consists of micro-structured titanium dioxide that acts as a carrier of silver chloride. In the case of moisture (*e.g.*, perspiration), silver ions with antimicrobial effect are set free from a virtually infinite deposit. The antibacterial activity of Co fabrics was tested against the Gram-negative bacterium *Escherichia coli* and the Gram-positive bacterium *Staphylococcus aureus*. Additionally, the stability of these textile nanocomposite materials was studied in artificial sweat at pH 5.5 and 8.0.

EXPERIMENTAL

Materials and methods

Desized and bleached woven Co fabric (168 g m^{-2}) was cleaned from surface impurities as described in a previous study.[13] Vat dyes Bezathren Olive T (BO) and Bezathren Grey FFB (BG), both products of Bezema AG, were used for dyeing the Co fabrics.

The schematic procedure of the dyeing of Co fabrics is shown in Fig. 1. Co fabrics were dyed in Polycolor (Werner Mathis AG) laboratory beaker dyer in the bath containing 2 % or 4 % (on weight of fabric – o.w.f.) of a vat dye and reducing agent $Na_2S_2O_4$ (5 g L^{-1}) at a liquor-to-fabric ratio of 10:1. Subsequently, the fabrics were oxidized in a bath containing H_2O_2 (1.5 g L^{-1}), rinsed once with water and treated in a solution of the surfactant Cotoblanc RS (2 g L^{-1}). After rinsing with water, the samples were dried at room temperature.

Silver nitrate ($AgNO_3$, Kemika) and the reducing agent sodium borohydride ($NaBH_4$, Fluka) of p.a. grade were used for the synthesis of the colloidal Ag NPs.[14,15] $AgNO_3$ (8.5 mg) was dissolved in 250 mL of water and purged with argon for 30 min. Under vigorous stirring, $NaBH_4$ (125 mg) was added to the solution and left for 1 h under an argon atmosphere. The concentration of the Ag colloid was 50 ppm. The synthesized colloid was comprised of nearly spherical nanoparticles with an average diameter of 10 nm.[13]

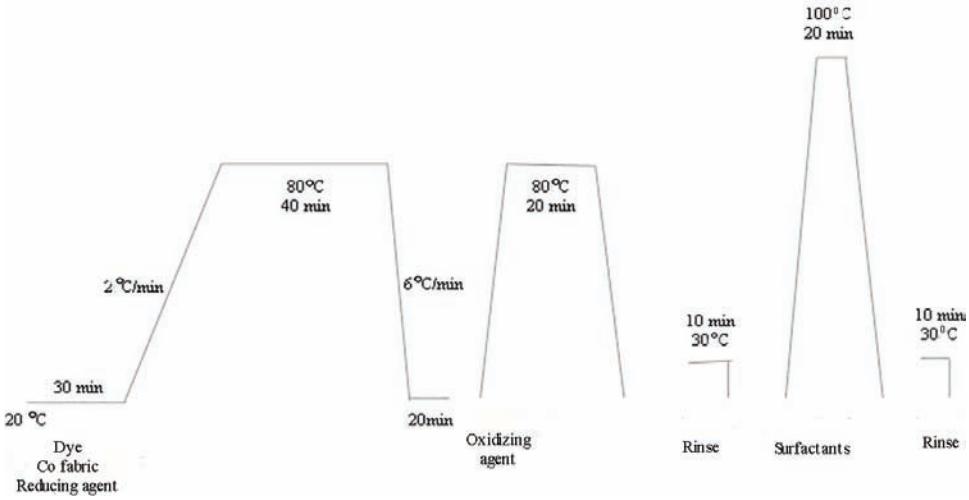

Fig. 1. Dyeing procedure for Co fabrics.

One gram of dyed Co fabric was immersed in 45 mL of the colloidal Ag NPs for 5 min and dried at room temperature. After 5 min of curing at 100 °C, the samples were rinsed twice (5 min) with deionized water and dried at room temperature.

Dyed samples were also treated with RUCO-BAC AGP, a highly concentrated hygiene and freshness system that comply with Öko-Tex Standard 100.[16] The recommended concentration of 0.50 % (o.w.f.) was applied. The samples were treated in a bath (liquor-to-fabric ratio 10:1) for 30 min at 50 °C. The pH value of 5–6 was adjusted using acetic acid. Subsequently, the samples were dried at 130 °C for 4 min.[17]

Fiber morphology was followed by scanning electron microscope (SEM, JEOL JSM--6610LV). Gold layer was deposited on the samples before analysis.

The color coordinates of the dyed fabrics (CIE L^*, a^* and b^*) were determined with a Datacolor SF300 spectrophotometer under illuminant D_{65} using the 10° standard observer. Based on the measured CIE color coordinates, the color difference (ΔE^*) was determined as:

$$\Delta E^* = \sqrt{(\Delta a^*)^2 + (\Delta b^*)^2 + (\Delta L^*)^2} \quad (1)$$

where ΔL^* is the color lightness difference between the treated (dyed Co fabric loaded with Ag NPs or RB) and the control (dyed Co fabric without Ag) samples; Δa^* is the red/green difference between the treated and control samples; Δb^* is the yellow/blue difference between treated and control samples.

The antibacterial efficiency of the differently modified Co fabrics was quantitatively assessed using the Gram-negative bacterium *E. coli* ATCC 25922 and the Gram-positive bacterium *S. aureus* ATCC 25923. Bacterial inoculums were prepared in 3 mL of tryptone soy broth (Torlak, Serbia) as the growing medium and left overnight at 37 °C (late exponential stage of growth). 70 mL of sterile potassium hydrogen phosphate buffer solution (pH 7.2) was added to sterile Erlenmeyer flask (300 mL), which was then inoculated with 0.7 mL of a bacterial inoculum. One gram of sterile Co fabric cut into small pieces was placed in the flask and shaken. After 1 h of shaking, 1.0 mL aliquots from the flask were diluted (1:10 and 1:100) with saline solution and 0.10 mL of the solution was placed onto tryptone soy agar (Torlak,

Serbia). After 24 h of incubation at 37 °C, zero time and one-hour counts of the viable bacteria were made. The percentage of bacteria reduction (*R*, %) was calculated using Eq. (2):

$$R = 100\frac{C_0 - C}{C_0} \quad (2)$$

where C_0 (CFU – colony forming units) is the number of bacterial colonies on the control Co fabric (dyed Co fabric without Ag) and C (CFU) is the number bacterial colonies on the Co fabric loaded with Ag NPs or RB.[5,18,19]

Artificial sweat at pH 5.5 and 8.0 was prepared according to ISO 105-E04:1989E.[20] One liter of acidic artificial sweat (pH 5.5) contained 0.5 g of *L*-histidine monohydrochloride monohydrate, 5 g of sodium chloride and 2.2 g of sodium dihydrogen orthophosphate dihydrate. One liter of alkaline artificial sweat (pH 8.0) contained 0.5 g of *L*-histidine monohydrochloride monohydrate, 5 g of sodium chloride and 5 g of disodium hydrogen orthophosphate dodecahydrate. The solutions were brought to pH 5.5 and 8.0 with a 0.1 M solution of sodium hydroxide. The Co fabrics (0.300 g) were soaked in artificial sweat at a liquor-to-fabric ratio of 1:50. The samples were incubated in a water bath at 37 °C. After 24 h of incubation, the artificial sweat was collected and the content of released silver was determined using a Perkin-Elmer 403 atomic absorption spectrometer (AAS). The results were calculated as the total amount of silver released into the artificial sweat and normalized with respect to the weight of the fabric sample. In order to determine the total amount of silver on the Co fabric, the samples were burnt and dissolved in nitric acid. The amount of silver was also measured by AAS.

The color fastness of the Co fabrics that had been exposed to artificial sweat was determined spectrophotometrically.

RESULTS AND DISCUSSION

The changes in fiber surface morphology after deposition of Ag NPs onto dyed Co fabric was assessed by SEM. The SEM image of the Co fiber dyed with 2 % BO and loaded with Ag NPs is shown in Fig. 2. It can be noticed that the surface of the Co fiber modified with Ag NPs was mainly covered with NP aggregates of dimensions around 100 nm.

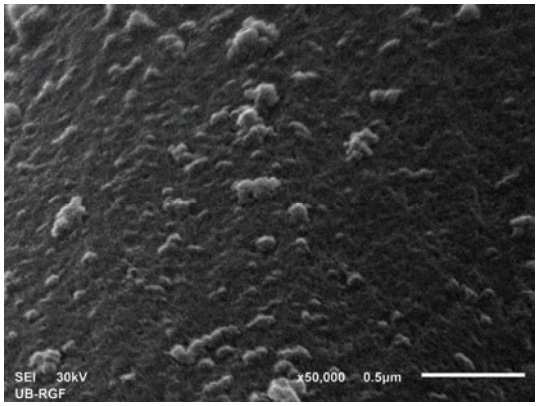

Fig. 2. SEM Image of Co fiber dyed with 2 % BO and loaded with Ag NPs.

The color difference between the Co fabrics loaded with Ag NPs or RB and the control fabric (only dyed Co fabric) was expressed *via* the CIE L^*, a^* and b^* color coordinates. The colorimetric data for the control Co fabrics and the Co fabrics loaded with Ag NPs or RB after dyeing with BG or BO are presented in Table I. The results clearly indicate that treatment of the dyed Co fabrics with RB caused a color change that could not be visually detected since the color difference (ΔE^*) was lower than one. The deposition of Ag NPs onto the Co fabrics dyed with BG also did not significantly affect the color of Co fabric ($\Delta E^* < 1$). However, the deposition of Ag NPs onto Co fabrics dyed with BO led to a considerable increase in color change. This was particularly prominent on the sample that had previously been dyed with 4 % BO.

TABLE I. Colorimetric data for Co fabrics dyed with BG or BO and modified with Ag NPs or RB

Dye	Sample	L^*	a^*	b^*	ΔL^*	Δa^*	Δb^*	ΔE^*
BG 2 %	Control[a]	37.87	–0.31	5.76	–	–	–	–
	Co+Ag NPs	37.56	–0.18	6.49	–0.31	0.13	0.73	0.80
	Co+RB	38.30	–0.30	5.75	0.43	0.01	–0.01	0.44
BG 4 %	Control	29.62	–0.23	5.09	–	–	–	–
	Co+Ag NPs	29.96	–0.26	5.61	0.34	–0.03	0.52	0.62
	Co+RB	30.30	–0.34	5.13	0.68	–0.10	0.04	0.69
BO 2 %	Control	43.38	–44.32	–4.06	–	–	–	–
	Co+Ag NPs	43.31	–42.81	–3.25	–0.07	1.51	0.81	1.71
	Co+RB	43.87	–44.53	–4.16	0.48	–0.22	–0.09	0.54
BO 4 %	Control	34.66	–42.08	–3.21	–	–	–	–
	Co+Ag NPs	34.24	–39.55	–2.00	–0.42	2.53	1.21	2.83
	Co+RB	35.18	–42.42	–3.40	0.52	–0.34	–0.19	0.65

[a]Dyed fabric without Ag NPs or RB

The antibacterial activity of the Co fabrics was tested against the Gram-negative bacterium *E. coli* and the Gram-positive bacterium *S. aureus*. The Co fabrics dyed with BG and loaded with Ag NPs reached the maximum bacteria reduction (Table II). A similar behavior was exhibited by the Co fabrics modified with RB, although a few bacterial colonies grew in the Petri dishes, leading to a decrease in the reduction of *S. aureus* to 99.8 % in the case of the sample that was dyed with 4 % BG.

The values of bacteria reduction by the Co fabrics dyed with BO and loaded with Ag NPs or RB are given in Table III. Again, the Co fabrics loaded with Ag NPs provided the maximum bacteria reduction, irrespective of the BO dye concentration and bacteria type. The Co fabrics loaded with RB showed good antibacterial efficiency, but the maximum reduction of *S. aureus* bacteria was achieved only in the case of Co fabric dyed with 4 % BO.

The obtained results indicated that both colloidal Ag NPs and RB could be used as efficient antibacterial agents for Co fabrics. They also confirmed that both forms of silver (nanoparticles and ions) exhibited excellent bactericidal pro-

perties. However, the mechanism of bactericidal action of Ag NPs is not yet fully understood. One group of scientists supports the assumption that Ag NPs in an aqueous medium release silver ions which are responsible for killing the bacteria.[21–24] Another approach relies on the finding of Morones *et al*. who detected Ag NPs attached to the cell membrane and inside the bacteria.[25] It is very likely that Ag NPs react with sulfur rich proteins in the bacteria cell membrane and the interior of the cell or with phosphorous-containing compounds such as DNA.[26,27] Accordingly, the morphological changes in the bacteria cell membrane and possible damage of DNA caused by reaction with Ag NPs disturb the respiratory chain or cell division processes, leading to a cell death.[25]

TABLE II. Antibacterial efficiency of Co fabrics dyed with BG and loaded with Ag NPs or RB

Sample	Bacterium	Initial number of bacterial colonies, CFU	Number of bacterial colonies on the fabric, CFU	*R* / %
Control Co (2 % BG)	*E. coli*	6.4×10^5	2.3×10^5	–
Co+Ag NPs			<10	99.9
Co+RB			45	99.9
Control Co (4 % BG)		2.0×10^5	1.2×10^5	–
Co+Ag NPs			<10	99.9
Co+RB			<10	99.9
Control Co (2 % BG)	*S. aureus*	2.4×10^4	4.0×10^3	–
Co+Ag NPs			<10	99.9
Co+RB			<10	99.9
Control Co (4 % BG)		3.5×10^4	2.0×10^4	–
Co+Ag NPs			<10	99.9
Co+RB			60	99.8

TABLE III. Antibacterial efficiency of Co fabrics dyed with BO and loaded with Ag NPs or RB

Sample	Bacterium	Initial number of bacterial colonies, CFU	Number of bacterial colonies on the fabric, CFU	*R* / %
Control Co (2 % BO)	*E. coli*	2.3×10^5	2.2×10^5	–
Co+Ag NPs			<10	99.9
Co+RB			2.8×10^2	99.8
Control Co (4 % BO)		8.0×10^5	2.5×10^5	–
Co+Ag NPs			<10	99.9
Co+RB			1.4×10^2	99.9
Control Co (2 % BO)	*S. aureus*	2.5×10^5	7.4×10^4	–
Co+Ag NPs			<10	99.9
Co+RB			30	99.9
Control Co (4 % BO)		2.3×10^5	6.7×10^4	–
Co+Ag NPs			<10	99.9
Co+RB			<10	99.9

The slightly better antibacterial activity of the Co fabrics loaded with Ag NPs can be attributed to the larger amount of silver present, which was detected

by AAS (Table IV). The larger amount of silver that was found in the samples modified with Ag NPs can provide longer antibacterial activity during the exploitation of textile products. It is also clear that the silver content in the Co fabrics modified with RB was almost constant being independent of the applied dye and the dye concentration. On the contrary, the total amount of silver in the Co fabrics loaded with Ag NPs varied with the concentration of the dyes and was larger in the Co fabrics that were dyed with the higher concentration of the dyes (4 %), indicating the existence of some interaction between the dye molecules and Ag NPs.

TABLE IV. Initial silver content and total silver released into artificial sweat

Sample	Initial silver content μg g^{-1}	Silver released into artificial sweat, pH 5.5 μg g^{-1}	Silver released into artificial sweat pH 8.0 μg g^{-1}
Co+BG 2 %+Ag NPs	31.97	13.15	16.35
Co+BG 4 %+Ag NPs	52.41	12.83	18.63
Co+BO 2 %+Ag NPs	32.15	12.40	16.00
Co+BO 4 %+Ag NPs	63.67	12.93	17.35
Co+BG 2 %+RB	18.84	12.48	17.78
Co+BG 4 %+RB	17.36	12.20	16.33
Co+BO 2 %+RB	18.20	12.10	17.93
Co+BO 4 %+RB	18.75	12.13	18.58

The stability of the investigated systems is of major interest for the exploitation and maintenance of textile products. Therefore, the stabilities of the differently modified Co fabrics were examined in artificial sweat. Namely, the composition of sweat varies between individuals. However it also depends on the body region, age, season, diet, degree of acclimation, infection status and level of activity.[28] Hence, the stability of modified Co fabrics was tested in alkaline and acidic artificial sweat. AAS measurements of sweat solutions after 24 hours of contact with the Co fabrics modified with Ag NPs or RB revealed that silver was released. The amounts of silver released from the Co fabrics into artificial sweat are shown in Table IV. Obviously, all the investigated samples released almost the same amount of silver into sweat, independent of the dye type and concentration, as well as of the silver form applied. However, approximately 39 % more silver was released into alkaline sweat (pH 8.0) compared to acidic sweat (pH 5.5). Although the Co fabrics modified with Ag NPs and RB showed equivalent trends of silver release, a larger amount of Ag was retained in the Co fabrics loaded with Ag NPs.

Additionally, the color fastness of Co fabrics in artificial sweat was studied. The data on color change and color fastness of the Co fabrics loaded with Ag NPs and RB after exposure to acidic and alkaline sweat for 24 h are given in Table V. The color fastness was evaluated in accordance with the ISO 105-A05

standard and the AATCC standard.[29,30] The color changes after 24 h of rinsing in artificial sweat could not be visually detected as the color difference (ΔE^*) was lower than one. The only exception was the Co fabric dyed with 4 % BO and loaded with Ag NPs that was exposed to artificial sweat at pH 8.0. All samples exhibited good color fastness since the color fastness grades ranged from 4–5 according to both standards.

TABLE V. Color change of Co fabrics loaded with Ag NPs and RB after 24-h exposure to acidic and alkaline sweat

Sample	ΔL^*	ΔE^*	Color fastness, ISO A05	Color fastness, AATCC
		pH 5.5		
Co+BG 2 %+Ag NPs	0.30	0.71	4–5	4–5
Co+BG 4 %+Ag NPs	0.06	0.43	4–5	4–5
Co+BO 2 %+Ag NPs	0.30	0.98	4–5	4–5
Co+BO 4 %+Ag NPs	0.55	0.88	4–5	4–5
Co+BG 2 %+RB	0.52	0.55	4–5	4–5
Co+BG 4 %+RB	0.26	0.34	5	5
Co+BO 2 %+RB	0.59	0.94	4–5	4–5
Co+BO 4 %+RB	0.49	0.70	4–5	4–5
		pH 8.0		
Co+BG 2 %+Ag NPs	0.25	0.62	4–5	4–5
Co+BG 4 %+Ag NPs	–0.30	0.43	4–5	4–5
Co+BO 2 %+Ag NPs	0.09	0.69	4–5	4–5
Co+BO 4 %+Ag NPs	0.79	1.64	4	4
Co+BG 2 %+RB	–0.41	0.44	4–5	4–5
Co+BG 4 %+RB	–0.04	0.10	5	5
Co+BO 2 %+RB	0.22	0.73	4–5	4–5
Co+BO 4 %+RB	0.28	0.87	4–5	4–5

CONCLUSIONS

Cotton fabrics dyed with the vat dyes Bezanthren Olive T and Bezanthren Grey FFB and subsequently loaded with synthesized colloidal silver nanoparticles exhibited excellent antibacterial activity, reaching the maximum possible bacterial reduction (Gram-negative bacterium *E. coli* and Gram-positive bacterium *S. aureus*). Although the dyed Co fabrics modified with commercial RUCO--BAC AGP agent with silver chloride as an active component also provided good antibacterial properties, the maximum bacteria reduction was not always achieved. The better antibacterial properties of the Co fabrics modified with the silver nanoparticles could be due to the larger amount of silver in these samples, which was confirmed by atomic absorption spectroscopy. The larger amount of silver in these Co fabrics could provide longer antibacterial activity during the exploitation. The treatment with RUCO-BAC AGP did not significantly affect the color of the cotton fabrics. However, the cotton fabrics dyed with Bezanthren Olive T

underwent considerable color change after the treatment with colloidal silver nanoparticles.

The results also indicated that silver was released from the cotton fabrics during 24-h long exposure to sweat at pH 5.5 and 8.0. All the studied samples released almost the same amount of silver into the sweat, independent of the dye type and concentration, as well as of the silver form applied. However, about 39 % more silver was released into the alkaline sweat compared to the acidic sweat. The color fastness of the cotton fabrics exposed to sweat was satisfactory.

Acknowledgement. This study was supported by the Ministry of Education and Science of the Republic of Serbia – Projects 45020 and 172056. We gratefully acknowledge Dr A. Pačevski (University of Belgrade, Serbia) for providing the SEM measurements.

ИЗВОД

ИСПИТИВАЊЕ АНТИБАКТЕРИЈСКЕ АКТИВНОСТИ И СТАБИЛНОСТИ ОБОЈЕНЕ ПАМУЧНЕ ТКАНИНЕ МОДИФИКОВАНЕ РАЗЛИЧИТИМ ФОРМАМА СРЕБРА

ВЕСНА ЛАЗИЋ[1], ЗОРАН ШАПОЊИЋ[2], ВЕСНА ВОДНИК[2], СУЗАНА ДИМИТРИЈЕВИЋ[3], ПЕТАР ЈОВАНЧИЋ[1], ЈОВАН НЕДЕЉКОВИЋ[2] и МАЈА РАДЕТИЋ[1]

[1]*Катедра за текстилно инжењерство, Технолошко–металуршки факултет, Карнегијева 4, 11120 Београд,* [2]*Институт за нуклеарне науке Винча, п. пр. 522, 11001 Београд и* [3]*Катедра за биоинжењерство и биотехнологију, Технолошко–металуршки факултет, Карнегијева 4, 11120 Београд*

У овом раду се пореде ефекти колоидних наночестица сребра и комерцијалног антимикробног агенса RUCO-BAC AGP са сребро-хлоридом као активном компонентом на антибактеријску активност бојене памучне тканине. Памучне тканине су бојене редукционим бојама *Bezanthren olive T* и *Bezanthren green FFB*. Антибактеријска активност сребра је тестирана према Грам-позитивној бактерији *Staphylococcus aureus* и Грам-негативној бактерији *Escherichia coli*. За разлику од RUCO-BAC AGP, синтетисане наночестице сребра депоноване на обојену памучну тканину су обезбедиле максимум бактеријске редукције независно од примењене боје. Стабилност модификованих памучних тканина је анализирана у вештачком зноју при pH 5,5 и 8,0. Готово иста количина сребра се ослобађа са различито модификованих памучних тканина у вештачком зноју. Већа количина сребра се ослобађа у зноју при pH 8,0.

(Примљено 5., ревидирано 31. маја 2011)

REFERENCES

1. R. Czajka, *Fibers Text. East. Eur.* **13** (2005) 13
2. Y. Gao, R. Cranston, *Text. Res. J.* **78** (2008) 60
3. V. Ilić, Z. Šaponjić, V. Vodnik, R. Molina, S. Dimitrijević, P. Jovančić, J. Nedeljković, M. Radetić, *J. Mater. Sci.* **44** (2009) 3983
4. J. S. Kim, E. Kuk, K. N. Yu, J. H. Kim, S. J. Park, H. J. Lee, S. H. Kim, Y. K. Park, Y. H. Park, C. Y. Hwang, Y. K. Kim, Y. S. Lee, D. H. Jeong, M. H. Cho, *Nanomedicine* **3** (2007) 95
5. H. J. Lee, S. Y. Yeo, S. H. Jeong, *J. Mater. Sci.* **38** (2003) 2199
6. M. Gorenšek, P. Recelj, *Text. Res. J.* **77** (2007) 138

7. N. Vigneshwaran, A. A. Kathe, P. V. Varadarajan, R. P. Nachane, R. H. Balasubramanya, *J. Nanosci. Nanotechnol.* **7** (2007) 1893
8. D. Chun, J. A. Foulk, D. D. McAlister III, *Ind. Crop. Pro.* **29** (2009) 371
9. S. Ghosh, S. Yadav, N. Reynolds, *J. Text. I.* **101** (2010) 917
10. V. Ilić, Z. Šaponjić, V. Vodnik, B. Potkonjak, P. Jovančić, J. Nedeljković, M. Radetić, *Carbohyd. Polym.* **78** (2009) 564
11. M. Gorjanc, V. Bukošek, M. Gorenšek, M. Mozetič, *Text. Res. J.* **80** (2010) 2204
12. M. Gorjanc, V. Bukošek, M. Gorenšek, A. Vesel, *Text. Res. J.* **80** (2010) 557
13. M. Radetić, V. Ilić, V. Vodnik, S. Dimitrijević, P. Jovančić, Z. Šaponjić J. Nedeljković, *Polym. Adv. Technol.* **19** (2008) 1816
14. V. V. Vuković, J. M. Nedeljković, *Langmuir* **9** (1993) 980
15. Z. V. Šaponjić, R. Csencsits, T. Rajh, N. Dimitrijević, *Chem. Mater.* **15** (2003) 4521
16. Öko-Tex standard 100, http://www.oekotex.com/OekoTex100_PUBLIC/content.asp?-area=hauptmenue&site=chemischaktivesubstanzen&cls=02 (accessed 31.05.2011)
17. M. Gorenšek, M. Gorjanc, V. Bukošek, J. Kovač, Z. Petrović, N. Puač, *Text. Res. J.* **80** (2010) 1633
18. S. H. Jeong, S. Y. Yeo, S. C. Yi, *J. Mater. Sci.* **40** (2005) 5407
19. H. Y. Ki, J. H. Kim, S. C. Kwon, S. H. Jeong, *J. Mater. Sci.* **42** (2007) 8020
20. ISO 105-E04: *Colour fastness to perspiration* (1989)
21. D. Pohle, C. Damm, J. Neuhof, A. Rösch, H. Münsted, *Polym. Polym. Compos.* **15** (2007) 357
22. I. Perelshtein, G. Applerot, N. Perkas, G. Guibert, S. Mikhailov, A. Gedanken, *Nanotechnology* **19** (2008) 1
23. C. Damm, H. Muenstedt, A. Roesch, *J. Mater. Sci.* **42** (2007) 6067
24. X. Xu, Q. Yang, Y. Wang, H. Yu, X. Chen, X. Jing, *Eur. Polym. J.* **42** (2006) 2081
25. J. R. Morones, J. L. Elechiguerra, A. Camacho, K. Holt, J. N. Kouri, J. T. Ramirez, M. J. Yacaman, *Nanotechnology* **16** (2005) 2346
26. Q. L. Feng, J. Wu, G. Q. Chen, F. Z. Cui, T. N. Kim, J. O. Kim, *J. Biomed. Mater. Res.* **52** (2000) 662
27. J. S. Kim, *J. Ind. Eng. Chem.* **13** (2007) 718
28. K. Kulthong, S. Srisung, K. Boonpavanitchakul, W. Kangwansupamonkon, R. Maniratanachote, *Particle Fibre Tox.* **7** (2010) 8
29. ISO 105-A05 standard: *Instrumental assessment of change in colour for determination of grey scale rating* (1996)
30. AATCC Evaluation procedure 6: *Instrumental colour measurement* (1995).

Journal of the Serbian Chemical Society
JSCS-info@shd.org.rs • www.shd.org.rs/JSCS
J. Serb. Chem. Soc. *77* (2) 235–246 (2012)
JSCS–4264
UDC 628.3+667.281+547.79:66.099.72
Original scientific paper

A central composite design for the optimization of the removal of the azo dye, methyl orange, from waste water using the Fenton reaction

MAHSA AZAMI[1], MORTEZA BAHRAM[1], SIROUS NOURI[1] and ABDOLHOSEIN NASERI[2]*

[1]*Department of Chemistry, Faculty of Science, Urmia University, Urmia, Iran and* [2]*Department of Analytical Chemistry, Faculty of Chemistry, University of Tabriz, 51666–16471, Tabriz, Iran*

(Received 15 March, revised 9 May 2011)

Abstract: In this study the degradation of Methyl Orange, using Fenton reaction was studied and optimized using central composite design as a response surface methodology. The effects of various experimental parameters in this reaction were investigated using the central composite design. 28 experiments, with 4 factors and 5 levels for each factor were designed. These factors (or variables) were: the initial concentration of Fe(II), the initial concentration of H_2O_2, the initial concentration of oxalate and the reaction time. A full-quadratic polynomial equation between the percentage of dye degradation (as the response) and the studied parameters was established. After removing the non-significant variables from the model, response surface method was used to obtain the optimum conditions. The optimum ranges of variables were: 0.25–0.35 mM for the initial concentration of Fe(II), 5–17 mM for the initial concentration of H_2O_2, 4–9 mM for the initial concentration of oxalate, and 50–80 min for the reaction time. In addition, the results of extra experiments showed that these optimized values can be used for real samples and lead to a high value for the response.

Keywords: design of experiments; decolourization; Fenton reaction; Methyl Orange.

INTRODUCTION

There are many branches of industry which use various colorants (synthetic dyes).[1,2] The wastewater from the manufacture of dyes generally contains residual dyestuffs, dye intermediates as well as unreacted raw materials, such as aromatic amines with alkyl-, halogen-, nitro-, hydroxyl-, sulphonic acid-substituents, and inorganic sodium salts.[3] Dyes are organic compounds that can be dangerous

* Corresponding author. E-mail: a_naseri@tabrizu.ac.ir
doi: 10.2298/JSC110315165A

to the environment. The discharge of coloured waste is highly problematic, firstly due to the toxic nature of some dyes or of their biodegradation products and secondly due to their visual impact because dyes are visible even at low concentrations.[4] For example, the textile industry is one of the top water polluting Industries in terms of spent volume, as well as colour and chemical composition of the residual wastewater. Residual textile dyes usually transform into toxic aromatic amines which are light resistant and, once in the environment, they exhibit recalcitrant properties.[5,6] Effluents from the textile industry commonly contain high concentration of organic and inorganic chemicals and are characterized by very high chemical oxygen demand (*COD*) and total organic carbon (*TOC*) values as well as strong colour.[7] The release of such coloured wastewaters into the environment is a dramatic source of aesthetic pollution, eutrophication and perturbations in aquatic life.[8]

Azo dyes, constituting the largest class among the synthetic colorants, are considered as widespread environmental pollutants associated with many important industries, such as textile, food colorants, printing and cosmetic manufacture.[9] The release of azo dyes into the environment is of great concern, due to coloration of natural waters and toxicity, mutagenicity, and carcinogenicity of the dyes and their biotransformation products.[10]

Methyl Orange is an azo dye that can be used as an indicator in acid–base titrations. This dye is also used in textile industries and is an orange-coloured anionic dye which has an absorbance maximum at 464 nm. Methyl Orange is a harmful compound that exists in textile waste waters and has various harmful effects on human beings. For example, it may cause eye or skin irritation, or inhalation may cause gastrointestinal irritation with nausea, vomiting, and diarrhoea.[11,12] To avoid the dangerous accumulation of dyes in the environment, there is a need to develop effective methods for the degradation of such organic pollutants, either to less harmful compounds or, more desirable, to their complete mineralization.[13]

There are many different technological processes, such as adsorption,[1] biodegradation, chemical methods (*e.g.*, chlorination and ozonation), electrocoagulation, electrochemical reduction and oxidation, indirect electro-oxidation with strong oxidants and photocatalytic degradation, which can be used for the treatment of waste waters, including those containing synthetic dyes.[14,15]

In recent years, oxidation processes (OPs) have attracted attentions for the destruction of dyes. Fenton oxidation, in which hydroxyl radicals are generated from Fenton reagents, is one of the OPs methods.[1] The Fenton reaction is already in use for industrial wastewater purification processes. It is well-known that, in theory, the most important characteristic of the Fenton processes is the formation of OH radicals, which are highly oxidative, non-selective, and able to decompose many organic compounds.[7,16] It is also well-accepted that the advantages of Fen-

ton processes are the complete mineralization of organic compounds at ambient temperature and the easy separation of the heterogeneous catalysts from the treated wastewater. The Fenton reaction has many other advantages in the degradation of pollutants, for example its reagents are environmentally safe, cheap and easy to obtain and use.

The mechanisms of Fenton reactions are available in the literatures.[17,18] When using Fenton reactions, several parameters, such as the concentration of iron salt and H_2O_2 have an important effect on the percentage removal of a dye and therefore should be optimized. In addition, in the present study, the salt sodium oxalate was also used to catalyze the removal reaction.

Optimizing refers to improving the performance of a system, a process, or a product in order to obtain the maximum benefit from it. The term optimization has been commonly used in chemistry as a means of discovering conditions at which a procedure produces the best possible response.[19] The response surface methodology (RSM) is a statistical method that is useful for the optimization of chemical reactions and/or industrial processes and is widely used for experimental design. Whenever multiple system variables may influence the outputs; RSM can be utilized to assess the relationship between the dependent (response) and independent variables, as well as to optimize the relevant processes.[20,21] This methodology was already applied to study and optimize advanced oxidation processes.[22,23] The response surface methodology was used to assemble a model in order to describe the way in which the variables are related and the way in which they influence the response.

In this research, finding optimal conditions for the effective factors on degradation of Methyl Orange by a Fenton reaction using an experimental design method (Central Composite Design, CCD) was investigated.

EXPERIMENTAL

Instruments

The solutions were stirred on a MTOPO magnetic stirrer model MS3300 and the absorbance of the solutions were measured using a PG-mode T80 UV–Vis double-beam spectrophotometer (Japan) utilizing a 1-cm quartz cell. The adjustment of the pH of the solutions was controlled by a pH-meter BEHINEH (UK).

Reagents

Methyl Orange (M_w = 269.31 g mol^{-1}), $FeSO_4 \cdot 7H_2O$ (M_w = 278 g mol^{-1}), H_2O_2 (a = 30 % v/v, d = 1.11 kg m^{-3}) and $Na_2C_2O_4$ (M_w = 134 g mol^{-1}) all of analytical grade (Merck) were used and all the solution were prepared with freshly distilled water.

The solution of Fe^{2+} was prepared several times during a day and was used immediately to prevent the exchange of Fe^{2+} to Fe^{3+}. To adjust the final pH of the solutions, solutions of H_2SO_4 (0.010 M) and NaOH (0.010 M) were prepared and used.

Solutions

Each experiment included a solution of 10 ml Methyl Orange (2.5×10^{-2} mM) plus calculated amounts of H_2O_2 (30 % v/v), Fe(II) and oxalate. These amounts were extracted from the table of DOE. The pH of the solutions were adjusted in 3.5 using H_2SO_4 (0.010 M) and NaOH (0.010 M), because the appropriate pH for the Fenton reaction is in the range of 3–5. These reagents were mixed in a 50 ml flask and the flasks were filled to the mark with distilled water. In addition, blanks were prepared in the same manner as the real samples, but without H_2O_2 and oxalate ions. These blanks were also stirred with a magnetic stirrer during the reaction of the corresponding real samples.

After the predetermined time of reaction, the absorbances of these two solutions were measured on a UV–Vis spectrophotometer.

Statistical software

Essential Regression and Experimental Design for Chemists and Engineers (EREGRESS), as an MS Excel Add-In software, was used to design the experiments and to model and analyze the results.

Design of experiments

By using central composite design (CCD) method, 28 experiments (including 4 repetitions at the central point) were designed.

The factors (variables) were: initial concentration of Fe(II) ($[Fe(II)]_0$), initial concentration of H_2O_2 ($[H_2O_2]_0$), initial concentration of oxalate ($[Oxalate]_0$) and the reaction time. Although the initial concentration of Methyl Orange might be important, this factor was kept constant at a value of 5×10^{-3} mM. This value for the dye concentration was selected from calibration curve of Methyl Orange (the middle point of the linear range in spectrophotometric determination).

For each factor, 5 levels were defined. These values were designated by the codes: –2, –1, 0, +1 and +2 and are given in Table I.[21,24]

TABLE I. The variables, their codes and the real experimental values used in the central composite design

Variable	Name	Coded levels				
		−2	−1	0	+1	+2
F_1	$[Fe^{2+}]_0$ / mM	0	0.1	0.2	0.3	0.4
F_2	$[H_2O_2]_0$ / mM	0	4.85	9.7	14.55	19.40
F_3	$[Oxalate]_0$ / mM	0	5	10	15	20
F_4	Time, min	5	35	65	95	125

RESULTS AND DISCUSSION

A spectrum of a 5×10^{-3} mM solution of Methyl Orange showed a maximum absorbance in the visible region at 464 nm. This wavelength was used to construct a calibration curve of absorbance *vs*. concentration of Methyl Orange to find the linear range of Methyl Orange absorbance. The obtained calibration curve is shown in Fig. 1. A concentration in middle point of this curve was selected and used for the preparing the dye solution in all experiments.

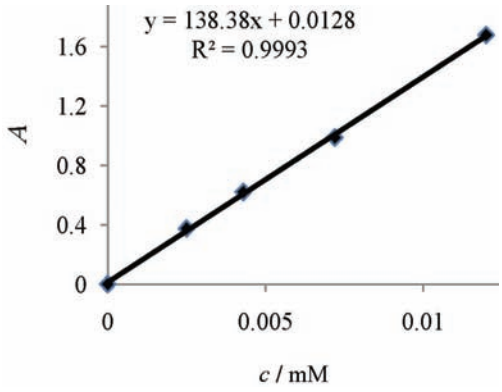

Fig. 1. The calibration curve for Methyl Orange (464 nm).

Analysis of data

After performing the experiments, the percentage of dye degradation for each experiment was calculated from Eq. (1), which was spotted as the response.

$$\text{Degradation} = 100\left[1-\left(\frac{\text{sample absorbance}}{\text{blank absorbance}}\right)\right] \quad (1)$$

The values of the blank absorbance, sample absorbance, the difference between the absorbance of blank and the absorbance of sample and the percentage of degradation for each experiment are given in Table II.

TABLE II. The coded values designed by the CCD and the responses

Run No.	$[Fe^{2+}]_0$ mM	$[H_2O_2]_0$ mM	$[Oxalate]_0$ mM	Time min	A_{blank}	A_{sample}	ΔA	Degradation %
1	0	–2	0	0	0.13	0.06	0.07	53.85
2	2	0	0	0	0.193	0.05	0.143	74.09
3	0	0	–2	0	0.162	0.075	0.087	53.7
4	1	–1	1	–1	0.122	0.007	0.115	94.26
5	0	0	0	–2	0.142	0.062	0.08	56.34
6	1	–1	–1	1	0.12	0.045	0.075	62.50
7	1	1	–1	–1	0.194	0.038	0.156	80.41
8	–1	1	1	–1	0.124	0.077	0.047	37.90
9	–1	–1	1	–1	0.092	0.05	0.042	45.65
10	–1	1	1	1	0.133	0.013	0.12	90.23
11	0	0	0	0	0.101	0.007	0.094	93.07
12	0	0	0	0	0.118	0.016	0.102	86.44
13	0	0	0	0	0.128	0.009	0.119	92.97
14	–1	1	–1	1	0.154	0.045	0.109	70.78
15	1	1	–1	1	0.133	0.026	0.107	80.45
16	0	0	0	0	0.115	0.017	0.098	85.22
17	1	1	1	1	0.205	0.002	0.203	99.02
18	–2	0	0	0	0.116	0.105	0.011	9.48
19	0	0	2	0	0.137	0.019	0.118	86.13

TABLE II. Continued

Run No.	$[Fe^{2+}]_0$ mM	$[H_2O_2]_0$ mM	$[Oxalate]_0$ mM	Time min	A_{blank}	A_{sample}	ΔA	Degradation %
20	0	2	0	0	0.145	0.024	0.121	83.45
21	–1	1	–1	–1	0.119	0.066	0.053	44.54
22	1	–1	1	1	0.134	0.011	0.123	91.79
23	0	0	0	2	0.127	0.003	0.124	97.64
24	1	–1	–1	–1	0.142	0.029	0.113	79.58
25	1	1	1	–1	0.104	0.016	0.088	84.62
26	–1	–1	–1	1	0.147	0.052	0.095	64.63
27	–1	–1	1	1	0.121	0.024	0.097	80.17
28	–1	–1	–1	–1	0.145	0.073	0.072	49.66

Among these 28 experiments, 4 experiments were repetition of the central point (run No. 11, 12, 13 and 16). These are the experiments in which all of the factors are in the centric point of their values. The closeness of the responses of these 4 experiments can be a sign of the accuracy of the experiment process. The relation between the collected response and the variables conforms to the following polynomial equation (full quadratic model as Eq. (2)).

$$Y = b_0 + b_1F_1 + b_2F_2 + b_3F_3 + b_4F_4 + b_{11}F_1F_1 + b_{22}F_2F_2 + b_{33}F_3F_3 + \\ + b_{44}F_4F_4 + b_{12}F_1F_2 + b_{13}F_1F_3 + b_{14}F_1F_4 + b_{23}F_2F_3 + b_{24}F_2F_4 + b_{34}F_3F_4 \quad (2)$$

where Y is a response variable of the decolourization efficiency; b_i are regression coefficients for linear effects; b_{ik} are regression coefficients for quadratic effects and F_i are coded experimental levels of the variables.

The analysis of variance (ANOVA) and least squares techniques were used to evaluate the statistical significance of the constructed models. The ANOVA consists of determining which factor(s) significantly affect the response, using the Fisher statistical test (F-test). The significance and the magnitude of the estimated coefficients of each variable and all their possible interactions on the response variable(s) were determined. Such coefficients for each variable represents the improvement in the response, that is, to expect as the variable setting is changed from low to high. Effects with a confidence level less than 95 % (effects with a p-value higher than 0.05) were discarded and pooled into the error term and a new analysis of variance was performed for the reduced model. Note that the p-value represents a decreasing index of the reliability of a result. Four replicates of the central points were performed to estimate the experimental error. In order to show the fitness of the model, regression coefficient (R) maybe be used. However, the adjusted regression coefficient (R_{adj}) and the prediction regression coefficient (R_{pred}) are better criteria than the absolute regression coefficient. Since the regression coefficient (R) always decreases when a regression variable is eliminated from the model, in statistical modelling, the R_{adj}, which takes the number of regression variables into account, is usually selected. In addition, R_{pred},

which indicates the predictive power of the model, is chosen for the same reason. This parameter was approximated using prediction error sum of squares, or *PRESS*, that is calculated from the residuals. Hence, R, R_{adj} and R_{pred} together are very convenient to obtain a quick impression of the overall fit and the predictive power of a constructed model.[24]

In order to find the important factors and build a model to optimize the procedure, initially the full quadratic model including all terms in Eq. (2) was employed. Then by the back elimination process, those terms which were not significant enough were eliminated. These terms included the variables or the interactions which had no effect or very low effect on the response. Each term with a p-value greater than 0.05 was removed from the main equation.

The reduced model using significant linear, quadratic and interaction parameters is defined in the form of the polynomial equation:

$$Y = b_0 + b_1[\text{Fe(II)}]_0 + b_{11}[\text{Fe(II)}]_0[\text{Fe(II)}]_0 + b_{22}[H_2O_2]_0[H_2O_2]_0 + b_{33}[\text{oxalate}]_0[\text{oxalate}]_0 + b_{14}[\text{Fe(II)}]_0\text{Time} + b_{24}[H_2O_2]_0\text{Time} + b_{34}[\text{oxalate}]_0\text{Time} \quad (3)$$

Obviously, $[\text{Fe(II)}]_0$, $[H_2O_2]_0$, $[\text{Oxalate}]_0$ and the interactions between the time and $[\text{Fe(II)}]_0$, the time and $[H_2O_2]_0$, and the time and $[\text{Oxalate}]_0$ are significant and have important effects on the percentage decolourization.

There were not large differences between the R values, which revealed that the experimental data showed a good fit to the quadratic equation and therefore an acceptable model had been achieved. The R values, standard error and prediction error sum of squares (*PRESS*) are presented in Table III.

TABLE III. Some characteristics of the constructed model

$\|R\|$	0.952
R^2	0.906
R^2 adjusted	0.873
R^2 for prediction	0.815
Standard error	7.738
Run No.	28
PRESS	2349.81

Response surfaces and selection of optimized values

After analysis of the data, the response surfaces of the full quadratic model between the response and the variables were depicted. *Via* these surfaces, the relations between the percentage of dye degradation and the effective factors are graphically given. These surfaces are shown in Fig. 2. The optimized ranges for each factor that leads to the best response (the highest percentage of dye degradation) were extracted from these surfaces. The optimized ranges are presented in Table IV.

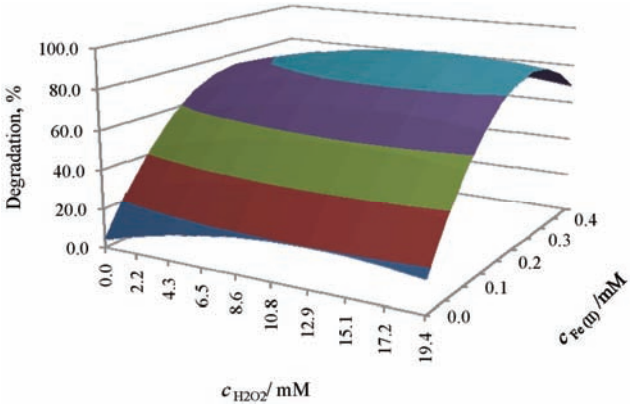

(A)

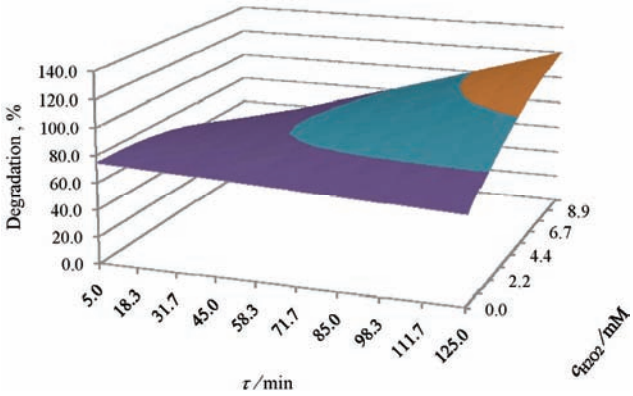

(B)

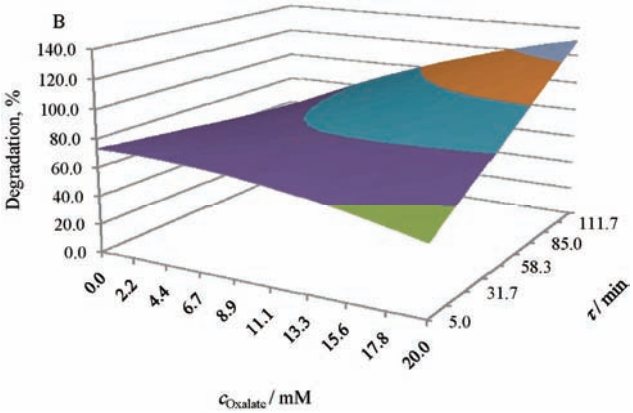

(C)

Fig. 2. Response surfaces of the full quadratic model between the percentage dye degradation and the three variables and the interaction between the variables. A – $[H_2O_2]$ and [Fe(II)], B – time and $[H_2O_2]$ and C – [oxalate] and time.

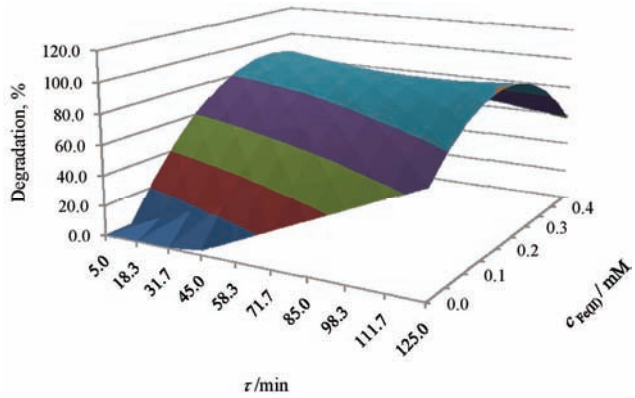

(D)

Fig. 2. (Continued) Response surfaces of the full quadratic model between the percentage dye degradation and the variable. D – time and [Fe(II)].

TABLE IV. The optimized ranges for the 4 relevant variables

Variable	Optimized range
$[Fe(II)]_0$ / mM	0.25–0.35
$[H_2O_2]_0$ / mM	5–17
$[Oxalate]_0$ / mM	4–9
Time, min	50–80

In order to test the accuracy of the obtained optimized ranges of the variables, it was necessary to select the middle point of each optimum range and repeat the experiments using these values. Five repetitive experiments were performed under these conditions. As can be seen, all the responses were similar to each other and yielded 92–100 % dye degradation. These results confirmed that the obtained optimized ranges for this reaction could lead to high percentages of dye degradation (Table V).

TABLE V. The results of 5 repetitions of the optimum conditions

Run No.	$[Fe^{2+}]_0$ / mM	$[H_2O_2]_0$ / mM	$[Oxalate]_0$ / mM	Time, min	A_{blank}	A_{sample}	ΔA
1	0.3	11	6.5	65	0.165	0.002	97
2	0.3	11	6.5	65	0.169	0.013	92
3	0.3	11	6.5	65	0.17	0.009	94
4	0.3	11	6.5	65	0.164	0	100
5	0.3	11	6.5	65	0.165	0.003	98

The relative standard deviation (*RSD*) of these repeated experiments was estimated for the responses to study the precision of the experiments and closeness of the responses. The value of the *RSD* was 3.31 %.

Effect of variables

Effect of [Fe(II)]$_0$. With increasing [Fe(II)]$_0$, an increasing trend was observed in the percentage of dye degradation; but increasing of the [Fe(II)]$_0$ more than a specific limit can lead to a plateau or a decrease in the percentage of dye degradation. This is because with increasing [Fe(II)]$_0$, the $^{\bullet}$OH generation increases; but the generation of high concentrations $^{\bullet}$OH could cause the undesirable reactions between OH and the H_2O_2 present in the solution.

Effect of [H_2O_2]$_0$. With increasing [H_2O_2]$_0$, the degradation increases because of the more intensive generation of $^{\bullet}$OH. Increasing the [H_2O_2]$_0$ to higher than the optimized value has no significant effect on the dye removal. The reason could be further reaction between $^{\bullet}$OH.

Effect of [oxalate]$_0$. According to Eq. (3) and Fig. 2, there is an interaction between the concentration of oxalate and the reaction time. Increasing the concentration of sodium oxalate (as a catalyst) increased the dye removal after long durations of the reaction.

Effect of time. Although during the passing the time, the reaction will go to completion, (increasing the time has a positive effect on the percentage of dye removal), it is advantageous (especially economically) to optimize the time simultaneously with the other parameters to have the best responses.

Interaction parameters. Eq. (3) and the response surfaces (Fig. 2) show that the time interacted with all three of the effective variables, more or less. Other interactions were non-significant or low-significant.

Real samples

After acquiring the optimized values for the effective variables and testing them with extra experiments, these experimental qualifications were applied on a real sample which was a derivative from the waste water of a local textile factory (Urmia, Iran).

The results showed that the optimum values that could lead to acceptable responses, had been achieved by CCD and the response surface method. The spectra of a real sample before and after treatment by the proposed method are presented in Fig. 3. Using Eq. (3), a percentage degradation of 79.87 % was achieved for the removal of Methyl Orange from the real sample.

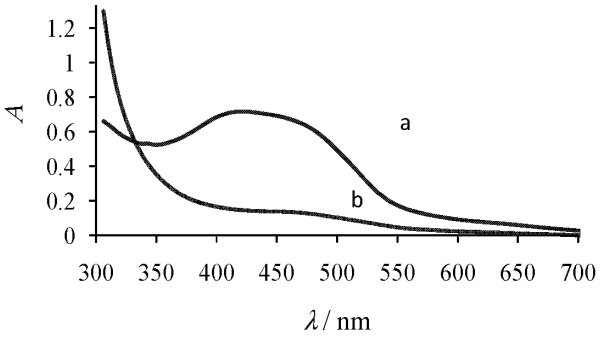

Fig. 3. a) The spectrum of a real sample before application of the Fenton reaction (blank solution) and b) the spectrum of the real sample after application of the Fenton reaction (sample solution).

CONCLUSION

The response surface methodology was shown to be a valuable approach to optimize a process based on the Fenton reaction. In order to obtain the optimized conditions for the removal of Methyl Orange from a textile wastewater, 28 experiments (including 4 repetitions of central points) were designed using CCD method. The optimized ranges were 0.25–0.35 mM for $[Fe(II)]_0$, 5–17 mM for $[H_2O_2]_0$, 4–9 mM for $[Oxalate]_0$, and 50–80 min for the reaction time. These conditions were applied on a real sample and an acceptable response was achieved.

ИЗВОД

ДИЗАЈН ЦЕНТРАЛНОГ КОМПОЗИТА У ОПТИМИЗАЦИЈИ УКЛАЊАЊА АЗО БОЈЕ, МЕТИЛ-ОРАНЖА, ИЗ ОТПАДНИХ ВОДА ФЕНТОНОВОМ РЕАКЦИЈОМ

MAHSA AZAMI[1], MORTEZA BAHRAM[1], SIROUS NOURI[1] и ABDOLHOSEIN NASERI[2]

[1]Department of Chemistry, Faculty of Science, Urmia University, Urmia, Iran and [2]Department of Analytical Chemistry, Faculty of Chemistry, University of Tabriz, 51666–16471, Tabriz, Iran

У овој студији је проучавана деградација метил-оранжа, коришћењем Фентонове реакције, и оптимизована помоћу дизајна централног композита и методологије површине одговора. Ефекти разних експерименталних параметара у овој реакцији испитивани су дизајнирањем централног композита. Дизајнирано је укупно 28 експеримената, са 4 фактора и 5 нивоа за сваки фактор. Ови фактори (или променљиве) били су: почетна концентрација Fe(II), почетна концентрација H_2O_2, почетна концентрација оксалата и време реакције. Утврђен је квадратни полином који повезује проценат деградације боје (као одговор) и проучаваних параметара. Након уклањања променљивих из модела које нису значајне, за одређивање оптималних услова употребљен је метод површине одговора. Оптимални опсези променљивих били су: 0,25 до 0,35 mM за почетну концентрацију Fe(II), 5 до 17 mM за почетну концентрацију H_2O_2, 4 до 9 mM за почетну концентрацију оксалата и 50 до 80 min за време реакције. Такође, резултати додатних експеримената су показали да се ове оптимизоване вредности могу употребити за стварне узорке и добијање одговора значајне висине.

(Примљено 15. марта, ревидирано 9. маја 2011)

REFERENCES

1. L. G. Devi, S. G. Kumar, K. M. Reddy, C. Munikrishnappa, *J. Hazard. Mater.* **164** (2009) 459
2. B. H. Hameed, T. W. Lee. *J. Hazard. Mater*. **164** (2009) 468
3. I. Arslan-Alaton, G. Tureli, T. Olmez-Hanci, *J. Photochem. Photobiol., A* **202** (2009) 42
4. C. Fernández, M. S. Larrechi, M. P. Callao, *Talanta* **79** (2009) 1292
5. E. Butron, M. E. Juarez, M. Solis, M. Teutli, I. Gonzalez, J. L. Navad, *Electrochim. Acta* **52** (2007) 6888
6. A. Özcan, M. A. Oturan, N. Oturan, Y. Şahin, *J. Hazard. Mater*. **163** (2009) 1213
7. A. Rodrıguez, G. Ovejero, J. L. Sotelo, M. Mestanza, J. Garcıa. *Ind. Eng. Chem. Res*. **49** (2010) 498
8. J. Garcıa-Montano, L. Perez-Estrada, I. Oller, M. I. Maldonado, F. Torrades, J. Peral, *J. Photochem. Photobiol., A* **195** (2008) 205
9. A. Pourbabaee, F. Malekzadeh, M. N. Sarbolouki, A. Mohajeri, *Iran. J. Chem. Chem. Eng.* **24** (2005) 41
10. R. Jain, S. Varshney, S. Sikarwar. *J. Colloid. Interf. Sci.* **313** (2007) 248
11. H. Wang, J. Niu , X. Long, Y. He, *Ultrason. Sonochem.* **15** (2008) 387
12. M. Diagne, N. Oturan, M. A. Oturan, *Chemosphere* **66** (2007) 841
13. M. Zarei, A. Niaei, D. Salari, A. R. Khataee. *J. Electroanal. Chem.* **639** (2010) 167
14. A. R. Khataee, M. Zarei, L. Moradkhannejhad. *Desalination* **258** (2010) 112
15. N. Daneshvar, M. J. Hejazi, A. R. Khataee, B. Rangarangy, *J. Environ. Health, B* **39** (2004) 285
16. T. Kurbus, Y. M. Slokar, A. M. L. Marechal, D. B. Voncinab, *Dyes Pigm.* **58** (2003) 171
17. S. P. Sun, C. J. Li, J. H. Sun, S. H. Shi, M. H. Fan, Q. Zhou. *J. Hazard. Mater.* **161** (2009) 1052
18. A. Gutowska, J. Ka1uzna-Czaplinska, W. K. Jozwiak. *Dyes Pigm.* **74** (2007) 41
19. T. Kurbusa,Y. M. Slokara, A. Majcen, L. Marechal, D. B. Voncinab. *Dyes Pigm.* **58** (2003) 171
20. N. Daneshvar, D. Salari, A. R. Khataee, *J. Photochem. Photobiol., A* **157** (2003) 111
21. M. Kincl, S. Turk, F. Vrecer, *Int. J. Pharm*. **291** (2005) 39
22. M. Ahmadi, F. Vahabzadeh, B. Bonakdarpour, E. Mofarrah, M. Mehranian, *J. Hazard. Mater*. **123** (2005) 187
23. C. Fernández, M. S. Larrechi, M. P. Callao, *J. Hazard. Mater.* **180** (2010) 474
24. S. Gorji, M. Bahram, *Anal. Methods* **2** (2010) 948.

Journal of the Serbian Chemical Society
JSCS-info@shd.org.rs • www.shd.org.rs/JSCS
J. Serb. Chem. Soc. *77* (2) 247–255 (2012) UDC 550.4:597+56.022:551.352.1:552.63(489)
JSCS–4265 *Original scientific paper*

Iridium anomaly in the Cretaceous–Paleogene boundary at Højerup (Stevns Klint, Denmark) and Woodside Creek (New Zealand): the question of an enormous proportion of extraterrestrial component

PAVLE I. PREMOVIĆ[1]*, BUDIMIR S. ILIĆ[2] and MILOŠ G. ĐORĐEVIĆ[1]

[1]*Laboratory for Geochemistry, Cosmochemistry and Astrochemistry, University of Niš, P. O. Box 224, 18000 Niš, Serbia and* [2]*Department of Pharmacy, Faculty of Medicine, University of Niš, 18000 Niš, Serbia*

(Received 4 April, revised 8 August 2011)

Abstract: The Cretaceous–Paleogene boundary clays at Højerup and Woodside Creek show anomalous enrichments of iridium compared with the marine sedimentary rocks. For the average iridium content of 465 ppb in CI chondrite the estimate of the carbonaceous chondritic proportions in the decarbonated iridium-rich boundary layers, based on the integrated iridium fluencies, is about 26 % at Højerup and 65 % at Woodside Creek. These proportions are most likely too high due to a significant Ir influx from the nearby marine or continental site to these sections.

Keywords: Fish Clay; Woodside Creek; iridium; carbonaceous chondrite.

INTRODUCTION

In the original paper, Alvarez *et al.*[1] first reported anomalously high Ir concentrations in the Cretaceous–Paleogene (KPB) boundary clays at Højerup (eastern Denmark, Fig. 1) and at Woodside Creek (the northern part of the South Island of New Zealand, Fig. 1). They proposed an impact of an extraterrestrial bolide to explain the elevated Ir content at the KPB. In general, Ir and other platinum-group elements (PGE: collectively the elements Ru, Rh, Pd, Os, Ir and Pt) are invariably enriched in the prominent KPB clays. Other trace elements (*e.g.*, heavy metals) are also relatively abundant in these clays.

Many researchers consider that the KPB impactor formed the *ca*. 180 km crater at Chicxulub (Yucatan Peninsula, Mexico). It was suggested that the impactor was a carbonaceous chondrite-type body,[2–6] although it is still unclear whether it was a carbonaceous chondrite or a comet. Indeed, comets are believed to be primitive bodies with a composition similar to that of carbonaceous chon-

* Corresponding author. E-mail: pavle.premovic@yahoo.com
doi: 10.2298/JSC110404178P

drites.[7] The anomalous Ir associated with the prominent boundary clay is, however, consistent with the high Ir content typical of most chondritic meteorites and inconsistent with the general proposition of comets. Indeed, a simple calculation shows that in the case of ice-rich comets (>70 % ice, *e.g.*, the Haley-Bopp comet), the amount of iridium produced by an impact energy for a crater of the Chicxulub size could be less than 0.001 % than that of an asteroid.

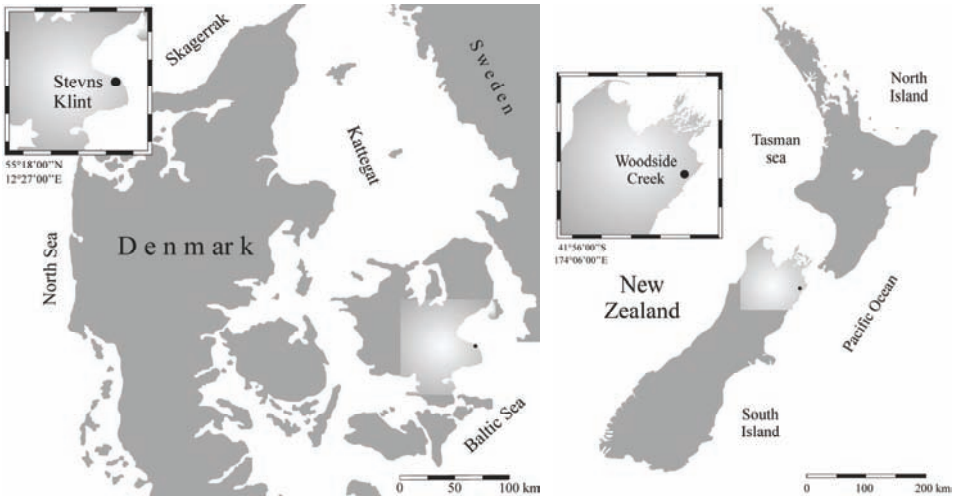

Fig. 1. Geographic location of Stevns Klint in Denmark and Woodside Creek in New Zealand.

In the past, many researchers used the iridium concentration and/or integrated amount of iridium to estimate the proportion of chondritic component in the renowned boundary clays. This brief paper aims to re-examine this method using comprehensive Ir data from the sites at Højerup and Woodside Creek, which are available and were published by Schmitz.[8]

RESULTS AND DISCUSSION

Fish Clay. The lowermost Danian Fish Clay Member of the Rødvig Formation near the village of Højerup is a classic marine KPB section. The lithology of the Fish Clay within this boundary section characterizes four distinctive layers: black-to-dark marl (hereinafter BDM) with a basal red (goethite-rich) layer, brown-to-grey marl and at the top light-grey marl (Fig. 2). The red layer is underlain by (latest) Maastrichtian bryozoan-rich limestone, whereas the top marl is overlain by (early) Danian Cerithium limestone.[8–12] Geochemical studies show that the Ir profile (on a whole rock basis) across the Fish Clay column is characterized by a sharp maximum in the base of the BDM with an upward gradual decrease (tailing-off) from its maximum (*e.g.*, Schmitz[10]). The BDM is considered to constitute the main part of the boundary section, since it probably contains more than 95 % of the total Ir in the Fish Clay.[13] The mineralogy of the BDM is

comparatively simple, smectite and authigenic (mainly biogenic) calcite being the principal components. Geochemical evidence indicates that the BDM was deposited under strong anoxic conditions but the red layer under strong oxic sedimentation conditions.[13]

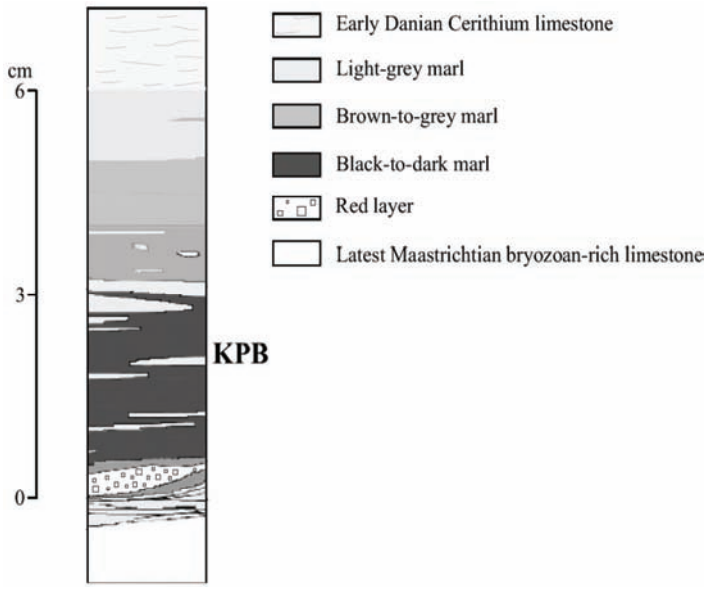

Fig. 2. Expanded lithological log of the Fish Clay at Højerup, based on Surlyk *et al.*[12]

As pointed out above, the Ir enrichment of the KPB clays is generally regarded as indicative of the presence of a carbonaceous chondrite (CC) component. Table I shows that carbonaceous chondrites typically contain 406.0–849.4 ppb Ir, while, on average, marine sedimentary rocks usually contain below 1 ppb (Table I); hence, little addition of a CC component would be necessary to critically increase the concentration of Ir in a marine sedimentary rock. Thus, Ir is a very sensitive means of examining the CC contribution to marine KPB clays such as the Fish Clay. Some authors suggested that Ir in the Fish Clay was sourced by iridium from seawater. However, the average iridium concentration in the decarbonated BDM (100 ppb) represents an enrichment factor of about 10^{17} compared to seawater (*ca.* 2×10^{-15} ppb, Table I). Moreover, according to these authors, the residence time of iridium in the oceans is about 1 million years. Thus, the excess of Ir in the BDM, therefore, could not have been derived from a sea reservoir.

Kyte *et al.*[14] estimated that the extraterrestrial component in the basal 1-cm part of the BDM from the measured Ir concentration (47.4 ppb) is about 10.5 %, corrected for about 20 % carbonate content. According to Grieve,[15] the chondrite-normalized relative abundance of Ir indicates that the Fish Clay (on a

whole-rock basis) contains an admixture of about 10 % chondrite. Trinquier *et al.*[6] showed that the Cr isotopic signature of the BDM represents a mixing of the CC matter with terrestrial material in a ratio of up to 6.8 %. Recently, Osawa *et al.*[16] estimated from the measured Ir concentration (29.9 ppb) that the extraterrestrial material in the basal part of BDM was diluted 1/19 (on a whole-rock basis), assuming that the Ir concentration of CC is 470 ppb. Of note, an impactor mass fraction globally dispersed after the Chicxulub impact ranged between 22[1] to 50 %.[17]

TABLE I. Concentrations of Ir in carbonaceous chondrites, marine sediments and seawater

Specimen		Ir content, ppb
Carbonaceous chondrites	Maximum	849.4[a]
	Minimum	406.0[a]
Marine sediments		<1[b]
Seawater		2×10^{-15}[c]

[a]Walker[29]; [b]Anbar *et al.*[30]; [c]Goldberg *et al.*[31]

Schmitz[8] reported instrumental neutron activation analysis (INAA) data for Ir in the carbonate-free fraction across the Fish Clay (Fig. 3a) as this metal is

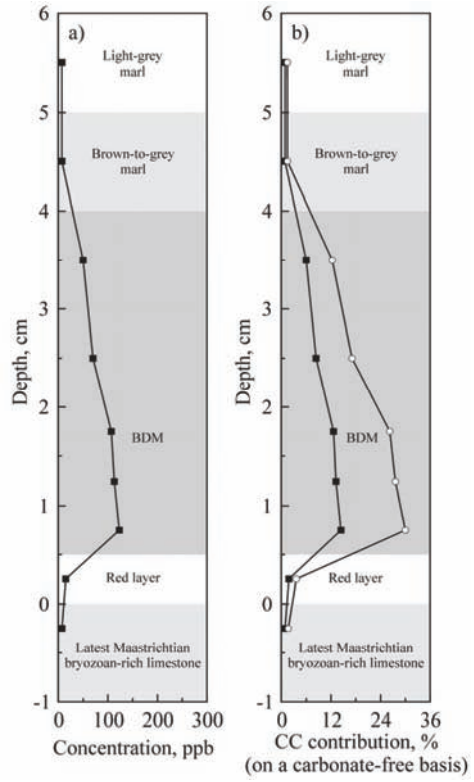

Fig. 3. a) Concentration profiles of Ir (on a carbonate-free basis) in the Cretaceous–Paleogene boundary clays at Højerup (Fish Clay). The samples were analyzed by instrumental neutron activation (INAA). The relative error in the precision of the analyses ranges from 5 to 10 %. The total uncertainties (including accuracy errors) were up to 20 %.[8] b) The CC contributions for the decarbonated Fish Clay based on the Ir concentrations. Lowest (■) and highest (○) CC contributions were calculated assuming that the Ir content of the carbonaceous chondrite was 406.0 and 849.4 ppb, respectively (Table I).

wholly located in this fraction. This profile shows that the peak and mean concentrations of Ir in decarbonated BDM is about 120 and 100 ppb, respectfully. Using these data and assuming that all the Ir found in the Fish Clay originated from the CC component, it was estimated that the decarbonated BDM is derived from about 6–30 % CC (Fig. 3b). This estimate assumed that the Ir content of the carbonaceous chondrites range from 406.0 to 849.4 ppb, Table I. If 465 ppb represents the average content of Ir in CI chondrites[18] then the CC contribution to the decarbonated BDM averages about 21 %.

A better measure of an Ir anomaly in boundary clay is the integrated Ir fluence. This fluence for the carbonate-free BDM (assuming a density of 2 g cm^{-3}) was estimated at about 600 ng cm^{-2} after integration in the interval from 0.5 to 4.0 cm. For comparison, an estimate of the Ir fluency for the global impact deposit for the KPB is about 40–55 ng cm^{-2}.[19] This value corresponds approximately to about 700 to 1500 mg cm^{-2} CC, based respectively on 406.0 to 849.4 ppb Ir in carbonaceous chondrites (Table I). These estimates correspond to about 14––30 % CC in the decarbonated BDM; for an average Ir content of 465 ppb in CI chondrite, the contribution is about 26 %. Such a significant proportion of CC, however, is not supported by any mineralogical evidence. Indeed, if initially the precursor material of BDM contained a high percentage of impact-derived ejecta fallout, then diagenetic alteration would have left a residue with high concentrations of the impact-derived markers. To the best of our knowledge, the BDM contains no altered meteoritic fragments[20] and only about 0–6 shocked quartz grains per gram.[21] On the other hand, similar calculation based on Ir fluency indicates that the underlying reddish layer (with 15. 2 ppb of Ir, Fig. 3a) contains as low as about 3.3 % of CC material. In sharp contrast, this layer is abundant with well-preserved, impact-related goethite-rich microspherules[10,22] and with nano--size goethite grains,[20,23] interpreted as altered meteorite fragments.[20] About 29––33 shocked quartz grains per gram were also identified in this layer.[21] Of note, the total iridium flux of the carbonate-free Fish Clay is about 615 ng cm^{-2}, which corresponds to about 27 % CC for an average Ir content in the CI chondrite of 465 ppb.

The present estimation (judging from the Ir concentrations and fluence) may substantially underestimate the actual CC contribution to the decarbonated BDM. There are two reasons for this. The anomalous amounts of Ir in the decarbonated Fish Clay display a gradual decrease from the BDM upwards but this metal is still relatively elevated (<5 ppb) in the light-gray marl (Fig. 3a). These stratigraphically extended enrichments of Ir may be explained by redox-controlled remobilization.[24] In addition, according to Peucker-Ehrenbrink and Hanningan,[25] between about 40 and 80 % of the initial Ir budget could have been lost due to surficial weathering of black shales (such as BDM) within roughly 13,000 years. Thus, because of the assumed remobilization and/or weathering loss of Ir, the

original proportion of CC in the carbonate-free part of the BDM could actually be even considerably higher than presented above. A more detailed discussion of this issue is beyond the scope of this paper.

The CC matter (and associated Ir) could have been deposited in the Fish Clay by the direct airborne ejecta fallout settling through the seawater column or transport from the nearby marine or continental site to the Fish Clay bed. Kyte *et al*.[14] reasoned that Ir (and other siderophiles) in the basal 1-cm-thick part of the BDM is only representative of primary Ir derived from the initial ejecta fallout deposited during a short time (a few days, months or years) after the impact. According to these researchers, Ir above this layer is probably secondary in origin and transported from the original nearby site, which increased the primary Ir values. Wolbach *et al*.[26] proposed that secondary Ir is ejecta material eroded from marine elevated sites to topographic lows already containing some primary fallout. Premović[13] has suggested that Ir in the Fish Clay was probably fluvially transported from the soil on the adjacent land and redeposited in a shallow marine basin at Højerup. This author argued that a predominant part of the Ir in the BDM ultimately came from CC material associated with ejecta fallout covering the nearby coastal soil. Consequently, overestimated proportions of the CC matter in the decarbonated BDM are probably due to the high Ir input from a marine or continental site.

The Woodside Creek section. The KPB at Woodside Creek is represented by a reddish goethite-rich clay layer that is up to 1-cm thick. The boundary clay at Woodside Creek (BW) is underlain by Maastrichtian siliceous limestone and overlain by siliceous claystone,[27] Fig. 4. Previous sedimentary studies showed that this clay (see for example)[28] is not primary fallout but redeposited (a feature that is difficult to reconcile with the high Ir anomaly) and affected by erosion or non-deposition. These studies also imply that the BW was deposited in a shallow marine region under well-oxygenated conditions.

Schmitz[8] also reported INAA data for Ir in the carbonate-free BW (Fig. 4a). Of note, the Woodside Creek sections also shows an Ir "tailing effect" as does the Fish Clay, but it is less pronounced, Fig. 4a.

Figure 4a shows that the peak concentration of Ir in the decarbonated BW is 460 ppb, which is one of the highest measured to date for any KPB interval. Using this data and assuming that all the Ir found in this boundary section originnated from the CC component, it was estimated that the decarbonated BW is derived from about 60 % up to bizarre 115 % CC (Fig. 4b). If 465 ppb represents an average content of Ir in CI chondrites[18] then the CC contribution to the decarbonated BW averages about >100 %.

The integrated Ir fluence for the carbonate-free red layer of the BW (assuming a density of 2 g cm^{-3}) was estimated at about 600 ng cm^{-2}**,** after integration in the interval from 0 to 1 cm, which is (fortuitously?) identical to that estimated

for the BDM. This value corresponds, as for the BDM case, to approximately 700 to 1500 mg cm^{-2} CC based on 406.0 to 849.4 ppb Ir in carbonaceous chondrites (Table I). These estimates correspond to about 35–75 % CC in the decarbonated BW. For an average Ir content of 465 ppb, the CI chondrite contribution to this decarbonated section is 65 % CC.

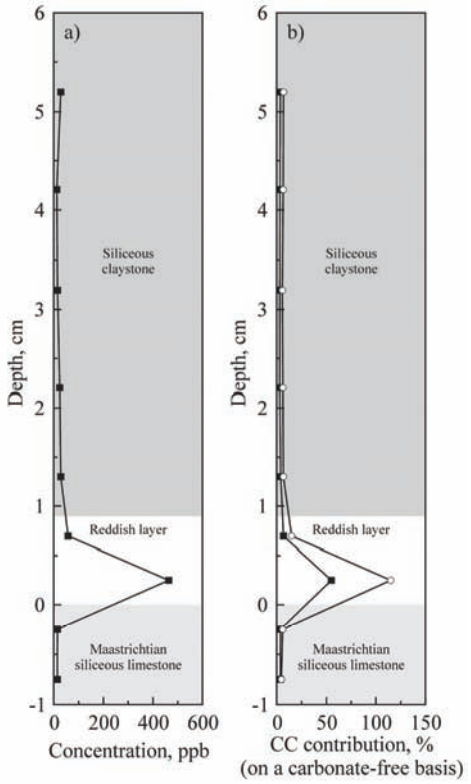

Fig. 4. a) The Ir concentration profile (on a carbonate-free basis) across the Cretaceous–Paleogene boundary section at Woodside Creek. The samples were analyzed by instrumental neutron activation (INAA). The relative error in the precision of the analyses ranges from 5 to 10 %. The total uncertainties (including accuracy errors) were up to 20 %.[8] b) The CC contributions for the decarbonated boundary section at Woodside Creek based on the Ir concentrations. Lowest (■) and highest (○) CC contributions are calculated assuming that the Ir content of the carbonaceous chondrite was 406.0 and 849.4 ppb, respectively (Table I).

As in the case of BDM, a high percentage of the impact-derived ejecta fallout would have left a residue after diagenesis with high concentrations of the impact-derived indicators in the BW. To the best of our knowledge, this thin reddish layer contains numerous (possibly?) impact-derived goethitic microspherules and about 2–8 shocked quartz grains per gram were identified in this layer.[21]

In analogy to the Fish Clay, it is assumed that the Ir in the BW probably originated from a carbonaceous chondritic component of ejecta fallout deposited on nearby adjacent land or marine area.

Assuming that 50 % represents the CC fraction in ejecta fallout (with an average density of about 2 g cm^{-3}), then about 0.7–1.5 g of the ejecta fallout would have sourced almost all the integrated amount (*ca.* 600 ng cm^{-2}) of Ir in the de-

carbonated BDM and BW. This corresponds to an approximately 0.35 – 0.75 cm thick ejecta deposit.

In summary, the Ir content of marine boundary clays may be influenced by various sedimentary and geochemical factors (*e.g.*, erosion, redeposition, geochemical remobilization and weathering). The extent to which these factors operate is dependent on the particular sedimentary site and the immediate seafloor environment. Consequently, Ir may have been concentrated or diluted in the boundary clay during sedimentation and diagenesis, and thereafter. This makes ambiguous any attempt to assess the contribution of the impactor Ir to the Ir enrichment of boundary clay or to use global fluence of Ir to calculate the chondritic impactor size. The same ambiguity goes for other PGE. In addition, in order to identify chondritic elements in the boundary clay, researchers usually present their trace element data after normalizing first to Ir and then to CI chondrites. It is clear from the above considerations that this method is also rather ambiguous.

CONCLUSION

Estimates based on the integrated Ir amount show that the decarbonated Ir-rich KPB layers at Højerup and Woodside Creek appear to contain respectfully as much as 26 and 65 % of the CC matter for the average Ir content of 465 ppb CI chondrite. These percentages are most probably an overestimation due to the high Ir input from nearby marine or continental sites, which presumably increased the primary Ir values in these clays.

И З В О Д

АНОМАЛНЕ КОНЦЕНТРАЦИЈЕ ИРИДИЈУМА У КРЕДА–ПАЛЕОГЕН ГРАНИЧНИМ СЛОЈЕВИМА СА ЛОКАЛИТЕТА HØJERUP (STEVNS KLINT, ДАНСКА) И WOODSIDE CREEK (НОВИ ЗЕЛАНД): ПИТАЊЕ ПОРЕКЛА ВИСОКОГ УДЕЛА ХОНДРИТСКЕ КОМПОНЕНТЕ

ПАВЛЕ И. ПРЕМОВИЋ[1], БУДИМИР С. ИЛИЋ[2] и МИЛОШ Г. ЂОРЂЕВИЋ[1]

[1]*Лабораторија за геохемију, космохемију и астрохемију, Универзитет у Нишу, п. п. 224, 18000 Ниш и* [2]*Одсек за фармацију, Медицински факултет, Универзитет у Нишу, 18000 Ниш*

Креда–палеоген граничне глине са локалитета Højerup и Woodside Creek показују значајно обогаћење иридијумом у поређењу са морским седиментима. Прорачун, заснован на интегрисаном приливу иридијума по cm^2, показује да је удео угљеничног хондрита у некарбонатним фракцијама њихових иридујумом богатим слојевима 26 (Højerup) и 65 % (Woodside Creek) за просечан садржај иридијума од 465 ppb у CI хондриту. Разлог за ове високе уделе је, вероватно, значајан унос иридијума са околних морских и копнених лежишта у наведене глине.

(Примљено 4. априла, ревидирано 8. августа 2011)

REFERENCES

1. L. W. Alvarez, W. Alvarez, F. Asaro, H. V. Michel, *Science* **208** (1980) 1095
2. F. T. Kyte, *Nature* **396** (1998) 237

3. A. Shukolyukov, G. W. Lugmair, *Science* **282** (1998) 927
4. R. Frei, K. M. Frei, *Earth Planet. Sci. Lett.* **203** (2002) 691
5. G. Quitté, E. Robin, F. Capmas, S. Levasseur, R. Rocchia, J. L. Birck, C. J. Allègre, *Carbonaceous or ordinary chondrite as the impactor at the K/T boundary? Clues from Os, W and Cr isotopes*, in *Proceedings of the 34th Lunar and Planetary Science Conference*, (2003), Lunar and Planetary Institute, Houston, TX, 2003, p. 1615
6. A. Trinquier, J. L. Birck, C. J. Alegret, *Earth Planet. Sci. Lett.* **241** (2006) 780
7. A. Gelinas, D. A. Kring, L. Zurcher, J. Urrutia-Fucugauchi, O. Morton, R. J. Walker, *Meteorit. Planet. Sci.* **39** (2004) 1003
8. B. Schmitz, *Geology* **16** (1988) 1068
9. L. Christensen, S. Fregerslev, A. Simonsen, J. Thiede, *Bull. Geol. Soc. Denmark* **22** (1973) 193
10. B. Schmitz, *Geochim. Cosmochim. Acta* **49** (1985) 2361
11. W. C. Elliott, *Clays Clay Miner.* **41** (1993) 442
12. F. Surlyk, T. Damholt, M. Bjerager, *Bull. Geol. Soc. Denmark* **54** (2006) 1
13. P. I. Premović, *Geochem. Int.* **47** (2009) 513
14. F. T. Kyte, J. Smit, J. T. Wasson, *Earth Planet. Sci. Lett.* **73** (1985) 183
15. R. A. F. Grieve, *Palaeogeogr. Palaeoclimatol. Palaeoecol.* **132** (1997) 5
16. T. Osawa, Y. Hatsukawa, K. Nagao, M. Koizumi, M. Oshima, Y. Toh, A. Kimura, K. Furutaka, *Geochem. J.* **43** (2009) 415
17. A. M. Vickery, H. J. Melosh, in *Global Catastrophes in Earth History*, B. Sharpton, P. Ward, Eds., Geological Society of America, Special Paper 247, Boulder, CO, 1990, p. 289
18. K. Lodders, B. Fegley Jr., *The Planetary Scientist's Companion*, Oxford University Press, New York City, New York, 1998, p. 371
19. F. T. Kyte, AGU Fall Meeting 2004, CA: B33C-0272
20. B. Bauluz, D. R. Peacor, W. C. Elliott, *Earth Planet. Sci. Lett.* **182** (2000) 127
21. J. Morgan, C. Lana, A. Kearsley, B. Coles, C. Belcher, S. Montanari, E. Díaz-Martínez, A. Barbosa, V. Neumann, *Earth Planet. Sci. Lett.* **251** (2006) 264
22. G. Graup, H. Palme, B. Spettle, *Trace element stratification in the Stevns Klint Cretaceous/Tertiary boundary layers*, in *Proceedings of the 23th Lunar and Planetary Science Conference*, (1992), Lunar and Planetary Institute Houston, TX, 1992, p. 446
23. T. J. Wdowiak, L. P. Armendarez, D. G. Agresti, M. L. Wade, Y. S. Wdowiak, P. Claeys, G. A. Izett, *Meteorit. Planet. Sci.* **36** (2001) 123
24. D. C. Colodner, E. A. Boyle, J. M. Edmond, J. Thomson, *Nature* **358** (1992) 402
25. B. Peucker-Ehrenbrink, R. E. Hannigan, *Geology* **28** (2000) 475
26. W. S. Wolbach, I. Gilmour, E. Anders, C. J. Orth, R. R. Brooks, *Nature* **334** (1988) 665
27. C. J. Hollis, C. P. Strong, K. A. Rodgers, K. M. Rodgers, *New Zeal. J. Geol. Geophys.* **46** (2003) 177
28. C. P. Strong, *New Zeal. J. Geol. Geop.* **20** (1977) 687
29. R. J. Walker, *Chem. Erde-Geochem.* **69** (2009) 101
30. A. D. Anbar, K. J. Zahnle, G. L. Arnold, S. J. Mojzsis, *J. Geophys. Res.* **106** (2001) 3219
31. E. D. Goldberg, V. Hodge, P. Kay, M. Stallard, M. Koide, *Appl. Geochem.* **1** (1986) 227.

Journal of the Serbian Chemical Society
JSCS-info@shd.org.rs • www.shd.org.rs/JSCS
J. Serb. Chem. Soc. *77* (2) 257–258 (2012)

Errata (printed version only)

Issue No. 1 (2012), Vol. 77, paper No. *JSCS-4247*:

– page 43, lines 5–11 from above should read:

MOHAMED ABUGHREN[1], MILICA POPOVIĆ[1#], RAJNA DIMITRIJEVIĆ[2#], LIDIJA BURAZER[3], MILICA GROZDANOVIĆ[1#], MARINA ATANASKOVIĆ-MARKOVIĆ[4,5] and MARIJA GAVROVIĆ-JANKULOVIĆ[1*#]

[1]Faculty of Chemistry, University of Belgrade, Belgrade, Serbia, [2]Innovation Center of the Faculty of Chemistry, University of Belgrade, Belgrade, Serbia, [3]Institute of Virology, Vaccines and Sera, Torlak, Belgrade, Serbia, [4]University Children's Hospital, Serbia and [5]Medical Faculty, University of Belgrade, Belgrade, Serbia

– page 45, line 2 from above should read:

…according to the manufacturer's instructions. Complementary-DNA (cDNA) was transcribed by a…

– page 45, line1 1–18 from below should read:

Recombinant GST-Mus a 5 was purified from a BL21 cell culture (100 mL), after 12 h of protein expression at 25 °C. The cells were harvested by centrifugation (3000×*g*, 15 min), and the pellet was suspended in 25 mL of ice-cold L buffer (50 mM Tris–HCl, pH 8.0, 100 mM NaCl, 5 mM EDTA, 0.1 % NaN_3 and 0.1 % Na-deoxycholate). Immediately before use, phenylmethylsulfonyl fluoride (PMSF) (0.1 mM) and dithiothreitol (DTT) (1 mM) were added to the L buffer. After sonication (3×20 s, 20 rms, Branson Sonifier 150, USA), $MgSO_4$ (1 mM), benzonase (0.01 mg mL^{-1}, Novagen, USA) and lysozyme (0.1 mg mL^{-1}, Serva, Germany) were added to the cell lysate, which was further incubated at RT for 15 min. To collect the insoluble fraction (IF), the cell lysate was centrifuged (3000×*g*, for 15 min). After two washings with the buffer (50 mM Tris–HCl, pH 8.0, 100 mM NaCl, 5 mM EDTA, 0.1 % NaN_3), the IF was solubilized in S buffer (100 mM Tris, 50 mM glycine, 6 M urea, pH 8.0). Protein refolding was achieved by rapid mixing of denatured protein solution with R buffer (300 mM NaCl, 20 mM Na_2HPO_4, 3.6 mM KH_2PO_4, pH 7.50; 1:7, v:v), in which a cocktail of protease inhibitors (1 mL L^{-1} of buffer) and oxidized (0.3 mM GSSG) and reduced glutathione (3 mM GSH) were added. The rGST-Mus a 5 solution was applied onto a pre-equilibrated GST-Bind® resin (Novagen, USA) according to the manufacturer's instruction.[18] The concentration of the rGST-Mus a 5 protein was determined using a molar extinction coefficient of 1.434, which was calculated from the amino acid sequence by ProtParam (http://expasy.org/cgi-bin/protparam).

– page 46, line 6 from above should read:

…immunization. Every 30 days, for four months, the rabbits were boosted with a mixture of…

Issue No. 1 (2012), Vol. 77, paper No. *JSCS-4248*:

– page 53, line 6 from above should read:

SOFIJA P. SOVILJ[1*#], DRAGANA MITIĆ[1#], BRANKO J. DRAKULIĆ[2#]

– page 58, Table II should read:

TABLE II. ^{1}H- and ^{13}C-NMR chemical shifts for complexes **1–5** in ppm downfield from TMS. Assignment of the atoms given according to the Scheme 1

Complex	δ^{1}H	δ^{13}C	δ^{13}C
1	2.51 (2H, *t* (C1), ^{3}J = 1.8 Hz); 1.91 (2H, *s* (C2)); 1.68 (2H, *s* (C3)); 2.00 (2H, *s* (C4)); 3.36 (2H, *s* (C5))	S_2CN, 190.91	C1(C5), 52.35; C2, 22.13; C3, 25.97; C4, 23.54
2	2.73 (2H, *s* (C1)); 3.51 (2H, *m* (C2)); 3.67 (2H, *s* (C4)); 3.17 (2H, *s* (C5))	S_2CN, 195.42	C1(C5), 51.82; C2, 66.5; C4, 66.5
3	3.27 (2H, *t* (C1), ^{3}J = 5.0 Hz); 2.58 (2H, *s* (C2)); 2.82 (2H, *m* (C4)); 3.27(2H, *t* (C5), ^{3}J = 5.0 Hz)	S_2CN, 201.66	C1(C5), 53.88; C2, 29.54; C4, 29.54
4	2.92(2H, *s* (C1)); 2.51 (2H, *t* (C2), ^{3}J = 1.6 Hz); 1.91 (H, *s* (C3)); 2.46 (2H, *s* (C4)); 2.99 (2H, *s* (C5))	S_2CN, 201.93	C1(C5), 66.42; C2, 45.43; C4, 45.43
5	3.39 (2H, *s* (C1)); 2.51 (2H, *d* (C2)); 2.25 (3H, *t* (C3), ^{4}J = 1.6 Hz); 2.40 (2H, *s* (C4)); 3.39 (2H, *s* (C5))	S_2CN, 197.40	C1(C5), 49.13; C2, 54.96; C4, 54.96; C6, 45.71

– page 63, the titles of Tables IV and V should read:

TABLE IV. Minimal inhibitory concentrations (*MIC* / μg ml^{-1}) of the tested compounds

TABLE V. Minimal inhibitory concentrations (*MIC* / μg ml^{-1}) of the standard antibiotics against the tested microbial strains (n.t. – not tested)

– page 64, line 13 from below should read:

“тих хетероатома утиче на промену положаја ν(C═H) и ν(C═S) вибрација, које опадају“

– page 65, line 18 from below should read:

“24. N. Katsaros, M. Katsarou, S. P. Sovilj, K. Babić-Samardžija, D. M. Mitić, *Bioinorg*.”